AD_____

Award Number: W81XWH-07-1-0428

TITLE: Nanotechnology-Enabled Optical Molecular Imaging of Breast Cancer

PRINCIPAL INVESTIGATOR: Rebekah Drezek, Ph.D.

CONTRACTING ORGANIZATION: Rice University
Houston, TX 77005

REPORT DATE: July 2012

TYPE OF REPORT: Annual

PREPARED FOR: U.S. Army Medical Research and Materiel Command
Fort Detrick, Maryland 21702-5012

REPORT DOCUMENTATION PAGE

Form Approved
OMB No. 0704-0188

1. REPORT DATE	**2. REPORT TYPE**	**3. DATES COVERED**
July 2012	Annual	15 June 2011 – 14 June 2012

4. TITLE AND SUBTITLE

Nanotechnology-Enabled Optical Molecular Imaging of Breast Cancer

5a. CONTRACT NUMBER

5b. GRANT NUMBER
W81XWH-07-1-0428

5c. PROGRAM ELEMENT NUMBER

6. AUTHOR(S)

Rebekah Drezek, Ph.D.

E-Mail: drezek@rice.edu

5d. PROJECT NUMBER

5e. TASK NUMBER

5f. WORK UNIT NUMBER

7. PERFORMING ORGANIZATION NAME(S) AND ADDRESS(ES)

Rice University
Houston, TX 77005

8. PERFORMING ORGANIZATION REPORT NUMBER

9. SPONSORING / MONITORING AGENCY NAME(S) AND ADDRESS(ES)
U.S. Army Medical Research and Materiel Command
Fort Detrick, Maryland 21702-5012

10. SPONSOR/MONITOR'S ACRONYM(S)

11. SPONSOR/MONITOR'S REPORT NUMBER(S)

12. DISTRIBUTION / AVAILABILITY STATEMENT
Approved for Public Release; Distribution Unlimited

13. SUPPLEMENTARY NOTES

14. ABSTRACT

This project focuses on development of nanotechnology-enabled optical molecular imaging technologies for applications in both breast cancer diagnosis and monitoring therapeutic response. The project consists of two major efforts: (1) optical instrumentation technology development and (2) development of complementary engineered nanomaterials for use in conjunction with the instrumentation created to provide molecular specificity. A particularly significant effort is underway to develop needle-compatible fiber optic probes to enable in vivo imaging of tumors with micron resolution in order to provide a new microscopic, high resolution imaging modality. These microscopic devices will complement the macroscopic, wide-field optical imaging devices being developed in this project.

15. SUBJECT TERMS
nanotechnology, molecular imaging, optical imaging

16. SECURITY CLASSIFICATION OF:			**17. LIMITATION OF ABSTRACT**	**18. NUMBER OF PAGES**	**19a. NAME OF RESPONSIBLE PERSON**
a. REPORT	**b. ABSTRACT**	**c. THIS PAGE**			USAMRMC
U	U	U	UU	122	**19b. TELEPHONE NUMBER** *(include area code)*

Table of Contents

Introduction

There is a critical need to develop new imaging technologies which bridge the gap between our rapidly developing fundamental molecular understanding of breast carcinogenesis and our ability to rationally harness this understanding to develop more effective diagnostic and treatment strategies. Bridging that gap requires developing new tools which can rapidly detect, diagnose, and at times, intervene in the disease process based on recognition of specific molecular signatures of breast cancer *in vivo*. In this project, we focus on the development of photonics-based imaging technologies (SOW, Project 1 and Project 2) and complementary nanoscale molecular-targeted imaging agents for detection and monitoring applications (SOW, Project 3) in order to provide a new approach to molecular imaging of breast cancer. Medical imaging plays a prominent role in all aspects of the screening, detection, and management of breast cancer today. A variety of imaging methods including screening and diagnostic x-ray mammography and resonance imaging (MRI) are currently used to evaluate and monitor breast lesions. Although existing imaging technologies provide a useful approach to delineating the extent of tumors, these methods offer only low resolution, non-specific issues of tissue and cannot provide a detailed picture of the molecular profile of a tumor. In addition, techniques such as x-ray imaging and MRI are not able to detect small early cancers or pre-cancerous breast lesions and are difficult to use in settings such as the operating room where near real-time dynamic images are required. Thus, there is a substantial clinical need for novel imaging methods for the detection and monitoring of breast cancers which offer improved sensitivity, specificity, portability, and cost-effectiveness. In this project we develop portable optical technologies which promise high resolution, noninvasive functional imaging of tissue at competitive costs. Optical approaches can detect a broad range of morphological, biochemical, and architectural tissue features directly relevant to characterizing breast lesions including sub-cellular physical parameters such as nuclear size and nuclear to cytoplasm (N/C) ratios and biochemical indicators such as hemoglobin concentration, metabolic rate, and collagen cross-linking levels. To make these technologies even more powerful we are expanding the current capabilities of photonics-based imaging approaches with the additional capacity to quantitatively and dynamically detect molecular markers of breast cancer *in vivo* without tissue removal or directly after removal in a surgical environment (SOW, Project 3). While initial work focused on agents best classified as pure imaging agents (quantum dots, nanorods, and other gold based materials), a particular focus during the final year of the award will be on gold-based agents also incorporating therapeutic functionalities through delivery of peptides, oligonucleotides, or drugs. We have now completed five years of effort on this project. The SOW has been modified once to reflect revised goals at the time of a major change in the project directions (discontinuation of radiation project (SOW, Project 4) and replacement with macroscopic imaging project (SOW, Project 2)). More minor changes including the particular nanomaterials worked with (shift from high aspect nanorods to spherical materials for the gold work and additional biomolecule attachments beyond antibodies) have been described in the annual reports. In addition, an exempt protocol was approved by Rice University's IRB and DoD for acquisition of human breast cancer tissue specimens so that work could extend beyond the cell level studies originally proposed.

Progress Report Body

To briefly review the overall structure of our project, we originally proposed three areas of work: development of a needle compatible imaging system for high resolution breast cancer imaging applications, development of nanoengineered molecular imaging agents for breast cancer, and development of nanotechnology based methods for more accurately monitoring delivered radiation. The radiation project was ultimately stopped when it became evident the approach was not clinically viable given the level of radiation needed to detect a signal. When this project was ended, a new project building a macroscopic imaging system to complement the microscopic imaging system under development was added. The SOW was formally revised via DoD to reflect this major change. More minor changes have been adjustments in the specific nanomaterials used for Project 3 as synthesis techniques have advanced over the course of award and the gradual use of a broader range of bioconjugates (peptides, oligonucleotides, glucose, and dendrimers in addition to antibodies). These changes are described in the annual reports.

We begin this year's report with a relatively extensive background section not included in prior year reports. We do this largely to provide literature background regarding why we believe using molecular markers for tumor margin identification, one of the areas we have investigated most heavily through our Era of Hope project, is an important and viable approach. The literature review summarizes current knowledge in the area including a number of new papers from 2011 and 2012 providing additional support for exploring the use of molecular indicators in this area. The new data section begins on approximately page 21. As was the case for Year 4, we integrate the description of our imaging and contrast agent development efforts in the report which follows. While prior year reports on the imaging development focused largely on Project 1 (needle-based high resolution microscopic imaging), over the past year we have worked predominantly on the final generation of the macroscopic imaging system for tumor margins (Project 2) and focus our description on that work. For a more complete technical description of our work, please see the copy of a paper currently under review in J. of Oncology provided in the appendix. In our technical description, rather than repeating the content of this paper, we focus in much more detail than that provided in the paper on the specific question of how we have verified that the macroscopic images we are generating are what we believe them to be (that is, that we are in fact visualizing signal generated from specifically bound anti-HER2 gold nanoparticles.) After providing the technical description of that work, we move on to describing the final macroscopic optical imaging device being developed in this project – an inexpensive handheld instrument we believe will be useful for applications such as tumor margin imaging. In prior years, we described a somewhat more expensive stationary macroscopic imaging instrument useful for whole breast imaging applications while this newer instrument is desgined for applications needing a small hand held device. Finally, we describe recent work in development of nanoparticle based imaging agents for breast cancer. In this year's report we focus on a continuation of the effort described in last year's report towards development of glucose conjugated gold nanoparticles. This work has been motivated by suggestions at prior LINKS meetings to expand our imaging agents beyond HER2. Also, on the basis of LINKS and Era of Hope meeting suggestions we have initiated efforts at pursuing gold nanoparticle based breast cancer theranostic opportunities beyond the pure photothermal applications already reported on. The final year of the award will focus highly in this area.

Part I: Macroscopic Tissue Level Assessment of Nanoengineered Imaging Agents (Project 2/3)

Introduction

In the United States (U.S.) in 2011, there were approximately 230,480 new cases of breast cancer and nearly 39,250 deaths from breast cancer (DeSantis et al. 2011). Nationally, breast cancer mortality rates have been in decline from the 1990s (2.2% per year), whereas incidence rates have been increasing. This increase is thought to be a result of the increase in the number of mammograms that has come about in the U.S (DeSantis et al. 2011).

Ninety-five percent of breast cancers are classified as adenocarcinomas; the other classifications include: squamous cell carcinomas, phyllodes tumors, sarcomas, and lymphomas (Lester 2004). There are two divisions of carcinomas: in situ and invasive. In situ indicates that the cancerous cells have not broken through the ducts or lobules in which the cancer has originated, and the cells are still limited by the basement membrane. Ductal carcinoma in situ (DCIS) is seen approximately four times more frequently (80% vs. 20%) than lobular carcinoma in situ. In situ incidences have increased recently due to technology improvements and the increased number of mammograms due to increased breast cancer awareness (DeSantis et al. 2011; Lester 2004; Nguyen et al. 2009; Atkins et al. 2012). Even though in situ carcinomas have not spread beyond the duct or lobule of origin, they can still be very dangerous because the malignant cells can spread throughout the entire duct or lobule and take up a very large volume in the breast (Lester 2004).

There are six types of invasive carcinoma, about eighty percent of all invasive carcinomas are deemed no special type (NST), also known as invasive ductal carcinoma (IDC), which can not be classified as a specific subtype (Lester 2004). These cancers have a wide variety of protein and gene expression, and there have been recent studies that have looked to classify these cancers more specifically by their expression profiles so that more specific prognoses and treatments can be accomplished. These will be explored later in the manuscript. Invasive lobular carcinoma (ILC) is the second most common breast adenocarcinoma, occurring at a rate of ten percent of all invasive carcinomas. ILC requires a different type of treatment and monitoring regiment. First ILC metastasizes to different organs than other breast cancers (Lester 2004), such as the GI tract, ovaries, and uterus. Additionally, chemotherapeutic treatment of ILC is difficult to monitor using Positron Emission Tomography and Computed Tomography scans

(PET/CT) because detectors have more difficult time detecting the radioactive isotopes that target the malignant tissue (Schelling et al. 2000; Norbert Avril et al. 2001; Groheux et al. 2011; Chung et al. 2006), which may be due to the differences in cell densities between the cell types and their respective infiltration into surrounding tissues (N Avril et al. 2000; Lim et al. 2007).

Other breast adenocarcinomas include tubular carcinoma, which accounts for six percent of invasive carcinomas and ten percent of cancers less than one cm. Ninety-five percent of these cancers will express hormone receptors and they are well-differentiated (Lester 2004). Medullary carcinoma occurs in approximately two percent of invasive carcinomas. It is characterized by high nuclear grade and proliferation rates, yet despite these factors, it still has a higher prognosis than IDC. Invasive mucinous carcinoma also occurs in about two percent of invasive carcinoma and grows slowly over the course of years. It is very soft and looks like gray-blue gelatin. Two other invasive carcinomas include invasive papillary carcinoma and metaplastic carcinoma. These cases are both very rare, less than one percent of all invasive breast cancer; disease heterogeneity and rarity makes it difficult for physicians to institute patients' prognoses for these types of cancers.

There are also rare cases of stromal tumors in the breast that includes benign fibroadenomas, sarcomas, and phyllodes tumors. Fibroadenomas is the most common of benign tumors and is often presented as a palpable mass, which allows for patients to discover them with a self-examination. Phyllodes tumors originate in intra-lobular stroma that are palpable, but are rarely detected in mammography (Lester 2004). Most phyllodes tumors are benign, but those that are more aggressive have been shown to over-express epidermal growth factor receptor (EGFR), a receptor whose overexpression correlates with cell proliferation (Tse et al. 2009). Sarcomas of the breast are very rare that present as large masses. One area of concern for physicians is that there is a slight risk of angiosarcoma formation (0.3-4%) in the breast after a patient receives radiation therapy to treat the primary breast cancer (Lester 2004).

As mentioned previously, there have been studies to classify all breast carcinomas by receptor phenotype that are geared towards helping physicians determine treatment options and prognosis for patients (Lowery et al. 2011; Tamimi et al. 2008). Cell types have been broken into three main subtypes based on protein expression: luminal, HER2 overexpressing (HER2+), and basal-like. Luminal tumors are characterized by the expression of hormone receptors progesterone and estrogen (ER+/PR+) (Lowery et al. 2011; Tamimi et al. 2008). Tamimi further

differentiates the luminal subtype into luminal A&B depending on the overexpression of HER2 on the surface. HER2+ cells are classified as hormone receptor negative, but the HER2 receptor is over-expressed. Finally, basal-like cells are negative for all three receptors, and are also known as triple-negative cancers (TN). Luminal tumors have been targeted with an anti-estrogen drug, Tamoxifen, that has demonstrated success in lowering recurrence and increasing long-term survival of patients that are ER+ (Shao and Brown 2004). However, tamoxifen treatment can cause endometrial cancer and cells will develop tamoxifen resistance (Shao and Brown 2004). Additionally, ER+ patients can receive oophorectomy, to remove sources of estrogen from the body. These two treatments have been recommended for combinatorial use to remove malignant tissue and lower the chances of recurrence and metastasis (Rodríguez Lajusticia, Martín Jiménez, and López-Tarruella Cobo 2008). HER2+ cancers over-express the growth factor receptor ErbB2 (Wang et al. 2011). Breast cancers of this molecular phenotype will be discussed in greater detail in a later section. TN cancers are of major concern for physicians and patients because the lack of receptors on the surface do not allow for targeted therapy that is seen with the other two subtypes of cancer (Duffy, McGowan, and Crown 2012). Lowery et al. showed that TN patients were more than likely to have a recurrence of cancer when compared to the luminal type cancers (Lowery et al. 2011). This is a result of a lack of a properly targeted therapeutic that physicians can use to treat the tumors.

There are three major treatment methods for breast cancer patients: chemotherapy, radiation therapy, and surgery. Chemotherapy involves the administration of agents to the body that will cause damage to the malignant cells. However, these compounds are also toxic to healthy cells in the body, so physicians have to balance the drugs' potential health benefits with the overall health of the patient. Chemotherapeutics can be administered pre-surgery (neoadjuvant) to reduce tumor volume before patients undergo surgery (Kaufmann et al. 2006; Margenthaler 2011). They can also be administered after surgery to control tumor recurrence and metastasis. The two main types of chemotherapeutic agents are small molecule therapeutic agents and biologically specific targets (J. H. Lee and Nan 2012).

Small molecule agents include anthracyclines and taxanes Anthracyclines' mechanisms of therapy include inhibiting DNA synthesis and creating free radicals in the cells that attack DNA (J. H. Lee and Nan 2012). Studies have shown that using multiple anthracyclines in combination raises the efficacy of the drugs (Jassem et al. 2001), but there is cardiotoxicity

associated with anthracyclines that limits the amount that can be administered to the patient (Livi et al. 2009). Taxanes, which include the drug paclitaxel, disrupt microtubule formation and function to disrupt mitosis. Because taxanes and anthracyclines have different mechanisms (and therefore different mechanisms of toxicity to healthy cells), combination of these therapies has proven an effective method of prolonging survival of patients (Bria et al. 2005).

Biologically specific agents are targeted at specific receptors on the surface of cancers such as ER, PR, and HER2. VEGFR (vascular endothelial growth factor receptor) is another important surface receptor in tumor health because it stimulates angiogenesis and vasculogenesis that build blood vessels specifically for the tumor when bound with VEGF (J. H. Lee and Nan 2012). Bevacizumab is an anti-VEGFR (VEGF receptor) antibody that competitively inhibits VEGF binding and prohibits vessel formation for the tumor area. As a single therapeutic, there is a very low response (9.6%) (Cobleigh et al. 2003), but when boosted with an anthracycline, the time to disease progression in head and neck cancers more than doubles (Baselga et al. 2005). The combination of these drugs can also be used t lower toxicity of the small molecule drug. Cameron et al. showed that lapatinib (an anti-HER2 antibody) in combination with the anthracycline capecitabine raised survival time by 11 weeks in comparison to patients treated with capecitabine alone (Cameron et al. 2010). Chemotherapeutics play an important role in patients' treatment plan and have great uses both pre and post surgery. However, cytotoxicity issues will always arise with drugs because they inhibit both healthy and diseased tissue.

Whole breast radiation therapy has been used for decades as a conjunction to breast conservation therapy and has reduced the rate of recurrence and increased long-term survival of patients (Clarke et al. 2005; Vinh-Hung and Verschraegen 2004). However, it delivers a large amount of ionizing radiation to the breast that is dangerous and has potential long-term harmful effects. A newer technology is accelerated partial breast irradiation (APBI) that treats a smaller volume of breast, just around the area of excision and does not expose the whole breast to ionizing radiation. However, one disadvantage is that areas of the breast with a multi-focal tumor will not receive enough radiation and could lead to an increase in tumor recurrence (Margenthaler 2011). There have been recent advancements to improve APBI. The first is interstitial multicatheter brachytherapy that places multiple catheters around the lumpectomy cavity and then delivers radiation through these catheters to localize radiation delivery. The patients can be given high or low radiation dosages, and 5-year recurrence rates ranged from 0-

6% (Arthur et al. 2008). Mammosite is very similar to interstitial multicatheter brachytherapy, but in place of multiple catheters, a single balloon catheter that is filled with saline and fills the entire tumor cavity. Radiation is delivered through this balloon twice a day. A 2008 study by Steward et al. showed a local recurrence rate of 3.8% and good cosmetic results (>90%) after a 60-month follow up. One potential downside of Mammosite is that tumors that are in the deep breast might be too close to the heart and deliver too high of a dose to the organ (Stewart et al. 2008). The final option for ABPI delivery is using a 3-dimensional external beam to treat the tumor cavity. This requires extensive planning and modeling to ensure maximized dosage delivery to the tumor cavity because there is no catheter to deliver the radiation. Multiple studies showed no local recurrence three years after treatment (L. J. Lee and Harris 2009; Vicini et al. 2003). There have been many promising developments in radiotherapy to the tumor cavity in the breast, even though whole breast therapy is still the standard therapy for BCT, APBI offers a new method of maintaining cosmesis and minimizing local recurrence.

Surgery still remains the primary method of removing the bulk of breast cancers. There are two main surgical methods, modified radical mastectomy (MRM) and breast conservation therapy (BCT). MRM involves removal total removal of the breast tissue (Yu et al. 2012) that lowers the chance of disease recurrence and removes the need for post-operative radiation therapy (Yu et al. 2012). However, one major downside of MRM is the removal of the full breast, which can be traumatic for the patient. BCT involves the surgeon removing the part of the breast with the malignant tissue and attempting to preserve as much of the breast as possible to maintain cosmesis for the patient. However, there is a higher chance of recurrence (Fisher et al. 2002; McGuire et al. 2009) with this procedure whose factors will be explored in further detail later on in this section. Because of the amount of local recurrences during BCT, surgeons sometimes have to remove larger volumes of breast tissue that has adverse effects on patient cosmesis. A new surgical specialty has developed in response to this problem, termed "onco-plastics," which involves the use of volume replacement or reconstruction of the breast during the BCT after all malignant tissue has been removed (Margenthaler 2011). These are very difficult surgical procedures and are the source of some controversy because it is thought that surgeons who are skilled enough to perform the plastics aspect of the surgery do not have enough knowledge of cancer as breast cancer surgeons and vice versa (Audisio and Chagla 2007). Because of these complications Clough et al. developed a two-tier classification system (Clough

I&II) based on the percentage of tissue being removed from the breast (Clough I <20%) that helped surgical teams decide on specialty of the surgical procedure (Clough et al. 2010; Margenthaler 2011). Margenthaler defines Clough II surgeries as a surgery where two surgical specialists are present (breast and plastic) that work in tandem to complete the complicated procedure; these surgeries include radial excision lumpectomy, batwing mastopexy lumpectomy, and lumpectomy with concurrent reduction mammoplasty (Margenthaler 2011).

Technical advancements in breast cancer screening technologies have led to the detection of smaller and smaller cancerous lesions within the breast (Nguyen et al. 2009; Osborn et al. 2011). Due to the decreased size of the lesions, a higher amount of patients are opting to undergo BCT followed by radiotherapy than the more traditional MRM (Pleijhuis et al. 2009). Recent studies have shown that there is no difference in long-term survival rates for patients that undergo the respective treatments for early stage breast cancers (Veronesi et al. 2002; Fisher et al. 2002; Mahmood et al. 2012; Miles et al. 2012). While BCT is optimal for cosmesis because it preserves the original breast, many studies have shown that local recurrence occurs at a higher rate for patients receiving BCT, especially with younger patients (Beadle et al. 2009; Cabioglu et al. 2007; Tanis et al. 2012). Even though the rate of recurrence does not effect overall survival rate (Miles et al. 2012), patients must undergo re-excision and increased radiation dosage (Guidroz et al. 2011; Pleijhuis et al. 2009). Additionally, these patients undergo stress and psychological trauma that has an additive effect on the stress already seen with initial treatment (Mannell 2005; H.-C. Yang et al. 2008). Most importantly, local recurrences have been associated with increased rates of metastases in patients (Kreike et al. 2008; Voogd et al. 2005), which leads to an increased mortality rate.

Many retrospective studies have been conducted to determine the factors that lead to a local recurrence after therapy (Pleijhuis et al. 2009). These studies include patient age (Yildirim 2009; Komoike et al. 2006; Nottage et al. 2006; Cèfaro et al. 2006; Vargas et al. 2005), tumor size(Yildirim 2009; Cèfaro et al. 2006; Aziz et al. 2006), radiation treatment (Komoike et al. 2006; Nottage et al. 2006; Aziz et al. 2006), and lymph node status (Yildirim 2009; Gülben et al. 2007; Aziz et al. 2006) among many. Even though these studies found that these factors can be used as independent predictors of a local recurrence of breast cancer, tumor margin status is still thought of as the strongest predictor for recurrence (Karni et al. 2007; Ali et al. 2011; Houssami et al. 2010; Schwartz et al. 2006).

The tumor margin is the area around the edge of the resected tissue specimen of the patient. Tumor margin status refers to the question of whether or not there are microscopic cancer cells located at the edge of the excised tissue specimen; a positive status indicates microscopic disease, whereas negative indicates disease free tissue. It is generally thought that if there are cancerous cells on the edge of the tissue, then the patient has an increased chance of a local recurrence due to the increased chance of cancerous cells not being removed from the body (Houssami et al. 2010). However, this is where the consensus on margin status ends, and argument begins (Houssami et al. 2010). Many studies have argued and presented evidence as to what constitutes a proper negative margin for patients (Singletary 2002; Carlson et al. 2009; Zavagno et al. 2008; MacDonald and Taghian 2009; Luini et al. 2009). In particular, the argument over what is the proper distance from the edge of the tissue that must be disease free in order for the patient to have negative margins. For example, Zavagno used a distance of 3 mm whereas a panel led by Kauffman recommends that as long as there are no cells "touching ink" then the patient should be declared to have free margins, effectively a margin distance of 0 mm (Zavagno et al. 2008; Kaufmann et al. 2010). Additionally, some studies use a third diagnosis: a close margin. Close margins are defined as tissues that contain microscopic disease within the pre-determined margin width, but not at the edge of the tissue. This leads to the conclusion that it is very difficult to compare studies that use different indications of negative margins; however, it is still accepted the margin status (regardless of definition of distance) is still an important predictor of local recurrence.

The distance in margin status is important in BCT because surgeons are trying to strike a balance between treating the disease while also maintaining cosmesis for the patient. Studies have shown that having a more normal breast appearance has positive psychological effects for patients who have undergone breast cancer treatment (Rowland et al. 2000; Al-Ghazal, Fallowfield, and Blamey 2000; Chakravorty et al. 2012). Increasing margin width will add to the amount of excised tissue during surgery leading to a higher difficulty of maintaining cosmesis (Fentiman 2011) and perhaps leading to future psychological problems for a patient. In 2010, Houssami et al. performed a meta-analysis of 21 margin status studies to determine how well margin status and width correlated with local recurrence rates. The authors found that positive (or close) margins correlated positively with margin status and patients with a negative margin status had a lower rate of recurrence. However, the study also concluded that the increasing the

tumor margin width (ranges of different studies were 1-5) did not significantly lower the rate of recurrence, especially when they considered if the patient received a radiation therapy boost (Houssami et al. 2010). However, Houssami et al. did recommend that surgeons use at least a 1 mm margin width when determining margin status in contrast to the "touching the ink" method recommended by Kaufman (Kaufmann et al. 2010; Houssami et al. 2010).

Even though proper margin width is debatable throughout the medical community, the principle of removing as much diseased tissue as possible during surgery still holds paramount to reducing local recurrence. There are many ways that physicians can increase the amount of diseased tissue removed by obtaining information about the tumor preoperatively (Pleijhuis et al. 2009).

Pre-operative imaging includes mammography, which allows the surgeon to assess the borders and a palpable tumor before the procedure begins. Additionally, physicians can determine if there are micro calcifications in the breast, an indicator of possible DCIS presence (Cho et al. 2008). A recent study by Rauscher et al. discovered that mammography has a high sensitivity in cancerous detection (94%), however it is lacking in specificity (61%) due to the presence of islands of fibroglandular or fibrocystic tissue in the breast that are indistinguishable from malignant tissue (Rauscher et al. 2008; Ikeda et al. 2003). In some patients, ultrasound is used to supplement mammography findings because it provides better information on size and growth pattern of tumors (Pleijhuis et al. 2009). Magnetic resonance imaging (MRI) is a newer technology that provides significant improvement in pre-operative imaging of cancerous tissue when compared to mammography and ultrasound (Van Goethem et al. 2007). MRI provides patients and physicians with extensive information, such as multifocality of the disease, that can help determine if a patient should even undergo BCT (Jacobs 2008). A study by Houssami et al. demonstrated that MRI helped detect additional cancer in 16% of patients, leading 1.1% of patients select a mastectomy over BCT (Houssami et al. 2008). Even though MRI can help direct patients away from a surgery in order to decrease the chance of local recurrence, its preoperative use does not have a significant impact on margin status or local recurrence (Solin et al. 2008; Pengel et al. 2009). This is probably due to there not being a means to provide an intra(peri)-operative MRI (Morrow and Freedman 2006).

Due to limitations of implementing pre-operative techniques intra-operatively and their minimal effect on overall margin status and local recurrence, methods of peri-operative tumor

localization have been developed to improve resection of tissue. For 20 years the standard for intra-operative localization was wire-guided localization (WGL). WGL involves placing a pre-operative procedure in which a wire is placed in the tumor under the guidance of ultrasound, X-ray, or mammography. The surgeon would then use the wire's location during surgery to help extract diseased tissue. There were many problems with this procedure; firstly, the wire tended to move between procedure and surgery, the wire did not provide 3-dimensional information for the tumor (making edges of the tumor difficult to locate), and it was very uncomfortable for the patient (Pleijhuis et al. 2009; Kelly and Winslow 1996). Recent studies also demonstrate that WGL was ineffective, with 21-43% of patients diagnosed with positive margins (Thind et al. 2005; Burkholder et al. 2007; Medina-Franco et al. 2008) after surgeries implementing WGL. A newer technique is intra-operative ultrasound (IOUS) guided excision that uses ultrasound in the surgical suite to guide resection of both palpable and non-palpable tumors. Several studies have shown that positive margin rates for this technology range from 3 to 11% (Bennett, Greenslade, and Chiam 2005; Ngô et al. 2007; Rahusen et al. 2002; Moore et al. 2001), with Rahusen's study directly comparing IOUS to WGL and showing a much better sensitivity (11% positive margins for IOUS compared to 45% for WGL) (Rahusen et al. 2002). However, IOUS cannot detect the micro-calcifications that are associated with ductal carcinoma in situ (DCIS) which limits the usefulness of the technique. X-ray radiography of the excised tissue is another intra-operative technique to improve patients' margin status. However, this technique has very low sensitivity and is limited to detection of tumors without calcification (Huynh, Jarolimek, and Daye 1998). Cryoprobe-assisted localization (CAL) is another methodology that is helpful in resection of non-palpable tumors. An ultrasound helps guide a cryoprobe into the tumor, which then freezes the tumor into a detectable sphere that is easier to find and remove. Tafra et al. found that there was no significant difference between CAL and WGL in reducing the amount of positive margins or rates of re-excision; however, there was a significant reduction in excised tissue volume which improved cosmesis (Tafra et al. 2006). Even though these techniques have shown promise as an intra-operative technique for margin detection, each has its limitations and are still used as a supplement to surgery. They have also yet to replace the gold standard for peri-operative margin detection: intra-operative pathology.

Intra-operative pathology involves the use of an on-site pathological team that slices, stains, and analyzes the resected specimen while the patient is still under anesthesia. The

pathological team will stain the different edges of the tissue to give spatial orientation of the tissue so that the physician can tell the physical location of malignant tissue with regards to the edge of the resected specimen. The tissue or cells are then stained for hematoxylin and eosin (H&E) (Rusby et al. 2008). A pathologist then reads analyzes the samples and informs the surgeon where there is still microscopic disease present. The surgical team will then decide whether to proceed with a re-excision. Hematoxylin is a blue stain that stains DNA in the nucleus, and eosin is a pink dye that stains other cellular structures. There are two different methods of intra-operative pathology, frozen section analysis (FSA) and intra-operative touch prep cytology (IOPTC).

FSA involves freezing, slicing, staining, and a pathologist analyzing samples to determine the presence of malignant cells. The pathologist will work with the surgeon while the patient is under anesthesia, and the team of physicians will determine whether or not the surgeon needs to remove more tissue from the patient. This process adds an average of 30 minutes to each surgery (Riedl et al. 2009). While there is risk with holding the patient under anesthesia for an extended amount of time, the benefits outweigh the risks because this procedure decreases the chance that patients will have to undergo a second surgery (and subsequently go under more anesthesia) and increased radiation dosage. Since 1994, M.D. Anderson Cancer Center (MDACC), a leading cancer research institution, has been performing FSA during BCT. In a 2007 article published by Cabioglu et al., the authors evaluated the effectiveness of the FSA procedure at the institution and found that the overall accuracy of the procedure was 87.4% (Cabioglu et al. 2007). Studies by Camp, Riedl, and Olson showed that 24-27% of patients undergoing lumpectomy had additional tissue resected after FSA (Camp et al. 2005; Riedl et al. 2009; Olson et al. 2007) during the same surgery, however Camp and Riedl's studies did not show an overall improvement in local recurrence (Riedl et al. 2009; Camp et al. 2005). Additionally, studies have shown that FSA has high specificity but a lower and more inconsistent sensitivity rate (Cabioglu et al. 2007; Cendán, Coco, and Copeland 2005; Olson et al. 2007). Pleijhuis et al. concludes that while FSA lowers the need for a second excision, it does not reliably improve negative margin rates (Pleijhuis et al. 2009).

IOPTC has been promoted as an alternative to FSA because of its speed, simplicity, and relative low cost (Creager et al. 2002; Bakhshandeh et al. 2007). Its process involves placing a glass slide at the edge of the tissue. Surface characteristics of the cancerous cells will allow them

to stick to the slide, whereas the benign mammary cells do not. The cancerous cells are then stained with using H&E, or other cellular stains (Valdes et al. 2007; D'Halluin et al. 2009), and margin status is determined. A study by Weinberg et al. showed that IOPTC significantly lowered recurrence rates (2.8% vs. 8.8%) when compared to all other margin assessment procedures (Weinberg et al. 2004); however this study did not take differentiate between patients who received intra-operative pathology or just had permanent analysis performed post-operatively. Additionally, IOPTC is good for determining if there are malignant cells on the edge of the tissue, but does not give any indication if there are cells within the margin width, and pathologists will not be able to tell if there are close margins (Pleijhuis et al. 2009; Cabioglu et al. 2007). Additionally, there may be scarring, cell damage, and artifacts on the edge of the resected tissue as a result of the cauterization that the surgeon has to perform when the specimen is removed (Singletary 2002).

While both FSA and IOPTC are promising techniques, they still have limitations. Firstly, they require an on-site pathological team consisting of technicians and a pathologist. This is not feasible in many community hospitals due to costs and number of physicians (currently, <5% of hospitals offer this service) (Bydlon et al. 2010). There is a vast unmet need for surgeons to be able to visualize tissue peri-operatively without the use of a full pathological team. While there has been success in developing technologies and techniques that help physicians determine margin status, there is always room for improvement. We are now going to look at some future techniques that have a wide range in stages of development, from taking part in clinical trials to still being developed on the bench-top.

One device that has been developed for use in a clinical setting is the MarginProbe™ from Dune Medical Devices. The device is a spectroscope that measures the response of cells when interacting with broad range of radiofrequencies (Karni et al. 2007). The device has a detection volume of about 38.5 mm^3 that uses an algorithm to compare signal reflected from tissue to previously recorded signal from tissue. It gives the surgeon a simple readout of negative or positive using this algorithm. The sensitivity of the device over a range of margin widths averaged 67% sensitivity and a specificity of 68% (Karni et al. 2007). Another study by Allweis et al. demonstrated that the MarginProbe™ was effective at lowering rates of a second surgery (12.6% to 18.6%) that was not statistically significant. Additionally, the volume of excised tissue for the device was higher than that of the control group, which may have skewed

the results in the device's favor (Allweis et al. 2008). Even though the device is not as effective as other options, it does show that there is potential for development of an intra-operative tool for surgeons to use as a supplement to already existing technologies.

Positron Emission Tomography (PET) has been used for imaging malignant breast tissue for many years (Pons, Duch, and Fuster 2009; Schelling et al. 2000; Wahl et al. 1991), especially as noninvasive method of monitoring chemotherapeutic response (Kumar et al. 2009). PET uses a radio-labeled glucose analog ^{18}F-FDG that accumulates in areas of high metabolism, such as malignancies (Bos et al. 2002). PET has a high sensitivity value in detection of large lesions (>1 cm) (Minamimoto et al. 2007; Schelling et al. 2000; Kaida et al. 2008) but its specificity is low due to accumulation in non-malignant cells that are associated infection and inflammation (Gulec, Daghighian, and Essner 2006). In addition to the sensitivity and specificity concerns of PET, it originally was not a good candidate for intra-operative imaging because the device was large and not practical for a surgical suite. However, recent technological developments have enabled hand-held PET probes in colorectal (Strong et al. 2008), renal (Strong et al. 2008), ovarian (Cohn et al. 2008), and breast cancer (Hall et al. 2007). The handheld probes are a very nice proof of concept; however, for BCT implementation, there is still the issue that PET has trouble detecting lesions under 1 cm, and with recent screening technologies being able to detect lesions smaller than that, the handheld probe would not be very useful during BCT because it could not detect something below its resolution limit. Additionally, the use of a radio labeled tracer in the surgical suite not only has safety implications for the patient but for the entire surgical staff (Heckathorne, Dimock, and Dahlbom 2008), and repeated exposures may have long-term carcinogenic effects on surgeons.

Another radio labeled visualization technology is radio guided occult lesion localization (ROLL). This technology is described as a theranostic device that can both visualize and resect the desired tissue from the patient. ROLL is similar to WGL in that it uses a pre-operative procedure to inject a non-targeted radioisotope into the tumor. During the surgery, a handheld gamma probe locates the isotope in the tumor and guides excision. As with WGL, the placement of the isotope is paramount to maintain specificity and sensitivity. Studies have shown correct placement of the radiotracer in 95-100% of cases (Medina-Franco et al. 2008; Thind et al. 2005; Sarlos et al. 2009; De Cicco et al. 2002; Rampaul et al. 2004). This technique shows approximately the same clinical success as WGL, 20% of patients in the study by Sarlos et al.

had positive margins post-operatively (Sarlos et al. 2009) and surgeons were able to detect the lesions at a rate of 98%. Even though, ROLL achieved the same clinical results as WGL, it was found to be more comforting for the patients and an easier technique for surgeons to perform (Rampaul et al. 2004). Even though ROLL seems to be a healthy alternative to WGL, surgeons have yet to see an improvement in re-excision rates for this technique, which probably means that the limitations seen with both technologies are probably from the pre-operative placement and the imaging device used to implant the radiotracer or wire.

The next evolution of imaging breast cancer in the clinic is through the use of optical imaging with targeted contrast agents and autofluorescent signal of tissue. Currently, near-infrared fluorescence (NIRF) has shown strong development and progress as a clinically relevant breast cancer imaging modality (Pleijhuis et al. 2009); however, most clinically relevant trials have been limited to mapping sentinel lymph nodes with incodcyanine green (ICG) (Tagaya et al. 2008; Sevick-Muraca et al. 2008; Ogasawara et al. 2008; Troyan et al. 2009) and not breast malignancies (Pleijhuis et al. 2011). NIRF is considered a strong candidate for optical imaging of breast cancer because it has resolution down to 10 μm, higher penetration depth than light in the visual range, and autofluorescence of molecules in this wavelength is reduced (Troyan et al. 2009; Pleijhuis et al. 2011; Pansare et al. 2012). Even though NIRF has shown great potential in cancer studies, it still is still limited to the use of contrast agents that must be injected into the patient, and there are still many cytotoxicity issues involved with the agents inside the patient, especially at the levels needed to differentiate tissue (Pansare et al. 2012). However, NIRF contrast agents can still be used on excised tissue which would allow physicians to use the contrast agents' positive aspects while minimizing their negative impact. This possibility will be discussed in a different section.

Other imaging modalities use the endogenous signal differences between cancerous and non-cancerous tissue to attempt to differentiate tissues without contrast agents. These signal differences arise from a difference in oxygenation of blood, hemoglobin content, and cell density (Wilke et al. 2009; Tromberg et al. 2008). One of the most successful of these technologies is Diffuse Optical Imaging (DOI). DOI has been used to measure the absorption of a broad spectrum of NIR light that is directed into specimen. Due to the presence of absorbers such as deoxy-hemoglobin, hemoglobin, lipid, and water, light will propagate through a tissue in different time lengths. These lengths can be measured, and correlated to the presence of specific

absorbing molecules that characterize malignant or benign tissue (Tromberg and Cerussi 2010). This data can be combined with other imaging modalities such as mammography, and a quantitative 3-dimensional map of the breast can be created. Additionally, a study by Kurkredi et al. demonstrated tumor only spectra (650-1000 nm range) in 22 cancerous patients versus 43 normal patients (Kukreti et al. 2010). However, those studies were not used to study margin status and reconstructing an image intra-operatively would be very difficult. However, Wilke et al. developed a spectroscopic imaging device that measured β-carotene scattering coefficient in negative, close, and positive margins. The increased coefficient is due to decreased adipose tissue and higher cell density (Wilke et al. 2009). Though this study showed success, (identified 79% of positive tissues correctly), there was decreased accuracy with patients who received neoadjuvant therapy which affected physiologic and metabolic parameters that were used in their algorithm (Wilke et al. 2009); however, this device shows great potential for intra-operative margin assessment.

There are many technologies that have been developed to help physicians visualize diseased tissue intra-operatively. Whether it is through pre-operative procedures, radio-labeled tracers, or using endogenous tissue differences, there are many methods to delineate malignant tissue. As previously stated, less than 5% of BCT are completed with the use of intra-operative pathology assessment (Bydlon et al. 2010). With this in mind, the overall goal of this project has been to develop a method of differentiating malignant breast tissue that has the potential to be used in a portable, inexpensive, and rapid manner, with minimal processing performed on the tissue to maximize speed. Our aim is the construction of a system that can be used intra-operatively without the added cost and time of extra technicians or pathological staff. This system would enable the surgical team to take whole tissue at the margin area, add a targeted contrast agent, and visualize malignant tissue during surgery. Previous work has demonstrated the efficacy of using antibody targeted silica-gold nanoshells (NS) as a visual contrast agent in cells (L. Bickford, Sun, et al. 2008; L. Bickford, Chang, et al. 2008), tissue slices (L. R. Bickford et al. 2010), and even as a theragnostic (Carpin et al. 2011). These studies have demonstrated that the NS can be used in an efficient and rapid (<5 minutes) manner that can be differentiated using a variety of optical imaging techniques. However, these studies were performed on cell lines or tissues that needed to be sliced to obtain images. Tissue slicing requires an element of

time, equipment, and personnel that would add to the cost and complications of the surgical procedure.

Additionally, these studies were acquired with expensive imaging equipment, and with exception of the Bickford et al. study from 2010 that utilized a Lucid VivaScope 2500, images were acquired with modalities that do not readily translate to the clinic. There is still a vast unmet need to further research into developing methods of imaging whole tissue rapidly with a portable and inexpensive system used in conjunction with targeted contrast agents.

Our previous research has used silica-gold NS linked to the anti-HER2 antibody that attaches to HER2 on the surface of cells that over-express HER2. HER2 is an EGFR that is part of the ErbB family (Tse et al. 2009), a group of four tyrosine kinase receptors expressed on the surfaces of cells in various levels. When expressed in proper levels, the receptors have an important role in cell growth, proliferation, and differentiation; however, abnormal expression levels are apparent in malignancies of a variety of organs, not just breast, and lead to uncontrolled cell growth (Altintas et al. 2009). The other three receptors include HER3 and HER4, and the commonly known EGFR. The HER2 receptor is most commonly associated with breast cancer because it is found in 25% of all breast cancers and is thought to be a more aggressive subtype of cancer (Altintas et al. 2009; Laurinavicius et al. 2012; Vanden Bempt et al. 2008; Vranic et al. 2010) that is associated with worse clinical outcomes. Even though tumors that are HER2+ are considered to be a more dangerous subtype, the over-expression of the receptor has made its cells an easier target for targeted therapy using a monoclonal antibody against the receptor either trastuzumab (Purmonen et al. 2011; Smith et al. 2007) or lapatinib (Geyer et al. 2006; Gomez et al. 2008). This has also led to research in targeting the HER2 receptor for contrast agents, such as silica-gold NS (L. Bickford, Sun, et al. 2008; L. Bickford, Chang, et al. 2008; Carpin et al. 2011) that can help physicians visualize HER2 status in tissues and cells.

Visualization of growth factor receptors at the margin status could be more important for pathologists than previously thought. As mentioned previously, cells at the tumor margin are stained for H&E, and pathologists use these slides to determine disease extent and margin status. This helps the team of physicians determine the course of action for post-operative treatment of the patient. However, a recent study of oral squamous cell carcinoma by Vosoughhosseini et al. demonstrated that there were cells that over-expressed EGFR in the samples that were deemed to

be negative margins by normal H&E (Vosoughhosseini et al. 2012). This is very significant because patients who are declared cancer free, are, in fact, not, which is a possible explanation for local recurrence when patients are declared to have negative margins. Additionally, a false-negative leads to a different post-operative treatment regiment that could possibly allow the cancer to proliferate at a higher rate than if the proper diagnosis was made. Another growth factor, VEGF, has been studied as a possible marker of local recurrence, but there have only been three published studies, so conclusive evidence has yet to be established. Moran et al. found that in only a specific sub-group of patients with local relapse, was VEGF an independent indicator; however when performing multi-variate analysis with that same group, they were not able to reach statistical significance (Moran et al. 2011). Linderholm et al. found that VEGF status contributed to overall survival but did not mention VEGF as a predictor of local recurrence (Linderholm et al. 1999). A study by Manders et al. concluded that VEGF contributed to reducing the effectiveness of radiotherapy in patients with negative lymph node status (Manders et al. 2003). These studies show that physicians are delving deeper into receptor phenotype as indicators for all aspects of the treatment of breast cancer and that there is much to be gained from knowing these phenotypes.

Lowery et al. states that knowledge of the molecular phenotypes in breast cancer will not only help drive treatment decisions that will optimize patient care, but will offer valuable insight into prognosis (Lowery et al. 2011). There have been several recent reviews that have studied the relationship of tumor expression and results such as margin status and local recurrence (Tse et al. 2009; Wang et al. 2011; Miller et al. 2004). Ductal carcinoma in situ (DCIS) was of particular importance to these studies due to the increased incidence and smaller lesions that are a result of the improved screening technologies. Over-expression of HER2 occurs in up to 50% of lower grade DCIS; however, 50-100% of higher grade DCIS over-express the receptor (Altintas et al. 2009). Wang et al. found that patients that were ER-/PR- but HER2+ had a higher rate of recurrence than patients that were ER+/PR+ and HER2- (Wang et al. 2011).A 2004 study by Miller et al. states that in DCIS patients with HER2+ status it was much harder for surgeons to reach negative margins on patients with these characteristics than other types, including invasive carcinomas that were HER2+ (Miller et al. 2004). In 2011, Munirah et al. found that a higher percentage of HER2+ patients had positive lymph nodes (regardless of estrogen receptor status), indicating the aggressiveness of the subtype (Munirah et al. 2011); a 2006 study by Kim et al.

showed that HER2+ cancers were the most frequent subtype found in distant metastases (Kim et al. 2006).

Due to the increasing incidence of DCIS (Virnig et al. 2010; Sørum et al. 2010), the increased number of DCIS patients choosing BCT over mastectomy for DCIS (Altintas et al. 2009), the increased prevalence of HER2+ tissue in DCIS (Tamimi et al. 2008), and increased chances of local recurrence with HER2+ DCIS (de Roos et al. 2007; Provenzano et al. 2003) there needs to be a method not only for identifying cancerous tissue at the margins, but HER2+ cells at the margin during BCT for DCIS. As stated previously, Vosoughhosseini et al. demonstrated that normal H&E might not be good enough to identify all cancerous cells at the margin (Vosoughhosseini et al. 2012), and a method to identify HER2+ cells rapidly and intra-operatively gives physicians another tool to ensure negative margins are achieved during excision.

Our aim is to use these targeted contrast agents to differentiate tissue that over-expresses HER2+ tissue from HER2- tissue optically. An imaging system that combines proper optical settings with an agent with a strong signal, such as silica-gold NS, could be an invaluable tool for surgeons intra-operatively as they attempt to achieve negative margins that have been difficult to achieve in HER2+ cancers (Miller et al. 2004). As demonstrated with earlier research, our targeted nanoshells have shown great results in being able to differentiate individual HER2+ cells from noncancerous cells because an average of 1500 nanoshells were bound to each HER2+ cell (L. Bickford, Chang, et al. 2008). This is important because studies deem patients to be HER2+ when there is strong IHC staining in greater than 10 (Kim et al. 2006; Tamimi et al. 2008) – 20% (X. R. Yang et al. 2007) of the cells being examined. During an intra-operative procedure where cells will be visually detected, such a small percentage of cells might be difficult to detect optically using fluorescent markers. This is where the strong optical scattering properties of silica-gold NS offers vast potential for use as an intra-operative contrast agent. Proper excitation light that is tuned to the optical resonance of the NS can be used in conjunction with proper emission and imaging settings to detect the NS, which, in turn, leads to proper detection of HER2+ cells and tissue.

Work described in the paper included in the appendix (currently under review) has demonstrated the ability of the silica-gold NS to differentiate whole tissue sections that were HER2+ from HER2- sections. Additionally, we believed that the localization of the nanoshells

was confined to the surface of each tissue section using two-photon microscopy. In the section that follows, we take these findings further and use hyperspectral darkfield imaging to confirm the localization of the NS to the surface of the tissues. Additionally, we use the hyperspectral imaging to demonstrate the spectral changes of HER2+ tissue with nanoshells versus tissue without nanoshells to demonstrate the areas of nanoshell localization.

Materials and Methods

Silica-gold Nanoshell Fabrication and Antibody Conjugation

Silica-cores were synthesized as described in previous literature (Loo et al. 2004; Loo, Hirsch, et al. 2005; Loo, Lowery, et al. 2005). Briefly, silica cores were fabricated following the Stöber method (Stober, Fink, and Bohn 1968) whose surfaces were then terminated using amine groups. Dynamic light scattering (DLS) determined that the average diameter of the cores was 276 nm. Gold colloid (1-3 nm diameter) was then functionalized to the surface of the silica cores using the amine groups (Duff, Baiker, and Edwards 1993). Once the gold surface was formed, UV-VIS spectrophotometry (Varian Carry 300) (Fig. 1) was used to determine the final diameter and concentration of the particles in solution.

To determine concentration and size of the particles, the experimental absorption, scattering, extinction coefficients were calculated using Mie theory. The experimental theory was then compared to the spectra obtained with the spectrophotometer and final size was determined to be 305 nm peak plasmon resonance of 796 nm. The final concentration of particles was approximately was $1.25*10^9$ particles/ml.

To target the NS against cells that over-express the HER2 receptor, an antibody against HER2 was conjugated to the surface of the nanoshells using previously described methods (Loo et al. 2004). An anti-HER2 antibody was conjugated to the surface via a heterobifunctionalized polyethylene glycol orthopyridyl-disulfide-PEG-N-hyroxysuccinimide ester (OPSS-PEG-NHS) (L. Bickford, Chang, et al. 2008). 450 µl of NS in solution was incubated with 0.6 µl of anti-HER2-PEG solution for 2 hours at 4°C. Then, 2.0 µl of 1.0 mM PEG-SH was added to the solution overnight (12-16 hours) at 4°C to coat the rest of the surface of the NS with PEG to make the particle more biocompatible. Excess PEG-SH was then removed from solution by centrifugation, and the solution was resuspended in a 37°C antibody diluent buffer to a final solution of 165 µl. The nanoshells were now ready for incubation with resected tissue specimens.

Ex vivo breast specimens

Cancerous (HER2+ and HER2-) and normal breast tissue were acquired from the cooperative human tissue network (CHTN) under a institutional review board (IRB) approved protocol. Tumors were classified by both tumor type and recepotor phenotype by a physician at the medical institution that provided the tissue prior to arrival in the laboratory. The tissues arrived pre-frozen in liquid nitrogen and were stored in a -80 upon arrival. They stayed in storage until sampling.

Tissues were thawed in phosphate buffered saline (PBS) at 37°C and then placed on a biopsy board where a 5 mm punch biopsy was taken to maintain consistency between samples. The biopsies were then stained with pathology ink to maintain orientation. The tissues were then incubated with the nanoshell/diluent cocktail for 5 minutes at 37°C under rotation. Samples were then rinsed in PBS 3X and placed in clean PBS prior to imaging.

After incubation, tissues were rapidly frozen in OCT media and prepared for slicing using a cryotome. 8 μm tissue slices were cut at -20°C and placed on slides to dry overnight. A coverslip was then placed on each tissue and the slides were placed under a Cytoviva™ darkfield microscope. A darkfield image of each tissue was then acquired using a Qimaging Exi blue CCD. After this image was acquired, a hyperspectral image of the same field of view (FOV) was acquired using the Cytoviva™ hyperspectral imaging camera. This image not only gave spatial information, but also provided spectral data for each pixel in the FOV. Spectral data of slices on and below the surface of normal tissue and HER2- and HER2+ cancerous tissue was acquired. The spectra of the illumination lamp was calibrated for each image by dividing each spectral data point by the normalized data point for the lamp spectra. The fields of view were then compared between multiple specimens (n=3 for each tissue type).

Results

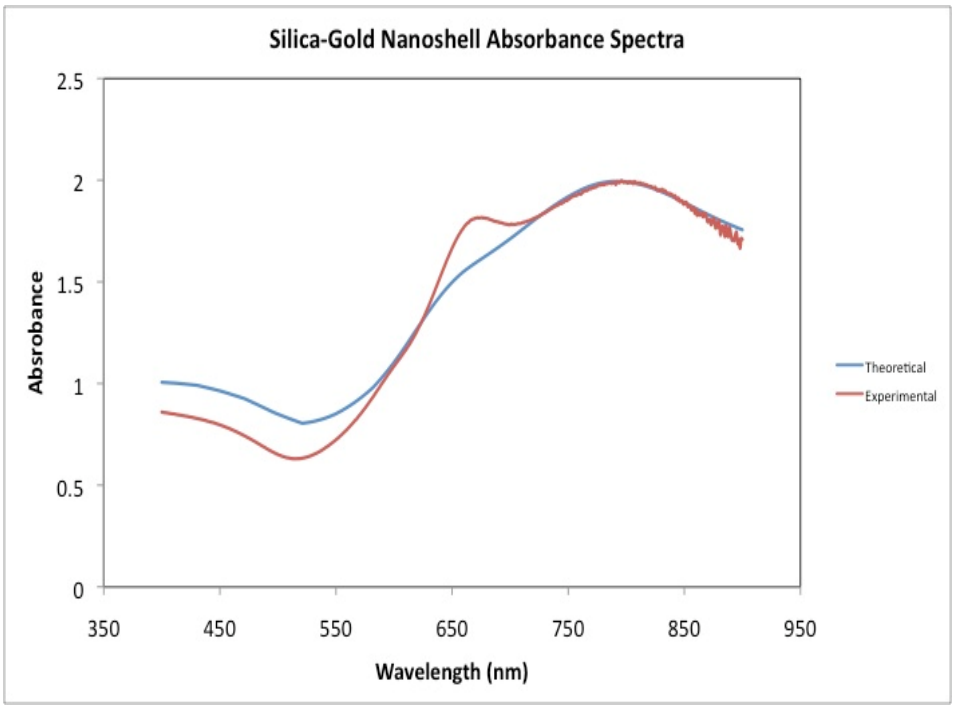

Figure 1. UV-VIS absorbance spectra of silica-gold NS with 276 nm silica-core diameter and a total diameter of 306 nm (red). The theoretical spectra as calculated by Mie Theory is displayed for comparison. Concentration of the particles in solution was calculated to be $1.25*10^9$ particles/ml.

Figure 1 displays the experimental (red) and theoretical (blue) UV-VIS absorbtion spectrum of silica-gold NS with a total diameter of 306 nm and a silica core diameter of 276 nm. Additionally, graphs display the plasmon resonance of the NS to be 796 nm. This is important for future experiments where we are designing an imaging system that will have optimized imaging settings for viewing silica-gold NS in excised tissue.

Figure 2 displays darkfield images of normal, HER2-, and HER2+ cancerous tissue taken with the Cytoviva hyperspectral imaging system taken on the same day and incubated with the same batch of nanoshell/antibody cocktail for 5 minutes at 37°C. 2(A) is the surface of normal mammary tissue after incubation, rinsing, and slicing in the cryotome. 2(B) displays the surface of HER2- malignant tissue (the blue ink is the pathological ink used for spatial orientation). 2(C) and 2(D) are from the same 5 mm punch biopsy of HER2+ tissue, but 2(C) represents the surface of the tissue and 2(D) represents a slice of tissue from approximately 24 μm below the surface of the same tissue. All of the tissues appear to be very different visually, but it is very difficult to visualize nanoshells on any of the tissues without the help of spectral data.

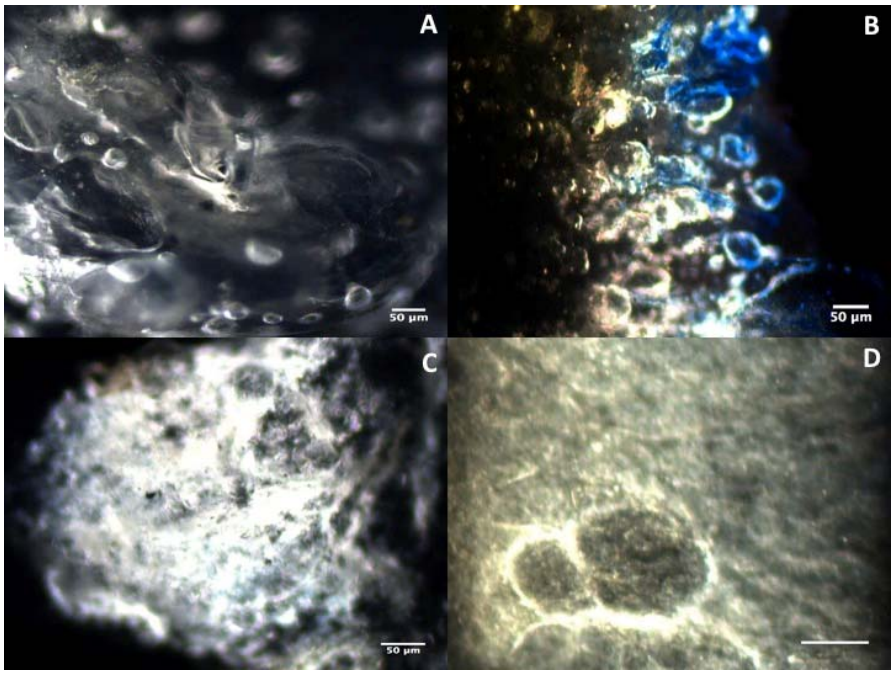

Figure 2. Darkfield images of (A) the surface of normal mammary tissue, (B) the surface of HER2- malignant tissue, (C) the surface of HER2+ tissue, and (D) 24 µm below the surface of the same tissue in 2(C). Scale bar in D represents 50 µm.

In previously submitted data, we had reported a localization of the nanoshells to the surface of the tissues. In Figure 3, the spectra of each of the FOV displayed in figure 2 are displayed. What is interesting is that the surface of the normal tissue and HER2- tissue seem to be more similar to the surface of the HER2+ than the HER2+ tissue below

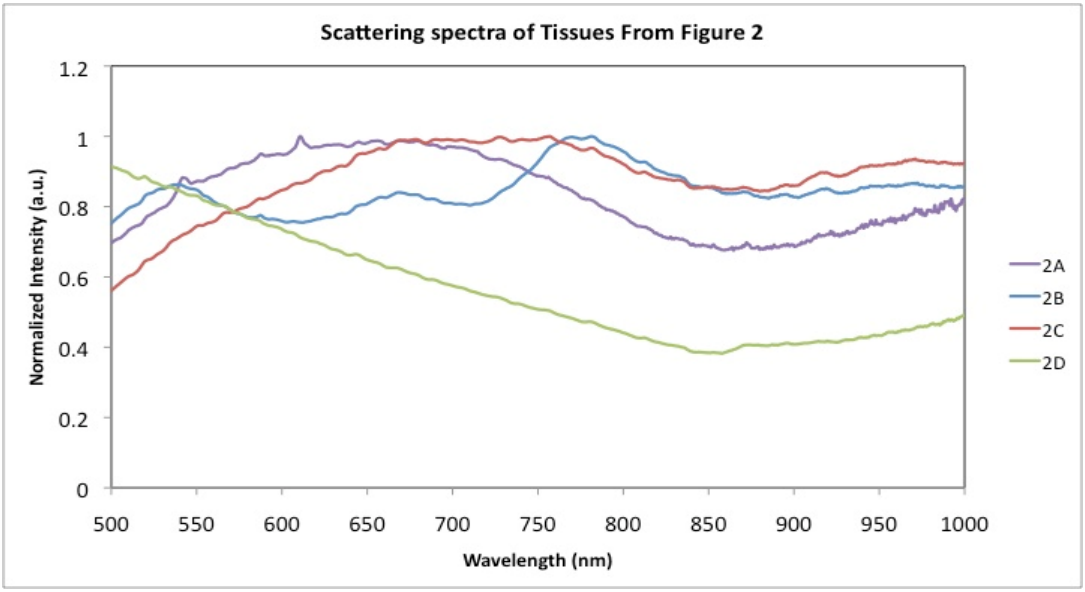

Figure 3. Scattering spectra of various tissue surfaces incubated with nanoshells that are displayed in Figure 2. 2D represents the spectra of HER2+ tissue 24 μm below the surface of the tissue displayed in 2C. The similar spectra of the surfaces of the tissue could be due to non-specific binding to the surface of the tissues that was seen in other imaging modalities.

the surface. Perhaps this is due to some non-specific binding of the nanoshells to the surface during the incubation period. Our previous data submitted (and currently in submission to a special issue "Molecular Imaging of Breast Cancer" in Journal of Oncology) showed that there were some instances of non-specific binding to the surface of these tissues after incubation, so this is not unexpected. However, there is a stark difference in scattering spectra of the surface of the HER2+ and the tissue below the surface (2C&D). Figure 4 is a side-by-side spectral comparison of the HER2+ tissue displayed in figure 2; additionally, spectra from HER2+ tissue without any nanoshells added is displayed as a negative control to show the similarity in spectra between tissue without nanoshells and the area below the surface of HER2+ tissue incubated with anti-HER2 silica-gold nanoshells. This demonstrates the localization of the NS to the surface of the tissue.

Figure 5 displays the spectra of the surface of three different HER2+ tissues after incubation with anti-HER2 NS and the negative control tissue spectra. Two of the specimens had very different spectra from the negative control, and surface 2 had a very similar spectra to the spectra of the negative control. One reason for this could be that there is low amount of nanoshell binding to the HER2 receptor. There were individual areas of nanoshells that were

localized in the hyperspectral image, but perhaps these areas were too small to make a significant contribution to the overall signal of the FOV.

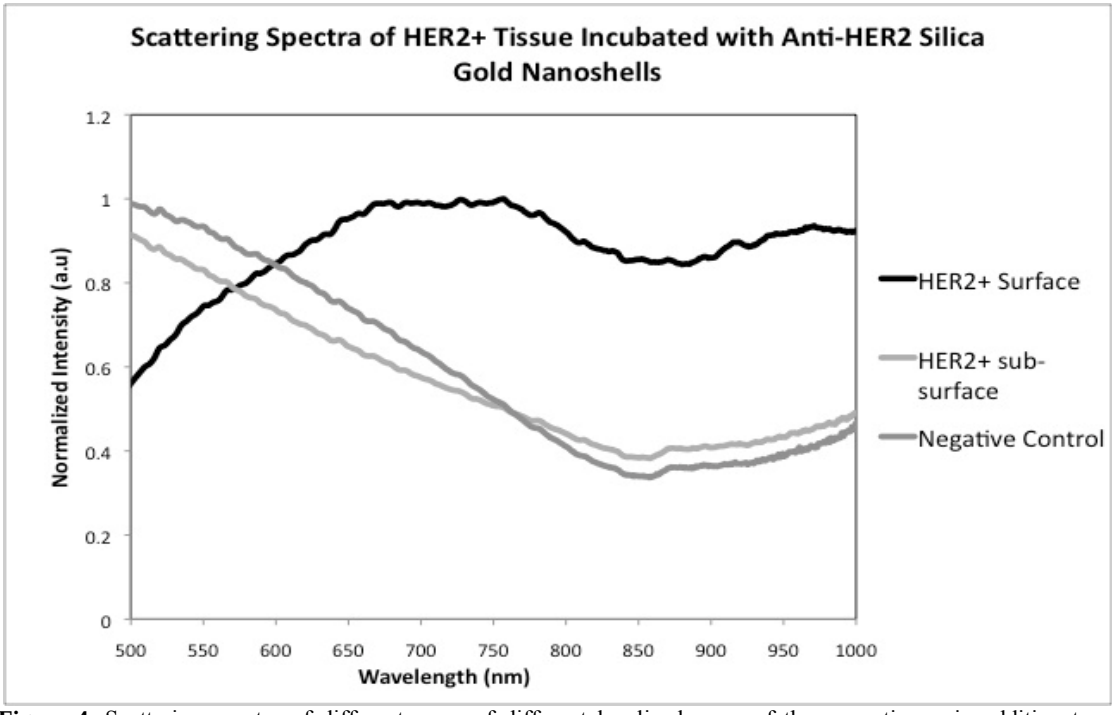

Figure 4. Scattering spectra of different areas of different localized areas of the same tissue, in addition to a negative control tissue that was not incubated with silica-gold nanoshells. The surface of the HER2+ tissue shows a much different spectra than that of the tissue 24 um below the surface of the tissue.

Figure 6 displays the FOV of the slide from surface 2. 6(A) demonstrates individual areas of the tissue that were sampled and showed a different spectra than that of the overall tissue (6(B)). However, the signal from these isolated areas were not enough to create a large difference in the overall spectra of the tissue. It is interesting to note that individual areas of silica-gold NS can be pictured, but due to the limited number of binding sites, they have a very small contribution to the overall signal.

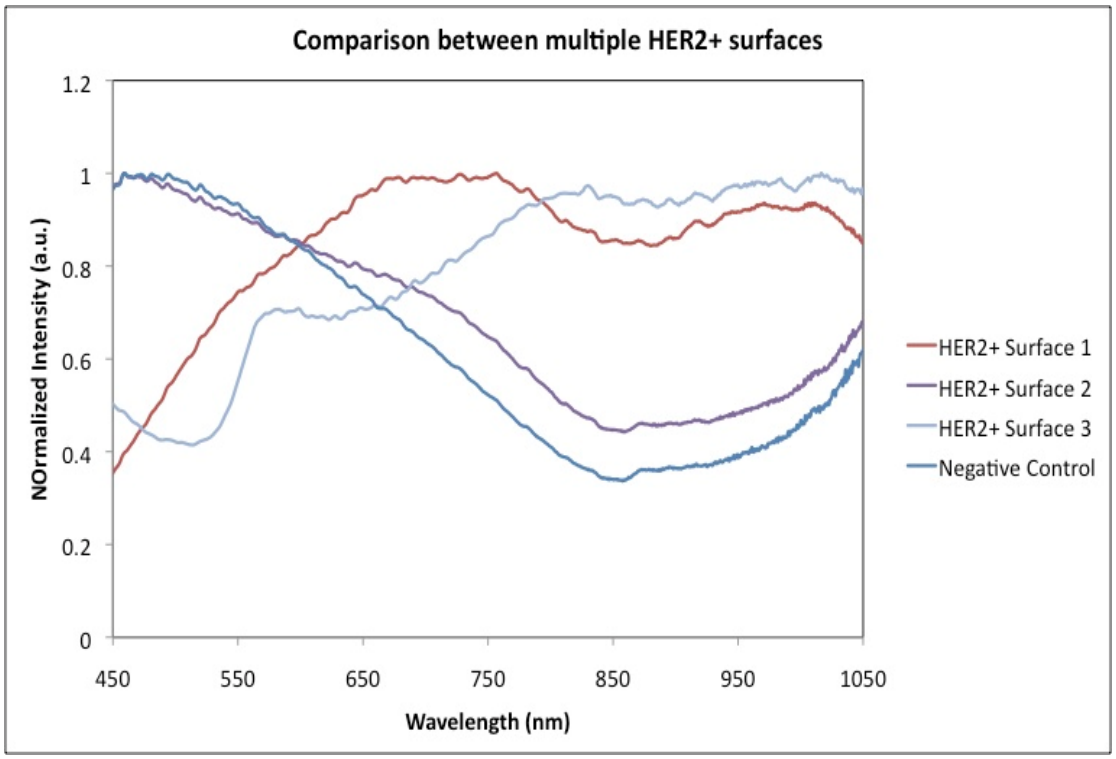

Figure 5. Scattering spectra of different HER2+ tissue surfaces that have been incubated with anti-HER2 nanoshells. Two of the three surfaces were very different from the negative control, where as surface 2 was very similar to tissue without NS.

Discussion

The data presented here verifies previous conclusions that anti-HER2 silica-gold nanoshells were limited to the surface of excised tissue. This is important information for physicians to be aware of because it allows them to understand the information that can be obtained using this technology. Additionally, for development of our intra-operative imaging device, we need to be able to confirm that signal from tissues is either from nanoshells, thus making knowledge of the localization of the nanoshells paramount.

Even though this technology has great potential for future clinical use, there are still some pitfalls that need to be addressed. First, there is always going to be intrinsic signal from the tissue that is going to contribute the signal collected. There are ways to control for this. For this experiment we used signal from tissue that had not been incubated with nanoshells for use as a comparison between tissues. This is not the most ideal method, but for this experimental set-up it was necessary. Future whole tissue experiments will attempt to use the same tissue as its own

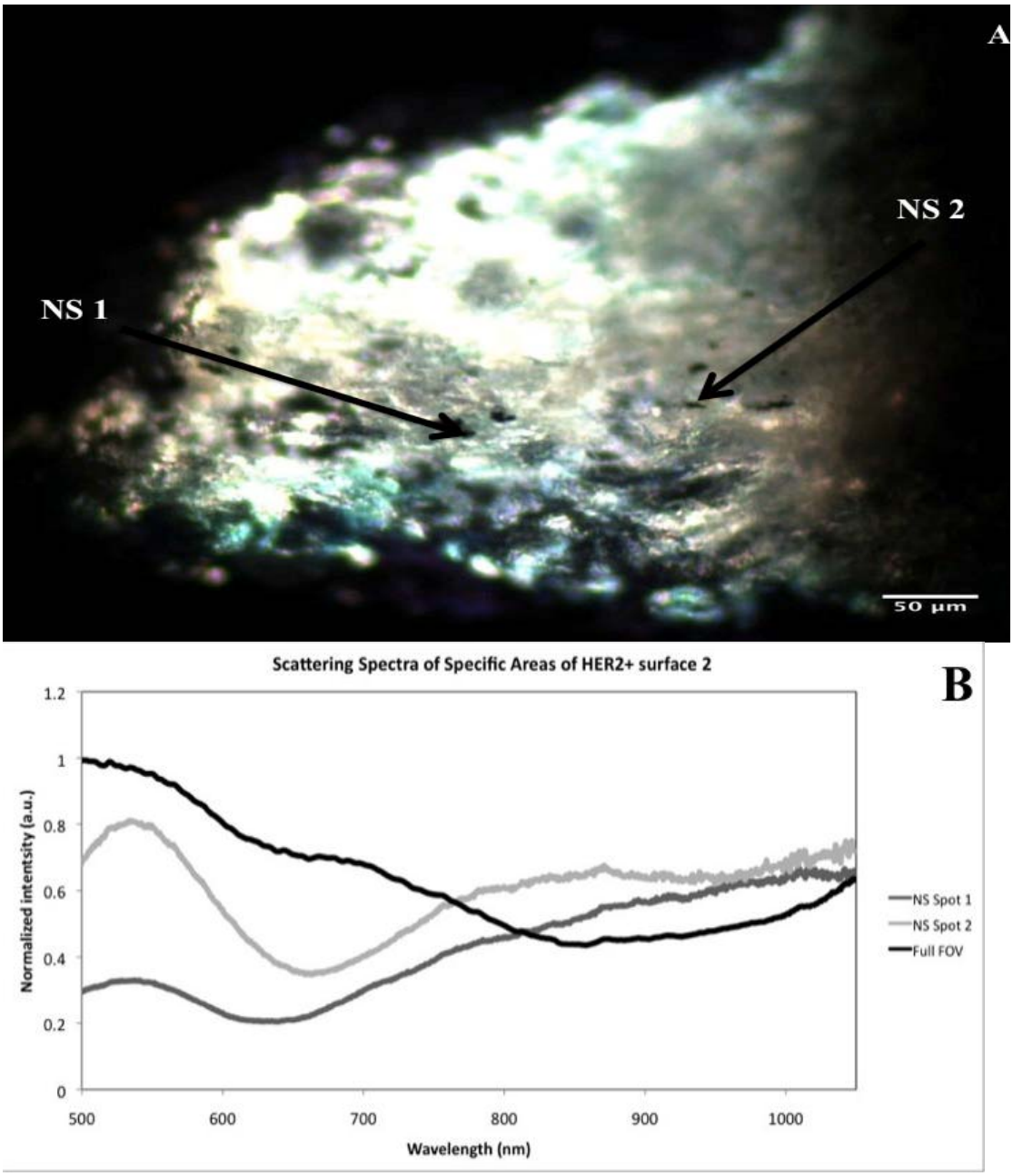

Figure 6. Darkfield image of HER2+ surface with areas of silica-gold NS pointed out with arrows. Spectral data of the individual NS spots shows different spectral data than the full FOV, showing local areas of NS. However, there was not sufficient binding of nanoshells to contribute to the signal of the full tissue changing.

control, so pre and post incubation data can be acquired from the same tissue and nanoshell effect can be measured with greater certainty.

Another result that is of some concern is from figure 5, which showed the spectra of "HER2+ surface 2" having a very similar spectra to that of the negative control. As stated

earlier, for a breast cancer to be deemed HER2+, only 10-20% of its cells need to have a 2+/3+ score from a pathologist (Kim et al. 2006; Tamimi et al. 2008; X. R. Yang et al. 2007). This means that the tissue sampled for imaging had a low percentage of HER2+ cells that were bound with NS, meaning that there were less NS to contribute to the overall signal of the FOV. Figure 6 displays the tissue in question and the areas of localized nanoshells that had a different spectral shape than the overall FOV. However, there does not seem to be enough contribution from the NS to the overall signal of the tissue to change its spectral shape. This is important too for margin status because it would be ideal for physicians to visualize where the individual HER2+ cells are and further elucidate the areas of high concern that a surgeon might be able to focus on during the re-excision procedure. Additionally, this shows that there is great difference in tissues' expression of HER2 in just one field of view, which means that areas that scan large volumes, (i.e., the MarginProbe™) might be obtaining inaccurate results due to the subtle tissue changes in a small area. This is a prime example of the heterogeneity of malignancies that all intra-operative margin technologies have to worry about and is one of the downsides of using receptor expression as a target for diagnostic imaging.

Conclusion

There are many elements that contribute to the discovery, treatment, and complete removal of breast cancer. The heterogeneity of the disease makes a difficult task even more treacherous. From tumor site to protein expression, each type of cancer has presents challenges to the team of physician trying to eradicate the disease. Our focus is on the development of a system that will help surgeons performing breast conserving therapy to remove as much diseased tissue as possible to decrease the chances of a patient having a recurrence of the disease. In this section, we used the over-expression of HER2+ cancerous cells in resected specimens to target an antibody targeted contrast agent that has strong optical properties in the NIR. We were able to confirm the location of these nanoshells to the surface of the tissues which gives valuable information as we move to the next section of our research development: the fabrication of a portable, intra-operative device that can visualize these targeted particles.

Part 2: Design and development of a portable, inexpensive macroscopic breast tissue imaging system (Project 2)

Introduction

There has been recent development in the field of optical imaging to develop low cost, portable imaging systems that use endogenous fluorescence of cancerous tissues as a screening tool for easy to reach areas such as the mouth, esophagus, and colon (Pierce et al. 2010; Pierce et al. 2011; Nadhi Thekkek, Anandasabapathy, and Richards-Kortum 2011; Roblyer et al. 2009). Additionally, the use of contrast agents to differentiate breast cancer and lymph nodes has also been recently published for both *in vivo* and *ex vivo* tissue specimens (Langsner et al. 2011; Rosbach et al. 2010; H. Lee et al. 2011; Mieog et al. 2011; Aoyama et al. 2011; Sano et al. 2012); however, only the studies by Rosbach and Mieog used a system that was portable and could be readily translated to a clinical setting. However, both of these studies were performed on lymph nodes of the breast. Our goal in this section is to develop an inexpensive and portable imaging system that is optimized for multi-marker imaging. As discussed previously, breast cancers can express certain hormone or tyrosine kinase receptors (ER/PR or HER2) that have been used as targets for monoclonal antibodies as therapeutics. We aim to build a system that can image both estrogen and HER2 in resected specimens that over-express these receptors using targeted anti-HER2 gold silica NS that have shown great efficacy in differentiating HER2+ tissue slices (L. R. Bickford et al. 2010) and in whole tissue specimens using a stereoscope (submitted to J of Oncology). This optical imaging system will be built with off-the-shelf imaging components to minimize cost; additionally, the system will be assembled so that the components all will fit into a standard backpack for ease of transport. In this section, we will show preliminary results of tissue incubated with nanoshells (both targeted and non-specific) that have been acquired with the first design prototype revision and discuss future studies and methods to improve the device so that it can be ready to use in the clinic.

System Design

Our goal is to fabricate a system that can image multiple markers on excised tissue so that tissues that over-express these markers can be differentiated from tissue that does not express these surface markers. Because of our past experience targeting HER2 over-expression in multiple tissues with silica-gold NS, we decided to optimize our system to visualize the NS signal in the tissue. The other marker we chose to visualize is the estrogen receptor (ER). We choose to image this receptor because, like HER2, its expression leads to treatment with a monoclonal antibody, Tamoxifen. Additionally, as discussed earlier, HER2+ that express ER have a different clinical prognosis than ER- tumors. The ability to image two markers at once

might also have significant impact on issues with false-negatives because physicians will be searching for two specific markers, and not just one. If there are low expression levels of one marker, physicians might still be able to identify malignant tissue using the other marker.

In addition to targeting the anti-HER2 antibody with silica-gold NS that can be imaged in the IR, estrogen needs to be tagged with a fluorescent marker to visualize binding in the tissue, in this case we are planning to use fluorescein (FITC), which can be excited with light in the blue spectra (460-500) and be imaged in the green (500-560). The device needs to be able to acquire both visible and NIR light to display the contrast agents. Additionally, excitation light must be filtered so that there is no bleed through into the emission filter, skewing the image. Finally, the tissues must receive 360° illumination so that not only one side of the tissue receives illumination light and signal is only collected from one area of the tissue.

We have built a prototype that accounts for all of these design parameters. Firstly, a Canon 450D digital SLR camera with its internal IR filter removed was purchased for $1,095. Two sets of LEDs (light emitting diodes) that were centered on 780 nm and 488 nm wavelength light, respectively, were purchased for $4.40 each. Short pass (800 and 500 nm) excitation filters for each set of excitation LEDs at a price of $73 each. A lens to attach to the camera was purchased for $215.00. Finally, an emission filter was attached to the end of the lens that transmits green light (500-560 nm) and any light above 825 nm. The LEDs and filters were arranged around an imaging station (design in figure 7a), and the LEDs were placed in a circuit with proper resistances and an on-off switch. The camera with emission filter and lens was then placed above the imaging acquisition and images are acquired.

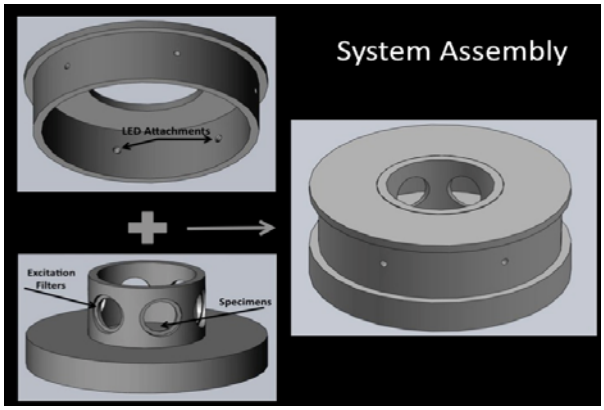

Figure 7. Two-piece assembly of imaging system to image multiple cell markers in resected specimens. The camera is attached to the top and images are acquired.

Materials and Methods

Anti-HER2 silica-gold nanoshells and tissues were prepared in the same method as stated in section 1. Pre-incubation images were taken of both tissues that were incubated with NS and the negative control. The tissues were then incubated with nanoshells for 5 minutes at 37°C and then rinsed 3X in PBS and stored in clean PBS until post-incubation images were acquired (<10 minutes after completion of incubation). All images were acquired with the same settings on the camera. The image acquisition settings include: an f-number of 5.6, exposure time 6 seconds, and a gain setting of 800. Images of tissues were collected side-by-side for comparison and individually. Additionally, different types of tissue that were incubated with NS were compared to determine if there was a higher signal from HER2+ than HER2- tissue.

Results

Figure 8 shows pre(A) and post(B) incubation images of HER2+ tissue from the same patient. 8(C) shows the average pixel intensity of the tissues and shows the difference between the tissues. 8(B) shows that the tissue incubated with nanoshells is much brighter than the negative control. However, the quantitative data is quite interesting in that the tissue incubated with nanoshells kept the same intensity while the negative control lost intensity. This could be due to the camera's internal dynamic range normalizing the signal it is acquiring, or it could be due to a change in the intensity of the signal coming from the LEDs. For future experiments, a optical power meter will be placed in the same location of the imaging system to ensure that the signal being seen by the tissues is consistent.

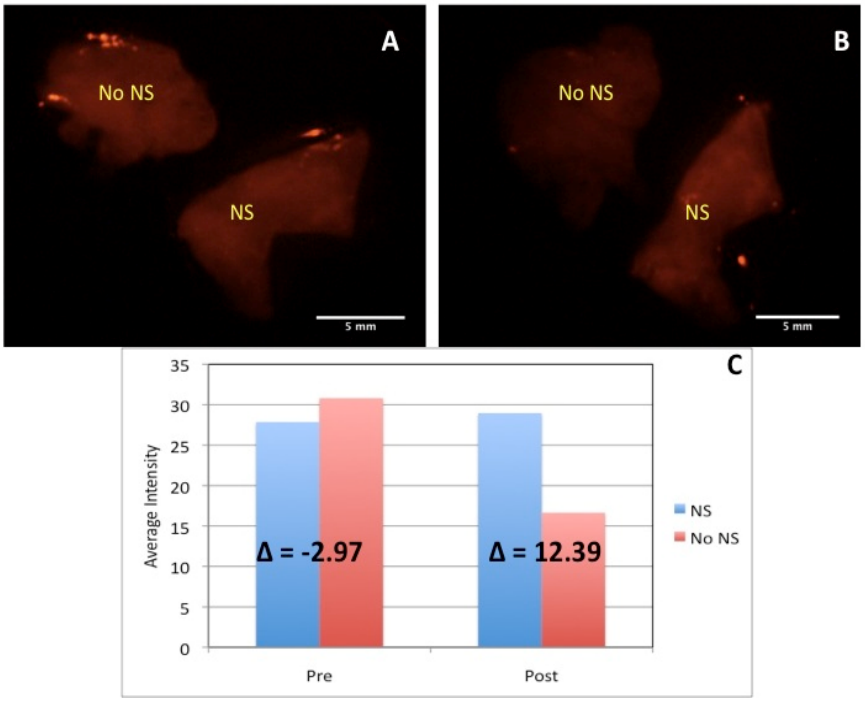

Figure 8. Pre (A) and Post (B) incubation images of HER2+ tissue that has been incubated with anti-HER2 silica-gold Nanoshells in addition to a negative control. 8(C) shows the pixel intensity of the tissues for both pre and post images and the differences between the two. The NS seem to increase the signal difference in the tissues, but not the actual signal of the tissue itself.

Figure 9 shows HER2- cancerous tissue from the same day with pre (A) and post (B) images of tissue incubated with nanoshells and its own control. Even though the tissue incubated with NS has a much brighter signal than the negative control, 9(C) shows that the signal difference was inherent in the tissues before the addition of nanoshells and that there was not much change due to incubation with nanoshells, which we hypothesize, implies that there was little to no nanoshell binding on the tissue that was incubated with nanoshells. Figure 10 shows the post incubation images of HER2+ tissue compared to normal (A) and HER2- tissue (B). While the normal tissue had a much lower signal than the HER2+ tissue, the HER2- was much higher than the HER2+ (Fig. 9(C)).

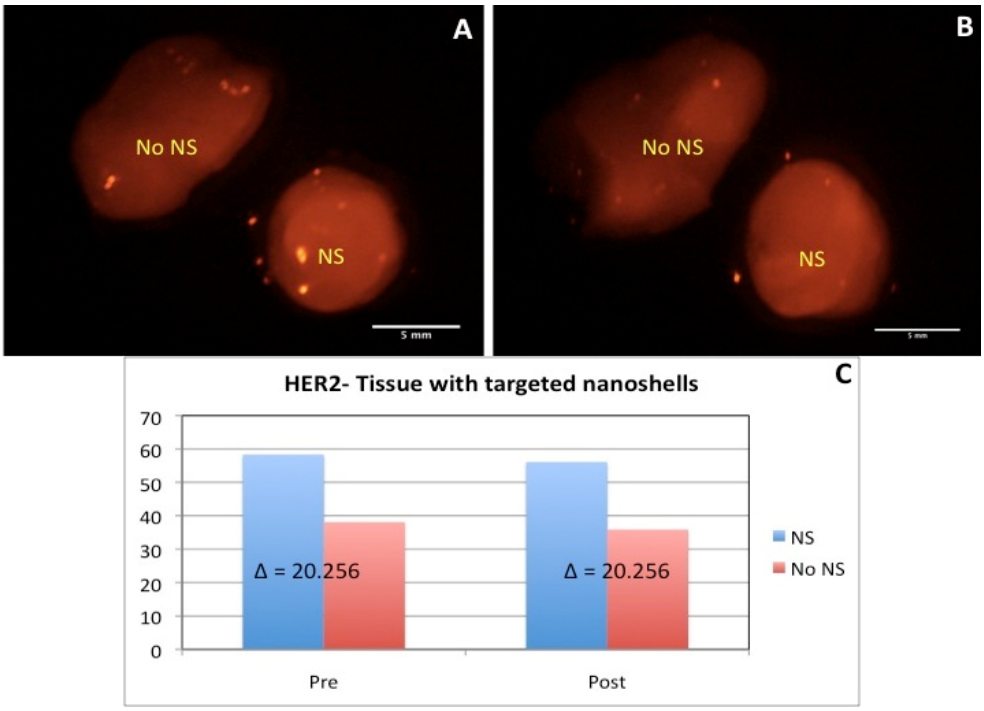

Figure 9. Pre (A) and Post (B) incubation images of HER2- tissue incubated with anti-HER2 silica gold NS. No signal difference between the tissues implies that there was no binding of anti-HER2 nanoshells to the tissue and that the signal difference is due to inherent tissue signal.

Figure 11 shows the results of a further experiment that acquired images of the tissues taken individually to ensure that the second tissue was not interfering with the excitation light coming from the excitation sources. It shows the difference in signal from nanoshells in tissues that were acquired individually so that there was no contributing signal from a separate tissue that might have affected the signal collected. This is interesting because it goes against the hypothesis that the nanoshells will enhance the NIR signal from the tissue, but the HER2+ tissue does have the smallest change in signal, which might mean that the nanoshells have an effect. However, this signal decrease might also be due to a change in signal from the excitation source, and further experiments will need to be completed to investigate what is happening.

These are promising results that show that incubation with anti-HER2 nanoshells seems to have a qualitative effect on the signal seen from the tissue. There are still many settings and optical set-ups that need to be considered before large amounts of quantitative data can be acquired. Additionally, a control for signal intensity needs to be acquired to confirm that the excitation light is staying within a consistent range during image acquisition.

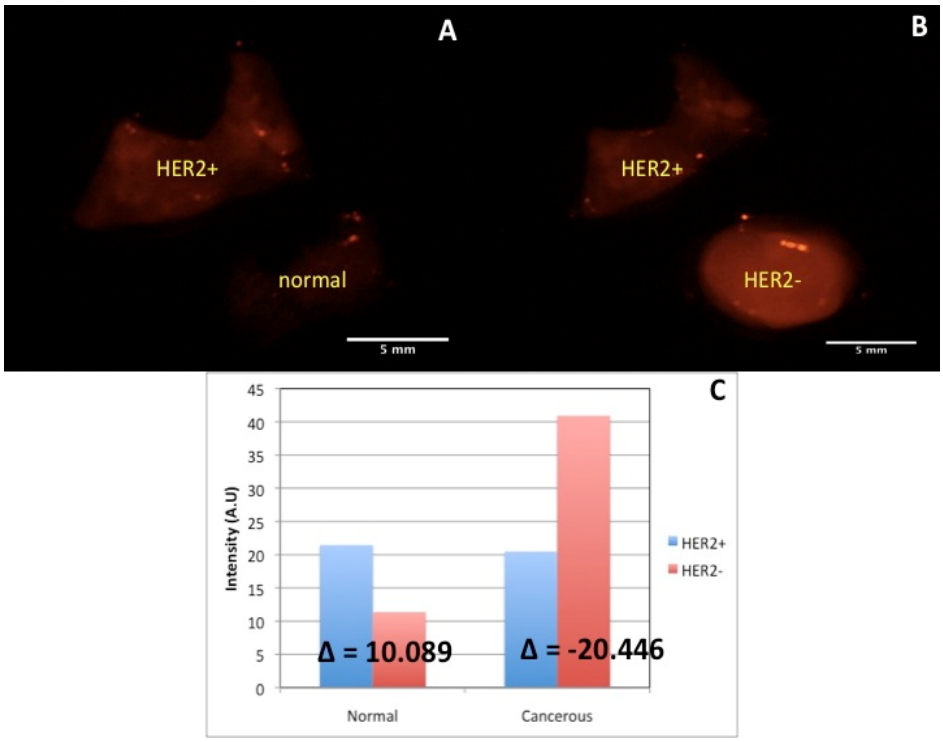

Figure 10. Post incubation images comparing HER2+ tissue to normal (A) and HER2- cancerous (B) tissue. The HER2- tissue was much brighter than the HER2+ tissue, but data from Fig. 9 shows that their was inherent signal tissue. Unfortunately, there was not pre incubation comparison images acquired to compare the signals of the tissue.

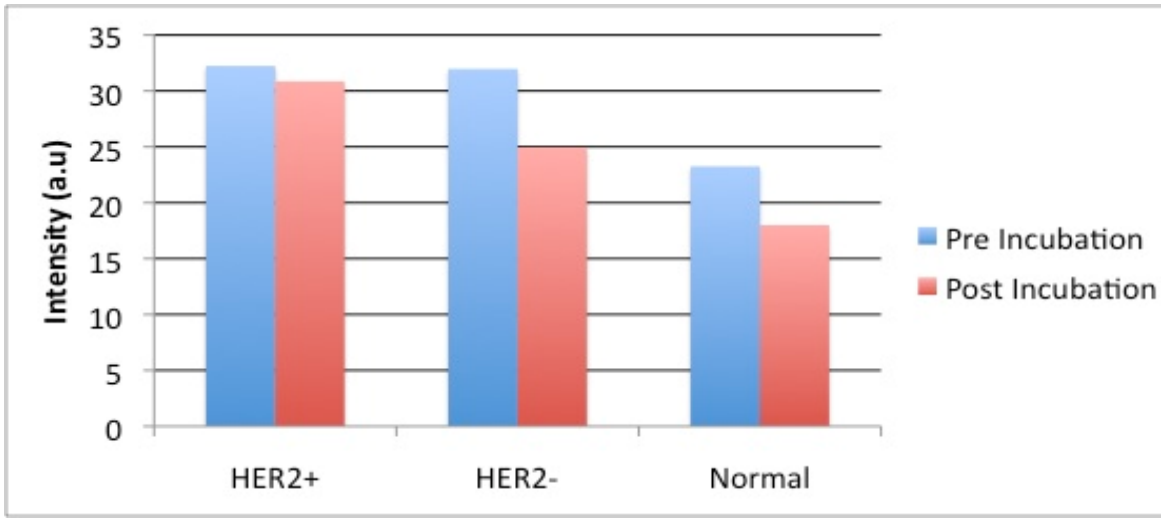

Figure 11. Signal intensities of individual tissues before and after incubation with silica-gold nanoshells. HER2+ tissue had the lowest signal drop of the three tissues.

Discussion

So far there have been promising results in using a portable, inexpensive imaging system in conjunction with anti-HER2 silica-gold nanoshells to differentiate HER2+ tissue from normal tissue. Most promising was the data presented in Figure 8. Good qualitative data showed little difference in tissue from the same patient before incubation with nanoshells, which was backed up with quantitative data confirming the difference after incubation with nanoshells. However, we are hesitant to add any specific value to any quantitative data for each of the graphs displayed currently because there seems to be inconsistencies between pre and post images, where the negative controls seem to have lost signal between incubations. Some possible explanations for this include the excitation light losing intensity between images, the camera performing some automated change in the signal being collected we have not yet been able to identify, or perhaps the presence of two tissues interfering with the excitation light that interacts with tissue. There are still many settings to optimize that will provide a more definite answer in the coming year.

Future experiments will include taking multiple images with the tissues at various angles inside the imaging system. Additionally, in order for good quantitative data to be obtained, signal interacting with the tissue from the excitation light has to be measured with every experiment to properly maintain a control. Finally, future experiments might include slicing the tissue and acquiring images using a reflectance confocal microscope or darkfield hyperspectral imaging to confirm binding of nanoshells to the tissue.

Additionally, future experiments include optimizing imaging settings for estrogen receptor labeled with FITC. When optimal settings have been acquired for both markers, then both contrast agents will be applied to the same tissues to demonstrate our ability to show multiple markers in a rapid, inexpensive, and portable system. This system will not only have the capability to improve margin status in breast cancer surgeries, but it can be applied to other organ systems and molecular markers as well such as the additional agents being developed as part of Project 3.

Part 3: Glucose conjugated gold nanoparticles as a new imaging agent and additional theranostic agents to be assessed

As described in the Year 4 report, based on suggestions received at the LINKS meetings about ouy heavy reliance on HER2 and estrogen receptor status, we have expanded the range of molecular markers being considered through this project. Here, we report on not yet published data using glucose targeted gold nanoparticles. As described in the prior section, we have not ended the work using established markers but rather continue to expand beyond those.

Introduction

Chemical agents have been conjugated to glucose with the purpose of targeting those agents to tissue that over-express glucose transporters (GLUTs), such as cancer (Macheda, Rogers, and Best 2005). These agents are then imaged and can be used to help differentiate cancerous tissue from non-cancerous tissue. These agents include ^{18}F-fluorodeoxyglucose (^{18}FDG), a radioactive labeled agent that emits positrons and is used to monitor chemotherapeutic response and stage breast cancer (Kumar et al. 2009; Lim et al. 2007). Additionally, a fluorescent deoxy-glucose, 2-[N-(7-nitrobenz-2-oxa-1,c-diazol-4-yl)amino]-2-deoxy-d-glucose (2-NBDG), accumulates in the cytoplasm of cells because after entering the cells through the GLUTs, it undergoes the first step of glycolysis but no further processing. The optical properties of 2-NBDG allow it to be detected fluorescently (excitation maximum 475, emission maximum 550 nm) (Yoshioka et al. 1996). Studies have demonstrated the ability of 2-NBDG to differentiate cancerous tissue from non-cancerous tissue in as little as 20 minutes for oral, esophageal, and breast cancer (Nitin et al. 2009; N Thekkek et al. 2011; Langsner et al. 2011). Glucose has already been shown as a new targeting agent to enhance contrast for malignant tissue We aim to take these findings further by targeting small (~2 nm diameter) gold nanoparticles (AuNPs) by capping them with glucose and using the GLUTs to deliver nanoparticles to the cells, rather than the traditional method of endocytosis.

A 2008 study by Kong et al. demonstrated that AuNPs (~10 nm diameter) capped with thioglucose could be used to enhance radiation cytotoxicity because the thioglucose allowed the AuNPs to enter the cytoplasm of the cell, rather than staying on the cell surface such as other cysteamine-capped AuNPs did (Kong et al. 2008). The authors supposed that the capping with glucose enhanced the entrance of the nanoparticles; however, if the glucose were to help with targeting of the AuNPs, then the particles would have entered the cells via the GLUTs. The GLUTs are very small (36 X 26 Å on the extracellular side, 46 X 27 Å on the cytosolic side)

(Salas-Burgos et al. 2004) and having a 10 nm diameter AuNP go through the transporter seems to be very difficult. Additionally, the authors did not present any endocytosis inhibition or glucose inhibition studies to show that the glucose targeting was the reason for the enhanced amount of AuNPS inside the cell. Finally, the authors incubated the cells for 2 hours, which is a significant amount of time for particles to enter the cell via receptor mediated endocytosis (Connor et al. 2005; Mironava et al. 2010). Previous studies have shown that 2-NBDG offers enhanced contrast in as short of a time as 10 minutes (O'Neil, Wu, and Mullani 2005) and that adding D-glucose (which enters cells through GLUT1) to cells with 2-NBDG decreases the amount of 2-NBDG entering the cell, demonstrating 2-NBDG's mechanism of entry (O'Neil, Wu, and Mullani 2005; Nitin et al. 2009).

The aim of this study is to demonstrate that 2 nm AuNPs can be capped with thioglucose and targeted to enter the cells via the GLUTs over-expressed in the cancerous cell line Sk-Br-3. We aim to show the mechanism of entry of 2 nm particles capped with thioglucose by doing both a D-glucose competitive inhibition assay and inhibiting endocytosis. Additionally, a final assay will be performed using varying sizes of AuNPs to demonstrate the size specificity of targeting AuNPs with thioglucose. Original research done with cells was done with colloid made in lab. However, transmission electron microscope (TEM) images showed that the size of the colloid was on average 2 nm, the same size of commercially available AuNPs from Ted Pella, Inc. To standardize between experiments, all future experiments will be done using Ted Pella particles. This will allow us to know the concentration of particles for all experiments.

Materials and Methods

Gold colloid was synthesized by spinning 45 mls of distilled H_2O in a glass beaker at 800 RPM. 1 ml of 1 N KOH was then added; 1 minute later, 12 ul of THPC (Tetrakis(hydroxymethyl)phosphonium chloride) was added; 2 mls of 1% $HAuCl_4$ (gold salt was added) for 2 minutes to form the colloid solution. 10 mls of colloid solution was then combined with 10 mls of 10 mM thioglucose and spun at 800 RPM for 15 minutes. The solution was then rinsed using a centrifugal dialysis filter (10,000 Dalton cutoff) spun 3X for 20 minutes at 2500 g. The final solution was then resuspended to a total of 10 ml and kept at 4°C. TEM images of the particles were acquired using a JEOL 2010 TEM; figure 12 (A) depicts a zoomed out view of the nanoparticles and 12(B) features a zoomed in version. Colloid from Ted Pella Inc ($1.25X\ 10^{14}$ particles/ml) was combined and filtered in the same manner as the "home-made" colloid.

However, TEM images were acquired with a JEMF-2100 Field Emission Gun Transmission Electron Microscope that is equipped with Energy Dispersive Spectroscopty (EDS) that uses electron energies to confirm the presence of certain atoms. EDS is a powerful tool because it can confirm the thiol binding of thioglucose to the surface of the nanoparticle. Figure 13 depicts the TEM images and subsequent EDS data.

The first experiment to demonstrate that thioglucose can be used to target AuNPs involved comparing different cappings of particles and showing that thioglucose preferentially entered the cells. 175,000 cells of the cancerous cell line Sk-Br-3 were plated onto two-well chamber slides for 48 hours at 37°C. Three different cappings (thioglucose, citrate, and no cap) and one negative control were added with fresh media to the cells for 20 minutes at 37°C. The cells were then rinsed with PBS, and imaged on a Cytoviva™ darkfield microscope. Figure 14 demonstrates images of the different cells from this experiment.

The next experiment involved the use of D-glucose as a competitive inhibitor with glucose AuNPs. For this experiment, the same number of cells were plated in the same type of well plates for the previous experiment. This time, there were two controls: cells only and cells with D-glucose added; then, glucose AuNPs were added to cells with and without D-glucose. Figure 15 depicts images from this experiment.

Results

Figure 12(A) depicts a zoomed out view of gold colloid with thioglucose conjugated on the outer core of the particle. 12(B) is a high zoom image depicting an area of AuNPs. As one can tell from the images, the solution of colloid seems to be very monodisperse; there does not seem to be any aggregates of particles in the solution. However, the particles are of an approximate size of 2 nm in diameter. This is no better than the size of particle that can be commercially bought and is fabricated with a more consistent process. Additionally, there is a known stock concentration of particles that are commercially available that allows us to control volume and number of particles added to cells at a more consistent rate than with the lab made colloid. Therefore, a switch was made to the particles visible in Figure 13. As well, figure 13 shows spectroscopic data that displayed the amount of an atom that was present in the area of interest. For this sample we compared the amount of sulfur to gold present on the inside and the outside (lighter) part of the particle. The inside (spot 1) had almost four times as

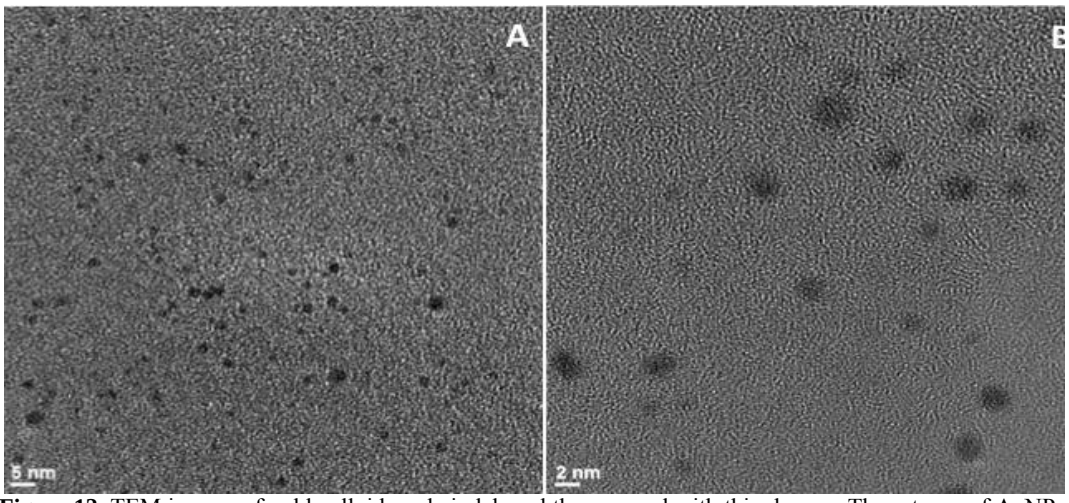

Figure 12. TEM images of gold colloid made in lab and then capped with thioglucose. These types of AuNPs were then added to the cells that are seen in Figs. 14&15

much gold present as sulfur and the outside, where the thioglucose was bound had almost 3 times as much sulfur. TEM-EDS is very powerful tool that we will be able to use to visualize and confirm thioglucose (or any molecule) binding to the surface of the particle. This technology will be used in future studies when TEM images of cells with nanoparticles are obtained.

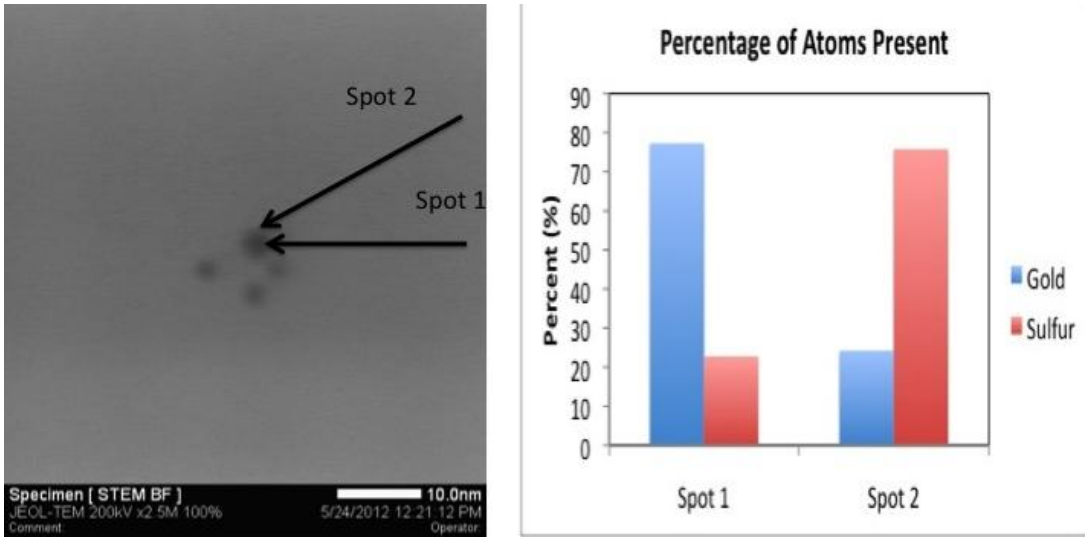

Figure 13. Gold colloid purchased from Ted Pella, Inc and then capped with thioglucose. EDS data acquired from spots delineated in the image demonstrate the concentration of sulfur and gold atoms with respect to each other at their respective locations of depicted in by the arrows. Spot 2 represents the area where the thioglucose has bound to the surface of the particle, whereas spot 1 represents the center of the particle.

Figure 14 displays darkfield images of Sk-BR-3 cells that were treated in four different manners (A) cells only, (B) bare AuNPs, (C) citrate capped AuNPs, and (D) thioglucose capped AuNPs. From the images, there are very obvious differences between each of the cells. What is quite interesting is that there seems to be a lot of signal from inside the cells that were treated

with the thioglucose-AuNPs. We hypothesize that this is due to the increased amount of AuNPs that were able to cross the GLUT and settle into the cytoplasm. Even though we do not see individual particles due to the limitations of microscopy, the increased signal might be due to the accumulation of a high number of particles in the cells. Additionally, it appears as if there is a dark circle in each cell that represents the nucleus. The cells treated with the other types of AuNPs seem to have increased signal on the edges of the cells which may be due to electrostatic or non-specific binding of the cells to the membrane. However, none of these can be concluded until controlled TEM images of the cells are acquired, a task currently underway.

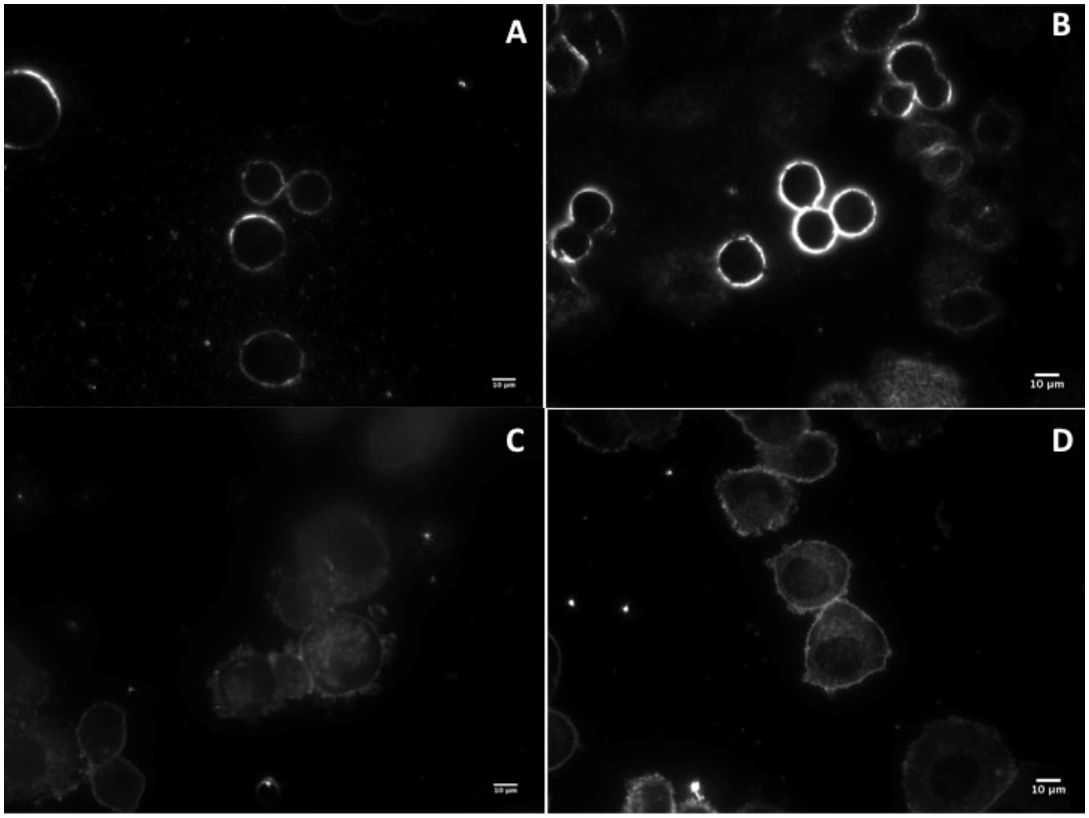

Figure 14. Darkfield images of Sk-Br-3 cells only (A), incubated with uncapped AuNPs (B), citrate AuNPs (C), and thioglucose capped AuNPs (D). 14(D) shows high signal inside the cell that is thought to be from gold AuNP accumulation. However, further tests are needed to verify this conclusion.

Once it was established that thioglucose-capped AuNPs interacted with the cancerous cell line Sk-Br-3 differently than other capped AuNPs, we hypothesized that the AuNPs were entering the cells via the GLUTs and not via endocytosis. Our first experiment to determine this was using a competitive inhibition assay using D-glucose. Figure 15 displays the darkfield images that were results of this experiment. Fig. 15(A) is the negative control of no cells, 15(B) displays cells incubated with 40 µM D-glucose only, (C) displays the cells after incubation with

both D-glucose and AuNPs(D) displays the cells after incubation with AuNPs only. Once again, there is good qualitative data displaying the high scatter signal from the cells that were incubated with AuNPs only, but very little signal from inside the cells where there was competitive inhibition. However, as with previous results, this cannot be confirmed until higher resolution images with TEM are acquired.

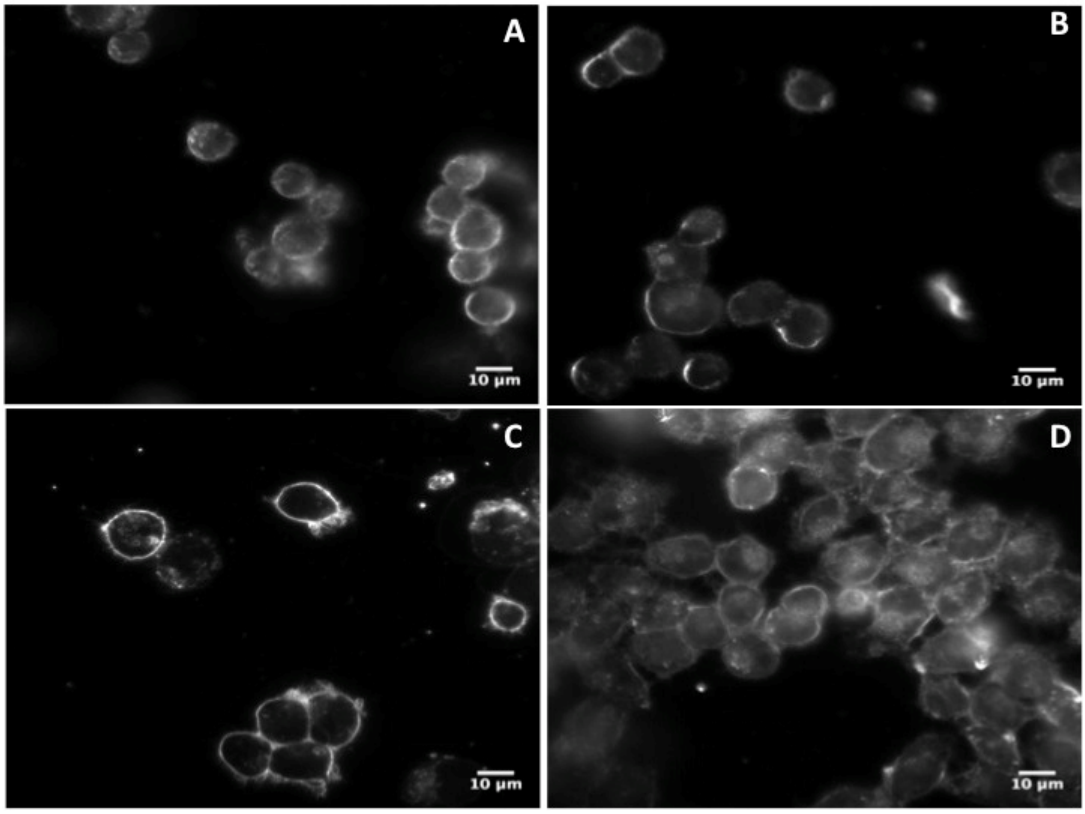

Figure 15. Sk-Br-3 breast cancer cells after incubation with (A) media only, (B) D-glucose, (C) D-glucose and thioglucose capped AuNPs, and (D) thioglucose capped AuNPs only. High scatter signal can be seen from the cells in (D) leading to the conclusion that there is gold colloid inside the cell membrane.

Discussion

Preliminary tests and results that show glucose capped AuNPs can enter cells in a twenty minute time frame are very promising. There is good qualitative data that shows enhanced signal from inside the cytoplasm of cells that have incubated with these particles and there is very little signal from cells that were incubated with something different. Additionally, there is strong scatter signal on the cell membrane of some of the samples that have been incubated with non glucose AuNPs which could mean that the particles are being localized to the cell membrane but have yet to enter the cell. This could be because of the time it takes to form endosomes to engulf

these other AuNPs or it could be due to electrostatic interactions between the membranes and the particles.

There are many more experiments that need to be run before any solid conclusions can be reached. First, there needs to be confirmation from TEM showing the AuNPs localized to the cell cytoplasm. Additionally, further experiments need to be completed to confirm the mechanism of entry for the particles. Inhibiting both clathrin dependent and independent endocytosis and then incubating the cells with the thioglucose AuNPs would show a different mechanism of entry of the particles into the cells. Second, the use of cells with RFP labeled endosomal DNA could also be used to show where endosomes have been forming inside the cell. If there are no endosomes formed, yet there is still high scatter signal coming from inside the cell, then that would be a secondary confirmation of entry into the cell via other mechanisms. Third, showing that larger AuNPs do not enter the cells as rapidly as the smaller AuNPs would also show that there is some size restriction for the NPs to enter the cells in a time frame of 20 minutes which would also imply that the AuNPs were entering via a non-endocytotic pathway.

Summary and Future Work

We have made significant progress on three aspects of using nanotechnology enabled contrast agents to improve diagnostic imaging in breast cancer. First, we used hyperspectral imaging to demonstrate localization of anti-HER2 silica gold NS to the surface of excised tissue. Second, we furthered our research in the development of a portable diagnostic imaging system that can be readily translated to clinical use for diagnostic imaging of tissues with multiple markers by tuning an optical set-up that is optimized to visualize certain contrast agents. Finally, we provided an important proof of concept that thioglucose can be used to target small (~2 nm diameter) gold nanoparticles in a rapid (<20 minute) manner. We hope to further develop this contrast agent and understand its mechanism of entry into cancerous cells, and further develop its use to enhance contrast in excised breast tissue.

In addition to the nanoparticles described in our reporting to date, over the past few years we have also developed a number of newer gold-based materials through other awards with significant potential as theranostic agents for breast cancer applications. In the final year of the DoD award, we plan to continue to develop these materials and assess both imaging and therapeutic potential for breast cancer applications. We have dedicated a portion of the remaining personnel funding to the supply category to enable this and purchased needed supplies

for this work prior to the original award end date in case of delays in processing the no cost extension request for the coming year. Specific materials to be included are dendrimer decorated gold nanoparticles, gold nanoparticles decorated with peptides or oligonucleotides (each offering potential delivery/therapeutic functionalities in addition to imaging), and gold nanoparticles also carrying a drug (paclitaxol). Finally, we have very recently discovered a potential method for generating a luminescent nanoparticle which would overcome the limitations of the cadmium-free luminescent nanocrystals (quantum dots) we had worked with in the early years of the award but abandoned largely on safety concerns. If we are able to validate our initial experiments, this will prove an additional material which we will test with the macroscopic imaging system we have already created. Throughout our DoD award we have focused most heavily on gold based nanomaterials. These materials can be imaged through scattering, absorption, and is some cases, two photon luminescence. Additionally, facile conjugation to biomolecules is enabled through the gold surface. It is this unique combination of optical and chemical properties which render these materials so powerful. Toxicity of these materials will continue to be assessed with an added emphasis on potential immune system impacts. By the conclusion of our award, we seek to have conclusively demonstrated the potential for targeted imaging and treatment of breast cancer, moving beyond the combined imaging/photothermal applications considered in the award early years to more sophisticated materials in which imaging potential is coupled with delivery of oligonucleotides, peptides, and chemotherapeutic agents, broadening the range of applications of these materials beyond the breast tumor margin area we have focused on to date.

One final small area of investigation is using the gold nanoparticles already developed for imaging applications for detection via a compressive sensing strategy using a random probes concept, which we are investigating together with collaborators at Rice. This concept removes the individual probe for each target restriction typically associated with array based analysis. Although very much at a proof of concept stage now, in the future such an approach could potentially be used to provide a more cost-effective approach to targeted large scale genetic screening valuable in applications such as determining more optimal chemotherapeutic regimens for breast cancer treatment. This effort was initiated based on the panel discussion at the 2011 LINKS meeting noting the difficulties in identifying optimal, and at times even reasonable, patient populations for drug studies and the need for new technologies to address this challenge.

KEY RESEARCH ACCOMPLISHMENTS

- During Year 5, we have continued to benefit from receiving protocol approval for the use of human tissue from the NCI Cooperative Human Tissue Network. Building on our prior published work using tissue slices, we were able to continue a shift to more translational work through working with whole tissue imaging, mimicking the conditions we would expect to encounter in the future in the surgical suite setting. A paper on our most recent work in now under review at *Journal of Oncology*.

- We have completed verification using a hyperspectral imaging approach that targeted nanoparticle binding was the origin of increased contrast in HER2+ tissue.

- Over the past year, we have completed construction of the final hand held instrument for intraoperative tumor margin delineation. This is the final macroscopic imaging system we have developed via Project 2 of this award. The device is fully functioning. During the next year, we will complete imaging studies using this system.

- We have continued to make progress on enhancing the range of molecular markers being addressed using gold nanoparticle technology in Project 3. We presented development of the glucose nanoparticles for metabolic imaging in Year 4. In Year 5, we progressed to cellular level studies described in the prior section. During the upcoming year we plan to conduct TEM studies to verify we understand our imaging data and write a manuscript on this work.

- A provisional patent was submitted on a new gold nanoparticle synthesis strategy. A paper describing the strategy was published and is included in the appendix. The method allows synthesis of gold nanoparticles over a broad range of sizes in a rapid and inexpensive fashion facilitating many of the theranostic applications now under development.

REPORTABLE OUTCOMES

Peer Reviewed Publications

Lissett R. Bickford*, Robert J. Langsner*, Joseph Chang, Laura C. Kennedy, Germaine D. Agollah, Rebekah A. Drezek. "Rapid stereomicroscopic imaging of HER overexpression in *ex vivo* breast tissue using topically applied silica-based gold nanoshells." J of Oncology. In review (2012).

Young, J. K., Figueroa, E. R., & Drezek, R. A. (2012). Tunable nanostructures as photothermal theranostic agents. *Annals of biomedical engineering*, *40*(2), 438-59. doi:10.1007/s10439-011-0472-5 (2012).

Joseph K Young, Nastassja A Lewinski, Robert J Langsner, Laura C Kennedy, Arthi Satyanarayan, Vengadesan Nammalvar, Adam Y Lin and Rebekah A Drezek. "Size-controlled synthesis of monodispersed gold nanoparticles via carbon monoxide gas reduction" Nanoscale Research Letters (2011). 6:428. doi:10.1186/1556-276X-6-428

Book Chapter

Bickford, L., Carpin, L, Sun, J., Lin, A., Loo, C., Yu, T., and Drezek, R. "Chapter 95: Non-invasive Optical and Functional Imaging of Breast Tissue" Book chapter in *Advanced Therapy of Breast Disease.* BC Decker (2012). *(This chapter is for a revised edition of this book. While it is not research based so not directly supported by DoD CDMRP, as part of our Era of Hope project we have been participating in writing opportunities that provide clinicians focused on breast cancer background on the potential of emerging optical technologies.)*

Abstracts

Drezek, R. Optical Molecular Imaging of Breast Cancer Using Nanoengineered Agents. Era of Hope Meeting. Florida. August 2011.

Joseph K. Young and Rebekah Drezek. "Synthesis and Characterization of Au2S/Au Core/Shell Nanostructures" 2011 Joint Annual Conference of NSBP and NSHP (2011).

Provisional Patent Application

Size Controlled Synthesis of Gold Nanoparticles Using Carbon Monoxide Based Reduction. 61/500,376. June 23, 2011 (Joseph Young)

Jobs

Lissett Bickford, whose PhD research as a graduate student was funded by this award, has accepted a faculty position at Virginia Tech beginning July 2012

Awards

Joseph Young, a portion of whose PhD research as a graduate student was funded by this award. was 1 of 20 United States graduate students selected by National Nanotechnology Initiative to attend global nanotechnology winter school in Brazil, Joseph Young (Winter 2012)**;** Joseph Young received the OSA/SPIE award for best presentation in photonics (2011); Joseph Young received the American Physical Society, Condensed Matter Division, 1st place poster (2011)

CONCLUSIONS

Our research team has focused the majority of its Era of Hope research efforts specifically in areas of breast cancer care where the combination of ***miniaturized optical devices*** and ***molecular-specific imaging agents*** offer the potential to address current gaps in care. There are two primary areas where I believe our technologies can make the biggest difference: ***early detection*** and ***integrated delivery and monitoring of therapy.*** Optical spectroscopy, implemented through small fiber optics, can provide clinically valuable information ranging from cellular metabolic status (via endogenous fluorescence) to nuclear size (correlated to optical scatter) to quantitative measurements of molecular markers (through targeted imaging agents under development in our lab). Most of our effort has focused on development of needle-compatible spectroscopic and direct imaging probes for breast cancer applications. The technology is being designed for clinical applications for which it is valuable to have a local high resolution imaging method to complement a more macroscopic imaging modality (for example, during ultrasound guided breast biopsy). Progressive design and evaluation of the needle-based technologies has been the focus of **Project 1** of our DOD project. In Year 3, we added in a new project, **Project 2**, to allow us to further develop a multi-modal, widefield optical imaging device. To complement our imaging technology development projects, the second primary effort underway is development of molecular-specific optical imaging probes (**Projects 3**). Much of the work underway in **Project 3** has been directly applicable to tumor margins assessment, and we have presented our results in this area in our series of annual reports.

REFERENCES

Al-Ghazal, S K, L Fallowfield, and R W Blamey. 2000. "Comparison of psychological aspects and patient satisfaction following breast conserving surgery, simple mastectomy and breast reconstruction." *European journal of cancer (Oxford, England : 1990)* 36 (15) (October): 1938-43. http://www.ncbi.nlm.nih.gov/pubmed/11000574.

Ali, A N, N Vapiwala, M Guo, W T Hwang, E E Harris, and L J Solin. 2011. "The impact of re-excision and residual disease on local recurrence after breast conservation treatment for patients with early stage breast cancer." *Clin Breast Cancer* 11 (6): 400-405. doi:S1526-8209(11)00160-1 [pii] 10.1016/j.clbc.2011.08.003. http://www.ncbi.nlm.nih.gov/entrez/query.fcgi?cmd=Retrieve&db=PubMed&dopt=Citation&list_uids=21993010.

Allweis, Tanir M, Zvi Kaufman, Shlomo Lelcuk, Itzhak Pappo, Tami Karni, Shlomo Schneebaum, Rona Spector, et al. 2008. "A prospective, randomized, controlled, multicenter study of a real-time, intraoperative probe for positive margin detection in breast-conserving surgery." *American journal of surgery* 196 (4) (October): 483-9. doi:10.1016/j.amjsurg.2008.06.024. http://www.ncbi.nlm.nih.gov/pubmed/18809049.

Altintas, Sevilay, Kathleen Lambein, Manon T Huizing, Geert Braems, Fernando Tjin Asjoe, Hilde Hellemans, Eric Van Marck, et al. 2009. "Prognostic significance of oncogenic markers in ductal carcinoma in situ of the breast: a clinicopathologic study." *The breast journal* 15 (2): 120-32. doi:10.1111/j.1524-4741.2009.00686.x. http://www.ncbi.nlm.nih.gov/pubmed/19292797.

Aoyama, Kei, Takako Kamio, Tetsuya Ohchi, Masako Nishizawa, and Shingo Kameoka. 2011. "Sentinel lymph node biopsy for breast cancer patients using fluorescence navigation with indocyanine green." *World journal of surgical oncology* 9 (January): 157. doi:10.1186/1477-7819-9-157. http://www.pubmedcentral.nih.gov/articlerender.fcgi?artid=3269998&tool=pmcentrez&rendertype=abstract.

Arthur, Douglas W, Kathryn Winter, Robert R Kuske, John Bolton, Rachel Rabinovitch, Julia White, William F Hanson, Raymond M Wilenzick, and Beryl McCormick. 2008. "A Phase II trial of brachytherapy alone after lumpectomy for select breast cancer: tumor control and survival outcomes of RTOG 95-17." *International journal of radiation oncology, biology, physics* 72 (2) (October 1): 467-73. doi:10.1016/j.ijrobp.2007.12.056. http://www.pubmedcentral.nih.gov/articlerender.fcgi?artid=2604132&tool=pmcentrez&rendertype=abstract.

Atkins, Jordan, Fatema Al Mushawah, Catherine M Appleton, Amy E Cyr, William E Gillanders, Rebecca L Aft, Timothy J Eberlein, Feng Gao, and Julie A Margenthaler. 2012. "Positive margin rates following breast-conserving surgery for stage I-III breast cancer: Palpable versus nonpalpable tumors." *The Journal of surgical research* (April 10). doi:10.1016/j.jss.2012.03.045. http://www.ncbi.nlm.nih.gov/pubmed/22516344.

Audisio, Riccardo A, and Leena S Chagla. 2007. "Oncoplastic fellowship: can we do better?" *Breast (Edinburgh, Scotland)* 16 (1) (February): 11-2. doi:10.1016/j.breast.2006.07.001. http://www.ncbi.nlm.nih.gov/pubmed/16987663.

Avril, N, C a Rosé, M Schelling, J Dose, W Kuhn, S Bense, W Weber, S Ziegler, H Graeff, and M Schwaiger. 2000. "Breast imaging with positron emission tomography and fluorine-18 fluorodeoxyglucose: use and limitations." *Journal of clinical oncology : official journal of the American Society of Clinical Oncology* 18 (20) (October): 3495-502. http://www.ncbi.nlm.nih.gov/pubmed/11032590.

Avril, Norbert, Manuela Menzel, Marcus Schelling, Wolfgang Weber, Fritz Ja, Walter Nathrath, and Markus Schwaiger. 2001. "Glucose Metabolism of Breast Cancer Assessed by 18 F-FDG PET : Histologic and Immunohistochemical Tissue Analysis." *Journal of Nuclear Medicine*: 9-16.

Aziz, Dalal, Ellen Rawlinson, Steven A Narod, Ping Sun, H Lavina A Lickley, David R McCready, and Claire M B Holloway. 2006. "The role of reexcision for positive margins in optimizing local disease control after breast-conserving surgery for cancer." *The breast journal* 12 (4): 331-7. doi:10.1111/j.1075-122X.2006.00271.x. http://www.ncbi.nlm.nih.gov/pubmed/16848842.

Bakhshandeh, Maryam, S Osman Tutuncuoglu, Gabor Fischer, and Shahla Masood. 2007. "Use of imprint cytology for assessment of surgical margins in lumpectomy specimens of breast cancer patients." *Diagnostic cytopathology* 35 (10) (October): 656-9. doi:10.1002/dc.20704. http://www.ncbi.nlm.nih.gov/pubmed/17854083.

Baselga, José, José M Trigo, Jean Bourhis, Jacques Tortochaux, Hernán Cortés-Funes, Ricardo Hitt, Pere Gascón, Nadia Amellal, Andreas Harstrick, and André Eckardt. 2005. "Phase II multicenter study of the antiepidermal growth factor receptor monoclonal antibody cetuximab in combination with platinum-based chemotherapy in patients with platinum-refractory metastatic and/or recurrent squamous cell carcinoma of the head and n."

Journal of clinical oncology : official journal of the American Society of Clinical Oncology 23 (24) (August 20): 5568-77. doi:10.1200/JCO.2005.07.119. http://www.ncbi.nlm.nih.gov/pubmed/16009950.

Beadle, Beth M, Wendy A Woodward, Susan L Tucker, Elesyia D Outlaw, Pamela K Allen, Julia L Oh, Eric A Strom, et al. 2009. "Ten-year recurrence rates in young women with breast cancer by locoregional treatment approach." *International journal of radiation oncology, biology, physics* 73 (3) (March 1): 734-44. doi:10.1016/j.ijrobp.2008.04.078. http://www.pubmedcentral.nih.gov/articlerender.fcgi?artid=3041273&tool=pmcentrez&rendertype=abstract.

Bennett, I C, J Greenslade, and H Chiam. 2005. "Intraoperative ultrasound-guided excision of nonpalpable breast lesions." *World journal of surgery* 29 (3) (March): 369-74. doi:10.1007/s00268-004-7554-6. http://www.ncbi.nlm.nih.gov/pubmed/15706446.

Bickford, L, J Chang, K Fu, J Sun, Y Hu, A Gobin, Tse-Kuan Yu, and R Drezek. 2008. "Evaluation of Immunotargeted Gold Nanoshells as Rapid Diagnostic Imaging Agents for HER2-Overexpressing Breast Cancer Cells: A Time Based Analysis." *Nanobiotechnology* 4 (1-4): 1-8.

Bickford, L, J Sun, K Fu, N Lewinski, V Nammalvar, J Chang, and R Drezek. 2008. "Enhanced multi-spectral imaging of live breast cancer cells using immunotargeted gold nanoshells and two-photon excitation microscopy." *Nanotechnology* 19 (31): -. doi:Artn 315102 Doi 10.1088/0957-4484/19/31/315102. <Go to ISI>://000257166800002.

Bickford, Lissett R, Germaine Agollah, Rebekah Drezek, and Tse-Kuan Yu. 2010. "Silica-gold nanoshells as potential intraoperative molecular probes for HER2-overexpression in ex vivo breast tissue using near-infrared reflectance confocal microscopy." *Breast cancer research and treatment* 120 (3) (April): 547-55. doi:10.1007/s10549-009-0408-z. http://www.ncbi.nlm.nih.gov/pubmed/19418216.

Bos, Reinhard, Jacobus J M van Der Hoeven, Elsken van Der Wall, Petra van Der Groep, Paul J van Diest, Emile F I Comans, Urvi Joshi, et al. 2002. "Biologic correlates of (18)fluorodeoxyglucose uptake in human breast cancer measured by positron emission tomography." *Journal of clinical oncology : official journal of the American Society of Clinical Oncology* 20 (2) (January): 379-87. http://www.ncbi.nlm.nih.gov/pubmed/11786564.

Bria, Emilio, Diana Giannarelli, Alessandra Felici, William P Peters, Cecilia Nisticò, Barbara Vanni, Federica Cuppone, Francesco Cognetti, and Edmondo Terzoli. 2005. "Taxanes with anthracyclines as first-line chemotherapy for metastatic breast carcinoma." *Cancer* 103 (4) (February 15): 672-9. doi:10.1002/cncr.20757. http://www.ncbi.nlm.nih.gov/pubmed/15637696.

Burkholder, Hans C, Laura E Witherspoon, R Phillip Burns, Jeffrey S Horn, and Michael D Biderman. 2007. "Breast surgery techniques: preoperative bracketing wire localization by surgeons." *The American surgeon* 73 (6) (June): 574-8; discussion 578-9. http://www.ncbi.nlm.nih.gov/pubmed/17658094.

Bydlon, Torre M, Stephanie A Kennedy, Lisa M Richards, J Quincy Brown, Bing Yu, Marlee K Junker, Jennifer Gallagher, Joseph Geradts, Lee G Wilke, and Nimmi Ramanujam. 2010. "Performance metrics of an optical spectral imaging system for intra-operative assessment of breast tumor margins." *Optics express* 18 (8) (April 12): 8058-76. http://www.pubmedcentral.nih.gov/articlerender.fcgi?artid=2939901&tool=pmcentrez&rendertype=abstract.

Cabioglu, N, K K Hunt, A A Sahin, H M Kuerer, G V Babiera, S E Singletary, G J Whitman, et al. 2007. "Role for intraoperative margin assessment in patients undergoing breast-conserving surgery." *Ann Surg Oncol* 14 (4): 1458-1471. doi:10.1245/s10434-006-9236-0. http://www.ncbi.nlm.nih.gov/entrez/query.fcgi?cmd=Retrieve&db=PubMed&dopt=Citation&list_uids=17260108.

Cameron, David, Michelle Casey, Cristina Oliva, Beth Newstat, Bradley Imwalle, and Charles E Geyer. 2010. "Lapatinib plus capecitabine in women with HER-2-positive advanced breast cancer: final survival analysis of a phase III randomized trial." *The oncologist* 15 (9) (January): 924-34. doi:10.1634/theoncologist.2009-0181. http://www.pubmedcentral.nih.gov/articlerender.fcgi?artid=3228041&tool=pmcentrez&rendertype=abstract.

Camp, E Ramsay, Priscilla F McAuliffe, Jeffrey S Gilroy, Christopher G Morris, D Scott Lind, Nancy P Mendenhall, and Edward M Copeland. 2005. "Minimizing local recurrence after breast conserving therapy using intraoperative shaved margins to determine pathologic tumor clearance." *Journal of the American College of Surgeons* 201 (6) (December): 855-61. doi:10.1016/j.jamcollsurg.2005.06.274. http://www.ncbi.nlm.nih.gov/pubmed/16310688.

Carlson, Robert W, D Craig Allred, Benjamin O Anderson, Harold J Burstein, W Bradford Carter, Stephen B Edge, John K Erban, et al. 2009. "Breast cancer. Clinical practice guidelines in oncology." *Journal of the National Comprehensive Cancer Network : JNCCN* 7 (2) (February): 122-92. http://www.ncbi.nlm.nih.gov/pubmed/19200416.

Carpin, L B, L R Bickford, G Agollah, T K Yu, R Schiff, Y Li, and R A Drezek. 2011. “Immunoconjugated gold nanoshell-mediated photothermal ablation of trastuzumab-resistant breast cancer cells.” *Breast Cancer Res Treat* 125 (1): 27-34. doi:10.1007/s10549-010-0811-5. http://www.ncbi.nlm.nih.gov/entrez/query.fcgi?cmd=Retrieve&db=PubMed&dopt=Citation&list_uids=20217215.

Cendán, Juan C, Dominique Coco, and Edward M Copeland. 2005. “Accuracy of intraoperative frozen-section analysis of breast cancer lumpectomy-bed margins.” *Journal of the American College of Surgeons* 201 (2) (August): 194-8. doi:10.1016/j.jamcollsurg.2005.03.014. http://www.ncbi.nlm.nih.gov/pubmed/16038815.

Chakravorty, A, A K Shrestha, N Sanmugalingam, F Rapisarda, N Roche, G Querci Della Rovere, and F A Macneill. 2012. “How safe is oncoplastic breast conservation? Comparative analysis with standard breast conserving surgery.” *European journal of surgical oncology : the journal of the European Society of Surgical Oncology and the British Association of Surgical Oncology* 38 (5) (May): 395-8. doi:10.1016/j.ejso.2012.02.186. http://www.ncbi.nlm.nih.gov/pubmed/22436560.

Cho, Kyu Ran, Bo Kyoung Seo, Chul Hwan Kim, Kyu Won Whang, Yun Hwan Kim, Baek Hyun Kim, Ok Hee Woo, Young Hen Lee, and Kyoo Byung Chung. 2008. “Non-calcified ductal carcinoma in situ: ultrasound and mammographic findings correlated with histological findings.” *Yonsei medical journal* 49 (1) (February 29): 103-10. doi:10.3349/ymj.2008.49.1.103. http://www.pubmedcentral.nih.gov/articlerender.fcgi?artid=2615255&tool=pmcentrez&rendertype=abstract.

Chung, Alice, Doug Liou, Scott Karlan, Alan Waxman, Kayo Fujimoto, Masanobu Hagiike, and Edward H Phillips. 2006. “Preoperative FDG-PET for axillary metastases in patients with breast cancer.” *Archives of surgery (Chicago, Ill. : 1960)* 141 (8) (August): 783-8; discussion 788-9. doi:10.1001/archsurg.141.8.783. http://www.ncbi.nlm.nih.gov/pubmed/16924086.

De Cicco, C, M Pizzamiglio, G Trifirò, A Luini, M Ferrari, G Prisco, V Galimberti, et al. 2002. “Radioguided occult lesion localisation (ROLL) and surgical biopsy in breast cancer. Technical aspects.” *The quarterly journal of nuclear medicine : official publication of the Italian Association of Nuclear Medicine (AIMN) [and] the International Association of Radiopharmacology (IAR)* 46 (2) (June): 145-51. http://www.ncbi.nlm.nih.gov/pubmed/12114878.

Clarke, M, R Collins, S Darby, C Davies, P Elphinstone, E Evans, J Godwin, et al. 2005. “Effects of radiotherapy and of differences in the extent of surgery for early breast cancer on local recurrence and 15-year survival: an overview of the randomised trials.” *Lancet* 366 (9503): 2087-2106. doi:S0140-6736(05)67887-7 [pii] 10.1016/S0140-6736(05)67887-7. http://www.ncbi.nlm.nih.gov/entrez/query.fcgi?cmd=Retrieve&db=PubMed&dopt=Citation&list_uids=16360786.

Clough, Krishna B, Gabriel J Kaufman, Claude Nos, Ines Buccimazza, and Isabelle M Sarfati. 2010. “Improving breast cancer surgery: a classification and quadrant per quadrant atlas for oncoplastic surgery.” *Annals of surgical oncology* 17 (5) (May): 1375-91. doi:10.1245/s10434-009-0792-y. http://www.ncbi.nlm.nih.gov/pubmed/20140531.

Cobleigh, Melody A, Virginia K Langmuir, George W Sledge, Kathy D Miller, Latrice Haney, William F Novotny, James D Reimann, and Amy Vassel. 2003. “A phase I/II dose-escalation trial of bevacizumab in previously treated metastatic breast cancer.” *Seminars in oncology* 30 (5 Suppl 16) (October): 117-24. http://www.ncbi.nlm.nih.gov/pubmed/14613032.

Cohn, David E, Nathan C Hall, Stephen P Povoski, Leigh G Seamon, William B Farrar, and Edward W Martin. 2008. “Novel perioperative imaging with 18F-FDG PET/CT and intraoperative 18F-FDG detection using a handheld gamma probe in recurrent ovarian cancer.” *Gynecologic oncology* 110 (2) (August): 152-7. doi:10.1016/j.ygyno.2008.04.026. http://www.ncbi.nlm.nih.gov/pubmed/18539314.

Connor, Ellen†E., Judith Mwamuka, Anand Gole, Catherine†J. Murphy, and Michael†D. Wyatt. 2005. “Gold Nanoparticles Are Taken Up by Human Cells but Do Not Cause Acute Cytotoxicity13.” *Small* 1 (3): 325-327. http://dx.doi.org/10.1002/smll.200400093.

Creager, Andrew J, Jo Ann Shaw, Peter R Young, and Kim R Geisinger. 2002. “Intraoperative evaluation of lumpectomy margins by imprint cytology with histologic correlation: a community hospital experience.” *Archives of pathology & laboratory medicine* 126 (7) (July): 846-8. doi:10.1043/0003-9985(2002)126<0846:IEOLMB>2.0.CO;2. http://www.ncbi.nlm.nih.gov/pubmed/12088456.

Cèfaro, Giampiero Ausili, Domenico Genovesi, Rita Marchese, Lucia Anna Ursini, Ettore Cianchetti, Enzo Ballone, and Marta Di Nicola. 2006. “Predictors of local recurrence after conservative surgery and whole-breast irradiation.” *Breast cancer research and treatment* 98 (3) (August): 329-35. doi:10.1007/s10549-006-9169-0. http://www.ncbi.nlm.nih.gov/pubmed/16555125.

DeSantis, Carol, Rebecca Siegel, Priti Bandi, and Ahmedin Jemal. 2011. "Breast cancer statistics, 2011." *CA: a cancer journal for clinicians* 61 (6): 409-18. doi:10.3322/caac.20134. http://www.ncbi.nlm.nih.gov/pubmed/21969133.

Duff, Daniel G, Alfons Baiker, and Peter P Edwards. 1993. "A new hydrosol of gold clusters. 1. Formation and particle size variation." *Langmuir* 9 (9): 2301-2309. doi:10.1021/la00033a010. http://dx.doi.org/10.1021/la00033a010.

Duffy, Michael J, Patricia M McGowan, and John Crown. 2012. "Targeted therapy for triple-negative breast cancer: where are we?" *International journal of cancer. Journal international du cancer* (May 14). doi:10.1002/ijc.27632. http://www.ncbi.nlm.nih.gov/pubmed/22581656.

D'Halluin, François, Patrick Tas, Sophie Rouquette, Cécile Bendavid, Fabrice Foucher, Habiba Meshba, Jérôme Blanchot, Olivier Coué, and Jean Levêque. 2009. "Intra-operative touch preparation cytology following lumpectomy for breast cancer: a series of 400 procedures." *Breast (Edinburgh, Scotland)* 18 (4) (August): 248-53. doi:10.1016/j.breast.2009.05.002. http://www.ncbi.nlm.nih.gov/pubmed/19515566.

Fentiman, I S. 2011. "Marginal effect in breast-conserving surgery." *International journal of clinical practice* 65 (5) (May): 519-20. doi:10.1111/j.1742-1241.2011.02608.x. http://www.ncbi.nlm.nih.gov/pubmed/21489074.

Fisher, Bernard, Stewart Anderson, John Bryant, Richard G Margolese, Melvin Deutsch, Edwin R Fisher, Jong-Hyeon Jeong, and Norman Wolmark. 2002. "Twenty-year follow-up of a randomized trial comparing total mastectomy, lumpectomy, and lumpectomy plus irradiation for the treatment of invasive breast cancer." *The New England journal of medicine* 347 (16) (October 17): 1233-41. doi:10.1056/NEJMoa022152. http://www.ncbi.nlm.nih.gov/pubmed/12393820.

Geyer, Charles E, John Forster, Deborah Lindquist, Stephen Chan, C Gilles Romieu, Tadeusz Pienkowski, Agnieszka Jagiello-Gruszfeld, et al. 2006. "Lapatinib plus capecitabine for HER2-positive advanced breast cancer." *The New England journal of medicine* 355 (26) (December 28): 2733-43. doi:10.1056/NEJMoa064320. http://www.ncbi.nlm.nih.gov/pubmed/17192538.

Van Goethem, M, K Schelfout, E Kersschot, C Colpaert, I Verslegers, I Biltjes, W A Tjalma, A De Schepper, J Weyler, and P M Parizel. 2007. "MR mammography is useful in the preoperative locoregional staging of breast carcinomas with extensive intraductal component." *European journal of radiology* 62 (2) (May): 273-82. doi:10.1016/j.ejrad.2006.12.004. http://www.ncbi.nlm.nih.gov/pubmed/17223002.

Gomez, Henry L, Dinesh C Doval, Miguel A Chavez, Peter C-S Ang, Zeba Aziz, Shona Nag, Christina Ng, et al. 2008. "Efficacy and safety of lapatinib as first-line therapy for ErbB2-amplified locally advanced or metastatic breast cancer." *Journal of clinical oncology : official journal of the American Society of Clinical Oncology* 26 (18) (June 20): 2999-3005. doi:10.1200/JCO.2007.14.0590. http://www.ncbi.nlm.nih.gov/pubmed/18458039.

Groheux, David, Sylvie Giacchetti, Jean-Luc Moretti, Raphael Porcher, Marc Espié, Jacqueline Lehmann-Che, Anne de Roquancourt, et al. 2011. "Correlation of high 18F-FDG uptake to clinical, pathological and biological prognostic factors in breast cancer." *European journal of nuclear medicine and molecular imaging* 38 (3) (March): 426-35. doi:10.1007/s00259-010-1640-9. http://www.ncbi.nlm.nih.gov/pubmed/21057787.

Guidroz, Julie A, Gregory Larrieux, Junlin Liao, Sonia L Sugg, Carol E H Scott-Conner, and Ronald J Weigel. 2011. "Sampling of secondary margins decreases the need for re-excision after partial mastectomy." *Surgery* 150 (4) (October): 802-9. doi:10.1016/j.surg.2011.07.064. http://www.ncbi.nlm.nih.gov/pubmed/22000194.

Gulec, Seza A, Farhad Daghighian, and Richard Essner. 2006. "PET-Probe: Evaluation of Technical Performance and Clinical Utility of a Handheld High-Energy Gamma Probe in Oncologic Surgery." *Annals of surgical oncology* (July 24). doi:10.1245/ASO.2006.05.047. http://www.ncbi.nlm.nih.gov/pubmed/16865592.

Gülben, Kaptan, Uğur Berberoğlu, Aziz Cengiz, and Hüseyin Altinyollar. 2007. "Prognostic factors affecting locoregional recurrence in patients with stage IIIB noninflammatory breast cancer." *World journal of surgery* 31 (9) (September 1): 1724-30. doi:10.1007/s00268-007-9139-7. http://www.springerlink.com/content/n752170246r84660/.

Hall, Nathan C, Stephen P Povoski, Douglas A Murrey, Michael V Knopp, and Edward W Martin. 2007. "Combined approach of perioperative 18F-FDG PET/CT imaging and intraoperative 18F-FDG handheld gamma probe detection for tumor localization and verification of complete tumor resection in breast cancer." *World journal of surgical oncology* 5 (January): 143. doi:10.1186/1477-7819-5-143. http://www.pubmedcentral.nih.gov/articlerender.fcgi?artid=2235860&tool=pmcentrez&rendertype=abstract.

Heckathorne, Elena, Colin Dimock, and Magnus Dahlbom. 2008. "Radiation dose to surgical staff from positron-emitter-based localization and radiosurgery of tumors." *Health physics* 95 (2) (August): 220-6. doi:10.1097/01.HP.0000310962.96089.44. http://www.ncbi.nlm.nih.gov/pubmed/18617803.

Houssami, Nehmat, Stefano Ciatto, Petra Macaskill, Sarah J Lord, Ruth M Warren, J Michael Dixon, and Les Irwig. 2008. "Accuracy and surgical impact of magnetic resonance imaging in breast cancer staging: systematic

review and meta-analysis in detection of multifocal and multicentric cancer." *Journal of clinical oncology : official journal of the American Society of Clinical Oncology* 26 (19) (July 1): 3248-58. doi:10.1200/JCO.2007.15.2108. http://www.ncbi.nlm.nih.gov/pubmed/18474876.

Houssami, Nehmat, Petra Macaskill, M Luke Marinovich, J Michael Dixon, Les Irwig, Meagan E Brennan, and Lawrence J Solin. 2010. "Meta-analysis of the impact of surgical margins on local recurrence in women with early-stage invasive breast cancer treated with breast-conserving therapy." *European journal of cancer (Oxford, England : 1990)* 46 (18) (December): 3219-32. doi:10.1016/j.ejca.2010.07.043. http://dx.doi.org/10.1016/j.ejca.2010.07.043.

Huynh, P T, A M Jarolimek, and S Daye. 1998. "The false-negative mammogram." *Radiographics : a review publication of the Radiological Society of North America, Inc* 18 (5): 1137-54; quiz 1243-4. http://www.ncbi.nlm.nih.gov/pubmed/9747612.

Ikeda, Debra M, Robyn L Birdwell, Kathryn F O'Shaughnessy, R James Brenner, and Edward A Sickles. 2003. "Analysis of 172 subtle findings on prior normal mammograms in women with breast cancer detected at follow-up screening." *Radiology* 226 (2) (February): 494-503. http://www.ncbi.nlm.nih.gov/pubmed/12563145.

Jacobs, L. 2008. "Positive margins: the challenge continues for breast surgeons." *Ann Surg Oncol* 15 (5): 1271-1272. doi:10.1245/s10434-007-9766-0. http://www.ncbi.nlm.nih.gov/entrez/query.fcgi?cmd=Retrieve&db=PubMed&dopt=Citation&list_uids=18320287.

Jassem, J, T Pieńkowski, A Płuzańska, S Jelic, V Gorbunova, Z Mrsic-Krmpotic, J Berzins, et al. 2001. "Doxorubicin and paclitaxel versus fluorouracil, doxorubicin, and cyclophosphamide as first-line therapy for women with metastatic breast cancer: final results of a randomized phase III multicenter trial." *Journal of clinical oncology : official journal of the American Society of Clinical Oncology* 19 (6) (March 15): 1707-15. http://www.ncbi.nlm.nih.gov/pubmed/11251000.

Kaida, Hayato, Masatoshi Ishibashi, Teruhiko Fuji, Seiji Kurata, Masafumi Uchida, Kenkichi Baba, Teruo Miyagawa, et al. 2008. "Improved breast cancer detection of prone breast fluorodeoxyglucose-PET in 118 patients." *Nuclear medicine communications* 29 (10) (October): 885-93. doi:10.1097/MNM.0b013e32830439d9. http://www.ncbi.nlm.nih.gov/pubmed/18769306.

Karni, T, I Pappo, J Sandbank, O Lavon, V Kent, R Spector, S Morgenstern, and S Lelcuk. 2007. "A device for real-time, intraoperative margin assessment in breast-conservation surgery." *Am J Surg* 194 (4): 467-473. doi:S0002-9610(07)00530-2 [pii] 10.1016/j.amjsurg.2007.06.013. http://www.ncbi.nlm.nih.gov/entrez/query.fcgi?cmd=Retrieve&db=PubMed&dopt=Citation&list_uids=17826057.

Kaufmann, Manfred, Gabriel N Hortobagyi, Aron Goldhirsch, Suzy Scholl, Andreas Makris, Pinuccia Valagussa, Jens-Uwe Blohmer, et al. 2006. "Recommendations from an international expert panel on the use of neoadjuvant (primary) systemic treatment of operable breast cancer: an update." *Journal of clinical oncology : official journal of the American Society of Clinical Oncology* 24 (12) (April 20): 1940-9. doi:10.1200/JCO.2005.02.6187. http://www.ncbi.nlm.nih.gov/pubmed/16622270.

Kaufmann, Manfred, Monica Morrow, Gunter von Minckwitz, and Jay R Harris. 2010. "Locoregional treatment of primary breast cancer: consensus recommendations from an International Expert Panel." *Cancer* 116 (5) (March 1): 1184-91. doi:10.1002/cncr.24874. http://www.ncbi.nlm.nih.gov/pubmed/20087962.

Kelly, P, and E H Winslow. 1996. "Needle wire localization for nonpalpable breast lesions: sensations, anxiety levels, and informational needs." *Oncology nursing forum* 23 (4) (May): 639-45. http://www.ncbi.nlm.nih.gov/pubmed/8735322.

Kim, Mi-Jung, Jae Y Ro, Sei-Hyun Ahn, Hak Hee Kim, Sung-Bae Kim, and Gyungyub Gong. 2006. "Clinicopathologic significance of the basal-like subtype of breast cancer: a comparison with hormone receptor and Her2/neu-overexpressing phenotypes." *Human pathology* 37 (9) (September): 1217-26. doi:10.1016/j.humpath.2006.04.015. http://www.ncbi.nlm.nih.gov/pubmed/16938528.

Komoike, Yoshifumi, Futoshi Akiyama, Yuichi Iino, Tadashi Ikeda, Sadako Akashi-Tanaka, Shozo Ohsumi, Mikihiro Kusama, et al. 2006. "Ipsilateral breast tumor recurrence (IBTR) after breast-conserving treatment for early breast cancer: risk factors and impact on distant metastases." *Cancer* 106 (1) (January 1): 35-41. doi:10.1002/cncr.21551. http://www.ncbi.nlm.nih.gov/pubmed/16333848.

Kong, T, J Zeng, X Wang, X Yang, J Yang, S McQuarrie, A McEwan, W Roa, J Chen, and J Z Xing. 2008. "Enhancement of radiation cytotoxicity in breast-cancer cells by localized attachment of gold nanoparticles." *Small* 4 (9): 1537-1543. doi:10.1002/smll.200700794.

http://www.ncbi.nlm.nih.gov/entrez/query.fcgi?cmd=Retrieve&db=PubMed&dopt=Citation&list_uids=18712753.

Kreike, Bas, Augustinus A M Hart, Tony van de Velde, Jacques Borger, Hans Peterse, Emiel Rutgers, Harry Bartelink, and Marc J van de Vijver. 2008. "Continuing risk of ipsilateral breast relapse after breast-conserving therapy at long-term follow-up." *International journal of radiation oncology, biology, physics* 71 (4) (July 15): 1014-21. doi:10.1016/j.ijrobp.2007.11.029. http://www.ncbi.nlm.nih.gov/pubmed/18234444.

Kukreti, Shwayta, Albert E Cerussi, Wendy Tanamai, David Hsiang, Bruce J Tromberg, and Enrico Gratton. 2010. "Characterization of metabolic differences between benign and malignant tumors: high-spectral-resolution diffuse optical spectroscopy." *Radiology* 254 (1) (January): 277-84. doi:10.1148/radiol.09082134. http://www.pubmedcentral.nih.gov/articlerender.fcgi?artid=2797652&tool=pmcentrez&rendertype=abstract.

Kumar, A, R Kumar, V Seenu, S D Gupta, M Chawla, A Malhotra, and S N Mehta. 2009. "The role of 18F-FDG PET/CT in evaluation of early response to neoadjuvant chemotherapy in patients with locally advanced breast cancer." *Eur Radiol* 19 (6): 1347-1357. doi:10.1007/s00330-009-1303-z. http://www.ncbi.nlm.nih.gov/entrez/query.fcgi?cmd=Retrieve&db=PubMed&dopt=Citation&list_uids=19214522.

Langsner, R J, L P Middleton, J Sun, F Meric-Bernstam, K K Hunt, R A Drezek, and T K Yu. 2011. "Wide-field imaging of fluorescent deoxy-glucose in ex vivo malignant and normal breast tissue." *Biomed Opt Express* 2 (6): 1514-1523. doi:10.1364/BOE.2.001514 145022 [pii]. http://www.ncbi.nlm.nih.gov/entrez/query.fcgi?cmd=Retrieve&db=PubMed&dopt=Citation&list_uids=21698015.

Laurinavicius, Arvydas, Aida Laurinaviciene, Valerijus Ostapenko, Darius Dasevicius, Sonata Jarmalaite, and Juozas Lazutka. 2012. "Immunohistochemistry profiles of breast ductal carcinoma: factor analysis of digital image analysis data." *Diagnostic pathology* 7 (January): 27. doi:10.1186/1746-1596-7-27. http://www.pubmedcentral.nih.gov/articlerender.fcgi?artid=3319425&tool=pmcentrez&rendertype=abstract.

Lee, Hyeran, Walter Akers, Kumar Bhushan, Sharon Bloch, Gail Sudlow, Rui Tang, and Samuel Achilefu. 2011. "Near-infrared pH-activatable fluorescent probes for imaging primary and metastatic breast tumors." *Bioconjugate chemistry* 22 (4) (April 20): 777-84. doi:10.1021/bc100584d. http://www.pubmedcentral.nih.gov/articlerender.fcgi?artid=3080440&tool=pmcentrez&rendertype=abstract.

Lee, Jun H, and Anjan Nan. 2012. "Combination drug delivery approaches in metastatic breast cancer." *Journal of drug delivery* 2012 (January): 915375. doi:10.1155/2012/915375. http://www.ncbi.nlm.nih.gov/pubmed/22619725.

Lee, Larissa J, and Jay R Harris. 2009. "Innovations in radiation therapy (RT) for breast cancer." *Breast (Edinburgh, Scotland)* 18 Suppl 3 (October): S103-11. doi:10.1016/S0960-9776(09)70284-X. http://www.ncbi.nlm.nih.gov/pubmed/19914528.

Lester, Susan C. 2004. The Breast. In *Pathologic Basis of Disease*, ed. Vinay Kumar, Abul Abbas, and Nelson Fausto, 1119-1154. 7th ed. Philadelphia: Elsevier Inc.

Lim, Hyo Soon, Woong Yoon, Tae Woong Chung, Jae Kyu Kim, Jin Gyoon Park, Heoung Keun Kang, Hee Seung Bom, and Jung Han Yoon. 2007. "FDG PET/CT for the detection and evaluation of breast diseases: usefulness and limitations." *Radiographics : a review publication of the Radiological Society of North America, Inc* 27 Suppl 1 (October): S197-213. doi:10.1148/rg.27si075507. http://www.ncbi.nlm.nih.gov/pubmed/18180227.

Linderholm, B, B Tavelin, K Grankvist, and R Henriksson. 1999. "Does vascular endothelial growth factor (VEGF) predict local relapse and survival in radiotherapy-treated node-negative breast cancer?" *British journal of cancer* 81 (4) (October): 727-32. doi:10.1038/sj.bjc.6690755. http://www.pubmedcentral.nih.gov/articlerender.fcgi?artid=2362894&tool=pmcentrez&rendertype=abstract.

Livi, Lorenzo, Icro Meattini, Carla De Luca Cardillo, Monica Mangoni, Daniela Greto, Alessia Petrucci, Andrea Rampini, et al. 2009. "Non-pegylated liposomal doxorubicin in combination with cyclophosphamide or docetaxel as first-line therapy in metastatic breast cancer: a retrospective analysis." *Tumori* 95 (4): 422-6. http://www.ncbi.nlm.nih.gov/pubmed/19856650.

Loo, C, L Hirsch, M H Lee, E Chang, J West, N Halas, and R Drezek. 2005. "Gold nanoshell bioconjugates for molecular imaging in living cells." *Opt Lett* 30 (9): 1012-1014. http://www.ncbi.nlm.nih.gov/entrez/query.fcgi?cmd=Retrieve&db=PubMed&dopt=Citation&list_uids=15906987.

Loo, C, A Lin, L Hirsch, M H Lee, J Barton, N Halas, J West, and R Drezek. 2004. "Nanoshell-enabled photonics-based imaging and therapy of cancer." *Technol Cancer Res Treat* 3 (1): 33-40. doi:d=3018&c=4130&p=12032&do=detail [pii].

http://www.ncbi.nlm.nih.gov/entrez/query.fcgi?cmd=Retrieve&db=PubMed&dopt=Citation&list_uids=14750891.

Loo, C, A Lowery, N Halas, J West, and R Drezek. 2005. "Immunotargeted nanoshells for integrated cancer imaging and therapy." *Nano Lett* 5 (4): 709-711. doi:10.1021/nl050127s. http://www.ncbi.nlm.nih.gov/entrez/query.fcgi?cmd=Retrieve&db=PubMed&dopt=Citation&list_uids=15826113.

Lowery, Aoife J, Malcolm R Kell, Ronan W Glynn, Michael J Kerin, and Karl J Sweeney. 2011. "Locoregional recurrence after breast cancer surgery: a systematic review by receptor phenotype." *Breast cancer research and treatment* (December 7). doi:10.1007/s10549-011-1891-6. http://www.ncbi.nlm.nih.gov/pubmed/22147079.

Luini, Alberto, Joel Rososchansky, Giovanna Gatti, Stefano Zurrida, Pietro Caldarella, Giuseppe Viale, Gabriela Rosali dos Santos, and Antonio Frasson. 2009. "The surgical margin status after breast-conserving surgery: discussion of an open issue." *Breast cancer research and treatment* 113 (2) (January): 397-402. doi:10.1007/s10549-008-9929-0. http://www.ncbi.nlm.nih.gov/pubmed/18386174.

MacDonald, Shannon, and Alphonse G Taghian. 2009. "Prognostic factors for local control after breast conservation: does margin status still matter?" *Journal of clinical oncology : official journal of the American Society of Clinical Oncology* 27 (30) (October 20): 4929-30. doi:10.1200/JCO.2009.23.6679. http://www.ncbi.nlm.nih.gov/pubmed/19720895.

Macheda, Maria L, Suzanne Rogers, and James D Best. 2005. "Molecular and cellular regulation of glucose transporter (GLUT) proteins in cancer." *Journal of cellular physiology* 202 (3) (March): 654-62. doi:10.1002/jcp.20166. http://www.ncbi.nlm.nih.gov/pubmed/15389572.

Mahmood, Usama, Christopher Morris, Geoffrey Neuner, Matthew Koshy, Susan Kesmodel, Robert Buras, Saranya Chumsri, Ting Bao, Katherine Tkaczuk, and Steven Feigenberg. 2012. "Similar Survival with Breast Conservation Therapy or Mastectomy in the Management of Young Women with Early-Stage Breast Cancer." *International Journal of Radiation Oncology*Biology*Physics* (January). doi:10.1016/j.ijrobp.2011.10.075. http://linkinghub.elsevier.com/retrieve/pii/S0360301611034833.

Manders, Peggy, Fred C G J Sweep, Vivianne C G Tjan-Heijnen, Anneke Geurts-Moespot, Doorléne T H van Tienoven, John A Foekens, Paul N Span, Jan Bussink, and Louk V A M Beex. 2003. "Vascular endothelial growth factor independently predicts the efficacy of postoperative radiotherapy in node-negative breast cancer patients." *Clinical cancer research : an official journal of the American Association for Cancer Research* 9 (17) (December 15): 6363-70. http://www.ncbi.nlm.nih.gov/pubmed/14695136.

Mannell, Aylwyn. 2005. "Breast-conserving therapy in breast cancer patients--a 12-year experience." *South African journal of surgery. Suid-Afrikaanse tydskrif vir chirurgie* 43 (2) (May): 28-30; discussion 30, 32. http://www.ncbi.nlm.nih.gov/pubmed/16035379.

Margenthaler, Julie A. 2011. "Optimizing conservative breast surgery." *Journal of surgical oncology* 103 (4) (March 15): 306-12. doi:10.1002/jso.21700. http://www.ncbi.nlm.nih.gov/pubmed/21337563.

McGuire, K P, A A Santillan, P Kaur, T Meade, J Parbhoo, M Mathias, C Shamehdi, M Davis, D Ramos, and C E Cox. 2009. "Are mastectomies on the rise? A 13-year trend analysis of the selection of mastectomy versus breast conservation therapy in 5865 patients." *Ann Surg Oncol* 16 (10): 2682-2690. doi:10.1245/s10434-009-0635-x. http://www.ncbi.nlm.nih.gov/entrez/query.fcgi?cmd=Retrieve&db=PubMed&dopt=Citation&list_uids=19653046.

Medina-Franco, Heriberto, Leonardo Abarca-Pérez, Miriam N García-Alvarez, José L Ulloa-Gómez, Cecilia Romero-Trejo, and Jesús Sepúlveda-Méndez. 2008. "Radioguided occult lesion localization (ROLL) versus wire-guided lumpectomy for non-palpable breast lesions: a randomized prospective evaluation." *Journal of surgical oncology* 97 (2) (February 1): 108-11. doi:10.1002/jso.20880. http://www.ncbi.nlm.nih.gov/pubmed/18181162.

Mieog, J Sven D, Susan L Troyan, Merlijn Hutteman, Kevin J Donohoe, Joost R van der Vorst, Alan Stockdale, Gerrit-Jan Liefers, et al. 2011. "Toward optimization of imaging system and lymphatic tracer for near-infrared fluorescent sentinel lymph node mapping in breast cancer." *Annals of surgical oncology* 18 (9) (September): 2483-91. doi:10.1245/s10434-011-1566-x. http://www.pubmedcentral.nih.gov/articlerender.fcgi?artid=3139732&tool=pmcentrez&rendertype=abstract.

Miles, Randy C, Rachel E Gullerud, Christine M Lohse, James W Jakub, Amy C Degnim, and Judy C Boughey. 2012. "Local recurrence after breast-conserving surgery: multivariable analysis of risk factors and the impact of young age." *Annals of surgical oncology* 19 (4) (April): 1153-9. doi:10.1245/s10434-011-2084-6. http://www.ncbi.nlm.nih.gov/pubmed/21989658.

Miller, Alexander R, Guillermo Brandao, Thomas J Prihoda, Cheryl Hill, Anatolio B Cruz, and I-Tien Yeh. 2004. "Positive margins following surgical resection of breast carcinoma: analysis of pathologic correlates." *Journal of surgical oncology* 86 (3) (June 1): 134-40. doi:10.1002/jso.20059. http://www.ncbi.nlm.nih.gov/pubmed/15170651.

Minamimoto, R, M Senda, K Uno, S Jinnouchi, T Iinuma, K Ito, C Okuyama, et al. 2007. "Performance profile of FDG-PET and PET/CT for cancer screening on the basis of a Japanese Nationwide Survey." *Ann Nucl Med* 21 (9): 481-498. doi:10.1007/s12149-007-0061-8. http://www.ncbi.nlm.nih.gov/entrez/query.fcgi?cmd=Retrieve&db=PubMed&dopt=Citation&list_uids=18030580.

Mironava, T, M Hadjiargyrou, M Simon, V Jurukovski, and M H Rafailovich. 2010. "Gold nanoparticles cellular toxicity and recovery: Effect of size, concentration and exposure time." *Nanotoxicology* 4 (1): 120-137. doi:Doi 10.3109/17435390903471463. <Go to ISI>://000275061000009.

Moore, M M, L A Whitney, L Cerilli, J Z Imbrie, M Bunch, V B Simpson, and J B Hanks. 2001. "Intraoperative ultrasound is associated with clear lumpectomy margins for palpable infiltrating ductal breast cancer." *Annals of surgery* 233 (6) (June): 761-8. http://www.pubmedcentral.nih.gov/articlerender.fcgi?artid=1421318&tool=pmcentrez&rendertype=abstract.

Moran, Meena S, Qifeng Yang, Sharad Goyal, Lyndsay Harris, Gina Chung, and Bruce G Haffty. 2011. "Evaluation of vascular endothelial growth factor as a prognostic marker for local relapse in early-stage breast cancer patients treated with breast-conserving therapy." *International journal of radiation oncology, biology, physics* 81 (5) (December 1): 1236-43. doi:10.1016/j.ijrobp.2010.07.031. http://www.ncbi.nlm.nih.gov/pubmed/21093162.

Morrow, Monica, and Gary Freedman. 2006. "A clinical oncology perspective on the use of breast MR." *Magnetic resonance imaging clinics of North America* 14 (3) (August): 363-78, vi. doi:10.1016/j.mric.2006.07.006. http://www.ncbi.nlm.nih.gov/pubmed/17098177.

Munirah, M A, M A Siti-Aishah, M Z Reena, N A Sharifah, M Rohaizak, A Norlia, M K M Rafie, et al. 2011. "Identification of different subtypes of breast cancer using tissue microarray." *Romanian journal of morphology and embryology = Revue roumaine de morphologie et embryologie* 52 (2) (January): 669-77. http://www.ncbi.nlm.nih.gov/pubmed/21655659.

Nguyen, Freddy T, Adam M Zysk, Eric J Chaney, Jan G Kotynek, Uretz J Oliphant, Frank J Bellafiore, Kendrith M Rowland, Patricia A Johnson, and Stephen A Boppart. 2009. "Intraoperative evaluation of breast tumor margins with optical coherence tomography." *Cancer research* 69 (22) (November 15): 8790-6. doi:10.1158/0008-5472.CAN-08-4340. http://www.pubmedcentral.nih.gov/articlerender.fcgi?artid=2782920&tool=pmcentrez&rendertype=abstract.

Ngô, Charlotte, Aymeric G Pollet, Juliette Laperrelle, Gregory Ackerman, Sandra Gomme, Fabienne Thibault, Virginie Fourchotte, and Remy J Salmon. 2007. "Intraoperative ultrasound localization of nonpalpable breast cancers." *Annals of surgical oncology* 14 (9) (September): 2485-9. doi:10.1245/s10434-007-9420-x. http://www.ncbi.nlm.nih.gov/pubmed/17541694.

Nitin, Nitin, Alicia L Carlson, Tim Muldoon, Adel K El-Naggar, Ann Gillenwater, and Rebecca Richards-Kortum. 2009. "Molecular imaging of glucose uptake in oral neoplasia following topical application of fluorescently labeled deoxy-glucose." *International journal of cancer. Journal international du cancer* 124 (11) (June): 2634-42. doi:10.1002/ijc.24222. http://www.pubmedcentral.nih.gov/articlerender.fcgi?artid=2700039&tool=pmcentrez&rendertype=abstract.

Nottage, Michelle K, Karen A Kopciuk, Anjela Tzontcheva, Irene L Andrulis, Shelley B Bull, and Martin E Blackstein. 2006. "Analysis of incidence and prognostic factors for ipsilateral breast tumour recurrence and its impact on disease-specific survival of women with node-negative breast cancer: a prospective cohort study." *Breast cancer research : BCR* 8 (4) (January): R44. doi:10.1186/bcr1531. http://www.pubmedcentral.nih.gov/articlerender.fcgi?artid=1779479&tool=pmcentrez&rendertype=abstract.

Ogasawara, Yutaka, Hirokuni Ikeda, Mina Takahashi, Kensuke Kawasaki, and Hiroyoshi Doihara. 2008. "Evaluation of breast lymphatic pathways with indocyanine green fluorescence imaging in patients with breast cancer." *World journal of surgery* 32 (9) (September): 1924-9. doi:10.1007/s00268-008-9519-7. http://www.ncbi.nlm.nih.gov/pubmed/18330628.

Olson, T P, J Harter, A Muñoz, D M Mahvi, and Tm Breslin. 2007. "Frozen section analysis for intraoperative margin assessment during breast-conserving surgery results in low rates of re-excision and local recurrence." *Annals of surgical oncology* 14 (10) (October): 2953-60. doi:10.1245/s10434-007-9437-1. http://www.ncbi.nlm.nih.gov/pubmed/17674109.

Osborn, John B, Gary L Keeney, James W Jakub, Amy C Degnim, and Judy C Boughey. 2011. "Cost-effectiveness analysis of routine frozen-section analysis of breast margins compared with reoperation for positive margins." *Annals of surgical oncology* 18 (11) (October): 3204-9. doi:10.1245/s10434-011-1956-0. http://www.ncbi.nlm.nih.gov/pubmed/21861234.

O'Neil, Roger G, Ling Wu, and Nizar Mullani. 2005. "Uptake of a fluorescent deoxyglucose analog (2-NBDG) in tumor cells." *Molecular imaging and biology : MIB : the official publication of the Academy of Molecular Imaging* 7 (6): 388-92. doi:10.1007/s11307-005-0011-6. http://www.ncbi.nlm.nih.gov/pubmed/16284704.

Pansare, Vikram J., Shahram Hejazi, William J. Faenza, and Robert K. Prud'homme. 2012. "Review of Long-Wavelength Optical and NIR Imaging Materials: Contrast Agents, Fluorophores, and Multifunctional Nano Carriers." *Chemistry of Materials* 24 (5) (March 13): 812-827. doi:10.1021/cm2028367. http://pubs.acs.org/doi/abs/10.1021/cm2028367.

Pengel, K E, C E Loo, H J Teertstra, S H Muller, J Wesseling, J L Peterse, H Bartelink, E J Rutgers, and K G A Gilhuijs. 2009. "The impact of preoperative MRI on breast-conserving surgery of invasive cancer: a comparative cohort study." *Breast cancer research and treatment* 116 (1) (July): 161-9. doi:10.1007/s10549-008-0182-3. http://www.ncbi.nlm.nih.gov/pubmed/18807269.

Pierce, Mark C, Peter M Vila, Alexandros D Polydorides, Rebecca Richards-Kortum, and Sharmila Anandasabapathy. 2011. "Low-cost endomicroscopy in the esophagus and colon." *The American journal of gastroenterology* 106 (9) (September): 1722-4. doi:10.1038/ajg.2011.140. http://www.pubmedcentral.nih.gov/articlerender.fcgi?artid=3191066&tool=pmcentrez&rendertype=abstract.

Pierce, Mark C., Richard a. Schwarz, Dong-Suk Shin, Darren Roblyer, Tim Muldoon, Mohammed Rahman, Ann M. Gillenwater, Sharmila Anandasabapathy, and Rebecca Richards-Kortum. 2010. "Low-cost, portable imaging systems for cancer detection." *Quality* 7556: 755606-755606-5. doi:10.1117/12.848553. http://link.aip.org/link/PSISDG/v7556/i1/p755606/s1&Agg=doi.

Pleijhuis, R G, M Graafland, J de Vries, J Bart, J S de Jong, and G M van Dam. 2009. "Obtaining adequate surgical margins in breast-conserving therapy for patients with early-stage breast cancer: current modalities and future directions." *Ann Surg Oncol* 16 (10): 2717-2730. doi:10.1245/s10434-009-0609-z. http://www.ncbi.nlm.nih.gov/entrez/query.fcgi?cmd=Retrieve&db=PubMed&dopt=Citation&list_uids=19609829.

Pleijhuis, R G, G C Langhout, W Helfrich, G Themelis, A Sarantopoulos, L M A Crane, N J Harlaar, J S de Jong, V Ntziachristos, and G M van Dam. 2011. "Near-infrared fluorescence (NIRF) imaging in breast-conserving surgery: assessing intraoperative techniques in tissue-simulating breast phantoms." *European journal of surgical oncology : the journal of the European Society of Surgical Oncology and the British Association of Surgical Oncology* 37 (1) (January): 32-9. doi:10.1016/j.ejso.2010.10.006. http://www.ncbi.nlm.nih.gov/pubmed/21106329.

Pons, F, J Duch, and D Fuster. 2009. "Breast cancer therapy: the role of PET-CT in decision making." *Q J Nucl Med Mol Imaging* 53 (2): 210-223. http://www.ncbi.nlm.nih.gov/entrez/query.fcgi?cmd=Retrieve&db=PubMed&dopt=Citation&list_uids=19293769.

Provenzano, E, J L Hopper, G G Giles, G Marr, D J Venter, and J E Armes. 2003. "Biological markers that predict clinical recurrence in ductal carcinoma in situ of the breast." *European journal of cancer (Oxford, England : 1990)* 39 (5) (March): 622-30. http://www.ncbi.nlm.nih.gov/pubmed/12628841.

Purmonen, Timo T, Emma Pänkäläinen, Juha H O Turunen, Christian Asseburg, and Janne A Martikainen. 2011. "Short-course adjuvant trastuzumab therapy in early stage breast cancer in Finland: cost-effectiveness and value of information analysis based on the 5-year follow-up results of the FinHer Trial." *Acta oncologica (Stockholm, Sweden)* 50 (3) (April): 344-52. doi:10.3109/0284186X.2011.553841. http://www.ncbi.nlm.nih.gov/pubmed/21299447.

Rahusen, Frans D, Andre J A Bremers, Hans F J Fabry, A H M Taets van Amerongen, Rob P A Boom, and S Meijer. 2002. "Ultrasound-guided lumpectomy of nonpalpable breast cancer versus wire-guided resection: a randomized clinical trial." *Annals of surgical oncology* 9 (10) (December): 994-8. http://www.ncbi.nlm.nih.gov/pubmed/12464592.

Rampaul, R S, M Bagnall, H Burrell, S E Pinder, A J Evans, and R D Macmillan. 2004. "Randomized clinical trial comparing radioisotope occult lesion localization and wire-guided excision for biopsy of occult breast lesions." *The British journal of surgery* 91 (12) (December): 1575-7. doi:10.1002/bjs.4801. http://www.ncbi.nlm.nih.gov/pubmed/15505875.

Rauscher, Garth H, Timothy P Johnson, Young Ik Cho, and Jennifer A Walk. 2008. "Accuracy of self-reported cancer-screening histories: a meta-analysis." *Cancer epidemiology, biomarkers & prevention : a publication of*

the American Association for Cancer Research, cosponsored by the American Society of Preventive Oncology 17 (4) (April): 748-57. doi:10.1158/1055-9965.EPI-07-2629. http://www.ncbi.nlm.nih.gov/pubmed/18381468.

Riedl, O, F Fitzal, N Mader, P Dubsky, M Rudas, M Mittlboeck, M Gnant, and R Jakesz. 2009. "Intraoperative frozen section analysis for breast-conserving therapy in 1016 patients with breast cancer." *European journal of surgical oncology : the journal of the European Society of Surgical Oncology and the British Association of Surgical Oncology* 35 (3) (March): 264-70. doi:10.1016/j.ejso.2008.05.007. http://www.ncbi.nlm.nih.gov/pubmed/18706785.

Roblyer, Darren, Cristina Kurachi, Vanda Stepanek, Michelle D Williams, Adel K El-Naggar, J Jack Lee, Ann M Gillenwater, and Rebecca Richards-Kortum. 2009. "Objective detection and delineation of oral neoplasia using autofluorescence imaging." *Cancer Prev Res (Phila Pa)* 2 (5) (May): 423-431. doi:1940-6207.CAPR-08-0229 [pii] 10.1158/1940-6207.CAPR-08-0229. http://www.pubmedcentral.nih.gov/articlerender.fcgi?artid=2719708&tool=pmcentrez&rendertype=abstract.

Rodríguez Lajusticia, Laura, Miguel Martín Jiménez, and Sara López-Tarruella Cobo. 2008. "Endocrine therapy of metastatic breast cancer." *Clinical & translational oncology : official publication of the Federation of Spanish Oncology Societies and of the National Cancer Institute of Mexico* 10 (8) (August): 462-7. http://www.ncbi.nlm.nih.gov/pubmed/18667376.

de Roos, Marnix A, Geertruida H de Bock, Jaap de Vries, Bert van der Vegt, and Jelle Wesseling. 2007. "p53 overexpression is a predictor of local recurrence after treatment for both in situ and invasive ductal carcinoma of the breast." *The Journal of surgical research* 140 (1) (June 1): 109-14. doi:10.1016/j.jss.2006.10.045. http://www.ncbi.nlm.nih.gov/pubmed/17291532.

Rosbach, Kelsey J, Dongsuk Shin, Timothy J Muldoon, Mohammad A Quraishi, Lavinia P Middleton, Kelly K Hunt, Funda Meric-Bernstam, Tse-Kuan Yu, Rebecca R Richards-Kortum, and Wei Yang. 2010. "High-resolution fiber optic microscopy with fluorescent contrast enhancement for the identification of axillary lymph node metastases in breast cancer: a pilot study." *Biomed. Opt. Express* 1 (3): 911-922. http://www.opticsinfobase.org/boe/abstract.cfm?URI=boe-1-3-911.

Rowland, J H, K A Desmond, B E Meyerowitz, T R Belin, G E Wyatt, and P A Ganz. 2000. "Role of breast reconstructive surgery in physical and emotional outcomes among breast cancer survivors." *Journal of the National Cancer Institute* 92 (17) (September 6): 1422-9. http://www.ncbi.nlm.nih.gov/pubmed/10974078.

Rusby, Jennifer E, Nirmala Paramanathan, Siobhan A M Laws, and Richard M Rainsbury. 2008. "Immediate latissimus dorsi miniflap volume replacement for partial mastectomy: use of intra-operative frozen sections to confirm negative margins." *American journal of surgery* 196 (4) (October): 512-8. doi:10.1016/j.amjsurg.2008.06.026. http://www.ncbi.nlm.nih.gov/pubmed/18809053.

Salas-Burgos, Alexis, Pavel Iserovich, Felipe Zuniga, Juan Carlos Vera, and Jorge Fischbarg. 2004. "Predicting the three-dimensional structure of the human facilitative glucose transporter glut1 by a novel evolutionary homology strategy: insights on the molecular mechanism of substrate migration, and binding sites for glucose and inhibitory molecules." *Biophysical journal* 87 (5) (November): 2990-9. doi:10.1529/biophysj.104.047886. http://www.ncbi.nlm.nih.gov/pubmed/15326030.

Sano, Kohei, Makoto Mitsunaga, Takahito Nakajima, Peter L Choyke, and Hisataka Kobayashi. 2012. "In vivo breast cancer characterization imaging using two monoclonal antibodies activatably labeled with near infrared fluorophores." *Breast cancer research : BCR* 14 (2) (April 17): R61. doi:10.1186/bcr3167. http://www.ncbi.nlm.nih.gov/pubmed/22510481.

Sarlos, D, L D Frey, H Haueisen, G Landmann, L A Kots, and G Schaer. 2009. "Radioguided occult lesion localization (ROLL) for treatment and diagnosis of malignant and premalignant breast lesions combined with sentinel node biopsy: a prospective clinical trial with 100 patients." *European journal of surgical oncology : the journal of the European Society of Surgical Oncology and the British Association of Surgical Oncology* 35 (4) (April): 403-8. doi:10.1016/j.ejso.2008.06.016. http://www.ncbi.nlm.nih.gov/pubmed/18692358.

Schelling, M, N Avril, J Nahrig, W Kuhn, W Romer, D Sattler, M Werner, et al. 2000. "Positron Emission Tomography Using [18F]Fluorodeoxyglucose for Monitoring Primary Chemotherapy in Breast Cancer." *J Clin Oncol* 18 (8): 1689-1695. http://jco.ascopubs.org/cgi/content/abstract/18/8/1689.

Schwartz, Gordon F, Umberto Veronesi, Krishna B Clough, J Michael Dixon, Ian S Fentiman, Sylvia H Heywang-Köbrunner, Roland Holland, et al. 2006. "Consensus conference on breast conservation." *Journal of the American College of Surgeons* 203 (2) (August): 198-207. doi:10.1016/j.jamcollsurg.2006.04.009. http://www.ncbi.nlm.nih.gov/pubmed/16864033.

Sevick-Muraca, Eva M, Ruchi Sharma, John C Rasmussen, Milton V Marshall, Juliet A Wendt, Hoang Q Pham, Elizabeth Bonefas, et al. 2008. "Imaging of lymph flow in breast cancer patients after microdose administration of a near-infrared fluorophore: feasibility study." *Radiology* 246 (3) (March): 734-41.

doi:10.1148/radiol.2463070962. http://www.pubmedcentral.nih.gov/articlerender.fcgi?artid=3166516&tool=pmcentrez&rendertype=abstract.
Shao, Wenlin, and Myles Brown. 2004. "Advances in estrogen receptor biology: prospects for improvements in targeted breast cancer therapy." *Breast cancer research : BCR* 6 (1) (January): 39-52. doi:10.1186/bcr742. http://www.pubmedcentral.nih.gov/articlerender.fcgi?artid=314456&tool=pmcentrez&rendertype=abstract.
Singletary, S Eva. 2002. "Surgical margins in patients with early-stage breast cancer treated with breast conservation therapy." *The American Journal of Surgery* 184 (5) (November): 383-393. http://www.sciencedirect.com/science/article/B6VHS-475NT83-3/2/62cd2a2269bef4ab66bd98f94184a246.
Smith, Ian, Marion Procter, Richard D Gelber, Sébastien Guillaume, Andrea Feyereislova, Mitch Dowsett, Aron Goldhirsch, et al. 2007. "2-year follow-up of trastuzumab after adjuvant chemotherapy in HER2-positive breast cancer: a randomised controlled trial." *Lancet* 369 (9555) (January 6): 29-36. doi:10.1016/S0140-6736(07)60028-2. http://www.ncbi.nlm.nih.gov/pubmed/17208639.
Solin, Lawrence J, Susan G Orel, Wei-Ting Hwang, Eleanor E Harris, and Mitchell D Schnall. 2008. "Relationship of breast magnetic resonance imaging to outcome after breast-conservation treatment with radiation for women with early-stage invasive breast carcinoma or ductal carcinoma in situ." *Journal of clinical oncology : official journal of the American Society of Clinical Oncology* 26 (3) (January 20): 386-91. doi:10.1200/JCO.2006.09.5448. http://www.ncbi.nlm.nih.gov/pubmed/18202414.
Stewart, Alexandra J, Desmond A O'Farrell, Robert A Cormack, Jorgen L Hansen, Atif J Khan, Subhakar Mutyala, and Phillip M Devlin. 2008. "Dose volume histogram analysis of normal structures associated with accelerated partial breast irradiation delivered by high dose rate brachytherapy and comparison with whole breast external beam radiotherapy fields." *Radiation oncology (London, England)* 3 (January): 39. doi:10.1186/1748-717X-3-39. http://www.pubmedcentral.nih.gov/articlerender.fcgi?artid=2612673&tool=pmcentrez&rendertype=abstract.
Stober, W, A Fink, and E Bohn. 1968. "Controlled Growth of Monodisperse Silica Spheres in Micron Size Range." *Journal of Colloid and Interface Science* 26 (1): 62-& <Go to ISI>://A1968A684600009.
Strong, Vivian E, John Humm, Paul Russo, Achim Jungbluth, W Douglas Wong, Farhad Daghighian, Lloyd Old, Yuman Fong, and Steven M Larson. 2008. "A novel method to localize antibody-targeted cancer deposits intraoperatively using handheld PET beta and gamma probes." *Surgical endoscopy* 22 (2) (February): 386-91. doi:10.1007/s00464-007-9611-3. http://www.ncbi.nlm.nih.gov/pubmed/18027053.
Sørum, Ragnhild, Solveig Hofvind, Per Skaane, and Tor Haldorsen. 2010. "Trends in incidence of ductal carcinoma in situ: the effect of a population-based screening programme." *Breast (Edinburgh, Scotland)* 19 (6) (December): 499-505. doi:10.1016/j.breast.2010.05.014. http://www.ncbi.nlm.nih.gov/pubmed/21071225.
Tafra, Lorraine, Richard Fine, Pat Whitworth, Michael Berry, James Woods, Gregory Ekbom, Jennifer Gass, et al. 2006. "Prospective randomized study comparing cryo-assisted and needle-wire localization of ultrasound-visible breast tumors." *American journal of surgery* 192 (4) (October): 462-70. doi:10.1016/j.amjsurg.2006.06.012. http://www.sciencedirect.com/science/article/pii/S0002961006004405.
Tagaya, Nobumi, Rie Yamazaki, Aya Nakagawa, Akihito Abe, Kiyoshige Hamada, Keiichi Kubota, and Tetsunari Oyama. 2008. "Intraoperative identification of sentinel lymph nodes by near-infrared fluorescence imaging in patients with breast cancer." *American journal of surgery* 195 (6) (June): 850-3. doi:10.1016/j.amjsurg.2007.02.032. http://www.ncbi.nlm.nih.gov/pubmed/18353274.
Tamimi, Rulla M, Heather J Baer, Jonathan Marotti, Mark Galan, Laurie Galaburda, Yineng Fu, Anne C Deitz, et al. 2008. "Comparison of molecular phenotypes of ductal carcinoma in situ and invasive breast cancer." *Breast cancer research : BCR* 10 (4) (January): R67. doi:10.1186/bcr2128. http://www.pubmedcentral.nih.gov/articlerender.fcgi?artid=2575540&tool=pmcentrez&rendertype=abstract.
Tanis, E, C J H van de Velde, H Bartelink, M J van de Vijver, H Putter, and J A van der Hage. 2012. "Locoregional recurrence after breast-conserving therapy remains an independent prognostic factor even after an event free interval of 10years in early stage breast cancer." *European journal of cancer (Oxford, England : 1990)* (March 23). doi:10.1016/j.ejca.2012.02.051. http://www.ncbi.nlm.nih.gov/pubmed/22446021.
Thekkek, N, D M Maru, A D Polydorides, M S Bhutani, S Anandasabapathy, and R Richards-Kortum. 2011. "Pre-clinical evaluation of fluorescent deoxyglucose as a topical contrast agent for the detection of Barrett's-associated neoplasia during confocal imaging." *Technology in cancer research & treatment* 10 (5) (October): 431-41. http://www.pubmedcentral.nih.gov/articlerender.fcgi?artid=3193280&tool=pmcentrez&rendertype=abstract.
Thekkek, Nadhi, Sharmila Anandasabapathy, and Rebecca Richards-Kortum. 2011. "Optical molecular imaging for detection of Barrett's-associated neoplasia." *World journal of gastroenterology : WJG* 17 (1) (January 7): 53-

62. doi:10.3748/wjg.v17.i1.53. http://www.pubmedcentral.nih.gov/articlerender.fcgi?artid=3016680&tool=pmcentrez&rendertype=abstract.
Thind, C R, S Desmond, O Harris, R Nadeem, L S Chagla, and R A Audisio. 2005. "Radio-guided localization of clinically occult breast lesions (ROLL): a DGH experience." *Clinical radiology* 60 (6) (June): 681-6. doi:10.1016/j.crad.2004.12.004. http://www.ncbi.nlm.nih.gov/pubmed/16038695.
Tromberg, Bruce J, and Albert E Cerussi. 2010. "Imaging breast cancer chemotherapy response with light. Commentary on Soliman et al., p. 2605." *Clinical cancer research : an official journal of the American Association for Cancer Research* 16 (9) (May 1): 2486-8. doi:10.1158/1078-0432.CCR-10-0397. http://www.pubmedcentral.nih.gov/articlerender.fcgi?artid=3204881&tool=pmcentrez&rendertype=abstract.
Tromberg, Bruce J, Brian W Pogue, Keith D Paulsen, Arjun G Yodh, David A Boas, and Albert E Cerussi. 2008. "Assessing the future of diffuse optical imaging technologies for breast cancer management." *Medical physics* 35 (6) (June): 2443-51. http://www.pubmedcentral.nih.gov/articlerender.fcgi?artid=2809725&tool=pmcentrez&rendertype=abstract.
Troyan, Susan L, Vida Kianzad, Summer L Gibbs-Strauss, Sylvain Gioux, Aya Matsui, Rafiou Oketokoun, Long Ngo, Ali Khamene, Fred Azar, and John V Frangioni. 2009. "The FLARE intraoperative near-infrared fluorescence imaging system: a first-in-human clinical trial in breast cancer sentinel lymph node mapping." *Annals of surgical oncology* 16 (10) (October): 2943-52. doi:10.1245/s10434-009-0594-2. http://www.pubmedcentral.nih.gov/articlerender.fcgi?artid=2772055&tool=pmcentrez&rendertype=abstract.
Tse, Gary M K, Philip C W Lui, Joaquim S L Vong, Kin-Mang Lau, Thomas C Putti, Rooshdiya Karim, Richard A Scolyer, et al. 2009. "Increased epidermal growth factor receptor (EGFR) expression in malignant mammary phyllodes tumors." *Breast cancer research and treatment* 114 (3) (April): 441-8. doi:10.1007/s10549-008-0030-5. http://www.ncbi.nlm.nih.gov/pubmed/18443904.
Valdes, Edna K, Susan K Boolbol, Jean-Marc Cohen, and Sheldon M Feldman. 2007. "Intra-operative touch preparation cytology; does it have a role in re-excision lumpectomy?" *Annals of surgical oncology* 14 (3) (March): 1045-50. doi:10.1245/s10434-006-9263-x. http://www.ncbi.nlm.nih.gov/pubmed/17206481.
Vanden Bempt, Isabelle, Peter Van Loo, Maria Drijkoningen, Patrick Neven, Ann Smeets, Marie-Rose Christiaens, Robert Paridaens, and Christiane De Wolf-Peeters. 2008. "Polysomy 17 in breast cancer: clinicopathologic significance and impact on HER-2 testing." *Journal of clinical oncology : official journal of the American Society of Clinical Oncology* 26 (30) (October 20): 4869-74. doi:10.1200/JCO.2007.13.4296. http://www.ncbi.nlm.nih.gov/pubmed/18794552.
Vargas, Carlos, Larry Kestin, Nel Go, Daniel Krauss, Peter Chen, Neal Goldstein, Alvaro Martinez, and Frank A Vicini. 2005. "Factors associated with local recurrence and cause-specific survival in patients with ductal carcinoma in situ of the breast treated with breast-conserving therapy or mastectomy." *International journal of radiation oncology, biology, physics* 63 (5) (December 1): 1514-21. doi:10.1016/j.ijrobp.2005.04.045. http://www.ncbi.nlm.nih.gov/pubmed/16005576.
Veronesi, Umberto, Natale Cascinelli, Luigi Mariani, Marco Greco, Roberto Saccozzi, Alberto Luini, Marisel Aguilar, and Ettore Marubini. 2002. "Twenty-year follow-up of a randomized study comparing breast-conserving surgery with radical mastectomy for early breast cancer." *The New England journal of medicine* 347 (16) (October 17): 1227-32. doi:10.1056/NEJMoa020989. http://www.ncbi.nlm.nih.gov/pubmed/12393819.
Vicini, Frank A, Vincent Remouchamps, Michelle Wallace, Michael Sharpe, Julie Fayad, Laura Tyburski, Nicola Letts, et al. 2003. "Ongoing clinical experience utilizing 3D conformal external beam radiotherapy to deliver partial-breast irradiation in patients with early-stage breast cancer treated with breast-conserving therapy." *International journal of radiation oncology, biology, physics* 57 (5) (December 1): 1247-53. http://www.ncbi.nlm.nih.gov/pubmed/14630258.
Vinh-Hung, Vincent, and Claire Verschraegen. 2004. "Breast-conserving surgery with or without radiotherapy: pooled-analysis for risks of ipsilateral breast tumor recurrence and mortality." *Journal of the National Cancer Institute* 96 (2) (January 21): 115-21. http://www.ncbi.nlm.nih.gov/pubmed/14734701.
Virnig, Beth A, Todd M Tuttle, Tatyana Shamliyan, and Robert L Kane. 2010. "Ductal carcinoma in situ of the breast: a systematic review of incidence, treatment, and outcomes." *Journal of the National Cancer Institute* 102 (3) (February 3): 170-8. doi:10.1093/jnci/djp482. http://www.ncbi.nlm.nih.gov/pubmed/20071685.
Voogd, A C, F J van Oost, E J T Rutgers, P H M Elkhuizen, A N van Geel, L J E E Scheijmans, M J C van der Sangen, et al. 2005. "Long-term prognosis of patients with local recurrence after conservative surgery and radiotherapy for early breast cancer." *European journal of cancer (Oxford, England : 1990)* 41 (17) (November): 2637-44. doi:10.1016/j.ejca.2005.04.040. http://www.ncbi.nlm.nih.gov/pubmed/16115758.

Vosoughhosseini, S, M Lotfi, A Fakhrjou, A Aghbali, M Moradzadeh, M Sina, and P Emamverdizadeh. 2012. "Analysis of epidermal growth factor receptor in histopathologically tumor-free surgical margins in patients with oral squamous cell carcinoma." *African Journal of Biotechnology* 11 (2): 516-520. doi:10.5897/AJB 10.489.

Vranic, Semir, Ossama Tawfik, Juan Palazzo, Nurija Bilalovic, Eduardo Eyzaguirre, Lisa Mj Lee, Patrick Adegboyega, Jill Hagenkord, and Zoran Gatalica. 2010. "EGFR and HER-2/neu expression in invasive apocrine carcinoma of the breast." *Modern pathology : an official journal of the United States and Canadian Academy of Pathology, Inc* 23 (5) (May): 644-53. doi:10.1038/modpathol.2010.50. http://www.ncbi.nlm.nih.gov/pubmed/20208479.

Wahl, R L, R L Cody, G D Hutchins, and E E Mudgett. 1991. "Primary and metastatic breast carcinoma: initial clinical evaluation with PET with the radiolabeled glucose analogue 2-[F-18]-fluoro-2-deoxy-D-glucose." *Radiology* 179 (3): 765-770. http://radiology.rsna.org/content/179/3/765.abstract.

Wang, Shi-Yi, Tatyana Shamliyan, Beth A Virnig, and Robert Kane. 2011. "Tumor characteristics as predictors of local recurrence after treatment of ductal carcinoma in situ: a meta-analysis." *Breast cancer research and treatment* 127 (1) (May): 1-14. doi:10.1007/s10549-011-1387-4. http://www.ncbi.nlm.nih.gov/pubmed/21327465.

Weinberg, Elizabeth, Charles Cox, Elisabeth Dupont, Laura White, Mark Ebert, Harvey Greenberg, Nils Diaz, et al. 2004. "Local recurrence in lumpectomy patients after imprint cytology margin evaluation." *American journal of surgery* 188 (4) (October): 349-54. doi:10.1016/j.amjsurg.2004.06.024. http://www.ncbi.nlm.nih.gov/pubmed/15474425.

Wilke, Lee G, J Quincy Brown, Torre M Bydlon, Stephanie a Kennedy, Lisa M Richards, Marlee K Junker, Jennifer Gallagher, William T Barry, Joseph Geradts, and Nimmi Ramanujam. 2009. "Rapid noninvasive optical imaging of tissue composition in breast tumor margins." *American journal of surgery* 198 (4) (October): 566-74. doi:10.1016/j.amjsurg.2009.06.018. http://www.pubmedcentral.nih.gov/articlerender.fcgi?artid=2764289&tool=pmcentrez&rendertype=abstract.

Yang, Hae-Chung, Lisa M Thornton, Charles L Shapiro, and Barbara L Andersen. 2008. "Surviving recurrence: psychological and quality-of-life recovery." *Cancer* 112 (5) (March 1): 1178-87. doi:10.1002/cncr.23272. http://www.pubmedcentral.nih.gov/articlerender.fcgi?artid=2435301&tool=pmcentrez&rendertype=abstract.

Yang, Xiaohong R, Mark E Sherman, David L Rimm, Jolanta Lissowska, Louise A Brinton, Beata Peplonska, Stephen M Hewitt, et al. 2007. "Differences in risk factors for breast cancer molecular subtypes in a population-based study." *Cancer epidemiology, biomarkers & prevention : a publication of the American Association for Cancer Research, cosponsored by the American Society of Preventive Oncology* 16 (3) (March): 439-43. doi:10.1158/1055-9965.EPI-06-0806. http://www.ncbi.nlm.nih.gov/pubmed/17372238.

Yildirim, E. 2009. "Locoregional recurrence in breast carcinoma patients." *European journal of surgical oncology : the journal of the European Society of Surgical Oncology and the British Association of Surgical Oncology* 35 (3) (March): 258-63. doi:10.1016/j.ejso.2008.06.010. http://www.ncbi.nlm.nih.gov/pubmed/18644692.

Yoshioka, K, K B Oh, M Saito, Y Nemoto, and H Matsuoka. 1996. "Evaluation of 2-[N-(7-nitrobenz-2-oxa-1,3-diazol-4-yl)amino]-2-deoxy-D-glucose, a new fluorescent derivative of glucose, for viability assessment of yeast Candida albicans." *Appl Microbiol Biotechnol* 46 (4): 400-404. http://www.ncbi.nlm.nih.gov/entrez/query.fcgi?cmd=Retrieve&db=PubMed&dopt=Citation&list_uids=8987729.

Yu, Jennifer, Fatema Al Mushawah, Marie E Taylor, Amy E Cyr, William E Gillanders, Rebecca L Aft, Timothy J Eberlein, Feng Gao, and Julie A Margenthaler. 2012. "Compromised margins following mastectomy for stage I-III invasive breast cancer." *The Journal of surgical research* (April 10). doi:10.1016/j.jss.2012.03.046. http://www.ncbi.nlm.nih.gov/pubmed/22520579.

Zavagno, Giorgio, Elena Goldin, Roberto Mencarelli, Giovanni Capitanio, Paola Del Bianco, Renato Marconato, Simone Mocellin, et al. 2008. "Role of resection margins in patients treated with breast conservation surgery." *Cancer* 112 (9) (May 1): 1923-31. doi:10.1002/cncr.23383. http://www.ncbi.nlm.nih.gov/pubmed/18327818.

Rapid stereomicroscopic imaging of HER2 overexpression in *ex vivo* breast tissue using topically applied silica-based gold nanoshells

Lissett R. Bickford[1,2,3*], Robert J. Langsner[1*], Joseph Chang[4], Laura C. Kennedy[1,5], Germaine D. Agollah[6], and Rebekah Drezek[1,7†]

[1]*Department of Bioengineering, Rice University, Houston, TX 77005, USA*

[2]*School of Biomedical Engineering and Sciences, Virginia Polytechnic Institute & State University, Blacksburg, VA 24061 USA*

[3]*Department of Mechanical Engineering, Virginia Polytechnic Institute & State University, Blacksburg, VA 24061 USA*

[4]*School of Medicine, University of California, San Francisco, San Francisco, CA 94143*

[5]*School of Medicine, Baylor College of Medicine, Houston, TX 77030*

[6]*Nanospectra Biosciences, Inc., Houston, TX 77054, USA*

[7]*Department of Electrical and Computer Engineering, Rice University, Houston, TX 77005, USA*

[†]*Corresponding author: Rice University, Department of Bioengineering, 6100 Main St., MS-142, Houston, TX 77005. Email, drezek@rice.edu; Phone, 713-348-3011; Fax, 713-348-5877*

* *These authors contributed equally to this work.*

Abstract

Tumor margin detection for patients undergoing breast conservation surgery primarily occurs postoperatively. Previously, we demonstrated that gold nanoshells rapidly enhance contrast of HER2-overexpression in *ex vivo* tissue sections. Our ultimate objective, however, is to discern HER2-overexpressing tissue from normal tissue in whole, non-sectioned, specimens to facilitate rapid diagnoses. Here, we use targeted nanoshells to quickly and effectively visualize HER2 receptor expression in intact *ex vivo* human breast tissue specimens. Punch biopsies of human breast tissue were analyzed after a brief 5-minute incubation with and without HER2-targeted silica-gold nanoshells using two-photon microscopy and stereomicroscopy. Labeling was subsequently verified using reflectance confocal microscopy, darkfield hyperspectral imaging, and immunohistochemistry to confirm levels of HER2-expression. Our results suggest that anti-HER2-nanoshells used in tandem with a near-infrared reflectance confocal microscope and a standard stereomicroscope may potentially be used to discern HER2-overexpressing cancerous tissue from normal tissue in near real time and offer a rapid supplement to current diagnostic techniques.

Key words: nanoshells; stereomicroscopy; reflectance confocal microscopy; breast cancer; rapid diagnosis; tumor margins; intraoperative detection

Introduction

Currently, breast cancer is the second leading cause of cancer-related deaths in women, and it accounts for approximately one-third of all cancers diagnosed in women in the United States [1]. To reduce cancer recurrence and progression, cancerous tissue must be completely eliminated, regardless of grade [2]. Surgical breast cancer therapy focuses on removing the primary tumor and identifying the possibility of metastatic disease from the evaluation of sentinel lymph nodes. Although some patients may require modified radical mastectomy, many patients with less-advanced breast cancer elect breast-conserving surgery. The presence of a positive surgical margin during these surgeries has been associated with lower rates of patient survival [3]. Due to residual cancer cells being left in many patients that undergo breast conservation therapy, as many as 40% of patients have experienced local breast cancer recurrence near the site of the original tumor [4]. Intraoperative treatment decisions are, therefore, absolutely critical.

Presently, intraoperative tumor margin detection occurs primarily in specialized tertiary centers, such as The University of Texas M.D. Anderson Cancer Center (MDACC). In these centers, the resected tissue receives a preliminary evaluation by a pathologist while the patient remains in the operating room; if necessary, additional tissue can be removed until the pathologist determines the tumor margins are negative. In community hospitals, however, pathologic analysis of excised tissue only occurs postoperatively [5]. Patients who consequently have positive tumor margins must return for surgical re-excision and receive increased doses of adjuvant radiation therapy [6,7]. Thus, the existence of positive tumor margins portends additional risks and costs to the patient. Due to the existing limitations of current intraoperative tumor margin detection,

there is an opportunity to develop superior diagnostic tools to assist in reducing the recurrence and progression of cancer due to inadequate tissue removal during primary surgery.

While histologic analysis remains the gold standard for tumor margin assessment, the macroscopic evaluation of whole, non-sectioned tissue specimens may also be used to provide an intraoperative estimate of tumor margin status prior to subsequent processing. This would be an invaluable tool in hospitals without onsite pathology suites. Macroscopic visualization of questionable tissue is attractive for enhancing the sensitivity and specificity of tumor margin delineation: if the number of suspicious regions that require further microscopic processing can be reduced, surgeons and pathologists can focus their attention and resources on areas that remain inconclusive. Currently, macroscopic evaluation only occurs for breast cancer specimens that involve microcalcifications or nonpalpable masses and does not occur for palpable breast masses [8]. For nonpalpable masses that have been resected, radiographic images are used to determine the extent of the breast disease and the proximity to the resected margins. Although specimen radiography appears to increase the accuracy of tumor margin detection, limitations have been noted. For instance, microcalcifications that appear as tumor on radiographic images may actually be areas of lymphocytic accumulation [9]. The use of contrast agents targeted to specific biomarkers associated with disease may present an opportunity to increase the sensitivity and specificity of macroscopic evaluations.

In preceding studies, we confirmed that silica-based gold nanoshells targeted to the Human Epidermal growth factor Receptor 2 (HER2) could be used for the rapid

contrast enhancement of both cells [10] and tissue sections [11] which overexpress HER2 biomarkers. While gold nanoshells can be conjugated to a variety of biomarkers [12,13], we have selected HER2 due to its association with increased cancer aggression, recurrence, and progression when amplified [14,15]. Amplification of this cell-surface bound tyrosine kinase receptor occurs in up to a quarter of all human breast cancer cases [16]. Importantly, using biomarkers for tumor margin detection has recently been shown to better identify patients at high risk of cancer recurrence over standard histological analysis [17].

To facilitate prompt tumor margin detection intraoperatively, the ability to assess tumor margins without physical sectioning is highly desirable as sectioning may incur significant time to the surgical procedure [5]. Thus, in this study, we advance our previous findings by examining the ability to rapidly target HER2 receptors in intact *ex vivo* human breast tissue specimens without sectioning. We first confirm the predominance of the surface targeting needed to identify the tumor margins and preferential labeling of HER2-positive tissue using two photon and hyperspectral imaging. Then, we demonstrate that anti-HER2 targeted gold nanoshells can be used as rapid diagnostic imaging agents for HER2-overexpression in intact breast tissue specimens using a standard stereomicroscope and confirm these results through reflectance confocal microscopy, and immunohistochemistry.

Materials and Methods

Nanoshell Fabrication and Antibody Conjugation

Nanoshells were fabricated as formerly described [18-20], and only a brief summary will be provided here. Silica cores were made using the Stöber method [21], followed by subsequent termination of the silica surfaces with amine groups. The final particles were measured by dynamic light scattering (DLS) to have an average diameter of 276 nm. Next, gold colloid (~1-3 nm diameter) was fabricated and adsorbed onto the surface of the silica cores via the amine groups [22]. After the gold layer over the silica cores was formed, the spectrum of the final nanoshell solution was visualized using a UV-vis spectrophotometer (Varian Cary 300) (Fig.1).

Nanoshells were targeted to biological HER2-antigens by linking the surfaces of the nanoshells to anti-HER2 antibodies using previously described methods [18]. Prior to beginning experimental studies, nanoshells were incubated with an anti-HER2-linker cocktail [18] for 2 hours at 4°C. To ensure nanoparticle stabilization in biological media, the nanoshells were next incubated with a 1 mM polyethylene glycol-thiol solution (PEG-SH, MW = 5kD, Nektar) for 12-16 hours at 4°C. Next, unbound antibodies and excess PEG-SH were removed from the nanoshells by centrifugation. Prior to experimental studies, the nanoshells were resuspended in antibody diluent (IHC World, pH 7.4) by gentle pipetting to a final volume of 165 μl.

Ex Vivo Human Breast Tissue Specimens

Normal and cancerous (HER2-negative and HER2-positive) breast tissue specimens were supplied by the Cooperative Human Tissue Network (CHTN) through a protocol approved by the Institutional Review Board (IRB). Tissues were designated as normal or cancerous by pathologists at the medical centers where the tissue samples were

obtained. Additionally, HER2 status was previously determined by pathologists at the respective medical centers prior to the patients undergoing any form of medical treatment.

Before use, samples were thawed briefly in a 37ºC water bath and cut on a disposable cutting board using a 5 mm punch biopsy to maintain size consistency. At least two punch biopsies were taken from each specimen for control and experimental conditions. Each cut specimen used was 5 mm in diameter with an average thickness of 1 mm. Tissue samples were subsequently incubated in pre-warmed antibody diluent for 1 minute at room temperature with gentle agitation in a 24-well plate. After pre-rinsing, the samples were incubated in either antibody diluent or the aforementioned targeted-nanoshell cocktail in polyethylene sample vials (Sigma Aldrich). The vials were placed on a nutator in an incubator at 37°C for 5 minutes. After incubation, the tissue samples were removed from the vials and rinsed 3 times in 1X PBS briefly in a 24-well plate. Samples were moved to a clean well of 1X PBS prior to imaging.

Two Photon Imaging of Human Breast Tissue Specimens

Both HER2-positive and HER2-negative cancerous samples were evaluated for surface labeling of HER2-targeted nanoshells by employing two-photon imaging of intact breast tissue specimens. Samples were placed directly on a glass coverslip (Fisher Scientific), and an additional coverslip was placed on top of the tissue in order to facilitate moderate tissue compression. For image acquisition, a Zeiss muti-photon confocal microscope (LSM 510 META NLO) was used in tandem with a Coherent Chameleon femtosecond-pulsed, mode-locked Ti:sapphire laser. This system was set to

operate as formerly described [23]. Specifically, an excitation wavelength of 780 nm and a power setting of 10% maximum excitation power were used. The collected emission wavelength range was 451-697 nm. Images were collected at a magnification of 20X and a z-stack (depth) increment of 5 μm. In order to calculate the percentage of area covered by nanoshells, ImageJ imaging software was implemented after image acquisition. An intensity threshold of 30 was used to distinguish areas with and without nanoshells. For areas that did not contain nanoshells, the associated intensities did not exceed the threshold.

Darkfield Hyperspectral Imaging of Human Breast Tissue Slices

To confirm the presence of nanoshells on the surface of the tissues, HER2-positive cancerous, HER2-negative cancerous and normal tissue samples were incubated with nanoshells as previously described. A thin layer of pathological ink was placed on the tissue surface for orientation. The tissues were embedded in OCT media (BBC chemical) and frozen rapidly over dry ice. The specimens were cut at a section thickness of 8 μm using a Leica CM1850 UV cryostat. Cancerous specimens were sectioned at −20ºC and normal specimens at − 30ºC, as recommended by Leica for maintaining optimal tissue morphology. The sections were immediately placed on superfrost slides (Fisher Scientific) and allowed to dry overnight. The next day the tissue slices were imaged with a 10X objective on an Olympus darkfield microscope equipped with a Cytoviva high-resolution illuminator. Hyperspectral images of the tissue slices were taken using a hyperspectral camera that provides both spatial and spectral data for each image.

Spectral data of each field of view (FOV) was used to determine if nanoshells were present on each slice of tissue. Comparisons were made between tissue surfaces and tissue beyond the surfaces to determine the presence of nanoshells; spectral data from tissue that was not incubated with nanoshells was also used as a negative control.

Macroscopic Imaging of Human Breast Tissue Specimens

Normal and HER2-positive cancerous breast tissue specimens (from patients who had and had not received neoadjuvant chemotherapy) were imaged using a Zeiss Discovery.V8 stereomicroscope equipped with a VisiLED MC1000 light source. For macroscopic imaging of breast tissue specimens, a thin plastic black stage was placed beneath a glass coverslip to enable ease of tissue placement and to provide a consistent black background among all samples. The specimens (controls and respective nanoshell-labeled counterparts) were placed alongside each other on top of the coverslip. Images were taken at both 1X and 2X magnification under the same lighting conditions.

Reflectance Confocal Microscopy Imaging of Human Breast Tissue Specimens

Following widefield imaging, the aforementioned samples were prepared for microscopic analysis under reflectance confocal microscopy. For this component of the study, a Lucid VivaScope 2500 inverted confocal microscope was used. Samples were placed directly on glass slides that were modified by the addition of an adhesive 1-mm-deep, 20-mm-diameter silicon isolator (Invitrogen). To compress the tissue slightly and consistently among samples, an adhesive tissue cassette (Lucid, Inc.) was placed directly on top of the silicone isolators above the tissue specimens. Multiple images were taken at

a power of 0.4 mW and at the same distance from the glass surface for both samples and controls. After reflectance imaging, the samples were prepared for histological processing. Additionally, reflectance intensity measurements were recorded using Image J processing software as formerly described [11].

Immunohistochemistry and Histology

Once images were collected under both stereomicroscopy and RCM imaging systems, normal and HER2-positive cancerous samples (with and without previous neoadjuvant chemotherapy) were embedded in OCT media and sectioned to a thickness of 5 μm. Multiple sections from each specimen were prepared for either immunohistochemistry (IHC) or hemotoxylin and eosin (H&E) staining. IHC for the HER2-antigen was executed using the Histostain Plus AEC Broad Spectrum Kit (Invitrogen) per manufacturer's instructions. H&E staining was also performed per manufacturer's instructions (Sigma Aldrich) for the alcoholic Eosin Y solution. For image acquisition, a standard brightfield microscope (Zeiss Axioskop 2 equipped with a Zeiss Axiocam MRc5 color camera) was used at a magnification of 20X.

Results

Distribution and Penetration of Gold Nanoshells in Intact Human Breast Tissue

The goal of this study was to evaluate the distribution of anti-HER2-conjugated gold nanoshells on resected intact tissue specimens. For comparison, the nanoshell labeling between HER2-positive and HER2-negative tissue samples was evaluated using a two photon imaging system. As previously reported, this imaging system is capable of

enhancing and capturing the luminescence signature of the gold nanoshells [23] while also collecting a stack of images taken through the depth of the tissue of interest. Figure 2 represents such images of HER2-positive and HER2-negative cancerous tissue samples incubated with HER2-targeted nanoshells. Each sequential increment in the z-direction represents 5 μm into the tissue. Qualitatively, the first image (taken at the surface, or at 0 μm) in Fig. 2 demonstrates that the nanoshells preferentially label HER2-receptors on the surface of the tissue. Additionally, Fig. 2 displays decreased signal as the focal spot from the confocal microscope penetrates further into the tissue. This is believed to be a minimal number of nanoshells being able to penetrate the tissue in the limited amount of incubation time, thus decreasing signal collected beyond the surface. A quantitative difference of the nanoshell signal at the surface of the HER2-positive and HER2-negative tissue was calculated. Using ImageJ imaging software, it was determined that approximately 66% of the FOV for HER2-positive tissue was covered in nanoshells versus just 2% for the FOV of the HER2-negative tissue. This confirms the preferential labeling and visualization of HER2-positive tissue using anti-HER2 nanoshells.

To further validate the surface binding of the nanoshells, hyperspectral images of different tissue sections were also acquired. Fig. 3 (a) shows a representative surface of a HER2-positive tissue section after incubation with anti-HER2 nanoshells. Fig. 3 (b) illustrates tissue 24 μm beyond the surface of the same tissue. Spectra from multiple (n=3) specimens that were incubated with anti-HER2 nanoshells were acquired and analysis showed that tissues without nanoshells had very similar spectra across different patients. Fig. 3 (c) displays the respective spectral information of each FOV shown in (a) and (b). Additionally, the spectra of HER2-positive tissue without nanoshells has been

included as a control. As can be seen in this graph, the spectra of the surface of the HER2-positive tissue incubated with anti-HER2 nanoshells is distinctive from that of the same tissue 24 μm beyond the surface. In fact, the spectra of the tissue beyond the surface of the nanoshell-labeled specimen is very similar to the spectra of the surface of the control. These results support our findings that the targeted nanoshells primarily localized to the surface of the tissue.

Enhanced Optical Imaging of Intact *Ex Vivo* Human Breast Cancer Tissue Using Gold Nanoshells

Based on previous results demonstrating the preferential labeling of HER2-targeted nanoshells on the surface of intact *ex vivo* HER2-positive tissue specimens, we assessed the potential of using a standard stereomicroscope to visualize this enhanced contrast. For this component of the study, human breast tissue specimens that over-expressed HER2 receptors at the time of patient diagnosis were evaluated and compared to normal breast tissue. Due to the ultimate goal of utilizing gold nanoshells to rapidly label tumor margins intraoperatively in diverse patient populations, we examined tissue from patients who had and had not undergone neoadjuvant chemotherapy. All tissue samples were incubated with either antibody diluent buffer or the anti-HER2-targeted nanoshells for 5 minutes at 37°C. As shown in Fig. 4, which represents raw images taken with a stereomicroscope, intact tissue specimens incubated with antibody diluent alone showed no markings or features characteristic of nanoshells. However, tissue specimens incubated with the anti-HER2-targeted nanoshells demonstrate numerous particles on the surfaces of the tissues. Qualitatively, the HER2-positive tissue from the patient who did

not undergo previous chemotherapy shows the greatest labeling with the targeted nanoshells. The HER2-positive tissue from the patient who did undergo neoadjuvant chemotherapy does demonstrate enriched nanoshell labeling when compared to normal tissue, though not to the same extent as the patient without previous chemotherapy. In contrast, the normal tissue shows the least amount of nanoshell labeling and only a few areas of nanoshells can be visually perceived.

While the degree of nanoshell labeling can be visualized without image adjustments under a standard stereomicroscope, the superior extent of this labeling can be seen more clearly after a simple contrast enhancement using imaging software (Image J). As seen in Fig. 5 (a.), the nanoshells are even more discernable against the tissue background regardless of inherent tissue constituents.

To validate the enhanced nanoshell labeling seen by macroscopic imaging, the surfaces of the same tissue samples were also imaged using reflectance confocal microscopy (Fig. 5 (b.)). Concurring with the stereomicroscopic images, we see dramatic nanoshell surface-labeling when using targeted nanoshells with previously untreated HER2-positive tissue. For the HER2-positive sample that had formerly undergone chemotherapy, we also see enhanced nanoshell labeling, though to a lesser degree than the untreated sample as suggested by the stereomicroscopy results. The normal breast tissue displays the least amount of surface labeling with only minimal nanoshells evident with either imaging system. Reflectance intensity measurements (data not shown) were ~2.5 to 3 times greater for both the HER2-positive tissue sample receiving chemotherapy and for the HER2-positive tissue not receiving chemotherapy when compared to the normal tissue sample.

Subsequent histological analysis shown in Fig. 5 (c.) reveals that the distribution of HER2 receptors seen with nanoshell-enabled contrast corresponds to that seen with IHC against HER2. The HER2 expression seen by IHC is greater for the previously untreated HER2-positive tissue sample than for the sample that had undergone neoadjuvant chemotherapy. This is believed to be due to the effects of chemotherapy. Rasbridge *et al.* previously demonstrated that patient response to chemotherapy is highly variable, with patients previously negative for HER2-overexpression occasionally becoming positive after treatment and patients previously positive for HER2-overexpression subsequently becoming negative [24]. Although patient response to chemotherapy varies, tissues previously identified as overexpressing HER2 receptors during initial diagnosis, regardless of chemotherapy exposure, demonstrate enhanced nanoshell labeling over normal tissue. Additionally, H&E-stained sections of all tissue samples have been included (Fig. 5 (d.)) to illustrate the microscopic characteristics and differences associated with cancerous vs. non-cancerous conditions.

Discussion

In this study we demonstrated the ability to use targeted gold nanoshells to rapidly improve visualization of a specific biomarker associated with disease aggression and progression (HER2) in intact *ex vivo* human breast tissue and confirmed binding location via confocal and darkfield hyperspectral microscopy. By utilizing silica-gold nanoshells designed as rapid diagnostic imaging agents, surgeons and pathologists may be able to realize tumor margin status directly in the operating room after both macroscopic and microscopic assessment. While multiple methods of intraoperative tumor margin

detection are currently under investigation [25-29], we are developing an inexpensive and portable system for rapidly analyzing *ex vivo* specimens based on the desire to enhance current methodologies without delay in clinical translation due to regulatory concerns associated with *in vivo* systems.

The ability to enhance contrast of malignancy using topically applied agents has previously been demonstrated for oral and breast tissue using fluorescently labeled deoxy-glucose and epidermal growth factor (EGF) conjugates [30-32] as well as cervical tissue using fluorescently labeled gold nanoparticles targeted to EGF receptors [33]. However, these studies employed incubation times ranging from 20-45 minutes, which exceeds the length of time currently needed to obtain tumor margin status using frozen section histology. Additionally, the aforementioned studies, utilized optical clearing agents, which may be necessary for particles that target intracellular biomarkers [34, 35]. Nevertheless, gold nanoshells targeted to extracellular biomarkers may offer more favorable opportunities for *ex vivo* intraoperative tumor margin detection without the need for lengthy incubation times or the use of optical clearing agents.

Recently, we verified that silica-based gold nanoshells could be used to enhance contrast of both HER2-overexpressing cells and tissue sections within 5 minutes of incubation time [10, 11]. However, translating this technology towards clinical relevancy requires the ability to assess whole, un-sectioned specimens. Here, we confirm that gold nanoshells, when targeted to HER2 receptors, can be used to distinguish intact HER2-overexpressing *ex vivo* tissue from normal tissue within the same incubation time and we demonstrate that this difference can be observed macroscopically. These results are supported by microscopic imaging and immunohistochemistry against HER2.

To translate these findings more readily to the clinic, we are presently developing a low cost widefield imaging system that can be used to detect the overexpression of HER2 (and other extracellular biomarkers) on account of contrast enhancement provided by gold nanoshells. In addition, we plan to collect data from diverse patient populations and assess results with fresh tissue samples. In this way, the use of gold nanoshells may demonstrate widespread efficacy or be limited only to specific patient subsets.

Our research indicates that *ex vivo* tissue specimens labeled topically with silica-based gold nanoshells can be visualized by both widefield (macroscopic) and high resolution (microscopic) imaging systems. By employing macroscopic imaging intraoperatively, clinicians may be better able to distinguish cancerous and normal breast tissue prior to further microscopic analysis and subsequent histological processing. Ultimately, this system could also be used for other diagnostic applications, for other anatomical locations, and for other biomarkers associated with disease. By facilitating fast and accurate tumor margin results intraoperatively and supplementing current diagnostic methods, the incidence of cancer progression and amount of time spent in surgery due to inadequate tissue removal is, correspondingly, expected to be reduced.

Acknowledgements

We thank the Cooperative Human Tissue Network for providing fresh frozen tissue samples. We thank Glenn P. Goodrich and Nanospectra Biosciences, Inc. for providing nanoshells used in the studies. We also thank Nadhi Thekkek for assistance with ImageJ data acquistion. This work was supported by a Department of Defense Congressionally Directed Breast Cancer Research Program Era of Hope Scholar Award to Rebekah Drezek, the Center for Biological and Environmental Nanotechnology (EEC-0118007 and EEC-0647452). L. Bickford thanks the Department of Defense (DoD) for training support through the National Defense Science & Engineering Graduate Fellowship (NDSEG) Program.

Figure Captions

Figure 1. Measured extinction spectra of nanoshells with an average core diameter of 276 nm and average shell thickness of 19 nm. Insert depicts corresponding image from scanning electron microscopy. Scale bar represents 500 nm.

Figure 2. Z-stack two-photon luminescence images of HER2-positive and HER2-negative tissue incubated with HER2-targeted nanoshells for 5 minutes at 37°C. Each progressive image represents an increase in depth penetration of 5 μm. Magnification = 20X. Scale bar = 50 μm.

Figure 3. Darkfield images of HER2-positive tissue sectioned after incubation with anti-HER2 targeted silica-gold nanoshells. (a.) Surface of HER2-positive tissue, (b.) 24 μm beyond the surface of the same tissue. (c.) Scattering spectra of the fields of view depicted in (a) and (b). Additionally, spectra from the surface of HER2-positive tissue not incubated with silica-gold nanoshells is shown as a negative control. Scale Bar = 50μm.

Figure 4. Raw stereomicroscope images of (a.,b.) HER2-overexpressing cancerous and (c.) normal tissue incubated with either buffer or HER2-targeted nanoshells for 5 minutes at 37°C. Cancerous tissue taken from a patient (a.) without chemotherapy and (b.) following neoadjuvant chemotherapy. Arrows represent nanoshells. Images taken at 2X. Scale bars = 2.5 mm.

Figure 5. (a.) Stereomicroscopic images of HER2-overexpressing breast tissue (with and without neoadjuvant chemotherapy) and normal breast tissue incubated with HER2-targeted nanoshells for 5 minutes at 37°C after contrast enhancement. Magnification at 2X; scale bar = 2.5 mm. Arrows represent nanoshells. (b.) Respective reflectance confocal microscopy images of tissue samples from (a.). Power = 0.4 mW and scale bar = 75 μm. Respective (c.) HER2 immunohistochemistry and (d.) H&E results taken under brightfield microscopy under 20X magnification. Scale bar = 0.35 mm.

References

1. American Cancer Society. (2005) Breast Cancer Facts and Figures 2005-2006. Atlanta: American Cancer Society, Inc. http://www.cancer.org/Research/CancerFactsFigures/BreastCancerFactsFigures/breast-cancer-facts--figures-2005-2006. Accessed 05 November 2010.

2. Steen RG (1993) A Conspiracy of Cells. Plenum Press, New York.

3. Mojica CM, Bastani R, Boscardin WJ, Ponce NA (2007) Low-Income Women With Breast Abnormalities: System Predictors of Timely Diagnostic Resolution. Cancer Control 14(2):176-182.

4. Fisher B, Anderson S, Bryant J, Margolese RG, Deutsch M, Fisher ER, Jeong JH, Wolmark N (2002) Twenty-year follow-up of a randomized trial comparing total mastectomy, lumpectomy, and lumpectomy plus irradiation for the treatment of invasive breast cancer. N Engl J Med 347(16):1233-1241

5. Pleijhuis RG, Graafland M, de Vries J, Bart J, de Jong JS, van Dam GM (2009) Obtaining adequate surgical margins in breast-conserving therapy for patients with early-stage breast cancer: Current modalities and future directions. Ann Surg Oncol 16 (10):2717-2730. doi:10.1245/s10434-009-0609-z

6. Oouchi A, Sakata K, Masuoka H, Tamakawa M, et al. (2009) The treatment outcome of patients undergoing breast-conserving therapy: the clinical role of postoperative radiotherapy. Breast Cancer Res Treat 16:49-57. doi:10.1007/s12282-008-0079-3

7. Smitt MC, Nowels KW, Zdeblick MJ, Jeffrey S, Carlson RW, Stockdale FE, Goffinet DR (1995) The Importance of the Lumpectomy Surgical Margin Status in Long Term Results of Breast Conservation. Cancer 76(2):259-267.

8. Cabioglu N, Hunt K, Aysegul AS, Kuerer HM, Babiera GV, Singletary SE, Whitman GJ, Ross MI, Ames FC, Feig BW, Buchholz TA, Meric-Bernstam F (2007) Role for Intraoperative Margin Assessment in Patients Undergoing Breast-Conserving Surgery. Ann Surg Oncol 14(4):1458-1471. doi:10.1245/s10434-006-9236-0

9. Graham RA, Homer MJ, Sigler CJ, Safaii H, Schmid CH, Marchant DJ, Smith TJ (1994) The Efficacy of Specimen Radiography in Evaluating the Surgical Margins of Impalpable Breast Carcinoma. Am J Roentgenol 162(1):33-36.

10. Bickford LR, Chang J, Fu K, Sun J, Hu Y, Gobin A, Yu T-K, Drezek RA (2008) Evaluation of Immunotargeted Gold Nanoshells as Rapid Diagnostic Imaging Agents for HER2-Overexressing Breast Cancer Cells: A Time-Based Analysis. Nanobiotechnol 4(1-4):1-8. doi:10.1007/s12030-008-9010-4

11. Bickford LR, Agollah G, Drezek R, Yu TK (2010) Silica-gold nanoshells as potential intraoperative molecular probes for HER2-overexpression in *ex vivo* breast tissue using near-infrared reflectance confocal microscopy. Breast Cancer Res Treat 120(3):547. doi:10.1007/s10549-009-0408-z

12. Sokolov K, Follen M, Aaron J, Pavlova I, Malpica A, Lotan R, Richards-Kortum R (2003) Real-time vital optical imaging of precancer using anti-epidermal growth factor receptor antibodies conjugated to gold nanoparticles. Cancer Research 63 (9):1999-2004

13. Liu X, Dai Q, Austin L, Coutts J, Knowles G, Zou J, Chen H, Huo Q (2008) A one-step homogeneous immunoassay for cancer biomarker detection using gold nanoparticle probes coupled with dynamic light scattering. Journal of the American Chemical Society 130 (9):2780-2782. doi:10.1021/ja711298b

14. Nahta R, Yu D, Hung MC, Hortobagyi GN, Esteva FJ (2006) Mechanisms of disease: understanding resistance to HER2-targeted therapy in human breast cancer. Nat Clin Pract 3(5):269-280.

15. Slamon DJ, Clark GM, Wong SG, Levin WJ, Ullrich A, McGuire WL (1987) Human breast cancer: correlation of relapse and survival with amplification of the HER-2/neu oncogene. Science 235(1):177-182.

16. Hicks DG, Kulkarni S (2008) Her2+ breast cancer. American Journal of Clinical Pathology 129 (2):263-273. doi:10.1309/99ae032r9fm8wnd1

17. Vosoughhosseini S, Lotfi M, Fakhrjou A, Aghbali A, Moradzadeh M, Sina M, Emamverdizadeh P (2012) Analysis of epidermal growth factor receptor in histopathologically tumor-free surgical margins in patients with oral squamous cell carcinoma. African Journal of Biotechnology 11 (2):516-520. doi:10.5897/AJB 10.489

18. Loo C, Lin A, Hirsch L, Lee MH, Barton J, Halas N, West J, Drezek R (2004) Nanoshell-enabled photonics-based imaging and therapy of cancer. Technol Cancer Res Treat 3(1):33-40.

19. Loo C, Hirsh L, Lee MH, Change E, West J, Halas N, Drezek R (2005) Gold nanoshell bioconjugates for molecular imaging in living cells. Opt Lett 30(9):1012-1014. doi:10.1364/OL.30.001012

20. Loo C, Lowery A, Halas N, West J, Drezek R (2005) Immunotargeted nanoshells for integrated cancer imaging and therapy. Nano Lett 5(4):709-711. doi: 10.1021/nl050127s

21. Stöber W, Fink A (1968) Controlled Growth of Monodisperse Silica Spheres in the Micron Size Range. J Colloid Interface Sci 26:62-69.

22. Duff DG, Baiker A, Edwards PP (1993) A new hydrosol of gold clusters. 1. Formation and particle size variation. Langmuir 9(9):2301-2309.

23. Bickford LR, Sun J, Fu K, Lewinski N, Nammalvar V, Chang J, Drezek RA (2008) Enhanced Multi-Spectral Imaging of Live Breast Cancer Cells Using Immunotargeted Gold Nanoshells and Two-Photon Excitation Microscopy. Nanotechnology 19: 315102. doi:10.1088/0957-4484

24. Rasbridge SA, Gillett CE, Seymour AM, Patel K, Richards MA, Rubens RD, Millis RR (1994) The effects of chemotherapy on morphology, cellular proliferation, apoptosis and oncoprotein expression in primary breast carcinoma. Br J Cancer 70(2):335-341.

25. Haid A, Knauer M, Dunzinger S, Jasarevic Z, Köberle-Führer R, Schuster A, Toeppker M, Haid B, Wenzl E, Offner F (2007) Intra-operative sonography: A valuable aid during breast-conserving surgery for occult breast cancer. Annals of Surgical Oncology 14 (11):3090-3101. doi:10.1245/s10434-007-9490-9

26. Karni T, Pappo I, Sandbank J, Lavon O, Kent V, Spector R, Morgenstern S, Lelcuk S (2007) A device for real-time, intraoperative margin assessment in breast-conservation surgery. The American Journal of Surgery 194 (4):467-473

27. Tafra L, Fine R, Whitworth P, Berry M, Woods J, Ekbom G, Gass J, Beitsch P, Dodge D, Han L, Potruch T, Francescatti D, Oetting L, Smith JS, Snider H, Kleban D, Chagpar A, Akbari S (2006) Prospective randomized study comparing cryo-assisted and needle-wire localization of ultrasound-visible breast tumors. The American Journal of Surgery 192 (4):462-470

28. Bakhshandeh M, Tutuncuoglu SO, Fischer G, Masood S (2007) Use of imprint cytology for assessment of surgical margins in lumpectomy specimens of breast cancer patients. Diagnostic Cytopathology 35 (10):656-659. doi:10.1002/dc.20704

29. Nitin N, Carlson AL, Muldoon T, El-Naggar AK, Gillenwater A, Richards-Kortum R (2009) Molecular imaging of glucose uptake in oral neoplasia following topical application of fluorescently labeled deoxy-glucose. Int J Cancer 124:2634-2642.

30. Strong V, Humm J, Russo P, Jungbluth A, Wong W, Daghighian F, Old L, Fong Y, Larson S (2008) A novel method to localize antibody-targeted cancer deposits intraoperatively using handheld pet beta and gamma probes. Surgical Endoscopy 22 (2):386-391. doi:10.1007/s00464-007-9611-3

31. Langsner RJ, Middleton LP, Sun J, Meric-Bernstram F, Hunt K.K., Drezek R.A. , Yu TK. (2011) Wide-field imaging of fluorescent deoxy-glucose in *ex vivo* malignant and normal breast tissue. Biomedical Optics Express 2(6): 1514-1523

32. Nitin N, Rosbach KJ, El-Naggar A, Williams M, Gillenwater A, Richards-Kortum R (2009) Optical Molecular Imaging of Epidermal Growth Factor Receptor Expression to Improve Detection of Oral Neoplasia. Neoplasia 11(6):542-551.

33. Aaron J, Nitin N, Travis K, et al. (2007) Plasmon resonance coupling of metal nanoparticles for molecular imaging of carcinogenesis in vivo. J Biomed Opt 12(3):034007. doi:10.1117/1.2737351

34. van de Ven A, Adler-Storthz K, Richards-Kortum R (2009) Delivery of optical contrast agents using Triton-X100, part 1: reversible permeabilization of live cells for intracellular labeling. J Biomed Opt 14(2):021012. doi:10.1117/1.3090448

35. van de Ven A, Adler-Storthz K, Richards-Kortum R (2009) Delivery of optical contrast agents using Triton-X100, part 2: enhanced mucosal penetration for the detection of cancer biomarkers. J Biomed Opt 14(2):021013. doi:10.1117/1.3090437

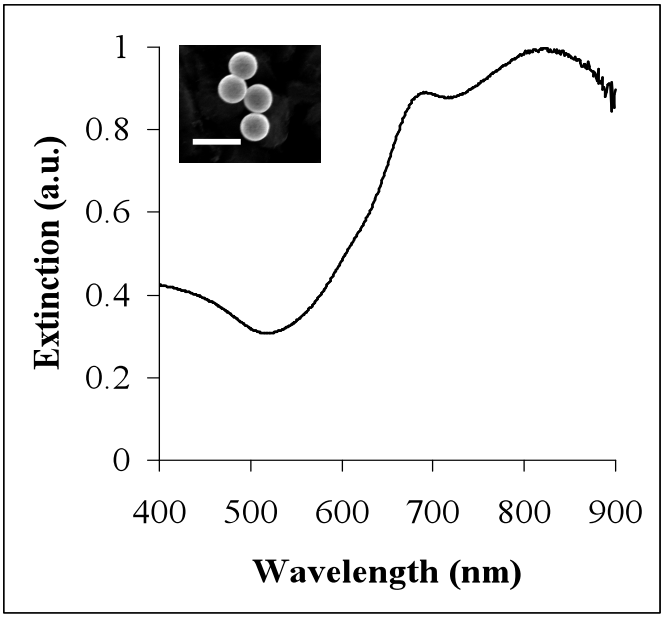
1
0.8
0.6
0.4
0.2
0
Extinction (a.u.)
400
500
600
700
800
900
Wavelength (nm)

Fig. 1

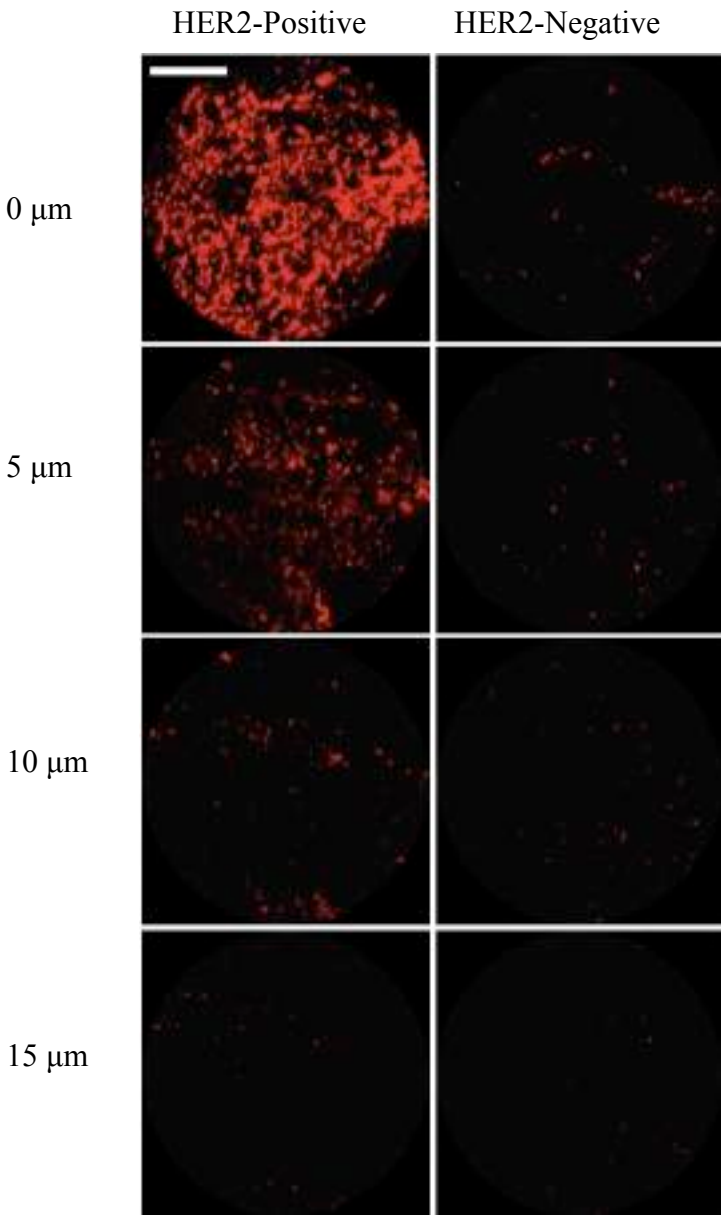

Fig. 2

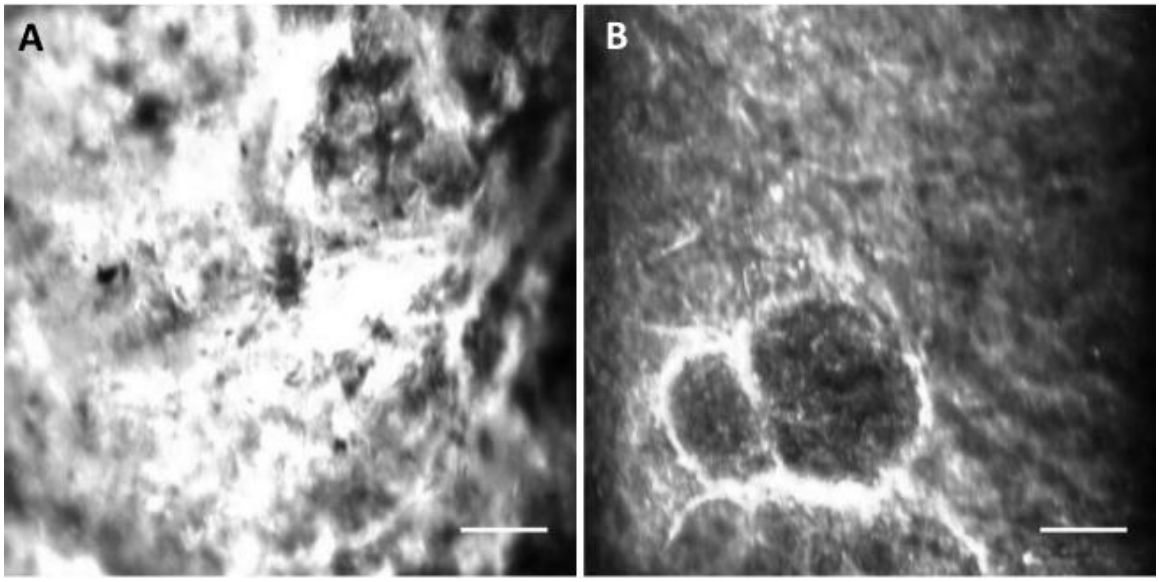
A
B

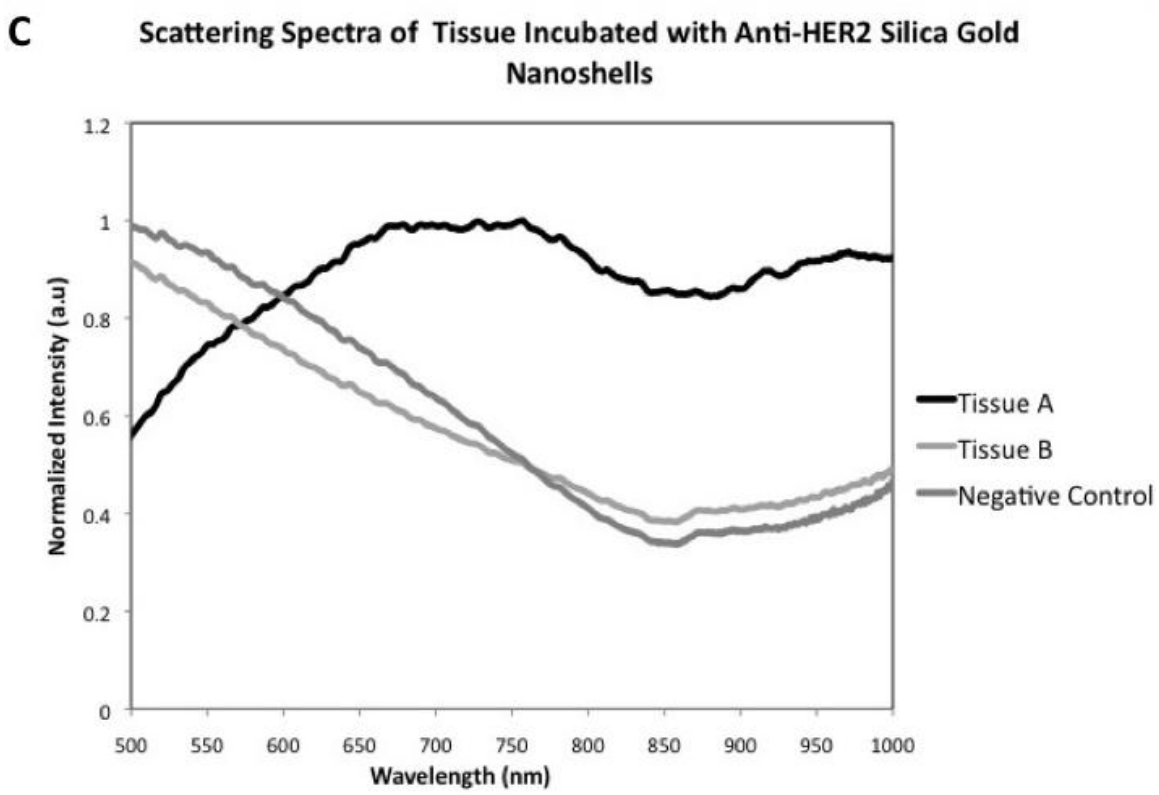
C
Scattering Spectra of Tissue Incubated with Anti-HER2 Silica Gold Nanoshells
Normalized Intensity (a.u)
1.2
1
0.8
0.6
0.4
0.2
0
500
550
600
650
700
750
800
850
900
950
1000
Wavelength (nm)
Tissue A
Tissue B
Negative Control

Fig. 3

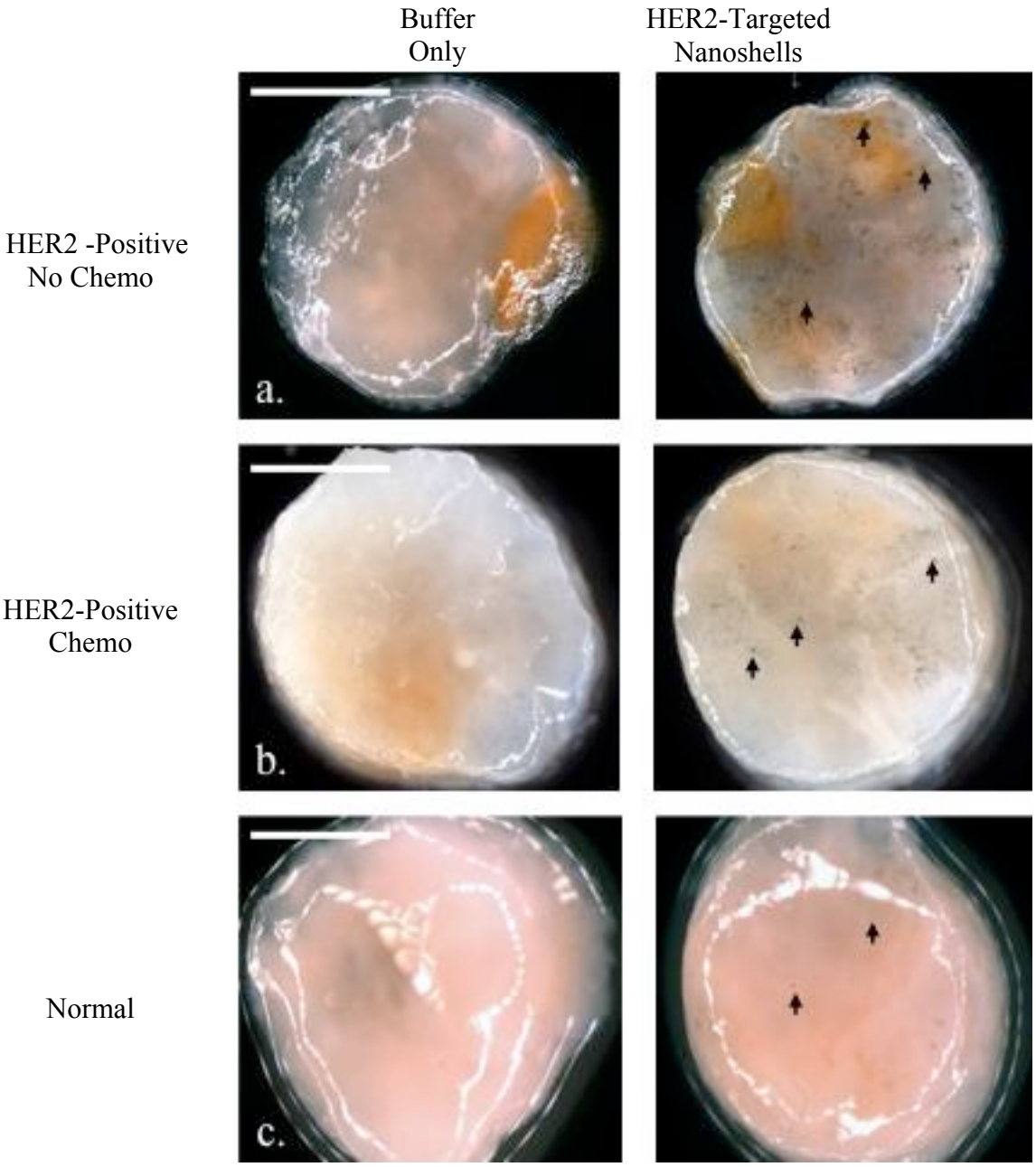
Buffer Only
HER2-Targeted Nanoshells
HER2 -Positive No Chemo
HER2-Positive Chemo
Normal
a.
b.
c.

Fig. 4

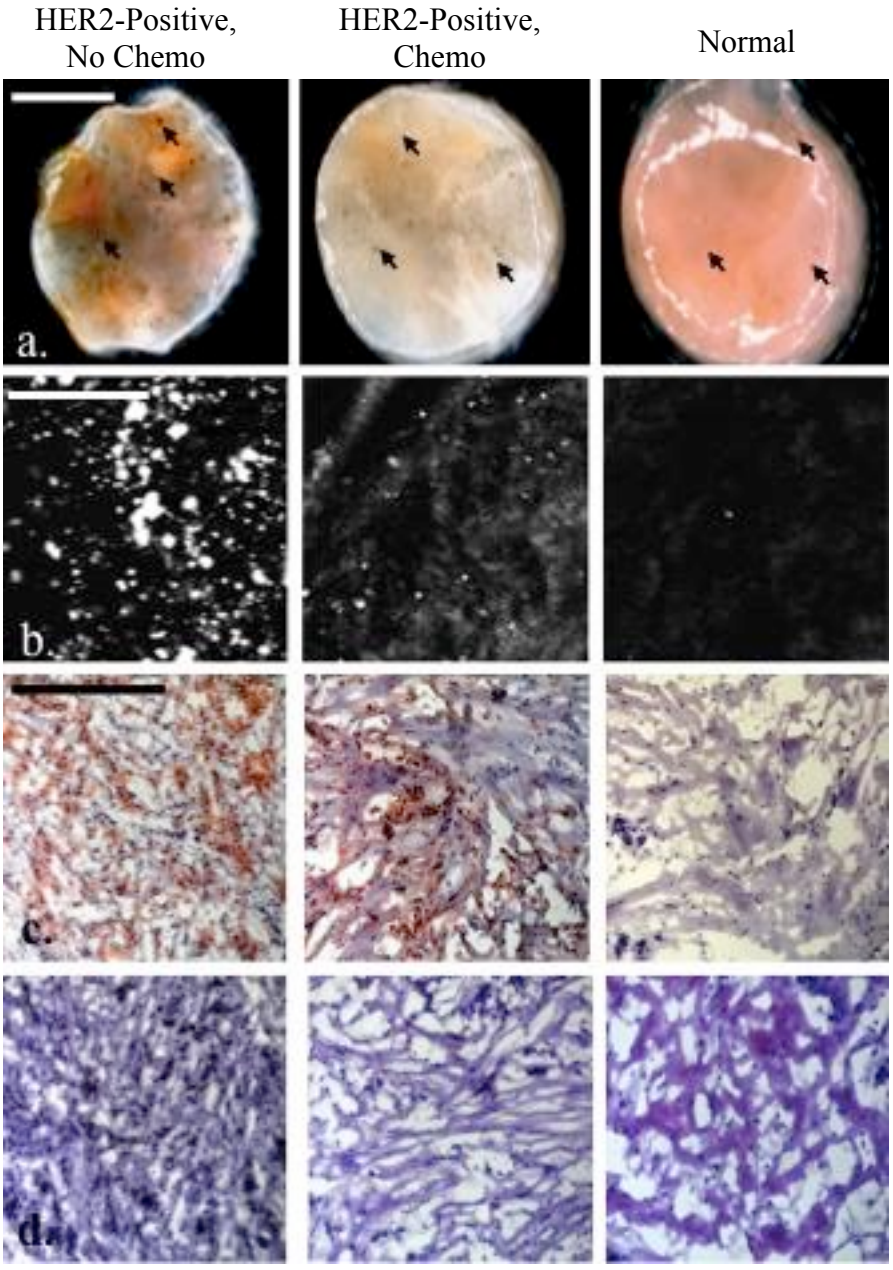

Fig. 5

Nanoscale Research Letters
a SpringerOpen Journal

NANO EXPRESS Open Access

Size-controlled synthesis of monodispersed gold nanoparticles via carbon monoxide gas reduction

Joseph K Young[1], Nastassja A Lewinski[2†], Robert J Langsner[2†], Laura C Kennedy[2], Arthi Satyanarayan[3], Vengadesan Nammalvar[2], Adam Y Lin[2] and Rebekah A Drezek[1,2*]

Abstract

An in depth analysis of gold nanoparticle (AuNP) synthesis and size tuning, utilizing carbon monoxide (CO) gas as a reducing agent, is presented for the first time. The sizes of the AuNPs are tunable from ~4 to 100 nm by altering the concentration of $HAuCl_4$ and inlet CO gas-injection flow rate. It is also found that speciation of aqueous $HAuCl_4$, prior to reduction, influences the size, morphology, and properties of AuNPs when reduced with CO gas. Ensemble extinction spectra and TEM images provide clear evidence that CO reduction offers a high level of monodispersity with standard deviations as low as 3%. Upon synthesis, no excess reducing agent remains in solution eliminating the need for purification. The time necessary to synthesize AuNPs, using CO, is less than 2 min.

Background

Metallic nanoparticles have attracted substantial attention due to their distinctive properties and various applications. AuNPs can exhibit a strong optical response to the extinction of surface plasmons by an alternating electromagnetic field [1]. By simply adjusting the size of the gold nanoparticles, this optical resonance can be positioned over hundreds of nanometers in wavelength across the visible into the near infrared spectrum [1,2]. Since these oscillations are located on the boundary of the metal and the external medium, these waves are very sensitive to changes in this boundary, such as the absorption of molecules to the metal surface [3]. These features render AuNPs useful as building blocks, and pave the way for fabricating biological labels, biological sensors, environmental detection of biological reagents, and clinical diagnostic technologies [4-6]. Many researchers have also exploited the unique optical properties of AuNPs for biomedical applications, such as thermal ablative cancer therapy and gene therapy [7-9].

Since the plasmon-derived optical resonance of gold nanoparticles is strongly related to the dimensions and morphology of the nanoparticles, the ability to synthesize monodispersed AuNPs is essential. The most popular and reliable method of producing AuNPs is an aqueous phase synthesis, which relies on the reduction of tetrachloroauric acid in the presence of a reducing agent to form colloid [10-15]. A number of different reducing agents can be used for the tetrachloroauric acid reduction. These agents have a significant influence on the morphology of the final product, and most of them lead to polydispersed nanoparticle solutions. To date, only a few methods have been established to synthesize AuNPs from about one nanometer to several hundred nanometers in diameter. A widely used method is based on the reduction of tetrachloroaurate ions in water using sodium citrate as a reductant to obtain AuNPs with diameters ranging from 16 to 147 nm [2,16,17]. While this method has demonstrated good quality control over particle size, a high level of monodispersity is limited to the synthesis of larger particles typically in the range of 22 to 120 nm. Another disadvantage to this synthesis method is that excess citrate remains in the solution. The residual citrate, which acts as a passivation layer on the surface of the nanoparticles, can reduce the effectiveness of surface functionalization with other biological markers [18].

Smaller-sized AuNPs, 1 to 5 nm, are usually prepared by borohydride reduction in the presence of thiol capping agents [19]. Disadvantages of this method include the use of toxic organic solvents and the potential presence of impurities introduced by using capping agents, which can also hinder the surface modification and functionality of particles for particular applications [20]. Also, AuNPs have been synthesized using formaldehyde as a reducing

* Correspondence: drezek@rice.edu
† Contributed equally
[1]Department of Electrical and Computer Engineering, Rice University, MS-366, 6100 Main St., Houston, TX 77005, USA
Full list of author information is available at the end of the article

agent. One disadvantage is that formaldehyde is toxic, and the excess formaldehyde in the solution leads to solution instability and eventual particle aggregation [13].

Non-chemical based reduction methods, to synthesize AuNPs, have also been employed. Size-selected AuNPs have been synthesized by use of laser irradiation in a surfactant based aqueous environment [21]. Yet this method limits AuNPs sizes to sub 10 nm diameters. Meunier et al. were able to synthesize gold nanoparticles from 3 to ~80 nm via a femtosecond laser-assisted method [22]. An involved multi-step process, including a seeding step, was necessary to produce the larger particles. This process requires a complicated femtosecond laser setup and nanoparticle synthesis was also dependent on polymer utilization. Dispersed AuNPs were also synthesized using glow discharge plasma [23-26]. Researchers showed that this method can produce particles in less than 5 min yet these particles were limited to ~4 nm diameters [26]. Takai et al. used discharge plasma to produce larger AuNPs of irregular shapes [24]. Polydispersed spherical AuNPs, ~20 nm in diameter, were only produced after exposure times greater than 45 min.

As compared to the current synthesis methods, CO has an advantage in that no excess reducing agent remains in solution. This eliminates the need for purification via multiple centrifugation steps. The reduction of $HAuCl_4$ with CO can also take place at room temperature, unlike other methods such as citrate reduction that require boiling of the solution. The time necessary to produce AuNPs using CO is less than 2 min compared to 20 min for comparable particle sizes using citrate reduction and 45 min for discharge plasma synthesis. CO reduction offers a cheap and flexible alternative to femtosecond laser-based AuNP synthesis processes while eliminating the need for surfactants and polymers to tune the nanoparticle sizes. To the best of our knowledge, there has never been an in depth study of AuNP synthesis, utilizing CO as a reducing agent, to enable size tuning from sub 5 to 100 nm diameters.

In this paper, an in depth analysis of AuNP synthesis utilizing CO gas as a reducing agent is presented. After synthesis, AuNP mono- and polydispersity was examined. The size and monodispersity of the AuNPs were tunable by controlling variables such as $HAuCl_4$ concentration and gas flow during synthesis. The CO reduction method offered excellent tunability over a broad range of sizes while maintaining a high level of monodispersity. Ensemble extinction spectra and TEM images provide clear evidence that CO reduction offers excellent AuNP tunability and is a viable alternative to other synthesis methods.

Results and discussion

AuNPs, synthesized by CO reduction, with average diameter ranging from 4 to 52 nm, were prepared as described below. A set of solutions consisting of $HAuCl_4$ concentrations ranging from 0.01 mM up to 0.09 mM was used. Each $HAuCl_4$ concentration was duplicated to ensure reproducibility. For each $HAuCl_4$ concentration, five 40 mL samples were prepared. Each sample was aerated at different flow rates controlled by a control valve. The five solutions were exposed to CO gas at flow rates of 16.9, 25.45, 31.59, 37.0, and 42.9 mL/min, respectively. The effect of stirring speed was examined, and it was found that the number of revolutions per minute (rpm), by which the solution was stirred, played a role in particle size and morphology. The optimal stir speed, for producing the most monodispersed particles, was found to be 500 rpm. For the following discussion, each solution was constantly stirred at a rate of 500 rpm during synthesis unless noted otherwise. Additionally, the effect of gas-injection flow rates and diffuser pore size on nanoparticle monodispersity and reaction completion times were investigated. It was found that a 60-μm average diffuser pore size was sufficient for producing monodispersed particles. The solution temperature, prior to aeration, was maintained between 20 and 22°C.

Formation of colloidal gold

The Au^{3+} reduction, by CO, to Au^0 takes place via a number of redox reactions. When the CO gas is introduced into the aqueous $HAuCl_4$ solution, electrons are donated to the $[AuCl_4]^-$ ions. For $[AuCl_4]^-$ ions to be reduced to gold atoms, a series of redox reactions take place. This includes the liberations of Cl^- ions and is described by Equations 1 and 2.

$$AuCl_4^- + 2e^- \rightarrow AuCl_2^- + 2Cl^- \quad (1)$$

$$AuCl_2^- + e^- \rightarrow Au^0 + 2Cl^- \quad (2)$$

The electrons are contributed from the reaction of CO and dihydrogen monoxide and the reducing half reactions are given in Equations 3 and 4.

$$CO(g) + H_2O \rightarrow CO_2(aq) + 2e^- + 2H^+ \quad (3)$$

$$CO(g) + 2H_2O \rightarrow HCO_3^- + 2e^- + 3H^+ \quad (4)$$

The thermodynamics of $HAuCl_4$ reduction in aqueous solutions using CO is presented (see Additional file 1).

Synthesis of AuNPs

To illustrate the effects of CO gas flow injection rates on nanoparticle synthesis, nanoparticles were synthesized from an aqueous solution of $HAuCl_4$ acid at a concentration of 0.01 mM. Even at this lower concentration, which is normally not used for the synthesis of AuNPs, the extinction spectra is clearly visible and well

formed as evident in Figure 1. A smoother, more pronounced spectrum was generated at the minimum flow rate of 16.9 mL/min when compared to the other injection flow rates. As the flow rate was increased from 16.9 to 42.9 mL/min the change in spectral symmetry was clearly visible. TEM micrographs of the corresponding nanoparticles are displayed in Figure 1. The gas-injection flow rate of 16.9 mL/min produced individual nanoparticles compared to the other injection rates. The nanoparticles produced by the 16.9 mL/min flow rate ranged in size from 5 to 11 nm in diameter. A flow rate of 25.45 mL/min, Figure 1B, produced nanoparticle aggregates and irregularly shaped particulate matter. Nanoparticles synthesized at a flow rate of 31.59 mL/min consisted of aggregated particle chains. A CO flow rate of 37 mL/min (Figure 1C) resulted in aggregated particle chains similar to that of nanoparticles produced at a flow rate of 25.45 mL/min. The particle aggregation in Figure 1B, D was evident by the broad spectral band. As the flow rate increased to 42.9 mL/min, the nanoparticles became elliptical in shape and very polydispersed. The nanoparticle sizes, when aerated at 42.9 mL/min, ranged from 5 to 40 nm in diameter with some aggregated particles; this size distribution is reflected in the broad spectral band.

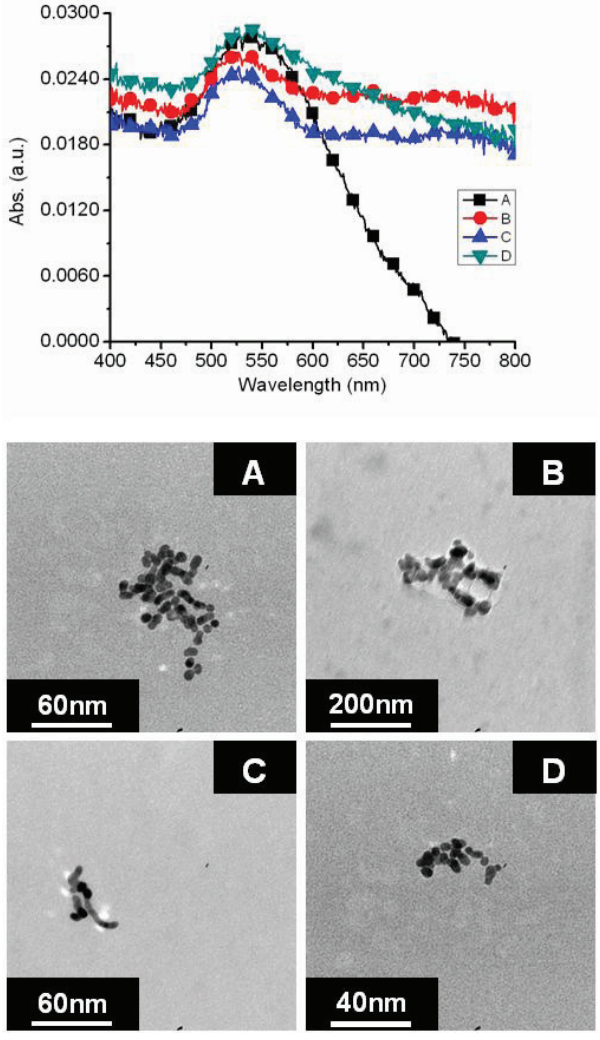

Figure 1 Effect of CO flow rate on nanoparticle morphology. UV-visible extinction spectra of nanoparticles synthesized from a chloroauric acid concentration of 0.01 mM aerated at flow rates of 16.9, 25.5, 37.0, and 42.9 mL/min corresponding to A, B, C, and D, respectively, with accompanying TEM micrographs. A smoother, more pronounced spectrum was generated at the minimum flow rate of 16.9 mL/min when compared to the other injection flow rates. As the flow rate was increased from 16.9 to 42.9 mL/min the change in spectral symmetry was clearly visible.

Increasing the chloroauric acid concentration reduced the polydispersity of the nanoparticles, yet the gas-injection flow rate continued to influence the AuNP size distribution profiles. Figure 2 shows the UV-visible spectra of AuNPs synthesized from a chloroauric acid concentration of 0.03 mM at flow rates of 16.9, 25.5, and 37.0 mL/min (Figure 2A, B, C). The polydispersity of the AuNPs aerated at 16.9 mL/min (Figure 2A) is represented by a broad particle distribution curve. The particle sizes for Figure 2A ranged from 2.5 to 17 nm in diameter. Increasing the CO flow reduced the width of the particle distribution curve where an optimum inlet gas flow was obtained at 25.5 mL/min (Figure 2B). The standard deviation for 2B was 7%, well below the 13 to 15% normally obtained for comparable sizes via citrate reduction [3]. To confirm the formation of Au atoms from $HAuCl_4$, the valence state of Au was identified by X-ray photoelectron spectroscopy (XPS). Figure 3 shows an XPS spectrum of AuNPs synthesized via CO gas reduction. The Au $4f_{7/2}$ peak appeared at a binding energy of 83.98 eV and the Au $4f_{5/2}$ peak appeared at a binding energy of 87.71 eV. This indicates the formation of metallic gold [27,28]. These particles remained stable in excess of 12 months when stored at 4°C.

A better understanding of the effect of the gas flow rates and chloroauric acid concentrations on nanoparticle synthesis can be obtained by considering the mechanisms involved in nanoparticle nucleation and growth. When aerating the aqueous $HAuCl_4$ solution with CO gas, the precursor concentration increases continuously with increasing time. As the concentration reaches supersaturation, nucleation takes place and leads to a decrease in concentration. The continued decrease of the concentration is due to the growth of the particles. During the growth process, two growth mechanisms could take place or a combination of the two. The first growth mechanism is due to the formation of particles from coalescence of the nuclei only. The second growth mechanism is due to the coalescence of nuclei into simple and multiple twins with further growth from monomer attachment of Au atoms on the surface [16].

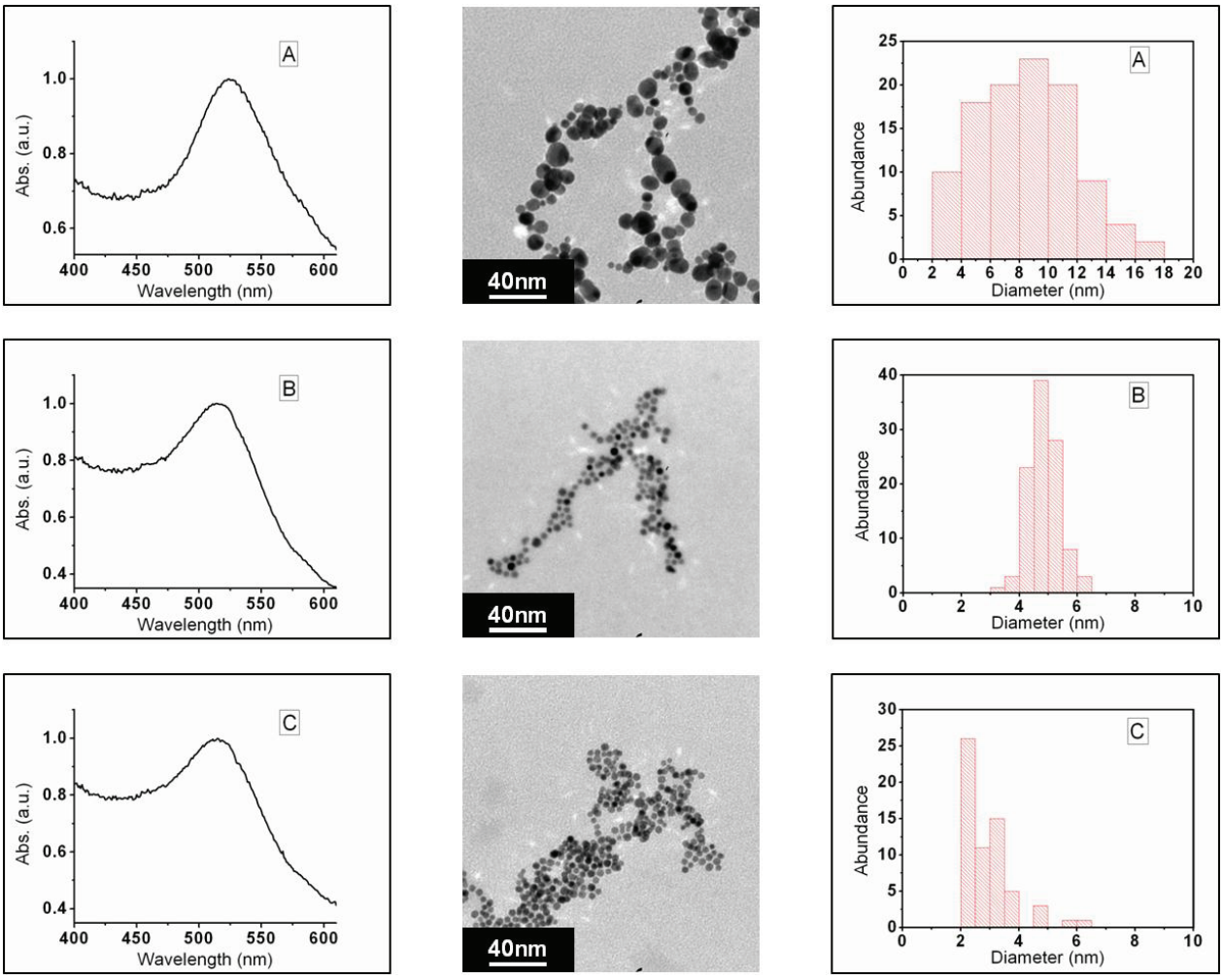

Figure 2 Effect of CO flow rate on nanoparticle distribution. UV-visible extinction spectra of nanoparticles synthesized from a chloroauric acid concentration of 0.03 mM aerated at flow rates of 16.9, 25.5, and 37.0 mL/min corresponding to A, B, and C, respectively, with accompanying TEM micrographs and histograms.

To produce monodispersed AuNPs with CO gas, the rate of nucleation must be high enough so that the precursor concentration does not continue to climb. Instead a large amount of nuclei are formed in a short period. Turkevich et al. found that the nucleation process consists of a polymerization step [29]. When the aqueous $HAuCl_4$ solution is neutral or acidic, the nucleus is formed by gold organic polymer. While the aqueous $HAuCl_4$ solution is alkaline, a polymerization of gold hydroxide takes place [16,30]. The rate of growth of these nuclei should be fast enough to decrease the concentration below the nucleation concentration rapidly. This results in the creation of a limited number of seed particles. The rate of growth must be slow enough that the growth period is long compared with the nucleation period. This produces AuNPs with narrowed size distributions which are the result of the limited nucleation period.

Factors affecting AuNP synthesis

Since the morphology is found to depend strongly on injection flow rates and $HAuCl_4$ concentrations, a relationship between the $HAuCl_4$ concentration and gas-injection flow rates on particle monodispersity can be found. Solution stir speeds during synthesis were examined and it was found that stir speeds had an effect on synthesis and played a role in nanoparticle size disparities. Slow solution stir speeds had the biggest affect on solutions aerated at a flow rate of 16.9 mL/min or below. Increasing the stir speed of the solution aided in the solubility and dispersal of the CO gas molecules during synthesis. It was found that adjusting the gas-injection flow rate compensated for a reduction or increase in solution stir speed. The gas diffuser pore size affected the synthesis process considerably when the solution was at a standstill or stirred at a relatively slow speed below

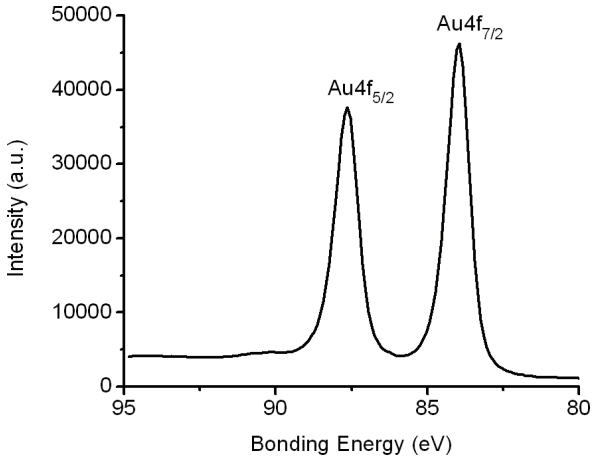

Figure 3 XPS spectrum of AuNPs synthesized via CO gas reduction. The Au $4f_{7/2}$ peak appeared at a binding energy of 83.98 eV and the Au $4f_{5/2}$ peak appeared at a binding energy of 87.71 eV. This indicates the formation of metallic gold [27,28].

75 rpm. Once the solution stir speed approached and/or crossed the 75 rpm threshold, injection-hole size produced only small variances. Once the stir speed reached 500 rpm, there was no difference between samples produced with different diffuser pore sizes, and only the Au concentration or gas-injection flow rates affected particle sizes. Therefore, the solution stirring speed was maintained at 500 rpm to isolate the gas-injection flow rate and Au concentration effect on nanoparticle synthesis.

A chloroauric concentration of 0.03 mM and an inlet gas flow of 16.9 mL/min stirred at 500 rpm resulted in coalescence and growth of nanoparticles before the nucleation reached equilibrium. In essence, the induction period was initiated with a slow autocatalytic rise in the number of nuclei due to the lack of sufficient reducing agent in the solution. Because of this slow nucleus formation, new nuclei were being formed while existing nuclei had already undergone coalescence resulting in polydispersity. Increasing the flow rate to 25.5 mL/min increased the autocatalytic rise in the number of nuclei. Particle growth took place after cessation of the nucleation process resulting in monodispersity. This is illustrated by the fact that the particle distribution curve for Figure 2B consisted of particle sizes in the range of 4 to 6 nm as opposed to the range of 2 to 17 nm (Figure 2A). By increasing the flow rate further (Figure 2C), rapid coalescence of the nuclei takes place. The resulting polydispersity of the sol at increased gas-injection flow rates is still marginal compared to the lower flow rate of 16.9 mL/min. When comparing the spectra of Figure 2A, B, C the more polydispersed sample possesses a broadened spectrum. This is illustrated in more detail (see Additional file 2).

Increasing $HAuCl_4$ concentration

When the chloroauric acid concentration approached 0.2 mM, the gas-injection flow rate had a less pronounced effect on the spectra symmetry yet the flow rate continued to dictate the monodispersity of the particles. When particles were synthesized from a chloroauric acid concentration of 0.3 mM, the most monodispersed sample was produced at a flow rate of 25.5 mL/min. The mean diameter for this sample was 9 nm with a standard deviation of 11%.

As the concentration increased to 0.5 mM, 20 to 25 nm particles were produced. Continual increase of the chloroauric acid concentration beyond 0.5 to 0.6 mM only produced small changes in nanoparticle size with increased absorbance. The standard deviation for the AuNPs produced at 0.6 mM was 8% indicating monodispersity. As the concentration was increased to 1 mM, nanoparticles approaching 30 nm in diameter were produced but the standard deviation approached 20%. Further doubling the concentration to 2 mM had no uniform effect on particle growth, with the majority of the particles in the 30 nm size regime and some of the particles in the 40 to 55 nm size regime with a standard deviation approaching 35%. The UV-visible spectra of the sol prepared at different concentrations (Figure 4), increasing from 0.02 to 1 mM, shows an increase in absorbance which correlates to an increase in particle concentration and volume. Figure 5 shows the pronounced red shifting of the plasmon, which is associated with increased nanoparticle size. The red shift of the plasmon is further illustrated (see Additional file 3). This shifting effect is in line with the prediction described by Mie theory [1,2]. The statistical analysis of

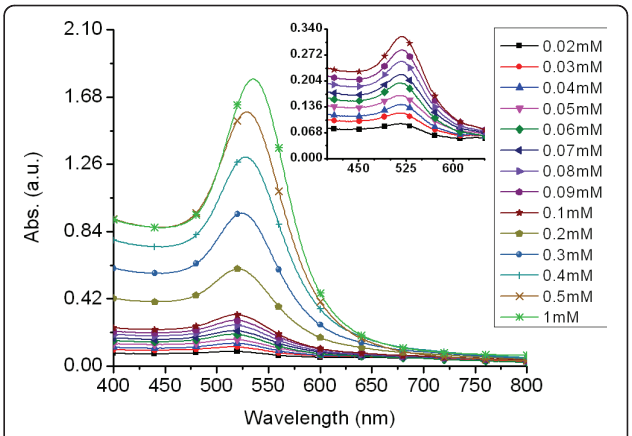

Figure 4 Effect of increasing chloroauric acid concentrations on nanoparticle spectral profile. UV-visible spectra of gold nanoparticles with increasing chloroauric acid concentrations from 0.02 to 0.05 mM in 0.01 mM increments, from 0.1 to 0.5 mM in .1 mM increments, and at 1 mM. The inset is the absorbance spectra of gold nanoparticles produced from concentrations of 0.02 to 0.1 mM.

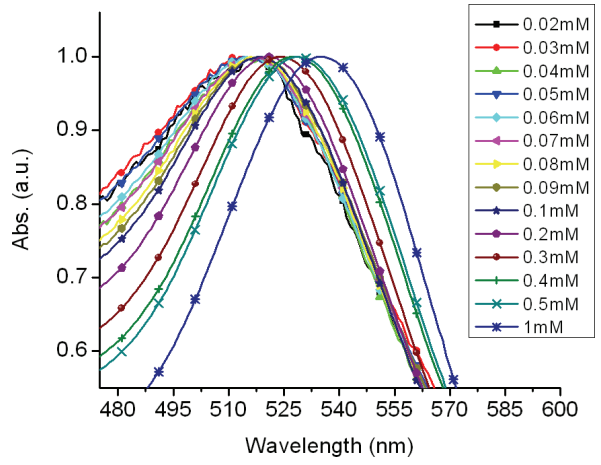

Figure 5 Spectral shift based on chloroauric acid concentrations. Normalized UV-visible spectra of gold nanoparticles with increasing chloroauric acid concentrations from 0.02 to 0.05 mM in 0.01 mM increments, from 0.1 to 0.5 mM in 0.1 mM increments, and at 1 mM. A red-shifting of the plasmon is observed as the chloroauric acid concentration is increased.

the particles synthesized from aqueous solutions of $HAuCl_4$ ranging from 0.02 to 0.6 mM revealed an average standard deviation of approximately 11%.

Influence of pH on AuNP synthesis

It is known that pH is a factor influencing the nucleation and growth of AuNPs [13,16,30]. Since the synthesis process takes place in an acidic environment, the particle is formed from gold polymer with a small contribution from gold hydroxide polymer reduction. As the concentration of chloroauric acid increases, the pH of the solution decreases (see Additional file 4) resulting in particle formation solely by gold polymer reduction. In an acidic environment, the effective monodispersed particle size threshold was reached at approximately 25 nm. The effective monodispersed threshold was defined as a standard deviation below 13%. As previously mentioned, continual increase of the chloroauric concentration eventually resulted in adverse affects on nanoparticle monodispersity. To further grow particles and maintain monodispersity, $HAuCl_4$ hydrolysis was explored. The addition of potassium carbonate (K_2CO_3) to generate an alkaline solution for gold hydroxide polymer reduction was systematically investigated. It was found that the speciation of $HAuCl_4$ had great influence on the size and monodispersity of the AuNPs. As the pH increased, speciation of aqueous $HAuCl_4$ occurred.

Adding K_2CO_3 raised the pH of the solution by allowing hydrolysis of $HAuCl_4$ to take place to form gold hydroxide solution. A 200 mL aqueous $HAuCl_4$ solution, with a concentration of 0.1 mM, was prepared by adding fresh gold to 200 mL of DI water. This solution was aged in an amber bottle, and light protected in a 4°C environment for a minimum of 72 h prior to use. A 0.5 N stock solution of K_2CO_3 was prepared and stirred for a minimum of 1 h. After aging, the chloroauric acid solution was allowed to gradually rise to 22°C. The pH was measured to be 3.6. $HAuCl_4$ (0.1 mM) aqueous solution with various pH values were prepared by the addition of K_2CO_3 aqueous solution into 20 mL of $HAuCl_4$ aqueous solution and shaken vigorously for a minimum of 1 min. This solution was allowed to age for 15 min before introduction of CO gas. The pH values of the aqueous solutions, measured prior to reduction, ranged from 4.25 to 11.4.

Figure 6 shows UV-visible absorption spectra of AuNPs prepared by reduction of hydrolyzed $HAuCl_4$ at various pH. At pH = 4.25, the acquired AuNPs exhibited a symmetric spectrum with a surface plasmon resonance (SPR) peak at 512 nm. When the pH increased to 6.6, there was a SPR shift to 527 nm. When the pH increased to 7.45, the SPR peak position did not change much at 528 nm, and the SPR peak remained symmetric. The SPR feature changed abruptly when the pH was 9.34 showing a broad feature originating at 559 nm. The SPR peak red-shifted further when the pH increased to 10.3. Absorption in the NIR region also gained significant intensity.

Previous experimental and theoretical results demonstrated that $AuCl_4$ undergoes a pH-dependant stepwise hydrolysis which gives way to $[AuCl_x(OH)_{4-x}]^-$ [30,31]. The extent of hydrolysis in turn depends on the pH which gives an indication of the amount of OH^- available for hydrolysis. When the pH is low, $[AuCl_4]^-$ ions dominate the solution. As the pH is increased to 4.25, $[AuCl_4]^-$ concentration is lowered and the contribution

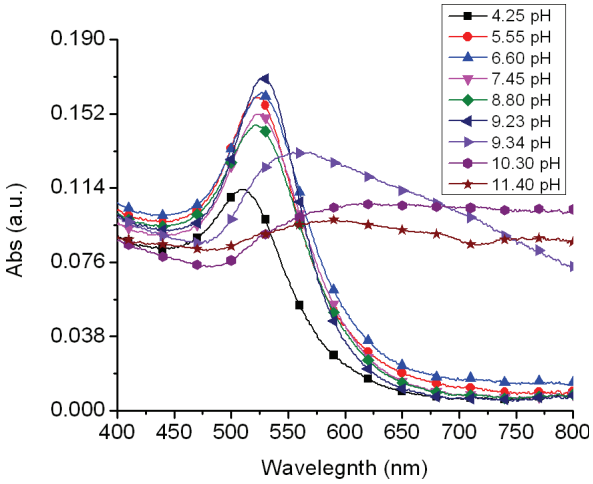

Figure 6 Effect of pH on nanoparticle spectrum. UV-visible spectra of AuNPs produced from a 0.1 mM $HAuCl_4$ aqueous solution synthesized at varying pH values.

from $[AuCl_3(OH)]^-$ ions is increased. Raising the pH of the solution to 6.66 reduced the concentration of $[AuCl_4]^-$ and $[AuCl_3(OH)]^-$ significantly, and the ionic composition was primarily made up of $[AuCl_2(OH)_2]^-$ ions. Further increasing the pH to 8.8 resulted in large ion contribution from $[AuCl(OH)_3]^-$ ions. Additional increase to 10.3 resulted in an overwhelming ion contribution from $[Au(OH)_4]^-$ ions with an appreciable contribution from $[AuCl(OH)_3]^-$ ions. This was because $[Au(OH)_4]^-$ is amphoteric. Its solubility increased due to the formation of $[Au(OH)_4]^-$ at higher pH, thus making the soluble $[Au(OH)_4]^-$ the most dominant species at high pH instead of the precipitating $[AuCl(OH)_3]^-$ [30]. It is the control of hydrolysis to tune the speciation of $[AuCl_x(OH)_{4-x}]^-$ that subsequently influenced the nanoparticle size.

It was observed that amongst the six species of $[AuCl_x(OH)_{4-x}]^-$ discussed earlier, $[Au(OH)_4]^-$ seems to have the lower tendency to be reduced in solution to form colloidal gold. This was evident from its slow and gradual color change when reduced, taking approximately 7 min for complete reduction to occur. This was in contrast to the reduction of other $[AuCl_x(OH)_{4-x}]^-$ species formed at lower pH where it was observed that the addition of CO gas caused a color change within seconds and total reduction within approximately 2 min. This observation may possibly be attributed to a weaker reduction potential of $[Au(OH)_4]^-$ compared to other species. It was found that adjustment to pH < 10 by addition of smaller amounts of K_2CO_3 resulted in the formation of other dominant species that had greater tendency to be reduced in solution to form colloidal gold. It was observed that the synthesis environment also affected nanoparticle stability. The stability of the nanoparticles was monitored for approximately 2 months to examine the pH effect on nanoparticle stability. As the pH increased, prior to synthesis, the nanoparticles became less stable. Table 1 illustrates the stability of the AuNP solutions produced at varying pH.

It was observed that hydrolysis of $[AuCl_4]^-$ started to occur within minutes after the addition of K_2CO_3 indicating immediate formation of the $[AuCl_x(OH)_{4-x}]^-$ species. It was further observed that Au colloid, of varying sizes, were produced when K_2CO_3 and $HAuCl_4$ concentrations and gas-injection flow rates remained constant and only aging times varied. This indicated that aging the gold hydroxide solution, before the addition of CO gas, had a strong influence on the outcome of the reaction.

By controlling the development of the $[AuCl_x(OH)_{4-x}]^-$ species, colloids of various sizes can be synthesized using CO as a reducing agent. When the pH is sufficiently high, the resultant aging process can generate coalescence of $Au(OH)_4$ initiating a limited nucleation process absent of a reducing agent. This nucleation process is out of favor with the requirements necessary for generating monodispersed nanoparticles. Thus proper aging times must be determined to synthesize monodispersed nanoparticles of a particular size from a given K_2CO_3 and $HAuCl_4$ concentration. Exploiting the control of $[AuCl_x(OH)_{4-x}]^-$ species development, by addition of K_2CO_3 and aging of the solution, Au colloid in the ranges of 15 to 100 nm in diameter were produced. Spectra A and B in Figure 7 show the UV-visible spectra of Au colloid produced from a mixture of 200 mL 0.38 mM $HAuCl_4$ aqueous solution and K_2CO_3 (2.71 mM) aged at 30 and 40 min, respectively, in solution reduction volumes of 40 mL. Both SPR peaks were well ordered with a SPR peak at 536 nm for the 30-min aged solution and 546 nm for the 40-min aged solution. Both solutions were aerated with CO gas at an inlet gas flow rate of 25.5 mL/min. The red-shift and dampening of the SPR peak indicated an increase in particle size. The effect of the solution volume being aerated was explored to determine if the amount of solution being aerated had an effect on nanoparticle size and monodispersity. Spectra C, D, and E in Figure 7 were produced from AuNPs synthesized from a 200 mL 0.38 mM $HAuCl_4$ aqueous solution with K_2CO_3 (3.62 mM) aged for

Table 1 Influence of pH upon stability of AuNPs

pH Before synthesis	pH After synthesis	Color	Stability After 1 h stored at 22°C	Stability After 6 h stored at 22°C	Stability After 2 months Stored at 4°C
4.25	3.72	Light pink	Stable	Stable	Small aggregation
4.25	3.72	Light pink	Stable	Stable	Small aggregation
5.55	4.75	Light red	Stable	Stable	Small aggregation
6.6	5.92	Light red	Stable	Stable	Stable
7.45	6.11	Light red	Stable	Stable	Stable
8.8	6.42	Light red	Stable	Stable	Stable
9.23	6.55	Medium red	Stable	Stable	Stable
9.34	6.32	Purple	Stable	Stable	Medium aggregation
10.3	8.10	Blue	Stable	Some aggregation	Heavy aggregation
11.4	10.96	Light blue	Crashed	Crashed	Crashed

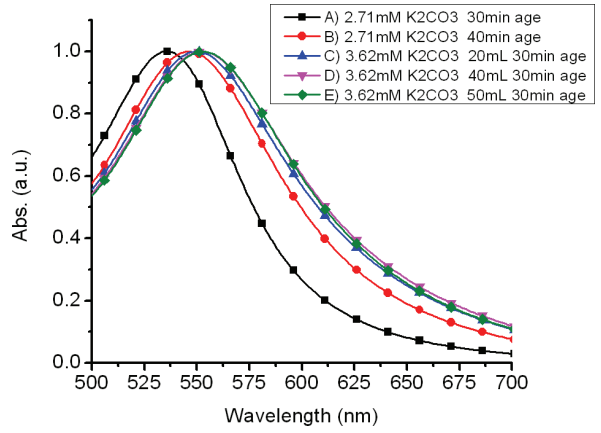

Figure 7 Nanoparticle spectra as a function of K_2CO_3 concentration and aging. UV-visible spectra of AuNPs produced from a mixture of 0.38 mM $HAuCl_4$ aqueous solution with 2.71 mM or 3.62 mM K_2CO_3. A and B are 2.71 mM K_2CO_3 aged at 30 and 40 min, respectively, at an aeration volume of 40 mL. C, D, and E are 3.62 mM K_2CO_3 aged for 30 min each at aeration volumes of 20, 40, and 50 mL, respectively. All samples were aerated at a gas flow rate of 25.5 mL/min.

30 min. The aeration volumes were 20, 40, and 50 mL, respectively. The amount of solution aerated had a small but noticeable effect on SPR peak position. The resulting SPR peak positions were 550, 553, and 554 nm for aeration volumes of 20, 40, and 50 mL, respectively. Increasing the amount of K_2CO_3, in a $HAuCl_4$ aqueous solution of known concentration, while decreasing the aging time, produced larger AuNPs while still maintaining monodispersity. Aqueous solutions of 200 mL 0.38 mM $HAuCl_4$ with 2.71 and 3.62 mM of K_2CO_3 aged for 30 min each produced AuNPs with SPR peak positions at 536 and 553 nm, respectively.

By employing a combination of gold polymer reduction and gold hydrolyzed polymer reduction, particles sizes from ~4 to 100 nm can be synthesized. Figure 8 shows a TEM micrograph illustrating the different sizes available using CO as a reducing agent. Figures 8A, B, C, D are TEM images of AuNPs synthesized without the addition of K_2CO_3. Figures 8E, F are AuNPs synthesized from a hydrolyzed solution of aqueous $HAuCl_4$ via the addition of K_2CO_3. The corresponding sizes of the AuNPs are 4, 6, 15, 25, 50, and ~100 nm with standard deviations of 7, 13, 8, 8, 10, and 11%, respectively.

Conclusions

These results indicate that AuNPs can be synthesized using CO as a reducing agent. CO offers tunability of nanoparticle sizes via altering $HAuCl_4$ concentration and flow rate. The fast synthesis rates, ease of tunability, and absence of cytotoxic by products allow for these CO-based AuNPs to be optimized and readily produced for biomedical and industrial applications. The manipulation of the solution pH and speciation of $HAuCl_4$ to control particle morphology may also be used as a means to tune the particle size. TEM micrographs and UV-visible spectral analysis confirm that the CO-based AuNPs are monodispersed upon synthesis. Future work will focus on how temperatures, upon synthesis, affect morphology. Nanoparticle surface chemistry and functionalization will also be explored. Cytotoxicity of the CO-based AuNPs in human cell lines will subsequently be investigated and compared against citrate-based nanoparticles.

Methods

Chemicals and materials

Hydrogen tetrachloroaurate III trihydrate ($HAuCl_4{\cdot}3H_2O$, 99.99%), and absolute ethanol (C_2H_5OH, 99.5%) where purchased from Sigma Aldrich and used as received. Carbon monoxide (CO, 99%) was supplied by Matheson-Trigas. All solutions were prepared using ultrapure water (18 Mohm Millipore Milli-Q water).

Pre-synthesis

All chloroauric acid solutions were aged in individual amber bottles under 4°C and light protected for a minimum of 3 days prior to use. All glassware used in the following procedures were cleaned in a bath of freshly prepared aqua regia solution (3 parts HCL acid to 1 part HNO_3 acid) and rinsed thoroughly with ethanol three times and then rigorously rinsed four times with copious amounts of pure grade water and oven dried prior to use. Stirring was conducted by a PTFE-coated magnetic stir bar which was cleaned and dried in the same manner as the glassware.

Carbon monoxide-based synthesis of pure aqueous $HAuCl_4$ solution

Several chloroauric acid solutions were prepared for utilization with CO reduction. Various weights of fresh chloroauric acid were dissolved in individual amber bottles containing water (200 mL). At least two separate batches of all solution concentrations were employed to confirm reproducibility. One set of solutions consisted of varying concentrations of chloroauric acid (0.01 to 0.09 mM in 0.01 mM increments) and $HAuCl_4$ (1 mM) and $HAuCl_4$ (2 mM) solutions were prepared. A solution of $HAuCl_4$ (1 wt%) was also prepared. Gold nanoparticles synthesized by CO reduction, with average diameter nanoparticles ranging from 4.5 to 52 nm were prepared as described below. For each $HAuCl_4$ concentration five volumes (40 mL) were prepared. Each sample was aerated at different flow rates controlled by a control valve. The gas entered the solution via a 60 um pore gas diffuser (Fisher Scientific) attached to the end of the gas supply line downstream of the control valve. The five solutions were exposed to CO

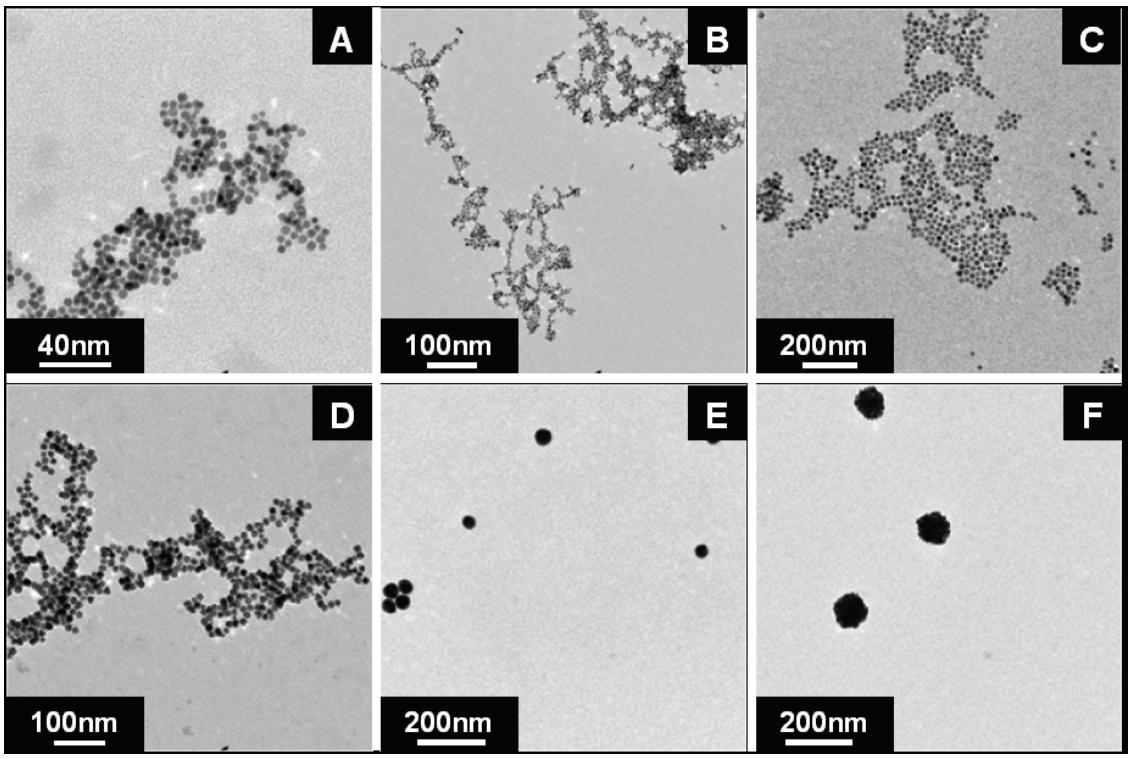

Figure 8 TEM images of AuNPs synthesized by CO reduction of $HAuCl_4$. A, B, C, and D are TEM images of AuNPs synthesized without the addition of K_2CO_3. E and F are AuNPs synthesized from a hydrolyzed solution of aqueous $HAuCl_4$ via the addition of K_2CO_3. The corresponding sizes of the AuNPs are 4, 6, 15, 25, 50, and ~100 nm respectively.

gas at flow rates of 16.9, 25.45, 31.59, 37.0, and 42.9 mL/min, respectively. The solution temperature, prior to aeration, was maintained between 20 and 22°C.

Carbon monoxide-based synthesis of pH adjusted $HAuCl_4$ solution and hydrolyzed $HAuCl_4$ solution

A 200 mL aqueous $HAuCl_4$ solution, with a concentration of 0.1 mM, was prepared by adding fresh gold to 200 mL of ultrapure Milli-Q water. This solution was aged in an amber bottle in light protected 4°C environment for a minimum of 72 h prior to use. After aging, the chloroauric acid solution was allowed to gradually rise to 22°C. A fresh stock solution of potassium carbonate (0.5 N) was prepared and stirred for a minimum of 1 h. $HAuCl_4$ aqueous solutions with various pH values were prepared by the addition of certain amounts of K_2CO_3 aqueous solution into of $HAuCl_4$ (0.1 mM) aqueous solution (20 mL) and shaken vigorously for a minimum of 1 min. This solution was allowed to age for 15 min before introduction of CO gas. The pH values of the aqueous solutions, measured prior to reduction, ranged from 4.25 to 11.4. Additionally several aqueous $HAuCl_4$ (0.38 mM) solutions (200 mL) were prepared by adding fresh gold to ultrapure Milli-Q water (200 mL). These solutions were allowed to age for a minimum of 72 h. K_2CO_3 (75 mg, 2.71 mM) was added to two $HAuCl_4$ (0.38 mM) solutions (200 mL) and aged for 30 and 40 min, respectively. K_2CO_3 (100 mg, 3.62 mM) was added to a $HAuCl_4$ (0.38 mM) solution (200 mL) and aged for 30 min. All solutions were aerated with CO gas at an inlet flow rate of 25.5 mL/min.

Nanoparticle characterization

Sample size distributions were determined by transmission electron microscopy (TEM) performed using a JEOL 1230 High Contrast-Transmission Electron Microscope (HC-TEM) operating between 80 and 100 kV. Samples were prepared for both instruments by contacting a AuNP (10 μL) drop with a carbon film coated 200 mesh copper grid. The grids were placed in a spotlessly clean container, covered and allowed to dry completely before use.

The optical response of the gold nanoparticles was determined by examining the optical extinction spectra of aqueous samples in 1 cm path length polystyrene cuvettes using a Varian Cary 300 UV-visible spectrophotometer. The UV-visible spectra were acquired at wavelengths between 400 to 800 nm. Distilled water was used as the reference and the blank for baseline subtraction.

XPS was carried out using a PHI Quantera SXM system. The soft X-ray source consisted of aluminum with

source energy of 1486.7 eV. The take off angle was set at 45°. Precut silicon wafers 4.5 mm × 5 mm were cleaned by immersion in a 3:1 H_2SO_4:H_2O_2 (piranha) solution for 15 min and rinsed with ultrapure Milli-Q water then dried. The sample was prepared by concentrating the AuNPs and dropping colloidal solution on precut silicon wafers. They were placed in a spotlessly clean container, covered and allowed to dry.

Additional material

Additional file 1: Thermodynamics of $HAuCl_4$ reduction in aqueous solutions using carbon monoxide as a reducing agent. The entire process is performed between 20 and 22°C and a pressure of 1 atm. The pH of the solution varies as a function of $HAuCl_4$ concentration. Nernst equation describes potential of electrochemical cell as a function of concentrations of ions taking part in the reaction:

$$E = E^0 - \frac{RT}{nF}\ln(Q) \quad \text{(M1a)}$$

where E^0 is the standard reduction potential, R is the absolute gas constant = 8.31441 J/(mol K), F is Faraday constant = 96484.6 C/mol, T is the absolute temperature = 295.15 K, n is number or electrons, and Q is the reaction quotient. RT/F can be considered constant.

$$Q = \frac{\{C\}^c\{D\}^d}{\{A\}^a\{B\}^b} \quad \text{(M2a)}$$

$$E = E^0 - \frac{RT}{nF} * 2.303 * \log(Q) \quad \text{(M3a)}$$

The CO gas is injected at a flow rate of 25.45 mL/min in 40 mL aqueous sample volumes. A water saturation constant of 0.26 g per 1 kg at 22°C is used.

$$Au^{3+} + 2e^- \rightarrow Au^0 \quad E^0(V) = 1.52 \quad \text{(M4a)}$$

$$AuCl_4^- + 2e^- \rightarrow AuCl_2^- + 2Cl^- \quad E^0(V) = 0.926 \quad \text{(M5a)}$$

$$AuCl_2^- + e^- \rightarrow Au^0 + 2Cl^- \quad E^0(V) = 1.154 \quad \text{(M6a)}$$

$$AuCl_4^- + 3e^- \rightarrow Au^0 + 4Cl^- \quad E^0(V) = 1.002 \quad \text{(M7a)}$$

$$CO(g) + H_2O \rightarrow CO_2(aq) + 2e^- + 2H^+ \quad E^0(V) = 0.11 \quad \text{(M8a)}$$

$$CO(g) + 2H_2O \rightarrow HCO_3^- + 2e^- + 3H^+ \quad E^0(V) = -0.101 \quad \text{(M9a)}$$

Redox potentials (7) and (8) are given at pH 0. The redox potentials are pH-dependent and must be adjusted for the varying pH values.

Additional file 2: Effect of CO flow rate on nanoparticle spectral profile. Normalized UV-visible spectra of nanoparticles synthesized from a chloroauric acid concentration of 0.03 mM aerated at flow rates of 16.9, 25.5, and 37.0 mL/min corresponding to A, B, and C, respectively. The effect of the gas flow rate during synthesis is illustrated by a comparison of the three spectra.

Additional file 3: Plasmon peak position and absorbance value as a function of chloroauric acid concentration. The chloroauric acid concentration ranging from 0.01 to 1 mM. The data is plotted on a logarithmic scale. As the $HAuCl_4$ concentration increases the absorbance intensity increases with an accompanying red-shift of the plasmon peak position.

Additional file 4: pH values before and after AuNP synthesis. pH values for given $HAuCl_4$ concentrations ranging from 0.02 to 0.1 mM in 0.01 mM increments and from 0.1 to 0.5 mM in 0.1 mM increments. The *x*-axis is plotted on a logarithmic scale. The inset shows the pH values of the AuNP solutions from 0.01 to 0.1 mM and is plotted on a linear scale. As the reduction of $HAuCl_4$ by CO takes place, H^+ ions are liberated decreasing the pH of the solution. All pH measurements were taken at room temperature.

Abbreviations

CO: carbon monoxide; AuNP: gold nanoparticle; HC-TEM: high contrast-transmission electron microscope; rpm: revolutions per minute; SPR: surface plasmon resonance; TEM: transmission electron microscopy; XPS: X-ray photoelectron spectroscopy.

Acknowledgements

This work was supported by a DoD Era of Hope Scholar Award, Welch Foundation Grant C-1598. We thank Lissett Bickford and Oara Neumann for their assistance and helpful suggestions.

Author details

[1]Department of Electrical and Computer Engineering, Rice University, MS-366, 6100 Main St., Houston, TX 77005, USA [2]Department of Bioengineering, Rice University, MS-142, 6100 Main St., Houston, TX 77005, USA [3]Department of Biochemistry and Cell Biology, Rice University, MS-140, 6100 Main St., Houston, TX 77005, USA

Authors' contributions

JKY is the primary author and conceived of the study, carried out the conception and design, synthesis and experiments, characterization, acquisition of data, analysis and interpretation of data, and drafting of the manuscript. NAL and RJL equally contributed as secondary authors by conducting cytotoxicity studies, data analysis and manuscript revisions. LCK carried out experiments, performed particle characterizations and aided in the drafting of the manuscript. AS participated in the design of the study, carried out synthesis and experiments and helped draft the manuscript. AYL and VN participated in the design of the study and coordination. RAD is the principal investigator.

Competing interests

The authors declare that they have no competing interests.

Received: 24 November 2010 Accepted: 16 June 2011
Published: 16 June 2011

References

1. Hovel H, Fritz S, Hilger A, Kreibig U: **Width of cluster plasmon resonance: Bulk dielectric functions and chemical interface damping.** *Phys Rev B* 1993, **48**:18178-18188.
2. Link S, El-Sayed MA: **Size and temperature dependence of the plasmon absorption of colloidal gold nanoparticles.** *J Phys Chem B* 1999, **103**:4212-4217.
3. Jain PK, Qian W, El-Sayed MA: **Ultrafast cooling of photexcited electrons in gold nanoparticle-thiolated DNA conjugates involves the dissociation of the gold-thiol bond.** *J Am Chem Soc* 2006, **128**:2426-2433.
4. Bickford L, Agollah G, Drezek R, Yu TK: **Silica-gold nanoshells as potential intraoperative molecular probes for HER2- overexpression in ex vivo breast tissue using near-infrared reflectance confocal microscopy.** *Breast Cancer Res Treat* 2009, **120**:547-555.
5. Yu L, Banerjee IA, Matsu H: **Direct growth of shape-controlled nanocrystals on nanotubes via biologicalrecognition.** *J Am Chem Soc* 2003, **125**:14837-14840.

6. Turner APF: **Biosensors-sense and sensitivity.** *Science* 2000, **290**:1315-1317.
7. Yeh C, Hung C, Chang TC, Lin HP, Lin YC: **An immunoassay using antibody-gold nanoparticle conjugate, silver enhancement and flatbed scanner.** *Microfluid Nanofluid* 2009, **6**:85-91.
8. Yang W, Wang J, Zhao S, Sun Y, Sun C: **Multilayered construction of glucose oxidase and gold nanoparticles on Au electrodes based on layer-by-layer covalent attachment.** *Electrochem Commun* 2006, **8**:665-672.
9. Wu ZS, Zhou GZ, Jiang JH, Shen GL, Yu RQ: **Gold colloid-bienzyme conjugates for glucose detection utilizing surfaced-enhanced raman scattering.** *Talanta* 2006, **70**:533-539.
10. Duff DG, Baiker A, Edwards PP: **A new hydrosol of gold clusters 1. Formation and particle size variation.** *Langmuir* 1993, **9**:2301-2309.
11. Brinson BE, Lassiter JB, Levin CS, Bardhan R, Mirin N, Halas NJ: **Nanoshells made easy: improving Au layer growth on nanoparticle surfaces.** *Langmuir* 2008, **24**:14166-14171.
12. Hu J, Wang Z, Li J: **Gold nanoparticles with special shapes: controlled synthesis, surface-enhanced raman scattering, and the application in biodetection.** *Sensors* 2007, **7**:3299-3311.
13. Park SE, Park MY, Han PK, Lee SW: **The effect of pH-adjusted gold colloids on the formation of gold clusters over APTMS-coated silica cores.** *Bull Korean Chem Soc* 2006, **27**:1341.
14. Polte J, Erler R, Thunemann AF, Sokolov S, Ahner TT, Rademann K, Emmerling F, Kraehnert R: **Nucleation and growth of gold nanoparticles studied via in situ small angle x-ray scattering at millisecond time resolution.** *ACS Nano* 2010, **4**:1076-1082.
15. Beattie JK: **Monodispersed colloids of transition metal and lanthanide compounds.** *Pure Appl Chem* 1989, **61**:937-941.
16. Turkevich J, Stevenson PC, Hillier J: **Formation of colloidal gold.** *J Phys Chem* 1953, **57**:670-673.
17. Sakai T, Alexandridis P: **Size and shape-controlled synthesis of colloidal gold through autoreduction of the auric cation by poly(ethylene oxide)-poly(propylene oxide) block copolymers in aqueous solutions at ambient conditions.** *Nanotechnology* 2005, **16**:S344-S353.
18. Majzik A, Patakfalvi R, Hornok V, Dekany I: **Growing and stability of gold nanoparticles and their functionalization by cysteine.** *Gold Bull* 2009, **42**:113-123.
19. Jana NR, Gearheart L, Murphy CJ: **Seeding growth for size control of 5-40 nm diameter gold nanoparticles.** *Langmuir* 2001, **17**:6782-6786.
20. Shan C, Li F, Yaun F, Yang G, Niu L, Zhang Q: **Size-controlled synthesis of monodispersed gold nanoparticles stabilized by polyelectrolyte-functionalized ionic liquid.** *Nanotechnology* 2008, **19**:285601.
21. Mafune F, Kohno J, Takeda Y, Kondow T: **Full physical preparation of size-selected gold nanoparticles in solution: laser ablation and laser-induced size control.** *J Phys Chem B* 2002, **106**:7575-7577.
22. Besner S, Kabashin AV, Winnik FM, Meunier M: **Synthesis of size-tunable polymer-protected gold nanoparticles by femtosecond laser-based ablation and seed growth.** *J Phys Chem C* 2009, **113(22)**:9526-9531.
23. Takai O: **Solution plasma processsing (SSP).** *Pure Appl Chem* 2008, **80**:2003-2011.
24. Saito N, Hieda J, Takai O: **Synthesis process of gold nanoparticles in solution plasma.** *Thin Solid Films* 2009, **518**:912-917.
25. Ashkarran AA, Iraji A, Mahbavi SM, Ahadian MM, Nezhad MRH: **Rapid and efficient synthesis of colloidal gold nanoparticles by arc discharge method.** *Appl Phys A* 2009, **96**:423-428.
26. Liang X, Wang ZJ, Liu CJ: **Size-controlled synthesis of colloidal gold nanoparticles at room temperature under the influence of glow discharge.** *Nanoscale Res Lett* 2010, **5**:124-129.
27. Thomas TD, Weightman P: **Valance electron structure of AuZn and AuMg alloys derived from a new way of analyzing Auger-parameter shifts.** *Phys Rev B* 1986, **33**:5406.
28. Seah MP, Smith GC, Anthony MT: **AES: energy calibration of electron spectrometers. I-an absolute, traceable energy calibration and the provision of atomic reference line energies.** *Surf Interface Anal* 1990, **15**:293-308.
29. Turkevich J: **Colloidal gold, part I.** *Gold Bull* 1985, **18**:86-91.
30. Wang S, Qian K, Bi X, Huang W: **Influence of speciation of aqueous HAuCl4 on the synthesis, structure, and property of Au colloids.** *J Phys Chem C* 2009, **113**:6505-6510.
31. Lemire C, Meyer R, Shaikhutdinov S, Freund HJ: **Do quantum size effects control CO adsorption on gold nanoparticles?** *Surface Chem Angew Chem Int Ed* 2004, **43**:118-121.

doi:10.1186/1556-276X-6-428
Cite this article as: Young *et al.*: Size-controlled synthesis of monodispersed gold nanoparticles via carbon monoxide gas reduction. *Nanoscale Research Letters* 2011 **6**:428.

Annals of Biomedical Engineering, Vol. 40, No. 2, February 2012 (© 2011) pp. 438–459
DOI: 10.1007/s10439-011-0472-5

Tunable Nanostructures as Photothermal Theranostic Agents

JOSEPH K. YOUNG,[1] ELIZABETH R. FIGUEROA,[2] and REBEKAH A. DREZEK[1,2]

[1]Department of Electrical and Computer Engineering, Rice University, 6100 Main Street, Houston, TX 77005, USA; and [2]Department of Bioengineering, Rice University, 6100 Main Street, Houston, TX 77005, USA

(*Received 15 July 2011; accepted 11 November 2011; published online 2 December 2011*)

Associate Editor Bahman Anvari oversaw the review of this article.

Abstract—The theranostic potential of several nanostructures has been discussed in the context of photothermal therapies and imaging. In the last several decades, the burden of cancer has grown rapidly, making the need for new theranostic approaches vital. Lasers have emerged as promising tools in cancer treatment, especially with the advent of photothermal therapies wherein light absorbing dyes or plasmonic gold nanoparticles are used to generate heat and achieve tumor damage. Recently, photoabsorbing nanostructures have materialized that can be employed in conjunction with lasers in the near-infrared region in order to enhance both imaging and photothermal effects. The incorporation of tunable nanostructures has resulted in improved specificity in cancer treatment. Silica-cored gold nanoshells and gold nanorods currently serve as the chief plasmonic structures for photothermal therapy. Although gold nanorods and silica-cored gold nanoshells have shown promise as therapeutic agents, over the past few years new nanostructures have emerged that offer comparable and even superior theranostic properties. In the present review, several theranostic agents and their impact on the development of more effective photothermal therapies for the treatment of cancer are discussed. These agents include hollow gold nanoshells, gold gold-sulfide nanoparticles, gold nanocages, carbon and titanium nanotubes, photothermal-based nanobubbles, polymeric nanoparticles and copper-based nanocrystals.

Keywords—Nanoparticles, Ablation, Therapy, Near-infrared, Cancer, Imaging, Plasmonics.

INTRODUCTION

Cancer is a leading cause of death worldwide; in 2007, it accounted for nearly 8 million deaths, and in 2030 this number is projected to increase to 12 million.[5] A critical challenge in dealing with such high incidence of cancer revolves around the separation between diagnosis, treatment and subsequent imaging to confirm therapeutic effect. Theranostics have emerged recently as a way to combine these three phases of medical treatment, thus decreasing time and improving efficacy of treatment. The ideal theranostic approach is capable of several tunable functions ranging from imaging to treatment with accurate targeting of cancer specific cells.

Photothermal therapy, in which photo-responsive agents such as gold-based nanoparticles (NPs) are employed to achieve selective heating, can be used as a theranostic treatment. The optical response is the result of the optical properties of metallic nanoparticles that are dominated by the plasmon, a collective excitation of the conduction electrons.[28,39] This collective oscillation is determined by the boundary conditions at the surface and when it reaches a maximum it is termed the surface plasmon resonance (SPR).[32] The optical response of the metallic nanoparticles depends on factors that affect the electron charge density on the surface such as atomic makeup, size, morphology and surrounding medium at the interface and can be described with Mie theory calculations.[39] For example, the generalized Mie theory scattering approach[3] can be employed to calculate the absorption and scattering cross sections of gold nanoshell geometries. The gold nanoshell geometry can be described as consisting of a spherical core of radius R_1 with a dielectric constant ε_1. Surrounding this core is a concentric gold shell for a total nanoparticle radius R_2 where the shell thickness is given as $R_2 - R_1$. The gold shell bulk dielectric function $\varepsilon(a, \omega)$ consists of a frequency dependent experimental dielectric function $\varepsilon(\omega)_{exp}$[35] and a size dependent modification of the bulk collisional frequency Γ,[39] and is written as

Address correspondence to Rebekah A. Drezek, Department of Bioengineering, Rice University, 6100 Main Street, Houston, TX 77005, USA. Electronic mail: jky1@rice.edu, lizfig@rice.edu, drezek@rice.edu

J. K. Young and E. R. Figueroa have contributed equally to this work.

$$\varepsilon(a,\omega) = \varepsilon(\omega)_{\text{exp}} + \omega_p^2/\left(\omega^2 + i\omega\gamma_{\text{bulk}}\right) - \omega_p^2/\left(\omega^2 + i\omega\Gamma\right)$$

where $\Gamma = \gamma_{\text{bulk}} + A \times V_F/a$, γ_{bulk} is the bulk collisional frequency, V_F is the fermi velocity, A depends on the theory used to derive the expression, a is the shell thickness ($R_2 - R_1$) and ω_p is the bulk plasmon frequency of gold.

For calculating the optical response of particles with non-spherical geometries, metallic or otherwise, Mie theory can be extended by Gan theory and discrete dipole approximation (DDA) and is described in detail by El-Sayed and coworkers.[32,44] While Gan theory was developed for short cylindrical shapes, DDA provides a practical and straightforward approach to analyze the effects of size and geometry on the plasmonic response of the nanoparticles possessing many different morphologies. An alternative and more rigorous mathematical approach, based on Maxwell's equations, to calculate the light scattering from non-spherical particles is the implementation of the T-matrix technique. Mishchenko and coworkers provide a detailed analysis of Waterman's T-matrix approach to compute light scattering characteristics of single, ensemble, aggregated, and extreme particle geometry sets.[63,95]

Utilization of such plasmonic agents, both spherical and non-spherical, allows for both imaging of cancerous tissue and initiation of cellular hyperthermia in a localized area. The theranostic effect is the result of surface plasmon oscillations and electronic transitions between states which produce thermal energy via light-to-heat conversions, and in some cases the result of mechanical action.[21,42,43,58,108] These processes are triggered by the irradiation of the photothermal agents which exhibit enhanced optical absorption properties in the visible and near-infrared (NIR) region. Furthermore, these optical properties are tunable which allows for the targeting of the transparency window, a region where NIR light is transmitted through biological tissue with relatively low scattering and minimal heating, since it is above the absorption of biological molecules like hemoglobin and below the absorption of water.[83] This is illustrated in Fig. 1. NIR light has also been shown to penetrate up to 2 mm depths with no normal tissue damage and little attenuation.[73]

Laser initiated hyperthermia, in which cellular tissue is raised to the denaturant temperature of 44 °C,[29] holds the potential to provide a minimally invasive alternative to current invasive treatments for millions of men and women who are diagnosed with cancer. Laser initiated hyperthermia is used in two main modes, continuous wave (CW) and pulsed laser. Halas and West conducted the first pioneering work on inducing CW mode for nanoshell-mediated near-infrared photothermal therapy.[29,66] Zharov *et al.* were

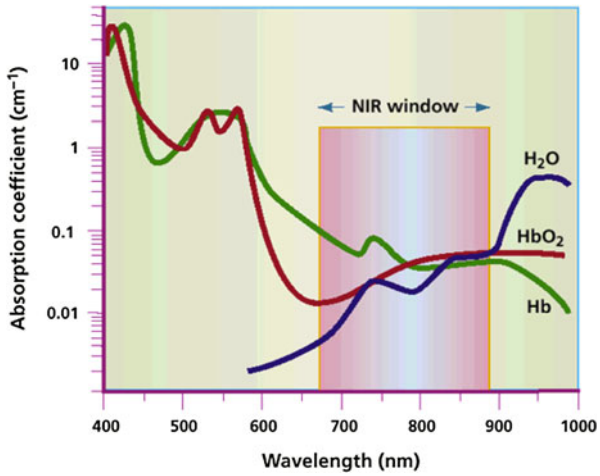

FIGURE 1. Near-infrared light (650–900 nm) is of particular interest in biological applications as it is minimally absorbed by biological chromophores and water. Reprinted by permission from Macmillan Publishers Ltd, Sarkar *et al.*[73], Copyright 2001.

first to explore pulsed mode in cancer applications for detection and killing of individual tumor cells via photothermal-induced bubbles around absorbing NPs and its clusters in cells.[108,109] These photothermal effects have been utilized to selectively target and ablate cancer cells, as well as for controlled gene release,[68] drug delivery[46] and imaging.[6,109] Pissuwan *et al.* provided a comprehensive analysis of the therapeutic possibilities of photothermally heated gold nanoparticles[67] while Hirsch *et al.* provide a detailed overview of metal nanoshell use in therapeutic applications.[29] Zharov *et al.* examined self-assembling nanoclusters in living systems that serve as applications for use in integrated photothermal nanodiagnostic and therapy.[109] Currently, silica-based gold nanoshells and gold nanorods are the chief structures that have been utilized in photothermal therapeutics.[28,33,67] However, in the present review, we will discuss several recently developed unconventional theranostic agents for photothermal therapy. These theranostic agents consist of gold-based plasmonic particles such as hollow gold nanoshells, gold nanocages, and gold gold-sulfide (GGS) NPs, as well as carbon and titanium oxide nanotubes, photothermal-based bubbles (PTB), polymeric NP composites and copper-based nanocrystals.

HOLLOW GOLD NANOSHELLS

Hollow gold nanoshells (HGNs) are similar structures to silica-cored gold nanoshells in which a gold shell of a certain thickness surrounds a core material of a given diameter. Unlike silica-based gold nanoshells, HGN cores are made up of the surrounding media.

Many researchers have taken advantage of templated galvanic replacement reactions of metals for gold to create simple and reproducible routes to synthesize 20–50 nm diameter HGNs for use in biomedical applications.[40,62,80,97] As in previous templated galvanic replacement methods, the core particle is sacrificed; the metal salt that makes up the nanoshell is reduced to metal if it has a greater standard reduction potential than the template metal, which is oxidized to a molecular solution.[43,69,79,85,86]

Zhang and coworkers have produced nearly monodispersed HGNs with tunable interior and exterior diameters by sacrificial galvanic replacement of cobalt nanoparticles.[79] In a typical HGN synthesis, sacrificial cobalt NPs are first synthesized by deoxygenating water that is kept under an argon purge. Cobalt(II) chloride is then added to the aqueous solution and reduced with sodium borohydride in the presence of sodium citrate. Upon ensuring complete hydrolysis of the sodium borohydride, chloroauric acid was added. Upon completion of the gold addition, the particles are exposed to ambient conditions to oxidize the remaining cobalt metal left in solution.[79]

The inner diameter and wall thickness can be adjusted leading to complete control of the optical properties of particles ranging from 20 to 70 nm. This makes it possible to tune the peak of the surface plasmon band absorption. In addition, Zhang and coworkers observed that by varying the wall thickness and particle size it is possible to tune the plasmon absorption across much of the visible spectrum as shown in Fig. 2a, UV–Vis–NIR data.

Li and coworkers also used cobalt cores as sacrificial templates to synthesize HGNs. They showed both the selective destruction of epidermal growth factor (EGFR)-positive cancer cells *in vitro* and the enhanced delivery to EGFR-positive tumors *in vivo* using anti-EGFR monoclonal antibody conjugated HGNs.[62] For

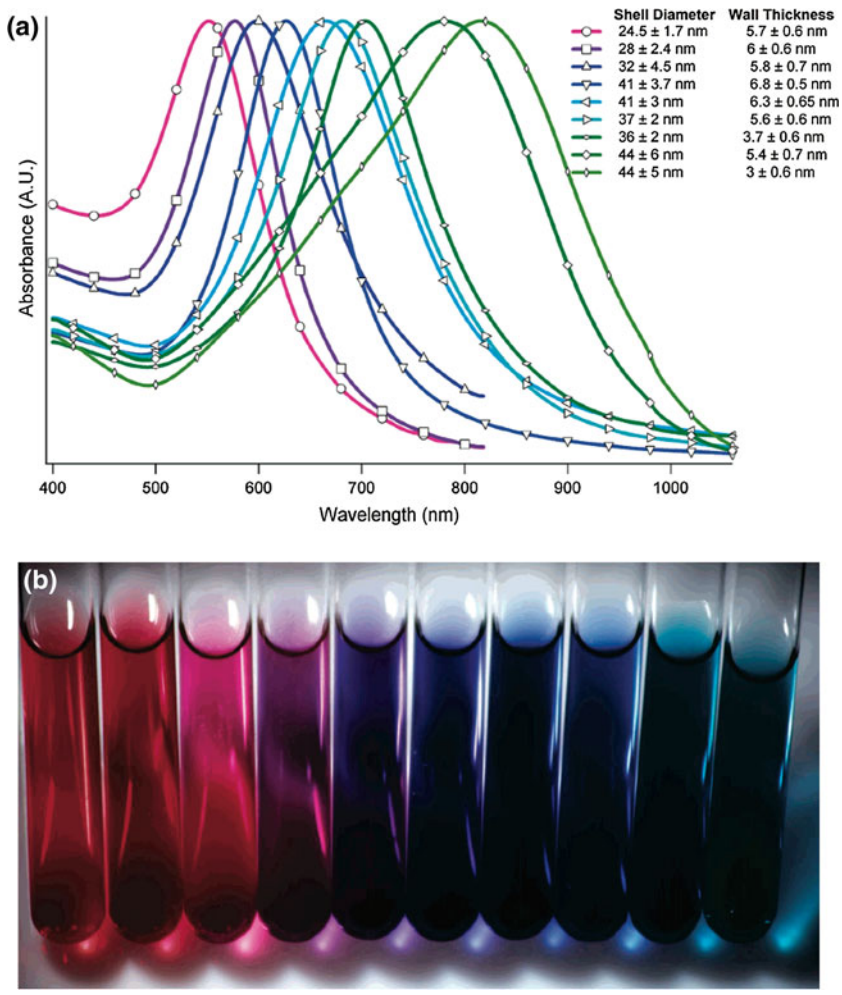

FIGURE 2. (a) UV–Vis–NIR absorption spectra of nine HGN samples with varying diameters and wall thicknesses. (b) Image showing the color range of HGN solutions. The vial on the far left contains solid gold nanoparticles, the rest are HNGs with varying diameters and wall thicknesses. Reprinted with permission from Luther *et al.*[61] Copyright 2007 American Chemical Society.

initial photothermal characterization studies, Li and coworkers incubated HGNs with C225 antibodies that shifted the plasmon peak from 828 nm to 810 nm. They tested the photothermal effects of the C225 conjugated HGNs in solutions using a continuous laser at 808 nm. Exposure of aqueous solutions of C225-HGNs to an 8 W/cm^2 laser intensity caused heating of the solutions. The temperature of the solutions containing 3.7×10^{10} and 7.3×10^{10} nanoshells/mL increased with increasing exposure time and reached plateaus at 34.8 and 41.5 °C after ~4 min of light exposure. Without HGNs there was a slight temperature increase observed.

For the *in vitro* studies, Li and coworkers incubated human squamous carcinoma cells with C225 conjugated HGNs tuned to the NIR region (810 nm) for 1 h. Light scattering images of the cells incubated with C225-HGNs and with IgG–HGNs were compared. They observed a 10-fold increase in scattering signal from the cells treated with C225-HGNs compared to those treated with IgG–HGNs. Cells were irradiated with NIR laser light centered at 808 nm at an intensity of 40 W/cm^2 for 5 min and then incubated for 24 h. The cells were then washed and stained with Calcein AM for visualization of live cells and ethidium homodimer-1 (EthD-1) for visualization of dead cells. Li observed that the control, C225-HGNs alone, irradiation alone, and IgG–HGNs plus laser groups showed no observable damage to the cancer cells. Contrastingly, most of the cells treated with C225-HGNs followed by NIR laser irradiation were lysed. The remaining cells stained with Calcein (green) were more rounded possibly as a result of condensation of skeleton proteins. Some of the cells that were stained with EthD-1 (red) 24 h after laser treatment had already lost cellular integrity. Li and coworkers have shown that immuno-HGNs targeted to EGFR selectively bind to EGFR-positive cells and destroy these cells via a photothermal effect.

Because of their relatively small size (~30 nm in diameter), optical properties, and ease of surface modification, targeted HGNs may find increasing applications in photothermal ablation therapy. A possible disadvantage of using HGNs is the potential for the particle shells to collapse under thermal stress, forming a colloidal structure. Zasadzinski and coworkers showed that under irradiation 350 μJ with a pulsed laser for 10 min, HGNs at the resonant frequency of the laser broke apart and/or collapsed forming stable smaller colloidal structures.[69] The loss of structural integrity within the shell under laser irradiation could lead to lower transduction efficiencies and ineffective ablative properties for use as a therapeutic agent if longer irradiation time is needed during photothermal therapy. It is possible to counteract this effect by coating the HGN surface with a thin silica layer thus making the HGNs more thermally stable. Emelianov and coworkers showed that adding a silica coating to gold nanorod surface increased thermal stability.[7] Teranishi and coworkers successfully coated AuNPs with silica that withstood temperatures in excess of 600 °C for 30 min.[36]

GOLD GOLD-SULFIDE NANOPARTICLES

Other researchers have explored replacing the silica-cores, found in traditional nanoshells, with other core structures. One popular core/shell configuration is based on a gold-sulfide core surrounded by a pure gold shell. Zhou *et al.* first synthesized GGS NPs that exhibited strong NIR absorbing properties.[110] GGS NPs are composed of a gold-sulfide core covered by an exterior gold layer. There has been debate as to the precise structure of the particles; that is, whether a discrete gold-sulfide core and gold shell exists, or whether gold-sulfide aggregates are formed.[2] Ultimately the core–shell NP model fits experimental data, and additionally X-ray diffraction has indicated the presence of a gold-sulfide composite core with a continuous gold surface.[71,78,105]

GGS NPs for therapeutic and imaging applications are generally synthesized in the range of 35–55 nm in diameter with a SPR near 800–900 nm, compared to gold silica nanoshells which range from 120 to 140 nm for the same resonant wavelength.[2] This size difference may prove advantageous, as models have suggested that particles with diameter <100 nm will move closer to the endothelium layer, potentially improving tumor extravasation[16] and experimental data suggests that peak gold uptake occurs for diameters between 30 and 50 nm.[14] When comparing absorbing efficiency of GGS NPs to gold silica using Mie scattering theory, it has been shown that GGS NPs absorb more efficiently at 98–99%, compared to gold silica which has been shown to absorb at 67–85%.[25] The increased absorption efficiency is attributed to the fact that the smaller GGS NPs have a higher absorption cross-sectional area ratio. This could result in lower laser power or fewer particles needed for GGS-mediated photothermal therapy compared to equivalent optical density of gold silica NPs.[26] Based on these advantages, GGS NPs are a promising candidate for treatment of cancer tumors using photothermal therapy.

Synthesis of GGS NPs proceeds by self-assembly using chloroauric acid and sodium sulfide. When the ratio of chloroauric acid and sodium sulfide is altered, the SPR of the particles ranges from 600 to >1000 nm.[83] During the synthesis process, the NIR peak of the NPs

shifts and narrows after each addition step. As a byproduct of the one pot synthesis method, small pure gold colloids are formed. These gold colloids are generally 5–10 nm in diameter, yet some colloids can be the same size as the GGS shells.[71] After the self-assembly, the smaller gold colloid may be removed so as to reduce reticulo-endothelial system uptake and other innate immune defense responses. The removal of the smaller colloidal byproduct requires multiple centrifugation steps. GGS NPs are synthesized with bare gold surfaces that allow surface functionalization with antibodies or other molecules for targeting capabilities. In order to avoid NP clearance and stabilize the particles, PEGylation of the GGS NPs is necessary for *in vivo* applications. The ease of the single step synthesis of GGS NPs is attractive, as it may reduce production costs, suggesting easy scale-up applications.[26] A disadvantage of using GGS presents itself when the colloidal byproducts produced during synthesis are the same size as the resultant GGS shells. Under these conditions the byproduct would not be able to be removed from the GGS sample.

Day *et al*. performed *in vitro* experiments using anti-HER2 conjugated GGS NPs (~40 nm) backfilled with PEG to target breast carcinoma cells that overexpress the HER2 receptor. Low pulsed laser powers of the range 1 J/cm^2 were utilized for visualization of the cells, while higher laser powers around 48 J/cm^2 were used for photothermal ablation of the cancerous cells. At the low range, no loss in cell viability was observed. On the contrary, at the higher laser power of 48 J/cm^2, EthD-1 fluorescence and membrane blebbing was observed within 30 s of irradiation, indicating successful cell death by photothermal ablation[15] (Fig. 3).

Gobin *et al*. evaluated *in vivo* distribution of GGS NPs after 24 and 48 h accumulation periods. By looking at the ratio of gold in the tumor compared to the spleen and liver, they were able to determine the efficiency of tumor uptake, taking into account NP clearance. These experiments indicated that GGS NPs avoid NP clearance and accumulate in tumors, and that they remain in the circulation for extended periods. Additionally, photothermal destruction of tumor cells was seen with CW NIR irradiation of the GGS particles (808 nm with 4 W/cm^2 intensity for 3 min), resulting in increased survival as seen in Fig. 4. Ultimately, with further optimization of laser power, accumulation time, and NP concentrations, GGS NPs may be a superior photothermal option to compliment the treatment of cancer.

GOLD NANOCAGES

Researchers have also developed other structures that are synthesized in a similar manner to HGNs that possess comparable optical, morphological and thermal properties. Examples of such structures are gold nanocages. Developed by Xia and coworkers, gold nanocages are a type of hollow and porous gold nanostructure that are formed by a galvanic replacement between silver nanocubes and chloroauric acid in aqueous solution. Gold nanocages represent a novel class of nanomaterials that are particularly attractive as photothermal transducers for therapeutic applications due to their absorbance in the NIR.[1,8–11,31,87,102]

In a typical reaction, an aqueous solution of chloroauric acid is slowly titrated into a boiling solution

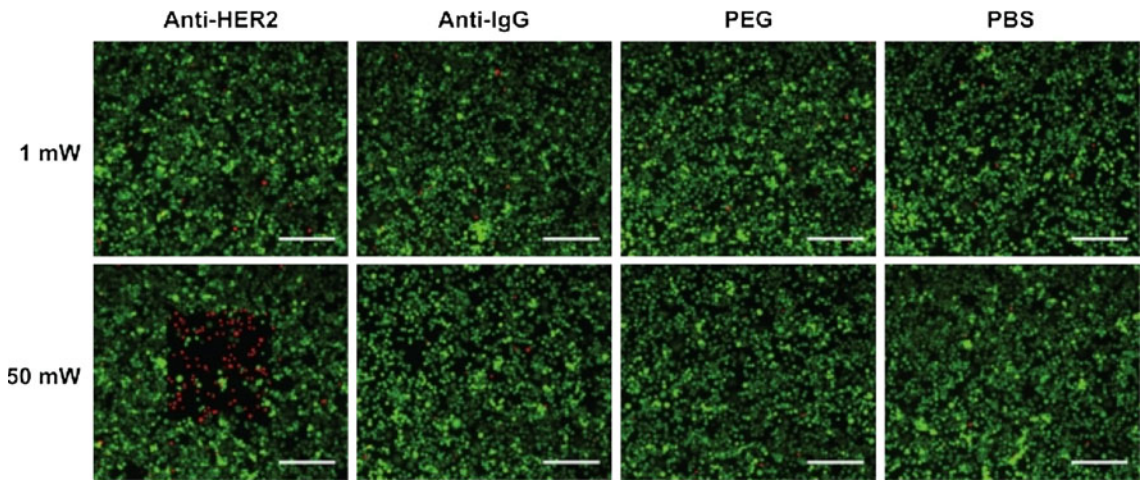

FIGURE 3. Calcein AM staining indicated that cancerous cells remained viable (evidenced by green fluorescent signal) when exposed to 1 mW laser power, regardless of nanoparticle presence. At 50 mW laser output a red fluorescent EthD-1 signal indicative of membrane damage was observed in cells exposed to anti-HER2 functionalized GGS NPs only where the laser was applied. Laser exposure alone was harmless to cells, as was laser exposure combined with nonspecifically targeted nanoparticles. Scale bar = 250 μm. Reprinted with permission from Cherukuri *et al.*[13]

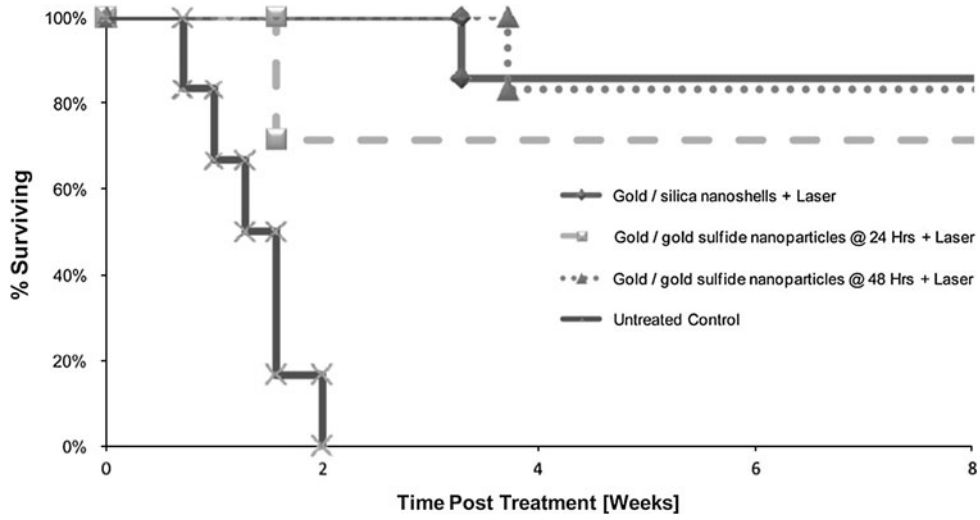

FIGURE 4. Kaplan–Meier survival of mice following treatment with GGS NPs and laser irradiation. There is a statistically significant increase in survival with 48 h accumulation compared to 24 h accumulation for the GGS NP treated mice and no difference for 48 h GGS NP treated mice as compared to gold silica nanoshell treated mice. Reprinted by permission from Garcia-Ripoll *et al.*[22]

suspension of silver nanocubes. Due to the different electrochemical potentials between silver and gold, the silver will give up its electrons and dissolve into the solution as ions while a thin layer of gold is deposited on the outer surface of the cube. By controlling the titrated amount of chloroauric acid into the reaction, the local SPR peak position of Au nanocages can be precisely tuned to any wavelength of interest in the range of 600–1200 nm.[87] The general size for nanocages tuned to 800 nm is around 45 nm to 50 nm edge width. Figure 5 shows the UV–Vis–NIR spectra and TEM images of Au nanocages.

Attempts using gold nanocages for photothermal therapy have also been made recently mainly by Xia and Li.[1,8–11,102] In *in vitro* studies by Li and coworkers, a NIR femtosecond pulse laser was used to treat breast cancer cells in combination with HER-2 targeted 45 nm gold nanocages. Li was able to demonstrate selective photothermal destruction of cancer cells *in vitro* (Fig. 6). Breast cancer cells that were treated with immunofunctionalized gold nanocages and then irradiated by a 810 nm laser at an intensity of 1.5 W/cm^2 for 5 min showed a well-defined circular zone of dead cells. Li and coworkers found that the transition power range for inducing damage is between 0.9 and 1.5 W/cm^2. It was observed that the cell viability exhibits significant decrease at an irradiation intensity of ~1.5 W/cm^2.

In the *in vivo* studies by Xia and coworkers,[8] they investigated the photothermal effect of the Au nanocages for selective destruction of neoplastic tissue using a bilateral tumor model. Ten athymic mice were subcutaneously injected into the right and left rear flanks with human glioblastoma cells. Five mice were injected with PEGylated Au nanocages in PBS and five mice were injected with saline. At 72 h post-injection, the tumor on the right rear flank of each mouse was subjected to photothermal treatment by exposure to the diode laser at an intensity of 0.7 W/cm^2 for 10 min. During laser treatment Xia and coworkers conducted full-body thermographic images as shown in Fig. 7. The average temperature of the irradiated area was plotted as a function of irradiation time. Xia observed that for the nanocage injected mice, the tumor surface temperature increased rapidly within 1 min to reach 50 °C and began to plateau after 2 min at ~54 °C. In the case of saline injected mice, the surface temperature remained below 37 °C during the entire treatment.

Xia and coworkers also monitored changes in tumor metabolism due to photothermal treatment using F-FDG PET. Measurement of tumor metabolism (Fig. 8) was performed before and after laser treatment for mice that had been intravenously injected with either saline or nanocages. Before laser irradiation, the images showed no significant difference between saline-injected mice and nanocage-injected mice. At 24 h post-laser treatment, Xia and coworkers reported a reduction in metabolic activity by 70% for nanocage laser treated mice. Xia also observed that there was no change in metabolic activity for saline treated mice, suggesting there is no benefit to laser treatment in the absence of Au nanocages. Photothermal damage of tumor cells in mice injected with Au nanocages was confirmed by histological examination showed marked degenerative changes of coagulative necrosis that was absent from tumors not treated with Au nanocages.

These results suggest that Au nanocages can serve as effective transducers for photothermal treatment of cancer. Like HGNs, Au nanocages present a drawback

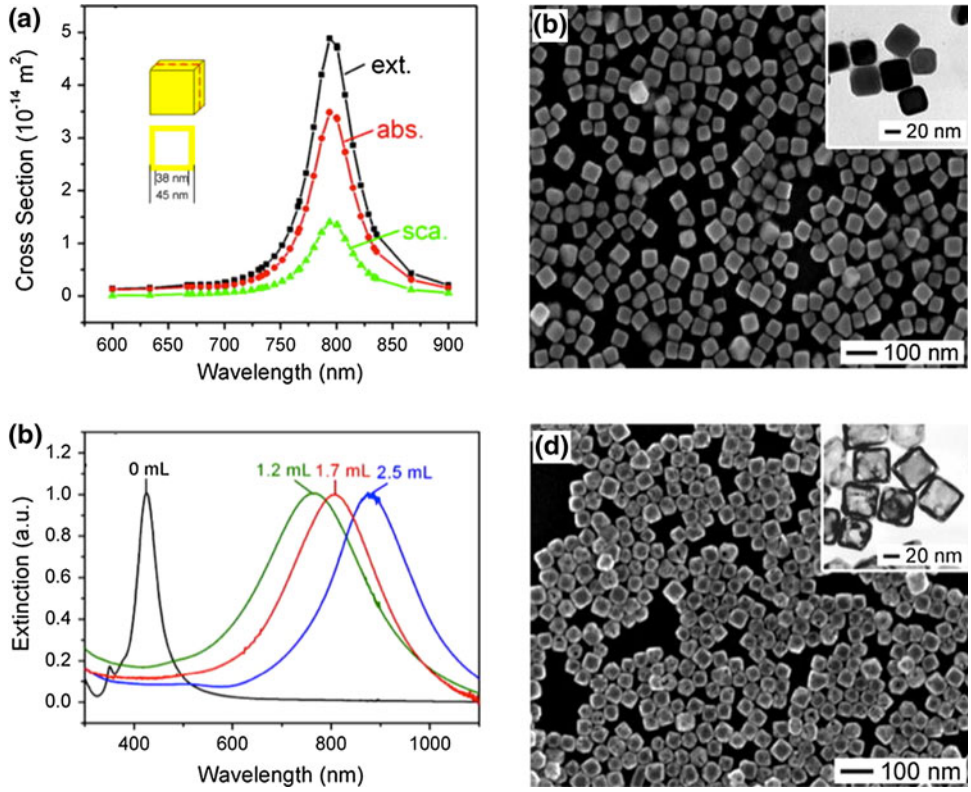

FIGURE 5. (a) The extinction (C_{ext}), absorption (C_{abs}), and scattering (C_{sca}) cross-sections (note that $C_{ext} = C_{abs} + C_{sca}$) calculated using the DDA method for a gold nanocage of 45 nm in edge length and 3.5 nm in wall thickness, and with the geometry depicted in the inset in (d). The alloy composition of the nanocages is Au_3Ag. (b) SEM images of Ag nanocubes prepared by sulfide-mediated polyol synthesis. The inset shows TEM image of the Ag nanocubes. (c) Normalized Vis–NIR extinction spectra recorded from aqueous suspensions of nanostructures after titrating Ag nanocubes with different amounts of a $HAuCl_4$ aqueous solution. Note that the spectrum in red is corresponding to the Au nanocages shown in (d). (d) SEM image of Au nanocages prepared by refluxing an aqueous solution containing both silver nanocubes and $HAuCl_4$. The inset shows a TEM image of the Au nanocages. Reprinted with permission from Chen *et al.*[11] Copyright 2007 American Chemical Society.

related to the thermal stability of the shell structure. Because the Au nanocages possess a hollow core, potential for shell collapse under sustained laser irradiation is high. The synthesis of Au nanocages is also more involved compared to the synthesis procedures for other NIR structures. The yield of Au nanocages during synthesis is small compared to other NIR particles due to the difficulty associated with scaling up the synthesis.[87]

CARBON NANOTUBES

Non gold-based nanostructures also hold great promise as theranostic agents. Carbon nanotubes are one such nanostructure that has shown great potential in various biological applications due to their unique physical and chemical properties.[38,53,54] Researchers have found that functionalized single-walled carbon nanotubes (SWNTs), made stable in physiological environments, are nontoxic *in vitro* and *in vivo*.[41,51,77,91,96,100] Furthermore SWNTs have many intrinsic optical properties useful for biomedical imaging.[13,52,93,94,103]

SWNTs have strong optical absorption in the NIR region. The high absorbance of SWNTs in the NIR originates from electronic transitions between the first or second van Hove singularities of the nanotubes.[4,65] By virtue of their high optical absorbance in the biological transparency window of ~700 nm–1.4 μm, SWNTs may also act as photothermal therapy agents for *in vitro* cell and *in vivo* tumor destruction.[21,23,24,55,64,72,81,98,111] Figure 9 shows the high NIR absorbance of SWNTs solubilized in water.

Dai and coworkers[81] exploited the optical properties of SWNTs at a single wavelength of 808 nm for *in vitro* radiation. They achieved selective cancer cell destruction by functionalization of SWNTs with a folate moiety that selectively targets the over expressed folate receptors on tumor cells, while the normal cells are unaffected. The nanotube samples used were Hipco SWNTs solubilized in the aqueous phase by noncovalently absorbing PEG-grafted phospholipids.

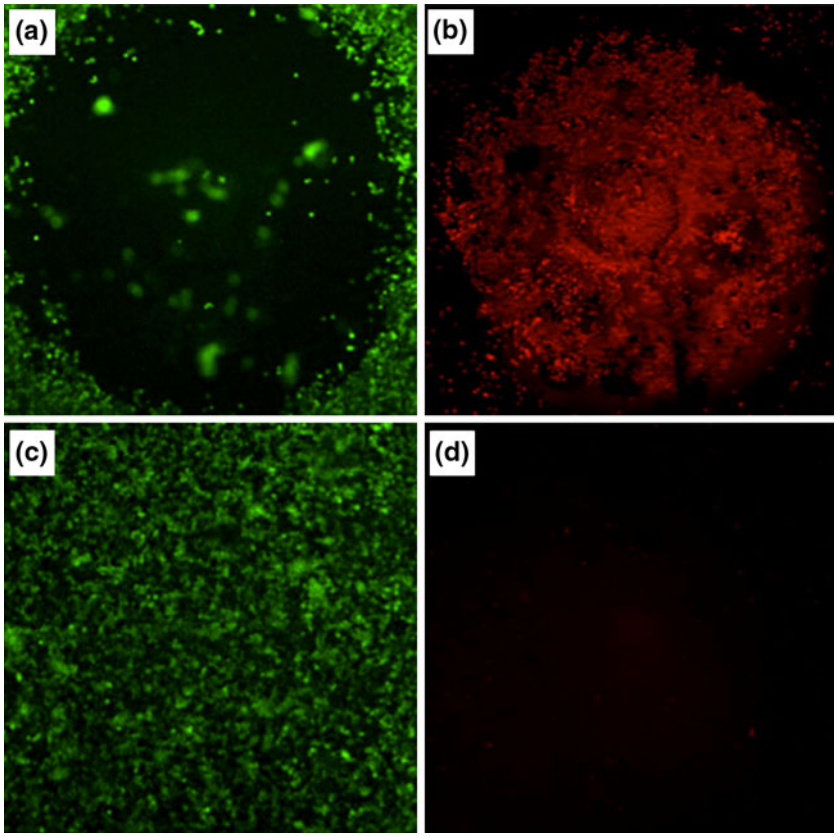

FIGURE 6. SK-BR-3 breast cancer cells that were treated with immuno gold nanocages and then irradiated by 810-nm laser at a power density of 1.5 W/cm^2 for 5 min showed a well-defined circular zone of dead cells as revealed by: (a) calcein AM assay (where green fluorescence indicates the cells were live), and (b) EthD-1 assay (where red fluorescence indicates the cells were dead). In the control experiment, cells irradiated under the same conditions but without immuno gold nanocage treatment maintained viability, as indicated by (c) calcein fluorescence assay, and (d) the lack of intracellular EthD-1 uptake. Modified with permission Chen *et al.*[11] Copyright 2007 American Chemical Society.

Figure 10 shows the selective targeting and killing of cancer cells *in vitro* using a NIR 808 nm laser.

Choi and coworkers[64] demonstrated *in vivo* ablation of solid malignant tumors by the combined treatments of SWNTs and NIR irradiation. Choi prepared an aqueous biocompatible SWNT-dispersed solution by noncovalently functionalizing Hipco SWNTs with PEG grafted phospholipids. The average lengths and the diameters of PEG–SWNTs were about 50–300 and 2–5 nm, respectively. *In vivo* therapeutic examinations were conducted against nude mice bearing human epidermoid mouth carcinoma tumor cells on their backs. Tumors were allowed to grow to approximately 70 mm^3. PEG–SWNTs were then injected into the tumor regions via intratumoral injection. Mice were irradiated at an intensity of 76 W/cm^2 for 3 min. Figure 11 shows tumor volume changes of representative mice treated in different experimental groups. As clearly shown in Fig. 11a, the mice treated with PEG–SWNTs and NIR irradiation showed complete destruction of tumors after 20 days of treatments. The photothermal therapeutic effect was also analyzed quantitatively by monitoring the tumor growth rates in terms of tumor volume changes as a function of time per each treatment Fig. 11c. While the tumors in treatment groups II through IV were continuously grown up, the tumor sizes of the mice treated with PEG–SWNTs and NIR laser displayed almost no volume.

The SWNT-based photothermal therapies in these experiments demonstrate the great potential for SWNTs to be utilized in cancer therapy as theranostic agents. Further exploration on the potential use of carbon nanotubes for systemic delivery needs to be conducted. Bio-distribution analysis after systemic delivery also needs to be further explored to address the potential toxicity effects of free carbon nanotubes traversing the circulatory system.

TITANIUM OXIDE NANOTUBES

Another non gold-based optically sensitive nanostructure that has potential to serve as a therapeutic agent is based on titanium oxide. Titanium oxide

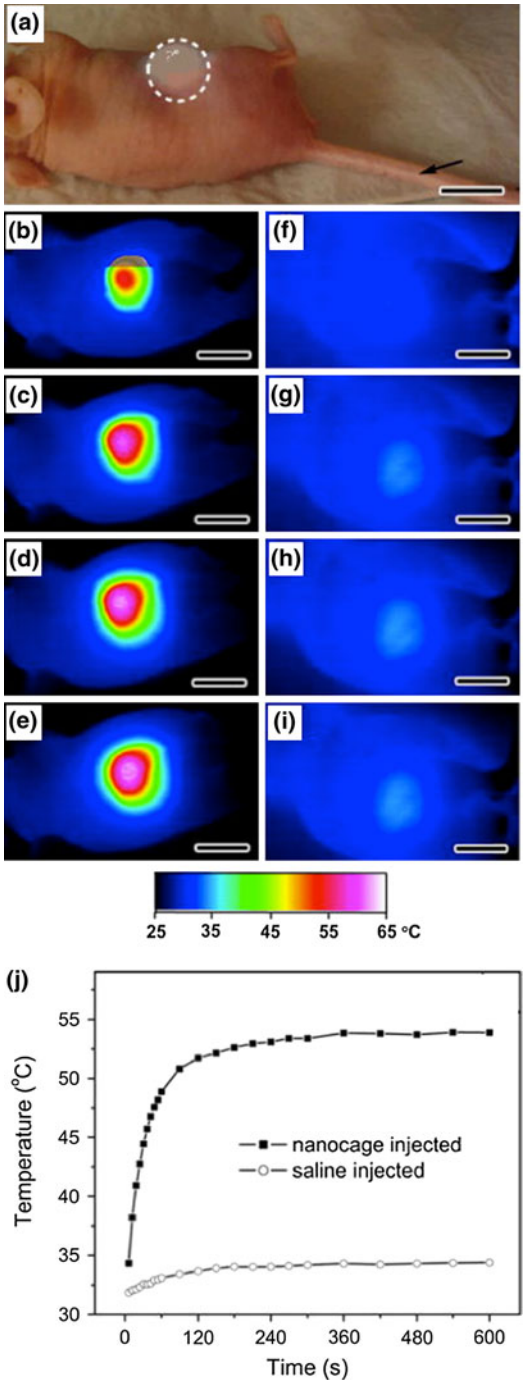

FIGURE 7. (a) Photograph of a tumor-bearing mouse under the photothermal treatment. 100 μL of PEGylated nanocages at a concentration of 9×10^{12} particles/mL or saline was administrated intravenously through the tail vein as indicated by an arrow. After the nanocages had been cleared from the circulation (72 h after injection), the tumor on the right frank was irradiated by the diode laser at 0.7 W/cm^2 with a beam size indicated by the dashed circle. (b–g) Thermographic images of (b–e) nanocage-injected and (f–i) saline-injected tumor-bearing mice at different time points: (b, e) 1 min (c, f) 3 min, (d, g) 5 min, and (e, i) 10 min. (j) Plots of average temperature within the tumors (dashed circle) as a function of irradiation time. All scale bars are 1 cm. Reprinted with permission from Chen *et al.*[10]

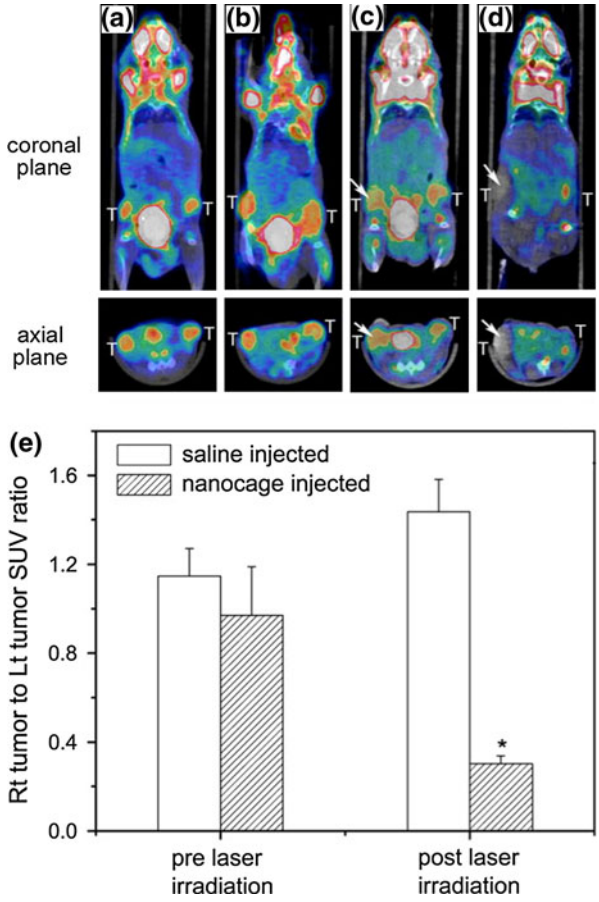

FIGURE 8. F-FDG PET/CT co-registered images of mice intravenously administrated with either saline or Au nanocages, followed by laser treatment: (a) a saline-injected mouse prior to laser irradiation; (b) a nanocage-injected mouse prior to laser irradiation; (c) a saline-injected mouse after laser irradiation; and (d) a nanocage-injected mouse after laser irradiation. The white arrows indicated the tumors that were exposed to the diode laser at a power density of 0.7 W/cm^2 for 10 min. (e) A plot showing the ratios of laser-treated tumor (Rt tumor) to non-treated tumor (Lt tumor) ^{18}F-FDG standardized uptake values (SUV, $p < 0.001$). Reprinted with permission from Chen *et al.*[10]

nanotubes (TiO_2 NTs) are highly functional materials with many interesting properties. TiO_2 NTs are known to be biocompatible and in recent years TiO_2 NTs have been explored for their potential use as *in vivo* photodecomposition catalysts, coatings for medical implants, augmentation of periimplant bone formation *in vivo*, and gene and drug delivery carriers.[22,34,74,84,88,101,104] More recently, Lee and coworkers have exploited the optical properties of TiO_2 NTs for use as potential therapeutic agents for cancer photothermal therapy in combination with NIR light.[30,45]

TiO_2 NTs were produced by electrochemical anodization of Ti thin foils in an electrolyte consisting of ammonium fluoride and water in ethylene glycol at 60 V for 17 h.[113] An SEM image of the TiO_2 NTs is

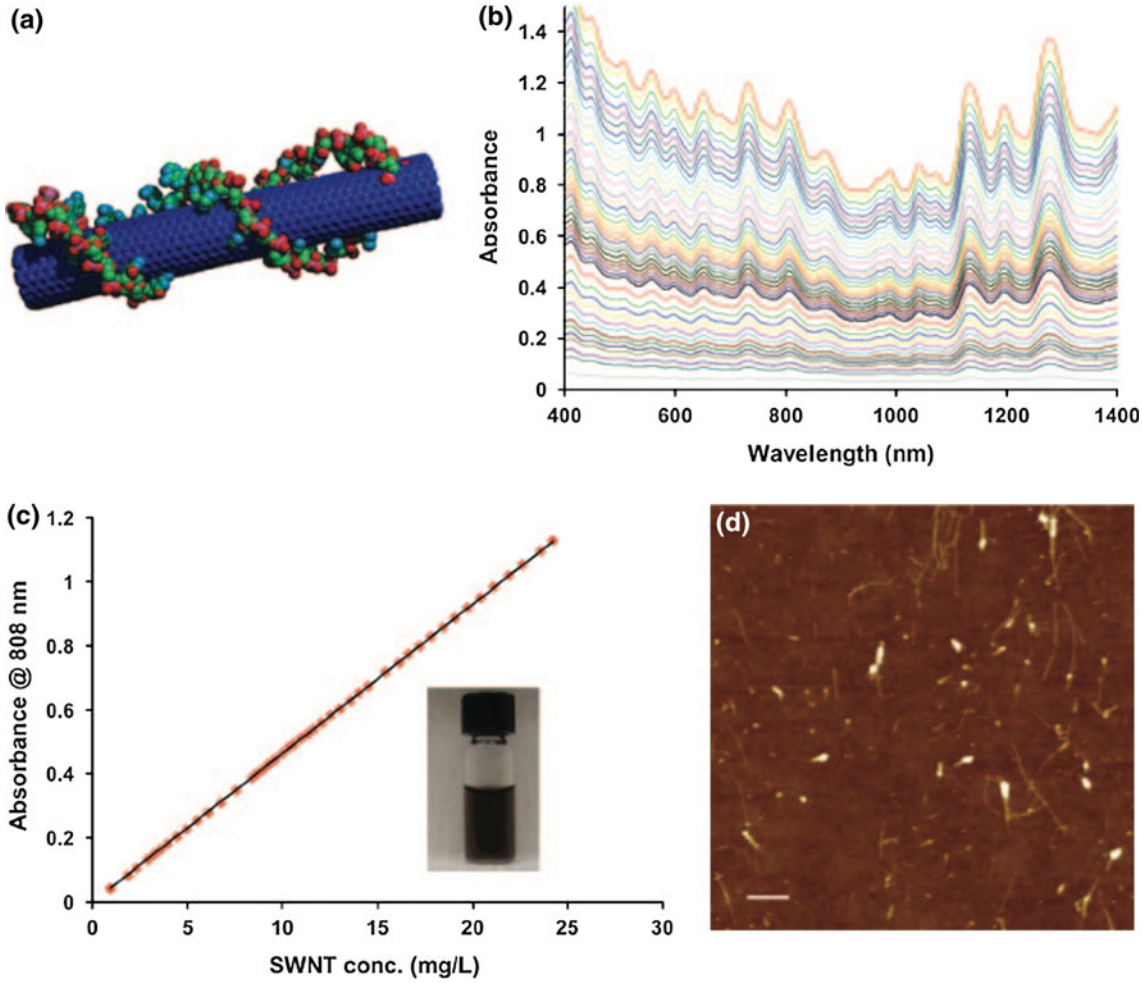

FIGURE 9. Carbon nanotubes with high NIR absorbance solubilized in water. (a) Schematic of a Cy3-DNA-functionalized SWNT. The drawing is only a graphic presentation and does not represent the precise way DNA binds on SWNTs. (b) UV–Vis spectra of solutions of individual SWNTs functionalized noncovalently by 15-mer Cy3 labeled-DNA at various nanotube concentrations (top curve, SWNT concentration ~25 mg/L in H_2O; lower curves correspond to consecutive 3% reduction in SWNT concentration). The well defined peaks in the UV–Vis spectra suggest lack of large aggregated SWNTs in the solution by removing bundles by centrifugation. (c) Absorbance at 808 nm vs. SWNT concentration (optical path = 1 cm). Solid line is Beer's law fit to obtain molar extinction coefficient of SWNT $\varepsilon = 7.9 \times 10^6\ M^{-1}\ cm^{-1}$. (Inset) A photo of a DNA-functionalized SWNT solution. (d) AFM image of DNA-functionalized individual SWNTs (height of 1–10 nm) deposited on a SiO_2 substrate (scale bar: 200 nm). Reprinted with permission from Melancon *et al.*[62] Copyright by the National Academy of Sciences.

shown in Fig. 12a. The TiO_2 NT layers were fragmented into small pieces with sizes <220 nm by using an ultrasonicator (Fig. 12b). A potential drawback to this synthesis method is the lack of monodispersity between the particles after sonication and fragmentation. Some of the particulate matter after fragmentation is larger than 500 nm, which limits the range of applications. The photothermal effects of TiO_2 NTs were studied by comparing with those of Au NPs and SWNTs. NIR light irradiation was carried out on TiO_2 NTs, Au NPs, and SWNTs using a high-power NIR laser (808 nm) source. The samples were irradiated continuously with an NIR laser at an intensity of 300 mW/cm^2 for 20 min. The temperature of the samples was measured at 30 s intervals and the results are shown in Fig. 13. The inner diameter of the TiO_2 NTs used in this experiment was ~100 nm. The diameter and length of the SWNTs were 1–1.2 nm and 5–20 μm, respectively, and the average diameter of the Au NPs was 50 nm.

To demonstrate the photothermal effect with TiO_2 NTs for use in *in vivo* applications, Lee and coworkers first performed initial studies *in vitro*.[30] Annexin V-fluorescein isothiocyanate (FITC) apoptosis assays were performed on 5 mouse colon carcinoma cell sample groups to see their modes of cell deaths. The cells were incubated with PEG modified TiO_2 NTs and irradiated with an NIR laser at 300 mW/cm^2 for 20 min. Five groups were evaluated: a TiO_2 NTs− and laser− control, a TiO_2 NTs− and laser+ group, a

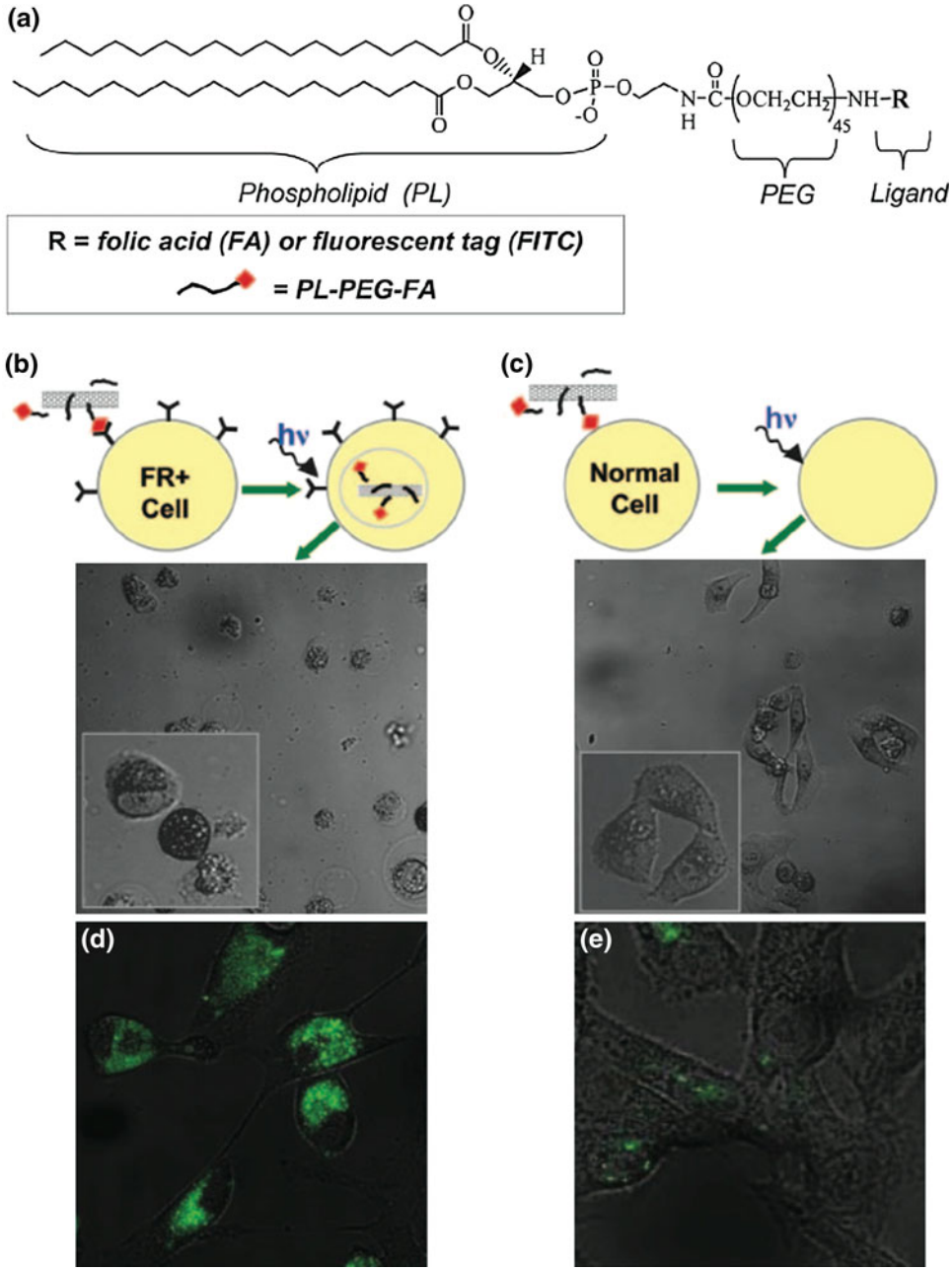

FIGURE 10. Selective targeting and killing of cancer cells. (a) Chemical structure of PL–PEG–FA and PL–PEG–FITC synthesized by conjugating PL–PEG–NH_2 with FA or FITC, respectively, for solubilizing individual SWNTs. (b) (Upper) Schematic of selective internalization of PL–PEG–FA–SWNTs into folate-overexpressing (FR^+) cells via receptor binding and then NIR 808-nm laser radiation. (Lower) Image showing death of FR^+ cells with rounded cell morphology after the process in Upper (808 nm laser radiation at 1.4 W/cm^2 for 2 min). (Inset) Higher magnification image shows details of the killed cells. (c) (Upper) Schematic of no internalization of PL–PEG–FA–SWNTs into normal cells without available FRs. (Lower) Image showing normal cells with no internalized SWNTs are unharmed by the same laser radiation condition as in "b". (Inset) Higher magnification image shows a live normal cell in stretched shape. (d) Confocal image of FR^+ cells after incubation in a solution of SWNTs with two cargoes (PL–PEG–FA and PL–PEG–FITC). The strong green FITC fluorescence inside cells confirms the SWNT uptake with FA and FITC cargoes. (e) The same as d for normal cells without abundant FRs on cell surfaces. There is little green fluorescence inside cells, confirming little uptake of SWNTs with FA and FITC cargoes. Reprinted with permission from Melancon *et al.*[62] Copyright by the National Academy of Sciences.

TiO_2 NT/NaCl+ and laser− group, a low concentration (12.5 mg/mL) TiO_2 NTs/NaCl suspension with laser + group, and high concentration (52.5 mg/mL) TiO_2 NTs/NaCl suspension with laser+ group.

Flow cytometry was performed and Lee and coworkers observed that the groups treated with TiO_2 NTs/NaCl suspensions and laser showed substantially higher cell death rates than those not given both laser

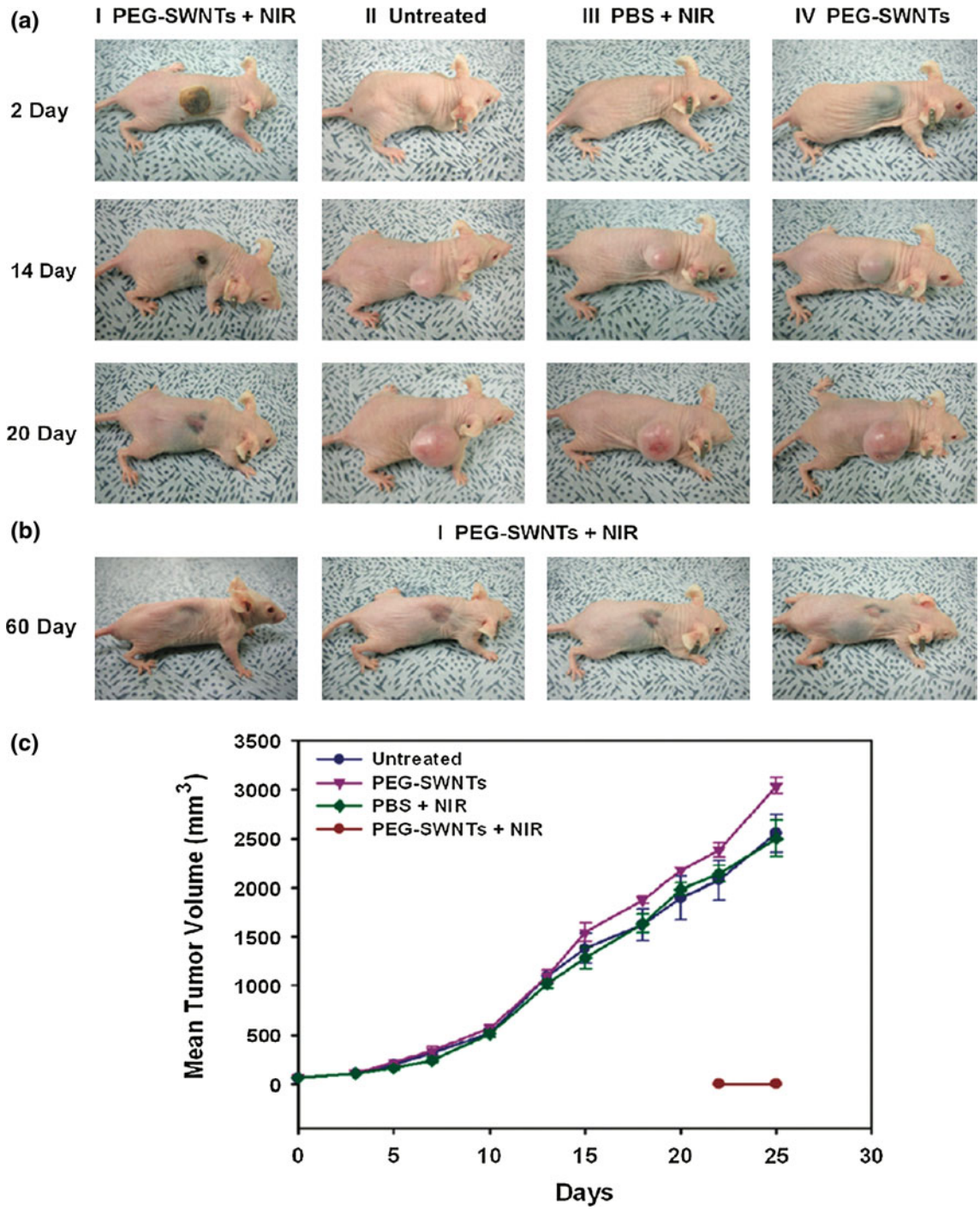

FIGURE 11. ***In vivo*** **photothermal effects of PEG–SWNTs for tumor obliteration. (a) Representative photographs of the mice treated in different groups at various time points after each treatment (I, PEG–SWNTs + NIR; II, untreated; III, PBS + NIR; IV, PEG–SWNTs). (b) Four mice after 60 days of photothermal treatments (I) from four independent sets. (c) Time-dependent tumor growth curves of KB tumor cell xenografts. Tumor volumes were measured three times a week after sample treatments. The results are presented as the arithmetic means with standard deviations of tumor volumes in each group ($n = 4$). Only the PEG–SWNTs + NIR treated group (I) shows significant suppression of tumor growth compared with other experimental groups ($n = 4$, $p < 0.05$, two-way ANOVA). Reprinted with permission from Li *et al.*[47] Copyright 2007 American Chemical Society.**

and TiO_2 NT treatments. They noticed that the cell death rate strongly depends on the concentration of TiO_2 NTs. Cells without TiO_2 NT treatment showed a viability of 97.8% and cells without laser treatment showed a viability of 96.4%. Combination of both laser and TiO_2 NTs shows cell viabilities of 0.77 and

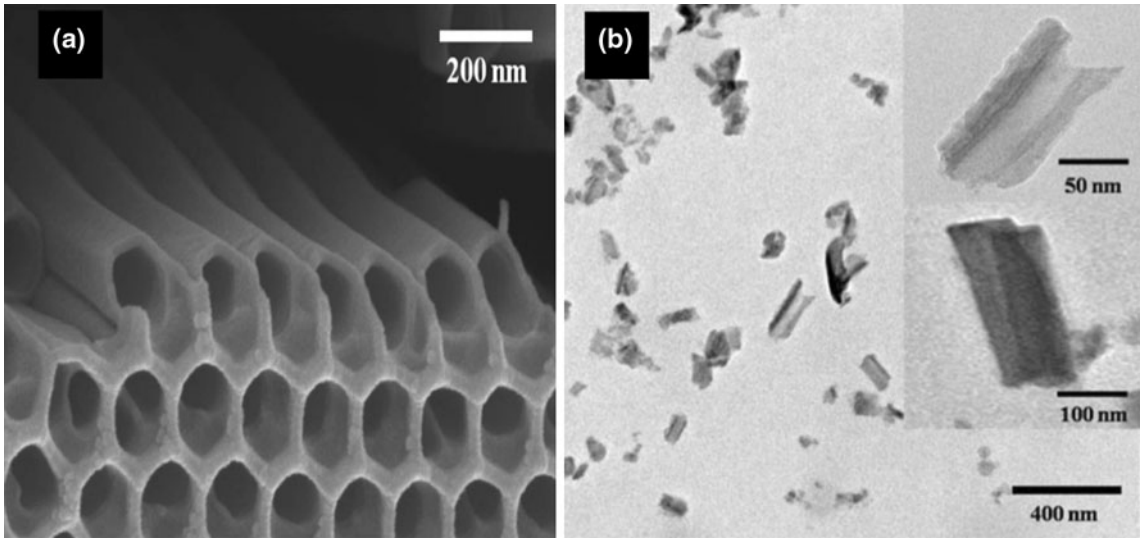

FIGURE 12. (a) Bird's eye view SEM images of TiO_2 NTs. TiO_2 NTs were formed by anodic etching of Ti thin foils in an electrolyte consisting of 0.3 wt.% NH_4F and 2 vol.% H_2O in ethylene glycol at 60 V for 17 h. (b) TEM image of the TiO_2 NT fragments with sizes <220 nm prepared by ultrasonication and filtration through a 220 nm microfilter. Modified with permission from Huang *et al.*[33]

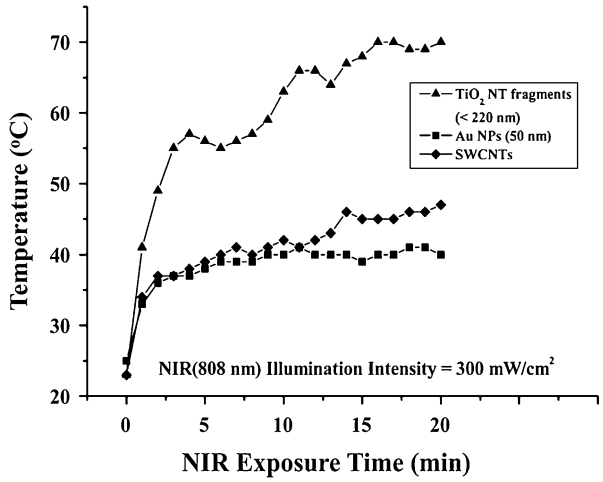

FIGURE 13. Comparison of the temperature of TiO_2 NTs with those of other inorganic nanomaterials such as Au NPs and SWCNTs which have recently been reported to be potential therapeutic agents for cancer thermotherapy during NIR laser irradiation at illumination intensities of 300 mW/cm^2. TiO_2 NT, Au NP and SWCNT samples are not in a state of suspension but are all in a state of dry solid; in other words, they have equal concentrations (100%). Reprinted with permission from Huang *et al.*[33]

0.0% for lower and higher TiO_2 NT concentrations, respectively, implying that most cells are killed.

Lee and coworkers conducted *in vivo* animal tests to confirm that TiO_2 NTs combined with NIR laser irradiation could efficiently destroy tumor cells, and to investigate the influence of the treatment parameters.[30] They inoculated murine colon carcinoma tumor cells into mice and grew them to ~1.0 cm in diameter prior to treatment. Two concentrations (27.5 or 52.5 mg/mL) of TiO_2 NTs/NaCl suspension were then directly injected into the tumor. NIR laser treatment was performed at either 300 or 400 mW/cm^2 for 20 min. Lee *et al.* observed that the ablated areas appeared black owing to carbonization of the skin and tumor tissue by the photothermal energy generated during laser treatment. Comparison of the treated tumors revealed that photothermal damage on tumor cells strongly depends on the intensity and duration of the laser delivered. According to their *in vivo* animal test results, increasing any of the following four parameters can enhance the photothermal destruction efficiency of tumor cells; namely, the laser intensity, laser exposure time, amount of TiO_2 NTs suspension and TiO_2 NTs concentration.

Based on their results, Lee suggested that phototherapy based on TiO_2 NTs, in combination with NIR laser, is anticipated to be effectively utilized to cure various cancers such as cancer of the esophagus, gastric cancer, cancer of the colon, cancer of the skin, breast cancer, and liver cancer due to the excellent photothermal property as well as the high biocompatibility of TiO_2 NTs.[30,45] Since the experiments utilizing TiO_2 NTs consisted of direct injections, there are many questions remaining concerning the delivery and specificity of the nanoparticles in a system where direct injection is not an option. Even so, TiO_2 nanoparticles are possible alternatives to current nanostructures as photothermal agents.

PHOTOTHERMAL-BASED BUBBLES

Another mechanism that shows great promise in theranostics is based on the vaporization of cellular

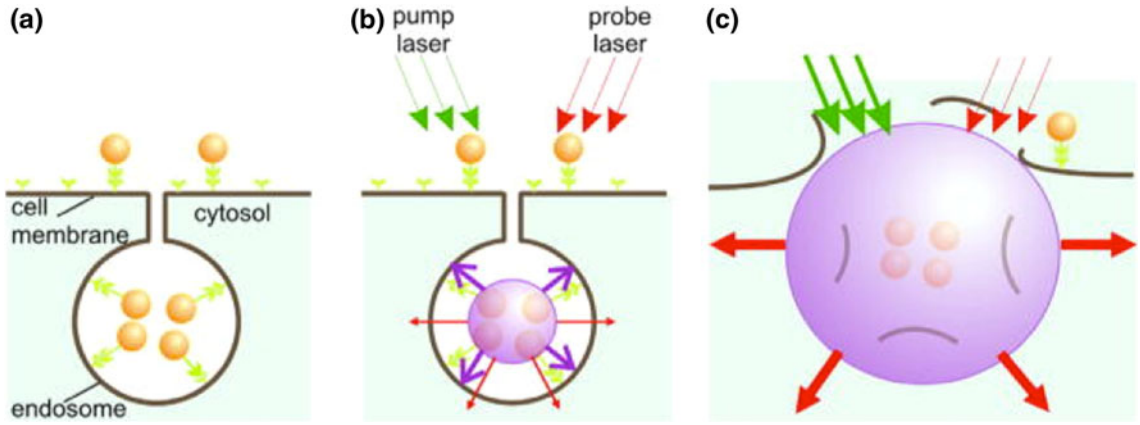

FIGURE 14. PNB cell theranostic with multi-stage tunable PNB: (a) cell is targeted with NP-antibody conjugates and intracellular NP clusters are formed through the receptor-mediated endocytosis, (b) the first (diagnostic) PNB provides the data on a cell and allows one to determine the parameters of the next laser pulse, (c) the second PNB delivers mechanical impact (cell damage though membrane disruption is shown) and this action is guided through the increased optical scattering (red arrows) of the second PNB; the PNB is tuned by varying the fluence of the pump pulse (green arrows). Reprinted with permission from Lacerda *et al.*[41]

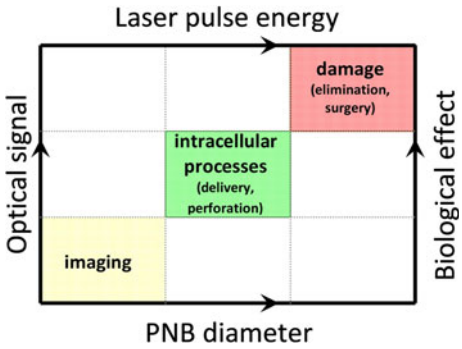

FIGURE 15. Tunability and guidance of the biological effects of PNBs: PNB diameter determines specific biological action and optical signal, while the pump pulse parameters determine the PNB diameter. Reprinted with permission from Hu *et al.*[31]

compartmental fluid using plasmonic NPs as a photothermal catalyst. The vaporization of the compartmental fluid leads to the formation of a bubble within the compartment and surrounding area. This phenomenon is termed photothermal-based bubbles (PTB). PTB therapy hinges on mechanical rather than thermal destruction of cancer cells. This is a slight deviation from the widespread use of plasmon resonant NPs for photothermal ablation. PTBs are transient photothermal vapor bubbles generated by various absorbing nanostructures including the AuNPs that combine high optical brightness with local mechanical impact.[42,43,56–60,82,92,108,109] The use of PTBs addresses the *in vivo* imaging limitations presented by low scattering from NPs due to background signals.

The generation of a PTB occurs in three phases (Fig. 14). First, a NP is activated by a laser pulse, resulting in the generation of heat. Second, there is thermal diffusion around the NP to surrounding medium, forming a thin vapor layer due to evaporation. Finally, the PTB expands to its peak diameter, and then collapses. The vapor–liquid border of the PTB creates a gradient of the refractive index, with the scattering efficiency and lifetime of the PTB determined by its diameter. Upon aggregation of AuNPs in cancer cells and laser pulse activation, the intracellular gold acts as a heat source and generates transient PTBs in the surrounding medium.[42,109] The optical and mechanical characteristics of PTBs are size- and lifetime-dependent, as illustrated in Fig. 15. Lukianova-Hleb *et al.* suggest that PTB diameters <300 nm are non-invasive imaging probes, 500–1000 nm PTBs produce localized reversible destruction, and 1–10 μm microbubbles result in mechanical destruction of target cells by disrupting the cell membrane due to their rapid expansion and collapse. The membrane disruption effect has also been utilized for selective gene transfection, where hydrodynamic injection was performed through the transient rupture that emerges during the PTB collapse.[60]

Lukianova-Hleb *et al.* used 50 nm gold spheres conjugated with anti-EGFR C225 *in vitro*, and exposed cells to a single pump laser pulse (532 nm, 0.5 ns). They then measured optical scattering and PTB lifetime after exposure to a probe laser (690 nm, 0.5 ns). These *in vitro* cell studies elucidated the threshold nature of PTBs. That is, the laser fluence level used was sufficient for PTB generation only around the larger NP clusters, with no PTB generation seen in smaller clusters or single NPs. Thus, NP clustering can improve the specificity of the PTBs. The *in vitro* study also demonstrated the ability to tune the PTBs from non-invasive imaging to invasive therapy. The first laser pulse allowed researchers to detect the PTB with

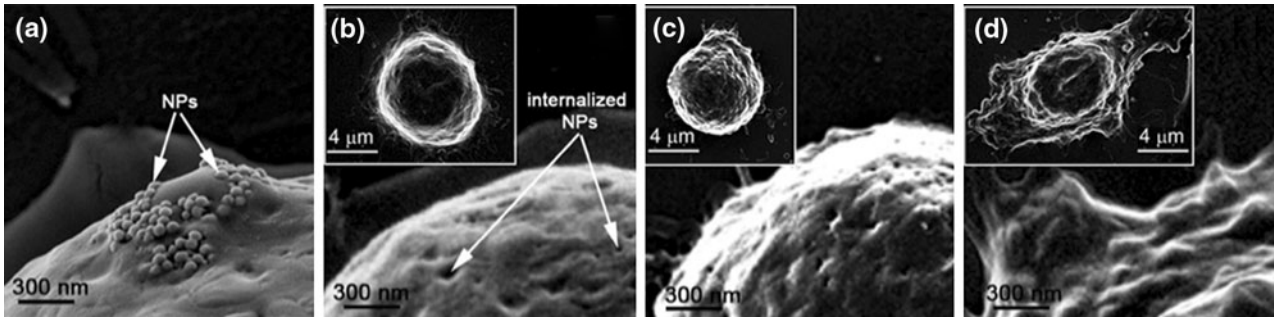

FIGURE 16. Scanning electron microscopy images of cancer cells after incubation with gold NPs show their membrane coupling (a) and internalization (b), and the result of the generation of a non-invasive PNB with a lifetime of 25 ± 5 ns (c) and an ablative PNB with a lifetime of 300 ± 42 ns (d).[94] The insets show images of the whole cells. The cells were fixed immediately after being treated with PNBs. Reprinted with permission from Qiu *et al.*[70] Copyright 2010, with permission from Elsevier.

almost 10-fold improvement in scattering relative to NPs, while the second pulse at an increased fluence (1.76 J/cm^2) resulted in brighter PTB scattering amplitude (290 times compared to NPs) and longer lifetime, with cellular disruption and formation of blebbing bodies seen 30–60 s after exposure.

Wagner *et al*. performed *in vivo* characterization of the PTBs in a zebrafish model hosting prostate xenografts using 60 nm gold spheres. Three conditions of zebrafish (NP+ and NP− xenografts, and ungrafted negative control) were exposed to a single pump laser pulse (pulse fluence of 125 mJ/cm^2) to observe localization of the cells by measuring optical scattering and darkfield fluorescence by the NPs and PTBs. When the pump laser pulse fluence was increased to 175 mJ/cm^2, targeted cancer cells in the NP+ xenograft were destroyed (Fig. 16), while the other two conditions were not and after 7 days, the NP treated zebrafish were still alive.[89]

A probe of such large diameter as PNBs (up to 200–500 nm) could never be delivered into cells without compromising their viability, however PTBs can be temporally generated non-invasively. With further optimization of laser fluence to meet the ANSI safety standard of 20 mJ/cm^2, PTBs may warrant further *in vivo* cancer studies in a clinically relevant animal model such as mice. However, changing the pulse laser to an NIR wavelength is vital before this approach can be expanded upon in order to increase penetration depths, which will be necessary for *in vivo* applications since very little tissue penetration will occur at 532 nm due to absorbance. Even after such alterations to the PNB design, this type of therapy may only prove applicable to superficial tumors.[49]

POLYMERIC NANOPARTICLE COMPOSITES

A more recent theranostic strategy has developed wherein the metal properties of NPs are coupled with thermally responsive polymers. These thermally responsive polymer–metal NP composites have been investigated for cancer therapy by combining the metal NP ability to generate heat with polymeric drug delivery.[12,19,28,37,47,90,106,107] Thus, the composite polymeric NPs can be irradiated with light, causing the metal NPs to generate heat, in turn resulting in polymer phase changes that can facilitate chemotherapy by drug release.

Thermally responsive polymers are a type of stimuli responsive smart polymer that exhibit fast and reversible conformational changes in the presence of external stimuli. In general, the conformational changes are a variation between hydrophilic and hydrophobic conformations as a result of changing chain arrangements.[20] The mechanism behind the conformational changes of thermally responsive polymers begins at the polymer's lower critical solution temperature (LCST). At the LCST, water molecules favorably form hydrogen bonds with the polar chain groups, resulting in swelling. As temperatures increase, the water moves away from the chains into the bulk solution, causing the polymer chains to collapse onto themselves.[75,76]

NPs that have been used in conjunction with thermally responsive polymers include solid Au NPs, GGS NPs, gold silica NPs, gold nanorods and superparamagnetic iron oxide NPs. Different methods have been used to synthesize and embed NPs within thermally responsive polymers. Langer *et al*. for example created a poly[*N*-isopropylacrylamide] (PNIPAAm) template by using both *N,N*-methylene bis-acrylamide (MBAAm) and *N,N*-cystamine bis-acrylamide (CBAAm) containing disulfide bridges which can bind AuNPs. Zhao *et al*. prepared gold encapsulated IPN-pNIPAAm nanogels in a two step process consisting of monolayer growth, followed by polymerization and crosslinking.[107] Li *et al*. synthesized poly(styrene-b-*N*-isopropylacrylamide) micelles and bound AuNPs to the surfaces.[47] Each of these approaches illustrates how

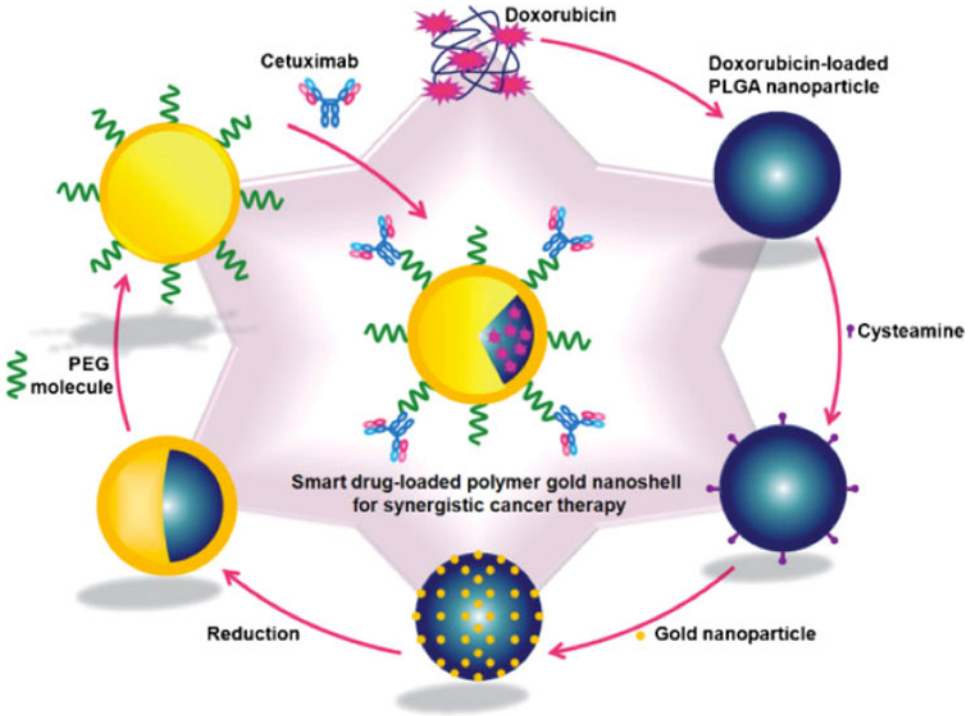

FIGURE 17. Schematic illustration of multifunctional drug-loaded gold nano-shells for synergistic cancer therapy. The novel nanostructure comprises three key parts for multidimensional therapeutic potentials, namely, (I) an anti-EGFR antibody, Cetuximab (CET), as a targeting moiety and signal-transduction inhibitor, (II) a gold nanoshell that has a photothermal effect due to plasmon resonance upon illumination by an NIR laser, and (III) DOX as a chemotherapeutic agent. These three components, incorporated into PLGA nanoparticles, provide synergistic tumoricidal efficacy. Reprinted with permission from Schwartzberg *et al.*[80] Advanced Materials, Copyright 2009.

hybrid polymer NPs vary widely from system to system.

In order to take advantage of the thermally responsive polymer properties, drug encapsulation is often incorporated in the design. An example of polymer NP composites for photothermal therapy utilized by Yang *et al.* consists of a thermally responsive poly(lactic-*co*-glycolic acid) (PLGA) matrix containing doxorubicin (DOX) and a gold outer layer, as illustrated in Fig. 17. This nanosystem was tested on epithelial cancer cells by targeting the over expressed EGFR receptor. Laser irradiation with 820 nm NIR light at 15 W/cm^2 intensity for 10 min facilitated a controlled 'burst' release of the DOX from the softened PLGA matrix, enhancing the photothermal effect. Despite the positive *in vitro* results, further *in vivo* testing of this multifunctional nanoplatform will be necessary before it is capable of producing cumulative cytotoxicity in tumors.[99] Additionally, the DOX-loaded PLGA NPs are around 80 nm before the final gold layer is even formed, which is on the larger range of desired diameters.

Recently, Cheng *et al.* developed a nanosystem consisting of polymer NP composites. Poly(lactic-*co*-glycolic acid) (PLGA) NPs encapsultating Taxol were functionalized with Fe_3O_4 NPs that were then covered with quantum dots (QDs) and Au nanorods. This nanoystem was the first of its kind tested in *in vitro* and *in vivo* models. Furthermore, experimental data showed that photothermal destruction using 808 nm laser at an intensity of 30 W/cm^2 for 7 min in conjunction with chemotherapy is more effective than either therapy alone.[12] This system was used as a contrast agent for MRI, but only preliminary image results were published. More work is still needed in developing the diagnostic and imaging components of this nanosystem. Overall, polymer NP composite structures are a promising theranostic agent for cancer therapy but are still in the very early stages of *in vitro* and *in vivo* development.

COPPER-BASED NANOCRYSTALS

While NPs encompass the group of amorphous or semicrystalline nanostructures, nanomaterials that are single crystalline are referred to as nanocrystals.[18] Nanocrystals tend to be smaller than other nanostructures at <100 nm and as such, metal nanocrystals exhibit different properties than their larger nanoparticle counterparts.[17,44,50] Recently, copper-based nanocrystals have gained interest due to their potential as a biocompatible replacement for cadmium-based

nanocrystals in applications such as contrast agents and *in vivo* cancer imaging. Two such nanocrystals are copper selenide (Cu_2Se) and copper sulfide (CuS). Interestingly, the NIR absorption of these particles is different from gold and other plasmonic particles we have discussed. While AuNP absorption is primarily a result of SPR, copper-based particle absorption is a combined effect from energy band–band transitions of the Cu^{2+} ions[48] as well as SPR bands.[61] Due to this property, the absorption wavelength of CuS and Cu_2Se is less affected by particle size, while the absorption intensity is highly affected by particle size due to quantum size confinement. As such, for small sizes, the absorbance is very large due to the confinement of bound excitons, while extending farther in the NIR range than other comparably sized plasmonic NPs that are difficult to obtain with a peak absorption >850 nm. Another advantage is that the absorption peak is less dependent of the surrounding solvent's dielectric constant, unlike with gold nanostructures whose plasmon absorption peak shifts depending on the surrounding matrix.[48]

Cu_2Se nanocrystals are one class of copper nanocrystals that exhibit NIR optical absorption. Synthesis of Cu_2Se particles uses a colloidal hot injection method followed by coating with amphiphilic polymer for biocompatibility. This process involves arrested precipitation in a hot solution of copper chloride and selenourea in oleylamine, followed by coating with a poly(maleic anhydride) polymer with carboxylic acid groups and oleylamine side chains. As a result of the amphiphillic polymer coating, micelles are formed in water, which protect the Cu_2Se nanocrystals by encapsulating them. Including the polymer coating, the nanoparticles have a hydrodynamic diameter of 39 nm. The Cu_2Se particles transfer heating at a photothermal conversion efficiency of 22% when irradiated with a laser tuned to 800 nm, which is reported to be comparable to Au NRs and nanoshells.[27] The NIR absorbance peak at 970 nm, shown in Fig. 18, is attributed to a combined plasmon and interband transition effect. In *in situ* and *in vitro* laser photothermal therapy of colorectal cancer cells, significant cell death was observed in the presence of Cu_2Se nanocrystals when cells were irradiated at an intensity of 30 W/cm^2 for 5 min. A possible limitation of these Cu_2Se nanocrystals is their small hydrodynamic diameter, which can result in unfavorable clearance *in vivo*. However, this issue could be addressed by the addition of nonimmunogenic targeting moieties such as proteins or antibodies in order to enhance their ability to stay in blood circulation for prolonged periods of time.[27] These biomolecules can potentially be functionalized on the distal carboxyl groups.

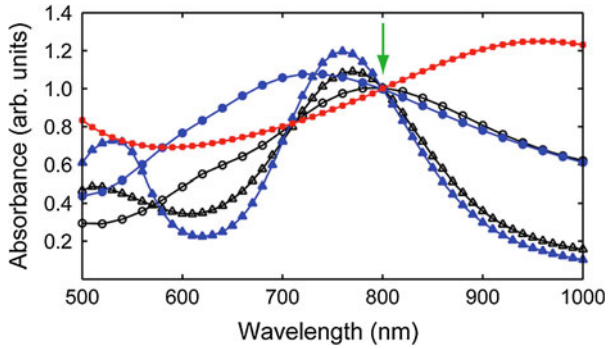

FIGURE 18. Absorbance spectra of Cu_2Se nanocrystals (red square), commercial Au nanoshells (blue circle), commercial Au NRs (blue triangle), synthesized Au nanoshells (black circle) and synthesized Au NRs (black triangle). Solutions were normalized to 1 OD at 800 nm (green arrow). Adapted with permission from Hessel *et al.*[27] Copyright 2011 American Chemical Society.

CuS nanocrystals are another emerging class of nanoparticles that exhibit NIR optical absorption. The synthesis proceeds by reacting $CuCl_2$ and thioacetamide in the presence of thioglycolic acid (TGA) for stabilization of the particles. In addition to the facile and quick synthesis, the cost of the synthesis is significantly less expensive than gold. While 1 mol of CuS particles costs \$330, 1 mol of Au atoms costs \$52,200.[48] Li *et al.* produced 3 nm diameter CuS using this process, with d–d transition peaks (and maximal absorption) at 900 nm. The laser used in Li *et al.*'s study was a CW diode laser. *In vitro* studies of the CuS nanocrystals were evaluated in a cervical cancer cell line, since NIR light can be used colposcopically clinically. The cells were exposed to 384 μM CuS and then irradiated at 808 nm at an intensity of 24 or 40 W/cm^2 for 5 min, or 64 W/cm^2 for 3 min. At 24 h post-laser irradiation, substantial cell death was observed. With higher output intensities, the region of cell death expanded beyond the laser spot size that indicates heat transfer to neighboring cells. As shown in Fig. 19, cell viability was 55.6% for 24 W/cm^2 and decreased to 21.2% at 40 W/cm^2, and finally 12.2% at 64 W/cm^2 laser intensity for 3 min exposure. In addition to laser intensity, the viability is also shown to be a function of CuS concentration. However, the laser intensity used in this study is too high to be translated *in vivo* at this point. As such, further optimization must occur. In order to move forward to *in vivo* studies, the photothermal conversion efficiency of the particles must be increased. One strategy is to coat the particles with zinc sulfide shells, since this would further confine excitons and increase the heating efficiency. Another approach is to simply switch to a 900 nm laser since the absorbance of CuS at 900 nm is stronger than 808 nm by a factor of 1.5.

Radioisotope passivated CuS particles have been synthesized recently to allow for noninvasive *in vivo* imaging in conjunction with PTT, and were shown to exhibit theranostic abilities *in vivo*. Zhou *et al*. utilized ^{64}Cu radioisotope due to its decay properties that facilitate PET imaging and radiotherapy.[112] They developed a synthesis process where [^{64}Cu]CuS particles were synthesized without the need to chelate ^{64}Cu to the CuS particles. This was accomplished by reacting $^{64}CuCl_2$ with $CuCl_2$ followed by SH-PEG addition and then sodium sulfide was added and the reaction proceeded overnight. This process produced larger particles than previously reported due to the addition of PEG, at around 11 nm, which is still much smaller than conventional plasmonic NPs. In addition to the small size of the particles, they absorb strongly in the NIR region and can be utilized for image-guided PTT. This was illustrated in human glioblastoma xenografts in a mouse model, with high uptake of the PEG–[^{64}Cu]CuS seen in the tumor, visualized in Fig. 20. The tumor was irradiated with 808 nm light at 12 W/cm^2 for 5 min. Intratumoral injections of the particles resulted in ~100% necrotic area, while intravenous injection resulted in ~70% necrosis.[112] While the cell death was extensive, there is still a clinical need to decrease the laser power in order to minimize damage to healthy tissues through heat transfer. Future work in theranostic [^{64}Cu]CuS particles will also focus on specific targeting moieties to increase tumoral accumulation and thus PTT efficiency.

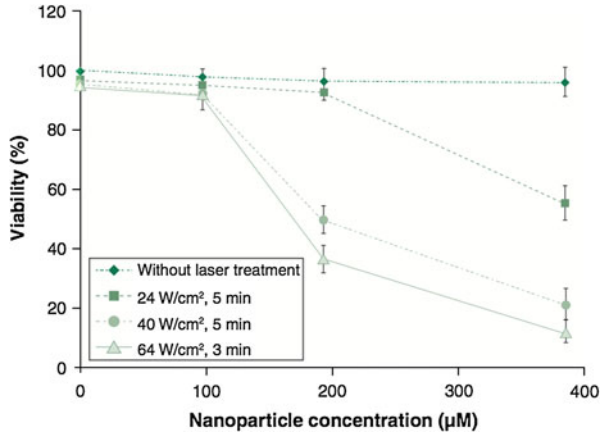

FIGURE 19. Cell viability after various concentrations of CuS NPs and laser intensities. Values present are mean ± standard deviation from triplicate samples. Reprinted with permission from Zhou *et al.*[112] Copyright 2011 American Chemical Society.

SUMMARY

Several unique nanostructures show great promise in theranostic applications of photothermal therapy for cancer treatment compared to conventional plasmonic-based gold nanoparticle approaches. These agents include HGNs, gold nanocages, GGS NPs, SWNTs, TiO_2 NTs, PTBs, polymeric NPs, and Cu-based nanocrystals. While these nanostructures are distinct, they have several properties in common. That is, they

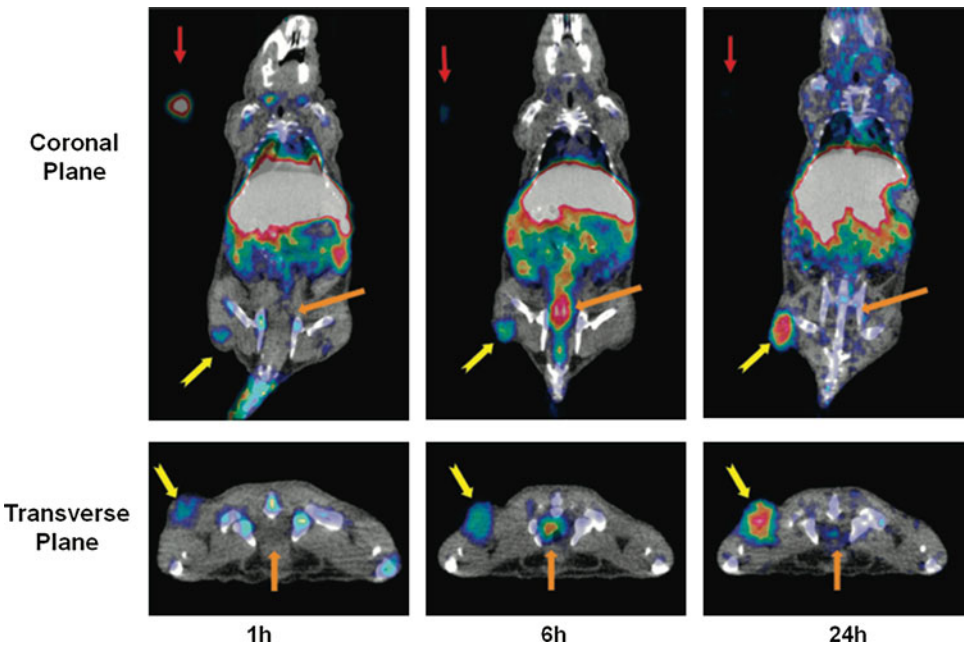

FIGURE 20. Nude mice with glioma xenografts (yellow arrow) imaged with Micro-PET/CT images at different time points after [^{64}Cu]CuS NP injection. Orange arrow, bladder. Red arrow, standard. Reprinted with permission from Zhou *et al.*[112] Copyright 2011 American Chemical Society.

are unique photoabsorbing agents that can be employed in conjunction with lasers in the NIR range in order to enhance imaging and photothermal effects and improve specificity in cancer treatment. More experimental studies are needed to further evaluate a number of variables such as particle concentration, laser power density and laser duration. Researchers anticipate the success of these unique approaches in clinical stages upon further optimization of parameters.

ACKNOWLEDGMENTS

We acknowledge financial support from the National Science Foundation, Dod CDMRP era of hope scholar award, and the NIH grand opportunities RC2 award.

CONFLICTS OF INTEREST

No benefits in any form have been or will be received from a commercial party related directly or indirectly to the subject of this manuscript.

REFERENCES

[1]Au, L., D. Zheng, F. Zhou, X. Y. Li, X. Li, and Y. Xia. A quantitative study on the photothermal effect of immuno gold nanocages targeted to breast cancer cells. *ACS Nano* 2(8):1645–1652, 2008.

[2]Averitt, R., D. Sarkar, and N. Halas. Plasmon resonance shifts of Au-coated Au_2S nanoshells: insight into multicomponent nanoparticle growth. *Phys. Rev. Lett.* 78(22):4217–4220, 1997.

[3]Averitt, R., S. L. Westcott, and N. J. Halas. Linear optical properties of gold nanoshells. *J. Opt. Soc. Am. B.* 16(10):1824–1832, 1999.

[4]Bachilo, S. M., M. S. Strano, C. Kittrell, R. H. Hauge, R. E. Smalley, and R. B. Weisman. Structure-assigned optical spectra of single-walled carbon nanotubes. *Science* 298:2361–2366, 2002.

[5]Bode, A. M., and Z. Dong. Cancer prevention research—then and now. *Nat. Rev. Cancer* 9(7):508–516, 2009.

[6]Boyer, D., P. Tamarat, A. Maali, B. Lounis, and M. Orrit. Photothermal imaging of nanometer-sized metal particles among scatterers. *Science* 297:1160–1163, 2002.

[7]Chen, Y., W. Frey, S. Kim, K. Homan, P. Kruizinga, K. Sokolov, and S. Emelianov. Enhanced thermal stability of silica-coated gold nanorods for photoacoustic imaging and image-guided therapy. *Opt. Expr.* 18(9):8867–8878, 2010.

[8]Chen, J., C. Glaus, R. Laforest, Q. Zhang, M. Yang, M. Gidding, M. Welch, and Y. Xia. Gold nanocages as photothermal transducers for cancer treatment. *Small* 6(7):811–817, 2010.

[9]Chen, J., F. Saeki, B. J. Wiley, H. Cang, M. J. Cobb, Z. Y. Li, L. Au, H. Zhang, M. B. Kimmey, and X. Li. Gold nanocages: bioconjugation and their potential use as optical imaging contrast agents. *Nano Lett.* 5(3):473–477, 2005.

[10]Chen, J., D. Wang, J. Xi, L. Au, A. Siekkinen, A. Warsen, Z. Y. Li, H. Zhang, Y. Xia, and X. Li. Immuno gold nanocages with tailored optical properties for targeted photothermal destruction of cancer cells. *Nano Lett.* 7(5):131813–131822, 2007.

[11]Chen, J., B. J. Wiley, Z. Li, D. Campbell, F. Saeki, H. Cang, L. Au, J. Lee, X. Li, and Y. Xia. Gold nanocages: engineering their structure for biomedical applications. *Adv. Mater.* 17:2255–2261, 2005.

[12]Cheng, F.-Y., C.-H. Su, P.-C. Wu, and C.-S. Yeh. Multifunctional polymeric nanoparticles for combined chemotherapeutic and near-infrared photothermal cancer therapy in vitro and in vivo. *Chem. Commun.* 46(18):3167–3169, 2010.

[13]Cherukuri, P., C. J. Gannon, T. K. Leeuw, H. K. Schmidt, R. E. Smalley, S. A. Curley, and R. B. Welsman. Mammalian pharmacokinetics of carbon nanotubes using intrinsic near-infrared fluorescence. *Proc. Natl Acad. Sci. USA* 103:18882–18886, 2006.

[14]Chithrani, B. D., A. A. Ghazani, and W. C. W. Chan. Determining the size and shape dependence of gold nanoparticle uptake into mammalian cells. *Nano Lett.* 6(4):662–668, 2006.

[15]Day, E. S., L. R. Bickford, J. H. Slater, N. S. Riggall, R. A. Drezek, and J. L. West. Antibody-conjugated gold–gold sulfide nanoparticles as multifunctional agents for imaging and therapy of breast cancer. *Int. J. Nanomed.* 5:445–454, 2010.

[16]Decuzzi, P., S. Lee, B. Bhushan, and M. Ferrari. A theoretical model for the margination of particles within blood vessels. *Ann. Biomed. Eng.* 33(2):179–190, 2005.

[17]El-Sayed, M. Small is different: shape-, size-, and composition-dependent properties of some colloidal semiconductor nanocrystals. *Acc. Chem. Res.* 37(5):326–333, 2004.

[18]Fahlman, B. Zero-dimensional nanomaterials. In: Materials Chemistry, edited by B. Fahlman. New York: Springer, 2011, pp. 473–484.

[19]Frimpong, R. A., S. Fraser, and J. Z. Hilt. Synthesis and temperature response analysis of magnetic-hydrogel nanocomposites. *J. Biomed. Mater. Res. A* 80:1–6, 2006.

[20]Galaev, I. Y., and B. Mattiasson. "Smart" polymers and what they could do in biotechnology and medicine. *Drug Deliv.* 7799:335–340, 1999.

[21]Gannon, C. J., P. Cherukuri, B. I. Yakobsen, L. Cognet, J. S. Kanzius, C. Kittrell, R. B. Weisman, M. Pasquali, H. K. Schmidt, R. E. Smalley, and S. A. Curley. Carbon nanotube-enhanced thermal destruction of cancer cells in a noninvasive radiofrequency field. *Cancer* 110:2654–2665, 2007.

[22]Garcia-Ripoll, A., A. M. Amat, A. Argues, R. Vicente, M. M. Ballesteros Martin, J. A. Sanchez Perez, I. Oller, and S. Malato. Confirming *Pseudomonas putida* as a reliable bioassay for demonstrating biocompatibility enhancement by solar photo-oxidative processes of a biorecalcitrant effluent. *J. Hazard. Mater.* 162:1223–1227, 2009.

[23]Ghosh, S., S. M. Bachilo, R. A. Simonette, K. M. Beckingham, and R. B. Weisman. Oxygen doping modifies near-infrared band gaps in fluorescent single-walled carbon nanotubes. *Science* 330:1656–1659, 2010.

[24]Ghosh, S., S. Dutta, E. Gomes, D. Carroll, R. D'Agostino, J. Olson, M. Guthold, and W. H. Gmeiner. Increased heating efficiency and selective thermal ablation of malignant tissue with DNA-encased multiwalled carbon nanotubes. *ACS Nano* 3:2667–2673, 2009.

[25]Gobin, A. M., M. H. Lee, N. J. Halas, W. D. James, R. A. Drezek, and J. L. West. Near-infrared resonant nanoshells for combined optical imaging and photothermal cancer therapy. *Nano Lett*. 7(7):1929–1934, 2007.
[26]Gobin, A. M., E. M. Watkins, E. Quevedo, V. L. Colvin, and L. West. Near infrared resonant gold/gold sulfide nanoparticles as a photothermal cancer therapeutic agent. *Small* 6(6):745–752, 2010.
[27]Hessel, C., V. Pattani, M. Rasch, M. Panthani, B. Koo, J. Tunnell, and B. Korgel. Copper selenide nanocrystals for photothermal therapy. *Nano Lett*. 11(6):2560–2566, 2011.
[28]Hirsch, L., A. Gobin, A. Lowery, F. Tam, R. Drezek, N. Halas, and J. West. Metal nanoshells. *Ann. Biomed. Eng*. 34(1):15–22, 2006.
[29]Hirsch, L., R. Stafford, J. Bankson, S. Sershen, B. Rivera, R. Price, J. Hazle, N. Halas, and J. West. Nanoshell-mediated near-infrared thermal therapy of tumors under magnetic resonance guidance. *PNAS* 100(23):13549–13554, 2003.
[30]Hong, C., J. Kang, J. Lee, H. Zheng, S. Hong, D. Lee, and C. Lee. Photothermal therapy using TiO_2 nanotubes in combination with near-infrared laser. *J. Cancer Ther*. 1:52–58, 2010.
[31]Hu, M., H. Petrova, J. Chen, J. M. McLellan, A. R. Siekkinen, M. Marquez, X. Li, Y. Xia, and G. V. Hartland. Ultrafast laser studies of the photothermal properties of gold nanocages. *J. Phys. Chem. B* 110(4):1520–1524, 2006.
[32]Huang, X., and M. A. El-Sayed. Gold nanoparticles: optical properties and implementations in cancer diagnosis and photothermal therapy. *J. Adv. Res*. 1:13–28, 2010.
[33]Huang, X., P. K. Jain, I. H. El-Sayed, and M. El-Sayed. Plasmonic photothermal therapy (PPTT) using gold nanoparticles. *Lasers Med. Sci*. 23(3):217–228, 2008.
[34]Jang, J. M., S. J. Park, G. S. Choi, T. Y. Kwon, and K. H. Kim. Chemical state and ultra-fine structure analysis of bio-compatible TiO_2 nanotube-type oxide film formed on titanium substrate. *Met. Mater. Int*. 14:457–464, 2008.
[35]Johnson, P. B., and R. W. Christy. Optical constants of the nobel metals. *Phys. Rev. Lett*. 11:541, 1963.
[36]Kanehara, M., Y. Watanabe, and T. Teranishi. Thermally stable silica-coated hydrophobic gold nanoparticles. *J. Nanosci. Nanotechnol*. 9:673–675, 2009.
[37]Kawano, T., Y. Niidome, T. Mori, Y. Katayama, and T. Niidome. PNIPAM gel-coated gold nanorods for targeted delivery responding to a near-infrared laser. *Bioconj. Chem*. 20(2):209–212, 2009.
[38]Kostarelos, K., A. Bianco, and M. Prato. Promises, facts and challenges for carbon nanotubes in imaging and therapeutics. *Nat. Nanotechnol*. 4:627–633, 2009.
[39]Kreibig, U., and M. Vollmer. Optical Properties of Metal Clusters. New York: Springer, 1995.
[40]Kumar, R., A. N. Maitra, P. K. Patanjali, and P. Sharma. Hollow gold nanoparticles encapsulating horseradish peroxidase. *Biomaterials* 26:6743–6753, 2005.
[41]Lacerda, L., A. Bianco, M. Prato, and K. Kostarelos. Carbon nanotubes as nanomedicines: from toxicology to pharmacology. *Adv. Drug Deliv. Rev*. 58:1460–1470, 2006.
[42]Lapotko, D. Plasmonic nanobubbles as tunable cellular probes for cancer theranostics. *Cancers* 3(1):802–840, 2011.
[43]Lee, H., C. Alt, C. Pitsillides, and C. Lin. Optical detection of intracellular cavitation during selective laser targeting of the retinal pigment epithelium: dependence of cell death mechanism on pulse duration. *J. Biomed. Opt*. 12(6):064034, 2007.
[44]Lee, K. S., and M. A. El-Sayed. Gold and silver nanoparticles in sensing and imaging: sensitivity of plasmon response to size, shape and metal composition. *J. Phys. Chem. B* 110(39):19220–19225, 2006.
[45]Lee, C., C. Hong, H. Kim, J. Kang, and H. M. Zheng. TiO_2 nanotubes as a therapeutic agent for cancer thermotherapy. *Photochem. Photobiol*. 86:981–989, 2010.
[46]Levi-Polyachenko, N. H., E. J. Merkel, B. T. Jones, D. L. Carroll, and J. H. Stewart. Rapid photothermal intracellular drug delivery using multiwalled carbon nanotubes. *Mol. Pharm*. 6(4):1092–1099, 2009.
[47]Li, J., W.-D. He, and X.-L. Sun. Preparation of poly (styrene-b-N-isopropylacrylamide) micelles surface-linked with gold nanoparticles and thermo-responsive ultraviolet–visible absorbance. *J. Polym. Sci. A: Polym. Chem*. 45:5156–5163, 2007.
[48]Li, Y., W. Lu, Q. Huang, M. Huang, C. Li, and W. Chen. Copper sulfide nanoparticles for photothermal ablation of tumor cells. *Nanomedicine* 5(8):1161–1171, 2010.
[49]Liang, H. P., L. J. Wan, C. L. Bai, and L. Jiang. Gold hollow nanospheres: tunable surface plasmon resonance controlled by interior-cavity sizes. *J. Phys. Chem. B* 109:7795–7800, 2005.
[50]Link, S., and M. El-Sayed. Shape and size dependence of radiative, non-radiative and photothermal properties of gold nanocrystals. *Int. Rev. Phys. Chem*. 19(3):409–453, 2000.
[51]Liu, Z., C. Davis, W. Cai, L. He, X. Chen, and H. Dai. Circulation and long-term fate of functionalized, biocompatible single-walled carbon nanotubes in mice probed by Raman spectroscopy. *Proc. Natl Acad. Sci. USA* 105:1410–1415, 2008.
[52]Liu, Z., X. Li, S. M. Tabakman, K. Jiang, S. Fan, and H. Dai. Multiplexed multi-color Raman imaging of live cells with isotopically modified single walled carbon nanotubes. *J. Am. Chem. Soc*. 130:13540–13541, 2008.
[53]Liu, Z., S. M. Tabakman, Z. Chen, and H. Dai. Preparation of carbon nanotube bio-conjugates for biomedical applications. *Nat. Protoc*. 4:1372–1382, 2009.
[54]Liu, Z., S. M. Tabakman, K. Welsher, and H. Dai. Carbon nanotubes in biology and medicine: in vitro and in vivo detection, imaging and drug delivery. *Nano Res*. 2:85–120, 2009.
[55]Liu, X., H. Tao, K. Yang, S. Zhang, S. T. Lee, and Z. Liu. Optimization of surface chemistry on single-walled carbon nanotubes for in vivo photothermal ablation of tumors. *Biomaterials* 32:144–151, 2011.
[56]Lukianova-Hleb, E., E. Y. Hanna, J. H. Hafner, and D. O. Lapotko. Tunable plasmonic nanobubbles for cell theranostics. *Nanotechnology* 21(8):85102, 2010.
[57]Lukianova-Hleb, E., Y. Hu, L. Latterini, L. Tarpani, S. Lee, R. Drezek, J. Hafner, and D. Lapotko. Plasmonic nanobubbles as transient vapor nanobubbles generated around plasmonic nanoparticles. *ACS Nano* 4(4):2109–2123, 2010.
[58]Lukianova-Hleb, E., I. I. Koneva, A. O. Oginsky, S. La Francesca, and D. O. Lapotko. Selective and self-guided micro-ablation of tissue with plasmonic nanobubbles. *J. Surg. Res*. 166(1):e3–e13, 2011.
[59]Lukianova-Hleb, E., A. O. Oginsky, D. L. Shenefelt, R. A. Drezek, and J. H. Hafner. Rainbow plasmonic nanobubbles: synergistic activation of gold nanoparticle clusters. *J. Nanomed. Nanotechnol*. 2(1):1–8, 2011.
[60]Lukianova-Hleb, E., A. P. Samaniego, J. Wen, L. Metelitsa, C.-C. Chang, and D. Lapotko. Selective gene transfection of

individual cells in vitro with plasmonic nanobubbles. *J. Control. Release* 152(2):286–293, 2011.
[61]Luther, J., P. Jain, T. Ewers, and P. Aliviatos. Localized surface plasmon resonances arising from free carriers in doped quantum dots. *Nat. Mater*. 10:361–366, 2011.
[62]Melancon, M. P., W. Lu, Z. Yang, R. Zhang, Z. Cheng, A. Elliot, J. Stafford, T. Olson, J. Z. Zhang, and C. Li. In vitro and in vivo targeting of hollow gold nanoshells directed at epidermal growth factor receptor for photothermal ablation therapy. *Mol. Cancer Ther*. 7:1730–1739, 2008.
[63]Mischenko, M., L. Travis, and D. Mackowski. T-matrix computations of light scattering by nonspherical particles: a review. *J. Quant. Spectrosc. Radiat. Transf*. 55(5):535–575, 1996.
[64]Moon, H. K., S. H. Lee, and H. C. Choi. In vivo near-infrared mediated tumor destruction by photothermal effect of carbon nanotubes. *ACS Nano* 3:3707–3713, 2009.
[65]O'Connell, M. J., S. M. Bachilo, C. B. Huffman, V. C. Moore, M. S. Strano, E. H. Haroz, K. L. Rialon, P. J. Boul, W. H. Noon, C. Kittrell, J. Ma, R. H. Hauge, R. B. Weisman, and R. E. Smalley. Band gap fluorescence from individual single-walled carbon nanotubes. *Science* 297:593–596, 2002.
[66]O'Neal, D., L. Hirsch, N. Halas, J. Payne, and J. West. Photo-thermal tumor ablation in mice using near infrared-absorbing nanoparticles. *Cancer Lett*. 209:171–176, 2004.
[67]Pissuwan, D., S. Valenzuela, and M. Cortie. Therapeutic possibilities of plasmonically heated gold nanoparticles. *Trends Biotechnol*. 24(2):62–67, 2006.
[68]Poon, L., W. Zandberg, D. Hsiao, Z. Erno, D. Sen, B. D. Gates, and N. R. Branda. Photothermal release of single-stranded DNA from the surface of gold nanoparticles through controlled denaturating and Au–S bond breaking. *ACS Nano* 4(11):6395–6403, 2010.
[69]Prevo, B. G., S. A. Esakoff, A. Mikhailovsky, and J. A. Zasadzinski. Scalable routes to gold nanoshells with tunable sizes and response to near-infrared pulsed-laser irradiation. *Small* 4(8):1183–1195, 2008.
[70]Qiu, L., T. Larson, D. Smith, E. Vitkin, S. Zhang, M. Modell, I. Itskan, E. Hanlon, B. Korgel, K. Sokolov, and L. Perelman. Single gold nanorod detection using confocal light absorption and scattering spectroscopy. *IEEE J. Sel. Top. Quant. Electron*. 13(5):1730–1738, 2007.
[71]Raschke, G., S. Brogl, A. S. Susha, A. L. Rogach, T. A. Klar, and J. Feldmann. Gold nanoshells improve single nanoparticle molecular sensors. *Nano Lett*. 4(10):1853–1857, 2004.
[72]Robinson, J. T., K. Welsher, S. M. Tabakman, S. P. Sherlock, H. Wang, R. Luong, and H. Dai. High performance in vivo near-IR (>1 μm) imaging and photothermal cancer therapy with carbon nanotubes. *Nano Res*. 3(11):779–793, 2007.
[73]Sarkar, S., J. Fisher, C. Rylander, and M. N. Rylander. Photothermal response of tissue phantoms containing multi-walled carbon nanotubes. *J. Biomech. Eng*. 132(4): 044505, 2010.
[74]Sasaki, K., K. Asanuma, K. Johkura, T. Kasuga, Y. Okouchi, N. Ogiwara, S. Kubota, R. Teng, L. Cui, and X. Zhao. Ultrastructural analysis of TiO_2 nanotubes with photodecomposition of water into O_2 and H_2 implanted in the nude mouse. *Ann. Anat*. 188(2):137–142, 2006.
[75]Sasaki, S., H. Kawasaki, and H. Maeda. Volume phase transition behavior of N-isopropylacrylamide gels as a function of the chemical potential of water molecules. *Biotechnol. Bioeng*. 19(9):1405, 1977.
[76]Schild, H. G. Poly(N-isopropylacrylamide): experiment, theory and application. *Prog. Polym. Sci*. 17:163–249, 1992.
[77]Schipper, M. L., N. R. Nakayama, C. R. Davis, N. W. S. Kam, P. Chu, Z. Liu, X. Sun, H. Dai, and S. S. Gambhir. A pilot toxicology study of single-walled carbon nanotubes in a small sample of mice. *Nat. Nanotechnol*. 3:216–221, 2008.
[78]Schwartzberg, A. M., C. D. Grant, T. van Buuren, and J. Z. Zhang. Reduction of $HAuCl_4$ by Na_2S revisited: the case for au nanoparticle aggregates and against Au_2S/Au core/shell particles. *J. Phys. Chem. C* 111(25):8892–8901, 2007.
[79]Schwartzberg, A. M., T. Y. Olson, C. E. Talley, and J. Z. Zhang. Synthesis, characterization, and tunable optical properties of hollow gold nanospheres. *J. Phys. Chem. B* 110(40):19935–19944, 2006.
[80]Schwartzberg, A. M., T. Y. Oshiro, J. Z. Zhang, T. Huser, and C. E. Talley. Improving nanoprobes using surfaced-enhanced Raman scattering from 30-nm hollow gold particles. *Anal. Chem*. 78:4732–4736, 2006.
[81]Shi, K. N. W., M. O'Connell, J. A. Wisdom, and H. Dai. Carbon nanotubes as multifunctional biological transporters and near-infrared agents for selective cancer cell destruction. *Proc. Natl Acad. Sci. USA* 102(33):11600–11605, 2005.
[82]Slifka, A., G. Singh, D. Lauria, P. Rice, and R. Mahajan. Observations of nanobubble formation on carbon nanotubes. *Appl. Phys. Expr*. 3:065103, 2010.
[83]Strong, L. E., and J. L. West. Thermally responsive polymer-nanoparticle composites for biomedical applications. Wiley interdisciplinary reviews. *Nanomed. Nanobiotechnol*. 3(3):307–317, 2011.
[84]Sul, Y. T., C. B. Johansson, Y. Jeong, and T. Albrektsson. The electrochemical oxide growth behaviour on titanium in acid and alkaline electrolytes. *Med. Eng. Phys*. 23(5): 329–346, 2001.
[85]Sun, Y., B. T. Mayers, and Y. Xia. Template-engaged replacement reaction: a one step approach to the large scale synthesis of metal nanostructures with hallow interiors. *Nano Lett*. 2(5):481–485, 2002.
[86]Sun, Y., and Y. Xia. Alloying and dealloying processes involved in the preparation of metal nanoshells through a galvanic replacement reaction. *Nano Lett*. 3(11):1569–1572, 2003.
[87]Sun, Y., and Y. Xia. Mechanistic study on the replacement reaction between silver nanostructures and chloroauric acid in aqueous medium. *J. Am. Chem. Soc*. 126: 3892–3901, 2004.
[88]von Wilmowsky, C., S. Bauer, R. Lutz, M. Meisel, F. W. Neukam, T. Toyoshima, P. Schmuki, E. Nkenke, and K. A. Schlegel. In vivo evaluation of anodic TiO_2 nanotubes: an experimental study in the pig. *J. Bio. Mater. Res*. 89(1):165–171, 2009.
[89]Wagner, D. S., N. A. Delk, E. Y. Lukianova-Hleb, J. H. Hafner, M. C. Farach-Carson, and D. O. Lapotko. The in vivo performance of plasmonic nanobubbles as cell theranostic agents in zebrafish hosting prostate cancer xenografts. *Biomaterials* 31(29):7567–7574, 2010.
[90]Wang, C., N. . T. Flynn, and R. Langer. Controlled structure and properties of thermoresponsive nanoparticle–hydrogel composites. *Adv. Mater*. 16(13):1074–1079, 2004.
[91]Wang, H. F., J. Wang, X. Y. Deng, H. F. Sun, Z. J. Shi, and Z. N. Gu. Biodistribution of carbon single-wall

carbon nanotubes in mice. *J. Nanosci. Nanotechnol.* 4:1019–10124, 2004.
[92]Weissleder, R. A clearer vision for in vivo imaging. *Nat. Biotechnol.* 19:316–317, 2001.
[93]Welsher, K., Z. Liu, D. Daranciang, and H. Dai. Selective probing and imaging of cells with single walled carbon nanotubes as near-infrared fluorescent molecules. *Nano Lett.* 8:586–590, 2008.
[94]Welsher, K., Z. Liu, S. P. Sherlock, J. T. Robinson, Z. Chen, D. Daranciang, and H. Dai. A route to brightly fluorescent carbon nanotubes for near-infrared imaging in mice. *Nat. Nanotechnol.* 4:773–780, 2009.
[95]Wielaard, D. J., M. I. Mishchenko, A. Macke, and B. E. Carlson. Improved T-matrix computations for large nonabsorbing and weakly absorbing nonspherical particles and comparison with geometrical-optics approximation. *Appl. Opt.* 36(18):4305–4313, 1997.
[96]Wu, P., X. Chen, N. Hu, U. C. Tam, O. Blixt, A. Zettl, and C. R. Bertozzi. Biocompatible carbon nanotubes generated by functionalization with glycodendrimers. *Angew. Chem. Int. Ed.* 47:5022–5025, 2008.
[97]Wu, G., A. Mikhailovsky, H. A. Khant, C. Fu, W. Chiu, and J. A. Zasadzinski. Remotely triggered liposomal release by near-infrared light absorption via hollow gold nanoshells. *J. Am. Chem. Soc.* 130:8175–8177, 2008.
[98]Xiao, Y., X. Gao, O. Taratula, S. Treado, A. Urbas, R. D. Holbrook, R. Cavicchi, C. T. Avedisian, S. Mitra, R. Savla, P. D. Wagner, S. Srivastava, and H. He. Anti-her2 IgY antibody-functionalized single-walled carbon nanotubes for detection and selective destruction of breast cancer cells. *BMC Cancer* 9:351, 2009.
[99]Yang, J., J. Lee, J. Kang, S. J. Oh, H.-J. Ko, J.-H. Son, K. Lee, J. Suh, Y. Huh, and S. Haam. Smart drug-loaded polymer gold nanoshells for systemic and localized therapy of human epithelial cancer. *Adv. Mater.* 21(43):4339–4342, 2009.
[100]Yang, S. T., X. Wang, G. Jia, Y. Gu, T. Wang, H. Nie, C. Ge, H. Wang, and Y. Liu. Long-term accumulation and low toxicity of single-walled carbon nanotubes in intravenously exposed mice. *Toxicol. Lett.* 101:181–182, 2008.
[101]Yao, C., G. Balasundaram, and T. Webster. Use of anodized titanium in drug delivery applications. *Mater. Res. Soc. Symp. Proc.* 951:0951-E12-28, 2007.
[102]Yavuz, M. S., Y. Cheng, J. Chen, C. M. Cobley, Q. Zhang, M. Rycenga, J. Xie, C. Kim, A. G. Schwartz, L. V. Wang, and Y. Xia. Gold nanocages covered by smart polymers for controlled release with near-infrared light. *Nat. Mater.* 8(12):935–939, 2009.
[103]Zavaleta, C., A. Zerda, Z. Liu, S. Keren, Z. Cheng, M. Schipper, X. Chen, H. Dai, and S. S. Gambhir. Noninvasive Raman spectroscopy in living mice for evaluation of tumor targeting with carbon nanotubes. *Nano Lett.* 8:2800–2805, 2008.
[104]Zhang, Y. M., P. Bataillon-Linez, P. Huang, Y. M. Zhao, Y. Han, M. Traisnel, K. W. Xu, and H. F. Hildebrand. Surface analyses of micro-arc oxidized and hydrothermally treated titanium and effect on osteoblast behavior. *J. Biomed. Mater. Res.* 68A(2):383–391, 2004.
[105]Zhang, J., A. M. Schwartzberg, T. Norman, C. Grant, J. Liu, F. Bridges, and T. Buuren. Comment on ''gold nanoshells improve single nanoparticle molecular sensors''. *Nano Lett.* 5(4):809–810, 2005.
[106]Zhao, X., X. Ding, Z. Deng, Z. Zheng, Y. Peng, C. Tian, and L. Xinping. A kind of smart gold nanoparticle hydrogel composite with tunable thermo-switchable electrical properties. *New J. Chem.* 30(6):915, 2006.
[107]Zhao, X., T. Wang, W. Liu, C. Wang, D. Wang, T. Shang, L. Shen, and L. Ren. Multifunctional Au@IPN-pNIPAAm nanogels for cancer cell imaging and combined chemo-photothermal treatment. *J. Mater. Chem.* 21(20):7240, 2011.
[108]Zharov, V., and V. Galitovsky. Photothermal detection of local thermal effects during selective nanophotothermolysis. *Appl. Phys. Lett.* 83(24):4897–4899, 2003.
[109]Zharov, V., J.-W. Kim, D. Curiel, and M. Everts. Self-assembling nanoclusters in living systems: application for integrated photothermal nanodiagnostics and nanotherapy. *Nanomedicine* 1(4):326–345, 2005.
[110]Zhou, H., I. Honma, H. Komiyama, and J. Haus. Controlled synthesis and quantum-size effect in gold-coated nanoparticles. *Phys. Rev. B Condens. Mat.* 50(16):12052–12056, 1994.
[111]Zhou, F., D. Xing, Z. Ou, B. Wu, D. E. Resasco, and W. R. Chen. Cancer photothermal therapy in the near-infrared region by using single-walled carbon nanotubes. *J. Biomed. Opt.* 14:021009, 2009.
[112]Zhou, M., R. Zhang, M. Huang, W. Lu, S. Song, M. Melancon, M. Tian, D. Liang, and C. Li. A chelator-free multifunctional [^{64}Cu]CuS nanoparticle platform for simultaneous micro-PET/CT imaging and photothermal ablation therapy. *JACS* 132(43):15351–15358, 2010.
[113]Zwilling, V., M. Aucouturier, and E. Darque-Ceretti. Anodic oxidation of titanium and TA6V alloy in chromic media. An electrochemical approach. *Electrochim. Acta* 45:921–929, 1999.